

DEVELOPMENT OF A BIOFIDELIC FLEXIBLE PEDESTRIAN LEGFORM IMPACTOR TYPE GTR PROTOTYPE

Part 1: DEVELOPMENT AND TECHNICAL EVALUATIONS

Atsuhiko Konosu and Takahiro Issiki

Japan Automobile Research Institute, Japan

Yukou Takahashi and Hideki Suzuki

Japan Automobile Manufacturers Association, Inc., Japan

Bernard Been and Mark Burleigh

First Technology Safety Systems, The Netherlands and the United Kingdom

Takahiro Hirasawa and Hitoshi Kanoshima

Ministry of Land, Infrastructure, Transport, and Tourism, Japan

Paper Number 09-0145

ABSTRACT

Prototypes of the latest version of a biofidelic flexible pedestrian legform impactor (Flex-GTR-PROTO) were developed in November 2008. In this research several technical evaluations on the Flex-GTR-PROTO were conducted. As a result, fairly good repeatability and reproducibility of the Flex-GTR-PROTO, and comparability of the Flex-GTR-PROTO output under the symmetric right and left bumper corner impacts were observed (majorities of CV values are less than 3%).

As for the comparability between the Flex-GT and Flex-GTR PROTO, some differences were observed between them. Most of the maximum value ratios of Flex-GTR-PROTO relative to the Flex-GT are less than 1.1. The difference between the Flex-GT and Flex-GTR-PROTO has a chance to affect the injury threshold values; therefore, a following research has been investigating the threshold values for the Flex-GTR-PROTO using the ratios of the Flex-GT and Flex-GTR outputs and/or using the correlations between the Flex-GTR-PROTO and human lower extremities outputs which can be obtained from a computer simulation analysis.

INTRODUCTION

In 1998, the European Enhanced Vehicle-Safety Committee proposed a test procedure to assess the protection vehicles provide to the lower extremity of a pedestrian during a collision [1]. This procedure utilizes a legform impactor composed of rigid long bones.

In order to improve biofidelity of the legform impactor, the Japan Automobile Research Institute (JARI) and the Japan Automobile Manufacturers Association, Inc. (JAMA) have been developing a biofidelic flexible pedestrian legform impactor (Flex-PLI) since 2002 [2]. The Flex-PLI has high biofidelity especially for its long bone parts, which have human-like bending characteristics under a car

impact condition, compared to other types of legform impactors, which have rigid long bone parts [3].

The Flex-PLI also provides extended injury assessment capability, including long bone bending moment at multiple locations and knee ligament elongations in comparison to other pedestrian legforms [3].

In 2005, the Flex-PLI Technical Evaluation Group (Flex-TEG) was settled under the UN/ECE/WP29/GRSP/Informal Group on Pedestrian Safety in order to evaluate its performance to adopt the impactor as a regulatory purpose test tool for a Global Technical Regulation on Pedestrian Safety (PS-GTR: gr 9).

The Ministry of Land, Infrastructure, Transport, and Tourism of Japan (J-MLIT) has been supporting this Flex-TEG activity, taking a task of a chair country of the group and conducting technical evaluation tests on the Flex-PLI.

After the settlement of the Flex-TEG, the Flex-PLI was evaluated and improved its performance under the Flex-TEG activity, and then its design of the final version, type GTR (Flex-GTR), was agreed by the Flex-TEG members in April 2008 [4], and its prototype (Flex-GTR-PROTO) was released in November 2008.

In the Flex-GTR-PROTO development, First Technology Safety Systems (FTSS) was involved as a dummy development specialist company.

This paper provides a brief introduction of the Flex-GTR-PROTO and technical evaluation test results on them under several impact conditions.

TECHNICAL EVALUATION ITEMS

In this research, following technical evaluations were conducted.

E1: Repeatability of the Flex-GTR-PROTO

- E2: Reproducibility of the Flex-GTR-prototype
- E3: Comparability between the Flex-GT and Flex-GTR-prototype
- E4: Comparability of the Flex-GTR-prototype output under the symmetric right and left bumper corner impacts

MATERIALS

Flexible Pedestrian Legform Impactor type GTR prototype (Flex-GTR-prototype)

Figure 1 shows a general construction of the Flex-GTR-prototype. Its femur and tibia have flexible long bones which can be bent under the car impact condition. Its knee has a ligament constraint system similar to the human one, and its movement is restrained by four knee ligaments as described in the figure. More detailed information of the Flex-GTR-prototype is described in the Part2 of this ESV paper series (Paper Number 09-0146) [5].

In this research three of the Flex-GTR-prototype (SN01, SN02, SN03) were used as shown in Figure 2. The three Flex-GTR-prototypes have the same constructions, and only data acquisition systems (DAS) which can be used are different. The SN01 can implement an off-board DAS only. On the other hand, the SN02 can implement an off-board DAS or on-board DAS (M=BUS, MESSRING, Germany), and the SN03 can implement an off-board DAS or on-board DAS (SLICE, DTS, USA), as shown in Figure 3. More detailed information of the DAS is described in the Part 2 of this ESV paper series [5].

Figure 4 shows the measurement items of the Flex-GTR-prototypes. In this research mainly injury assessment items and monitoring items were measured.

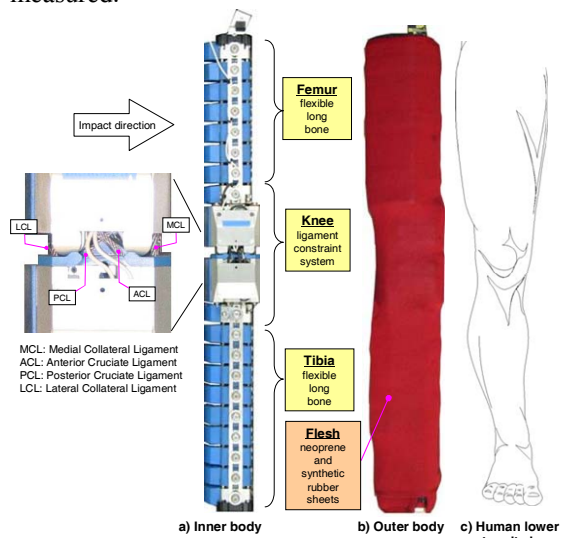


Figure 1. Flexible Pedestrian Legform Impactor type GTR prototype (Flex-GTR-prototype).

Flex-GTR-prototype (SN01, SN02, SN03)

Data Acquisition systems (DAS)

- SN01: Off-board DAS
- SN02: Can select On-board DAS (M=BUS) or Off-board DAS
- SN03: Can select On-board DAS (SLICE) or Off-board DAS

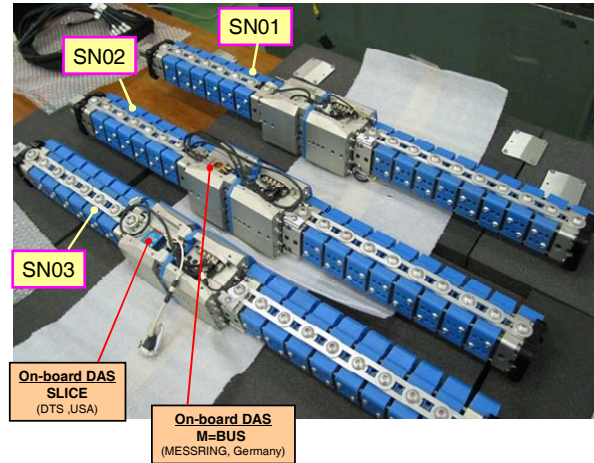


Figure 2. Flex-GTR-prototype (SN01, SN02, SN03) and Data Acquisition System (DAS).

On-board DAS (M=BUS) for SN02



On-board DAS (SLICE) for SN03

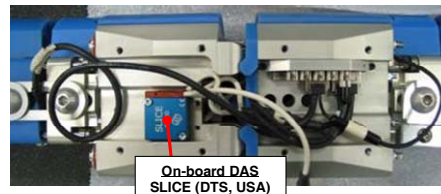


Figure 3. On-board Data Acquisition System (DAS) for the Flex-GTR-prototype (SN02 and SN03).

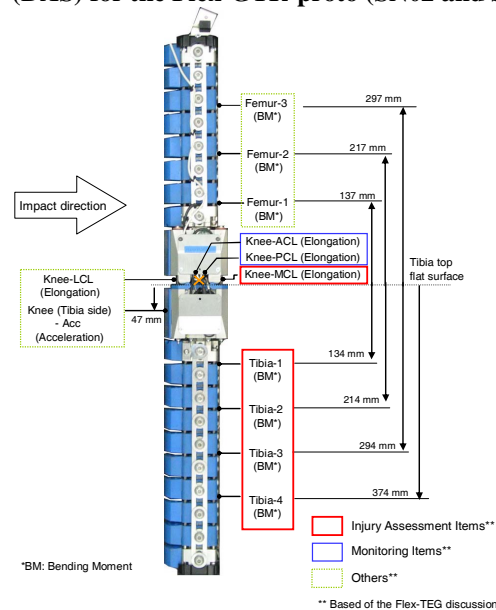


Figure 4. Flex-GTR-prototype Measurement Items.

Flexible Pedestrian Legform Impactor type GT (Flex-GT)

Figure 5 shows a general construction of the Flex-GT. Its construction is similar to the Flex-GTR-prot, however, knee ligaments arrangements are different. In the Flex-GTR-prot, the ACL (anterior cruciate ligament) and PCL (posterior cruciate ligament) are located on both sides of the knee, symmetry to the impact and longitudinal axes of the impactor [5]. On the other hand, in the Flex-GT, ACL and PCL are located on different sides of the knee, asymmetry to the impact and longitudinal axes of the impactor. The asymmetric knee ligament location of the Flex-GT tends to generate knee twist motion, therefore it tends to obtain different test results between symmetric left and right bumper corner impacts. As for the DAS of the Flex-GT, only an off-board DAS is available.

Figure 6 shows the measurement items of the Flex-GT. The measurement items are the same except the knee (tibia side) acceleration of the Flex-GTR-prot. In this research, we used the Flex-GT (SN03), and then measured injury assessment items and monitoring items mainly.

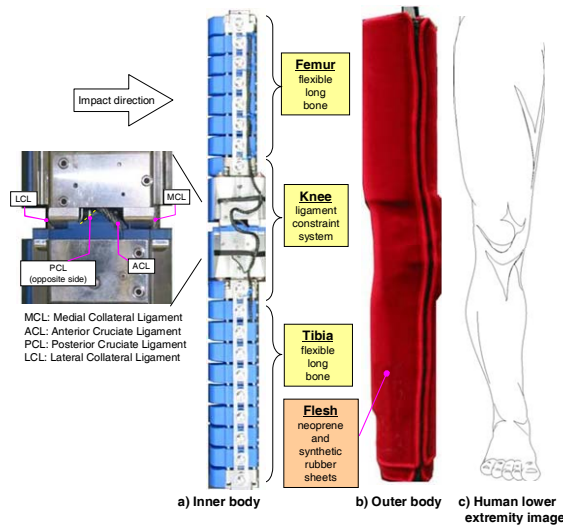


Figure 5. Flexible Pedestrian Legform Impactor type GT (Flex-GT).

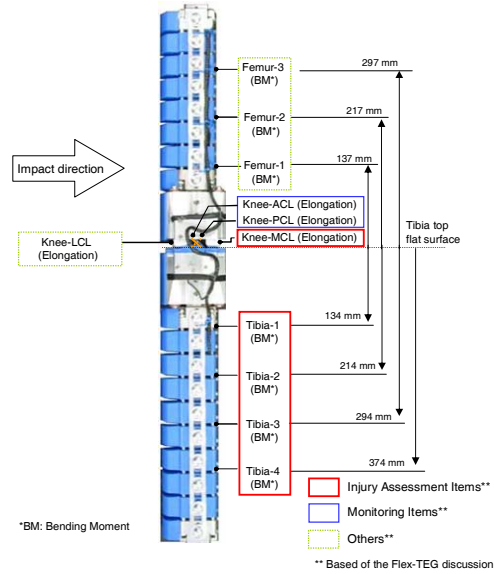


Figure 6. Flex-GT Measurement Items.

Assembly Pendulum Type Calibration Test Rigs

Type 1 – Figure 7 shows the assembly pendulum type calibration test rig (type 1). The rig was developed in order to calibrate the Flex-GT. However, the rig can accommodate not only the Flex-GT but also the Flex-GTR-prot. The test rig therefore was used for investigating E3: Comparability between the Flex-GT and Flex-GTR-prot in this research.



Figure 7. Assembly Pendulum Type Calibration Test Rig (Type 1).

Type 2 – Figure 8 shows the assembly pendulum type calibration test rigs (type 2). The rig was developed in order to calibrate of the Flex-GTR-prot. The rig can accommodate the Flex-GTR-prot only, therefore, the test rig was used for investigating E1: Repeatability and E2: Reproducibility of the Flex-GTR-prot.



Figure 8. Assembly Pendulum Type Calibration Test Rig (Type 2).

Simplified Cars

Type 1 – Figure 9 shows an over view of a simplified car (type 1). The car consisted of bonnet leading edge (BLE), bumper (BP), and spoiler (SP). Figure 10 shows its cross sectional dimensions at the center line of the car. The car was made from steel for automobile; therefore, the car was deformed after an impact test as shown in Figure 11.

This car was used for investigating E1: Repeatability and E2: Reproducibility of the Flex-GTR-proto and E3: Comparability between the Flex-GT and Flex-GTR-proto.

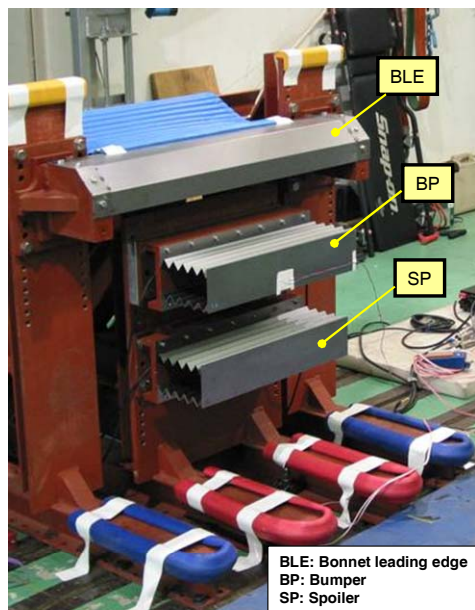


Figure 9. Simplified Car (Type 1).

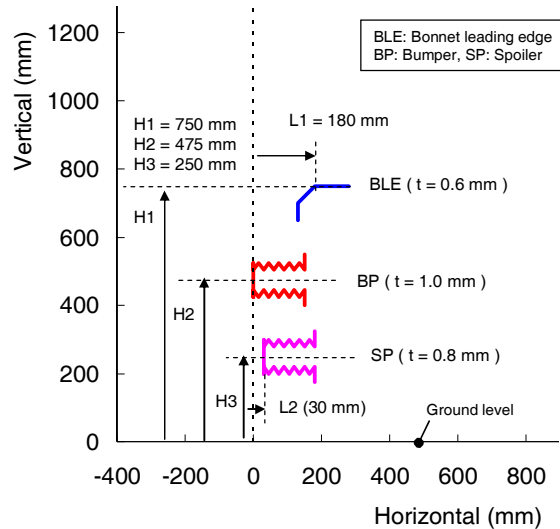


Figure 10. Cross Sectional Dimensions at the Car Center of the Simplified Car (Type 1).

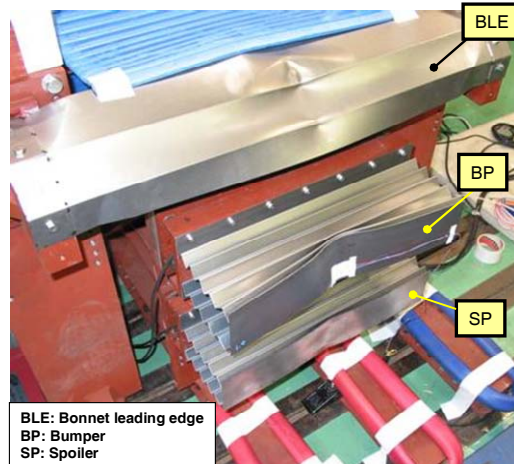


Figure 11. Deformation of the Simplified Car (Type 1) after an Impact Test.

Type 2, -R and -L – Figure 12 shows an over view of the simplified car (type 2, -R and -L). The car had the same configuration as that of the simplified car type 1, consisting of bonnet leading edge (BLE), bumper (BP), and spoiler (SP). Figure 13 shows its cross sectional dimensions at the center line of the car. The type 2 has two versions, -R and -L, by different setting of the car turned 30 degree right or left around the vertical axis, therefore both versions had exactly the same cross sectional dimensions at the car center. The type 2-R simulates right side of the bumper corner, and the type 2-L simulates left side of the bumper corner. The car was made from steel for automobile, which was also used for the simplified car type 1; therefore, the car is deformed after an impact test as shown in Figure 14.

These cars (Type 2, -R and -L) were used for investigating E4: Comparability of the Flex-GTR-proto under the symmetric right and left bumper corner impacts.

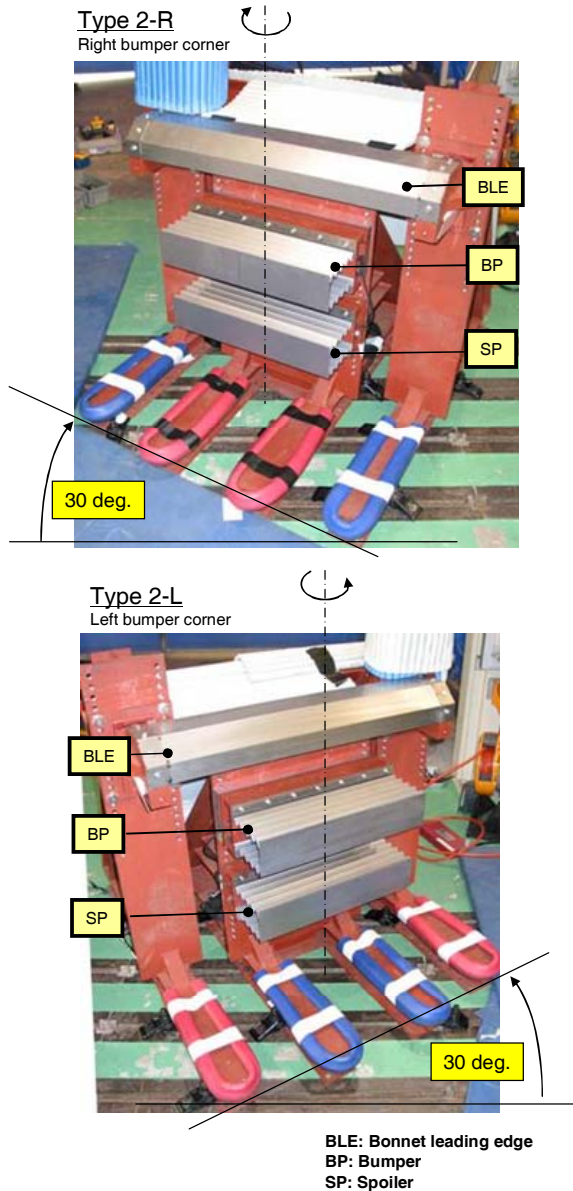


Figure 12. Simplified Car (Type 2, -L and -R).

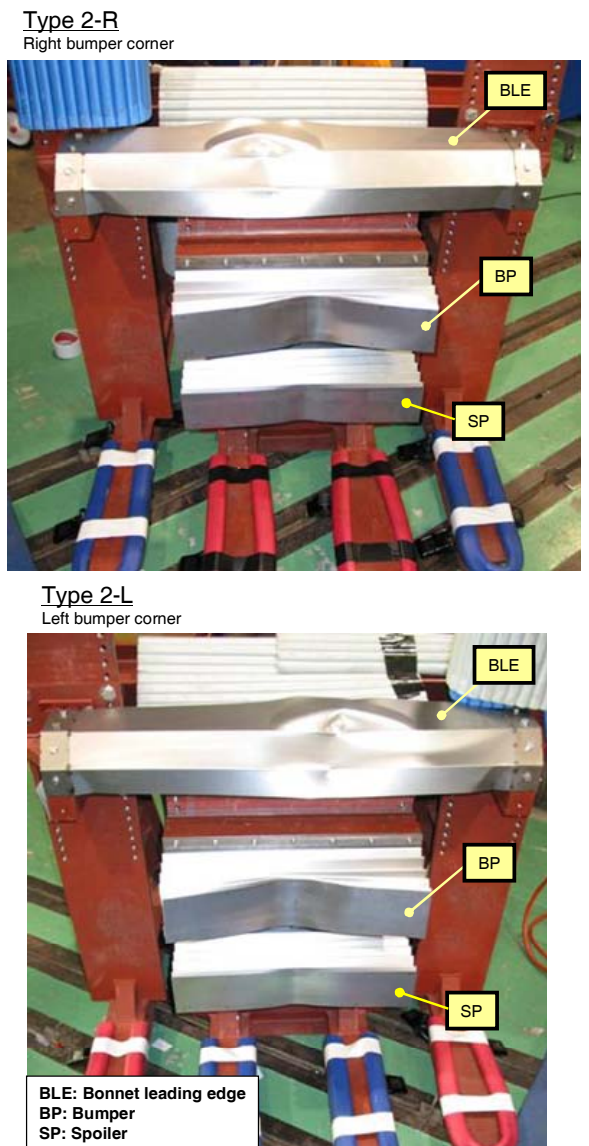


Figure 14. Deformation of the Simplified Car (Type 2, -R and -L) after an Impact Test.

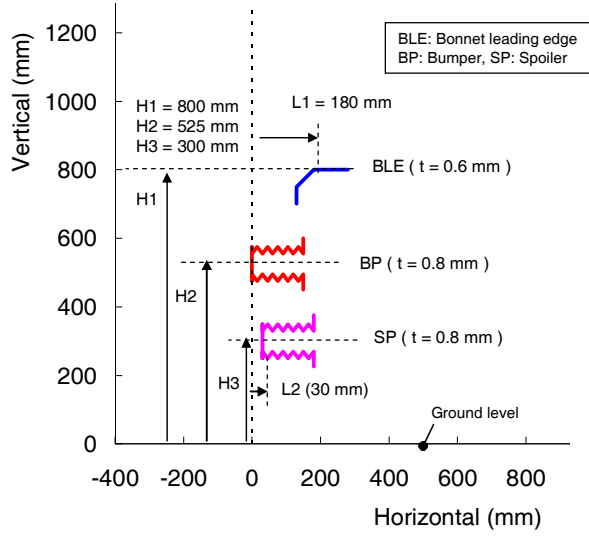


Figure 13. Cross Sectional Dimensions at the Car Center of the Simplified Car (Type 2).

METHODOLOGY

Assembly Pendulum Type Calibration Test Methods

Type 1 – Figure 15 shows the assembly pendulum type calibration test method (Type 1). In the test, the femur top of the Flex-GT or Flex-GTR-proto was attached to the assembly type calibration test rig (Type 1) via a pin joint, and then the tibia bottom was suspended at 15 degrees above the horizontal level. The legform was then released from the suspended position and then impacted the pad attached to the test rig. The same material as that of the flesh part of the Flex-GT and Flex-GTR-proto was used for the pad.

Assembly Pendulum type Calibration Test Method (Type 1)

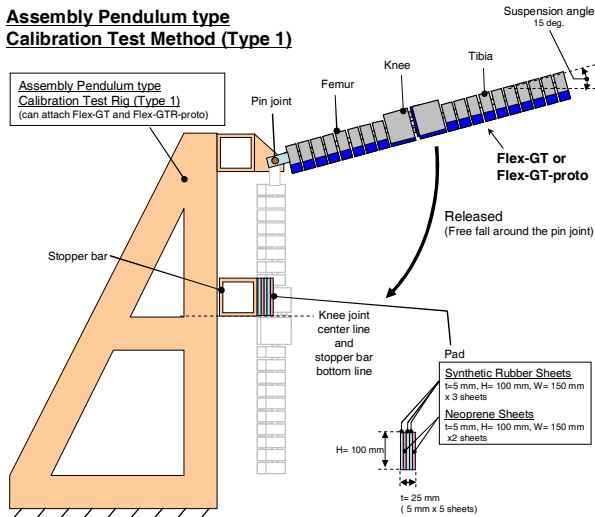


Figure 15. Assembly Pendulum type Calibration Test Method (Type 1).

Type 2 – Figure 16 shows the assembly pendulum type calibration test method (Type 2). In the test, the tibia bottom of the Flex-GTR-proto was attached to the assembly type calibration test rig (Type 2) via a pin joint, and then the top of the femur was suspended with a 5 kg additional mass at 15 degrees above the horizontal level. The legform was then released from the suspended position and then impacted the pad attached to the test rig. The same material as that of the flesh part of the Flex-GT and Flex-GTR-proto was used for the pad.

Assembly Pendulum type Calibration Test Method (Type 2)

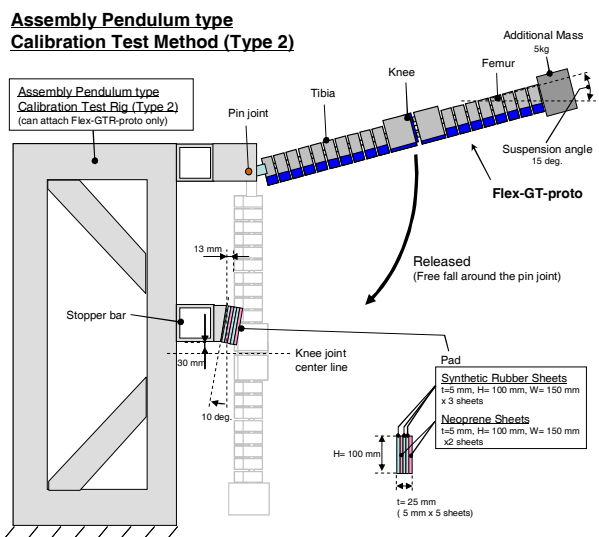


Figure 16. Assembly Pendulum type Calibration Test Method (Type 2).

Simplified Car Test Methods

Type 1 – Figure 17 shows the test method for the simplified car (Type 1). In the test, the Flex-GTR-proto or Flex-GT was propelled to the car under the free flight condition, and then impacted the center line position of the simplified car bumper at 11.1 m/s. The target impact height of the impactor was 75 mm above the ground level, and the target temperature and relative humidity of the test sight were 20 degree Celsius and 40 % respectively. The tolerance of each test condition was settled based on the current global technical regulation on the pedestrian safety (gr 9).

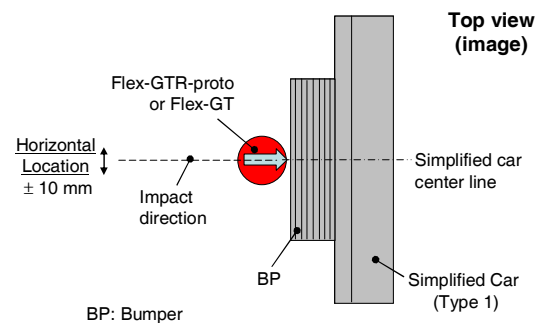
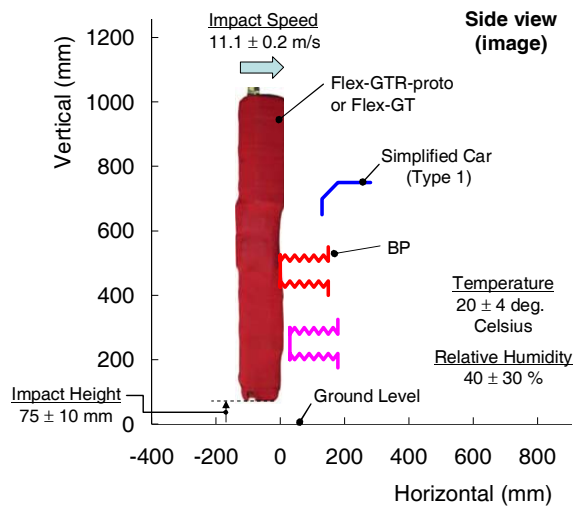


Figure 17. Simplified Car (Type 1) Test Method.

Type 2, -R and -L – Figure 18 shows the test method for the simplified car (Type 2, -R and -L). In the test, the Flex-GTR-proto was propelled to the car under the free flight condition, and then impacted the center line position of the simplified car bumper at 11.1 m/s. The target impact height of the impactor was 75 mm above the ground level, and the target temperature and relative humidity of the test sight were 20 degree Celsius and 40 % respectively. The tolerance of each test condition was settled based on the current global technical regulation on the pedestrian safety (gr 9).

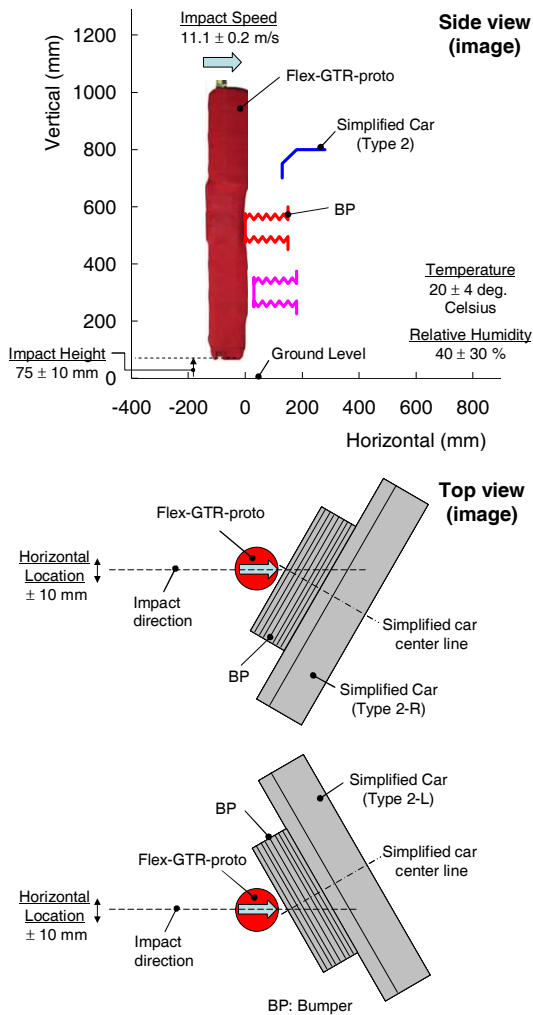


Figure 18. Simplified Car (Type 2, -R and -L) Test Method.

TEST MATRIXES

Assembly Pendulum Type Calibration Test Series

Table 1 shows the matrix for the assembly pendulum type calibration test series. In the test series, thirteen tests were conducted, and then the following items were evaluated; E1: Repeatability of the Flex-GTR-proto, E2: Reproducibility of the Flex-GTR-proto, and E3: Comparability between the Flex-GTR and Flex-GT.

Simplified Car Test Series

Table 2 shows the matrix for the simplified car test series. In the test series, eleven tests were conducted, and then the following items were evaluated; E1: Repeatability of the Flex-GTR-proto, E2: Reproducibility of the Flex-GTR-proto, E3: Comparability between the Flex-GTR and Flex-GT, and E4: Comparability of the Flex-GTR-proto under the symmetric right and left bumper corner impacts.

Table 1. Matrixes for the Assembly Pendulum Type Calibration Test Series.

Test ID	Impactor		DAS	Assembly Pendulum Type Calibration Test Method			
	Type	SN					
E1	P1	Flex-GTR-proto	SN01	Off-board	Type 2		
	P2						
	P3						
E2	P4		SN02	M-BUS		Type 1	
	P5						
	P6						
E1	P7		SN03	Off-board			Type 1
	P8						
	P9						
E3	P10	Flex-GTR-proto	SN01	Off-board	Type 1		
	P11		SN02	M-BUS			
	P12		SN03	SLICE			
	P13		Flex-GT	SN03		Off-board	

E1: Evaluation on the [Repeatability of the Flex-GTR-proto](#)
E2: Evaluation on the [Reproducibility of the Flex-GTR-proto](#)
E3: Evaluation on the [Comparability between the Flex-GT and the Flex-GTR-proto](#)

Table 2. Matrix for the Simplified Car Test Series.

Test ID	Impactor		DAS	Simplified Car Type	
	Type	SN			
E2	Flex-GTR-proto	SN01	Off-board	Type 1	
					SN02
		Off-board			
			SN03		
		Flex-GT			SN03
		E4	Flex-GTR-proto		SN03
Type 2-R					

E1: Evaluation on the [Repeatability of the Flex-GTR-proto](#)
E2: Evaluation on the [Reproducibility of the Flex-GTR-proto](#)
E3: Evaluation on the [Comparability between the Flex-GT and the Flex-GTR-proto](#)
E4: Evaluation on the [Comparability of the Flex-GTR-proto output under the symmetric right and left bumper corner impact](#)

TENTATIVE INJURY ASSESSMENT REFERENCE VALUES

Table 3 shows the tentative injury assessment reference values (t-IARV) in this research. These values were settled based on the proposal or discussion at the 7th Flex-TEG meeting [6-8].

The t-IARV values were used to evaluate standard deviation (St.Dev) levels of the maximum measurement values for injury assessment or monitoring items relative to the injury assessment levels by dividing St.Dev. by t-IARV (i.e. St.Dev/t-IARV).

Table 3. Tentative Injury Assessment Reference Values (t-IARV).

Injury Criteria	Purpose	Proposed/Discussed Injury Assessment Reference Values at the 7th Flex-TEG meeting			Tentative Injury Assessment Reference Values (t-IARV) in this research
		TEG-077	TEG-076	TEG-078	
Tibia BM*	Injury Assessment	318 (Nm)	-	-	318 (Nm)
Knee-MCL Elongation		-	23 (mm)	16, 20 (mm)	20 (mm)
Knee-ACL Elongation	Monitoring Only	-	-	12.7 (mm)	12.7 (mm)
Knee-PCL Elongation		-	-	12.7 (mm)	12.7 (mm)

* BM: Bending Moment

TEST CONDITIONS (TARGETS AND RESULTS)

Table 4 shows the test conditions for the simplified car test series. All of the impact conditions are within the targets, except for the horizontal location of the S1. However, the simplified car has a continuous similar shape in the horizontal direction, so the test results were used for our analysis.

As for the assembly pendulum type calibration test series, there were no concerns on the test conditions for the following reasons; 1) well air conditioned test sight is used, 2) not free freight test (well controlled pendulum test).

Table 4. Test Conditions for the Simplified Car Test Series (Targets and Results).

Test ID	Impact Speed (m/s)		Temperature (deg. Celsius)		Relative Humidity (%)	
	Targets	Results	Targets	Results	Targets	Results
S1	11.1 ± 0.2	11.1	20 ± 4	20.6	40 ± 30	40
S2		11.1		21.1		35
S3		11.2		20.5		40
S4		11.1		21.9		42
S5		11.1		21.4		34
S6		11.2		20.7		37
S7		11.1		20.4		48
S8		11.0		22.8		26
S9		11.1		22.2		30
S10		11.1		21.7		29
S11		11.1		22.8		32

Test ID	Impact Height (mm)		Horizontal Location (mm)	
	Targets	Results	Targets	Results*
S1	75 ± 10 above from the ground level	70	Simplified car center line ± 10	28
S2		73		-2
S3		72		-6
S4		71		0
S5		77		-2
S6		75		-10
S7		72		-2
S8		79		5
S9		78		-2
S10		77		-3
S11		80		0

* +: Right, -: Left (from driver's point of view)

TEST RESULTS

The test results are described by each evaluation item.

E1: Repeatability of the Flex-GTR-proto

Assembly Pendulum Type Calibration Test Series – Evaluation test results on the repeatability of the Flex-GTR-proto (SN01-SN03) in the assembly pendulum type calibration test series are shown in Figure 19 through Figure 21 and in Table 5 through Table 7. Each impactor shows repeatable waveforms. The Coefficient of Variation (CV) values with regard to the injury assessment or monitoring items are lower than 7.72% (SN03, Knee-PCL), with the majority of the CV values being less than 3%. When we see the standard deviation values related to the tentative injury assessment reference values (St.Dev./t-IARV), all of the values are lower than 4.52 % (SN03, Knee-ACL), and most of the values are less than 3 %.

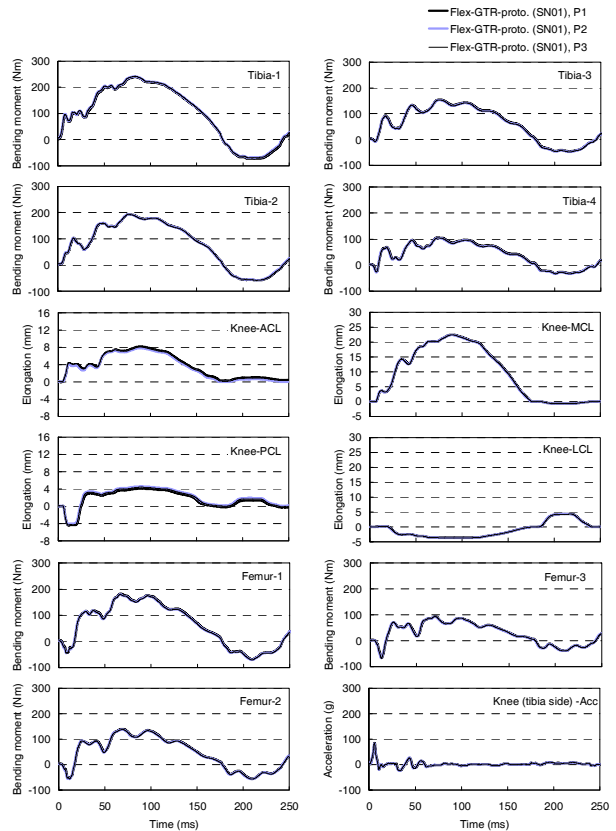


Figure 19. Waveforms (Test ID: P1-P3, Repeatability: Flex-GTR-proto (SN01)).

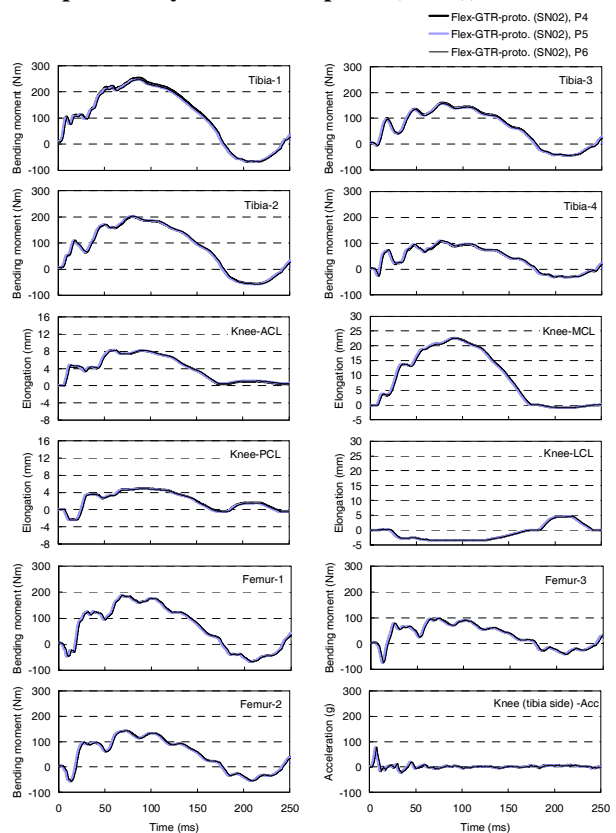


Figure 20. Waveforms (Test ID: P4-P6, Repeatability: Flex-GTR-proto (SN02)).

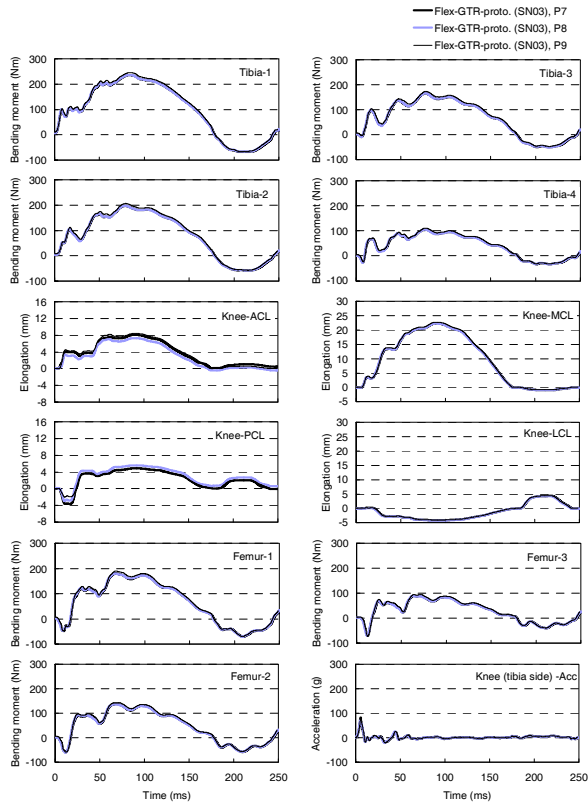


Figure 21. Waveforms (Test ID: P7-P9, Repeatability: Flex-GTR-proto (SN03)).

Table 5. Maximum Values and Variations (Test ID: P1-P3, Repeatability: Flex-GTR-proto (SN01)).

	Max. values**						
	Tibia-1 (Nm)	Tibia-2 (Nm)	Tibia-3 (Nm)	Tibia-4 (Nm)	Knee-ACL (mm)	Knee-PCL (mm)	Knee-MCL (mm)
Flex-GTR-proto. (SN01), P1	239.7	194.0	154.9	106.4	8.19	4.11	22.4
Flex-GTR-proto. (SN01), P2	241.2	193.6	152.8	104.1	7.65	4.62	22.3
Flex-GTR-proto. (SN01), P3	241.8	193.6	153.4	104.5	8.10	4.41	22.4
Avg.	240.9	193.7	153.7	105.0	8.05	4.38	22.4
St. Dev.	1.08	0.23	1.08	1.23	0.18	0.26	0.06
CV (%)	0.45	0.12	0.70	1.17	2.19	5.85	0.26
Judgement	Good	Good	Good	Good	Good	Acceptable	Good
t-IARV*	318	318	318	318	12.7	12.7	20
St.Dev./t-IARV (%)	0.34	0.07	0.34	0.39	1.39	2.02	0.29
Judgement	Good	Good	Good	Good	Good	Good	Good

* t-IARV: Tentative Injury Assessment Reference Values
 ** Injury assessment items and monitoring items were evaluated.



Table 6. Maximum Values and Variations (Test ID: P4-P6, Repeatability: Flex-GTR-proto (SN02)).

	Max. values**						
	Tibia-1 (Nm)	Tibia-2 (Nm)	Tibia-3 (Nm)	Tibia-4 (Nm)	Knee-ACL (mm)	Knee-PCL (mm)	Knee-MCL (mm)
Flex-GTR-proto. (SN02), P4	253.9	201.1	160.3	106.8	8.28	4.97	22.6
Flex-GTR-proto. (SN02), P5	247.4	203.1	157.4	110.0	8.24	4.90	22.5
Flex-GTR-proto. (SN02), P6	246.7	202.8	157.7	109.9	8.20	4.85	22.5
Avg.	249.3	202.3	158.5	108.9	8.24	4.91	22.5
St. Dev.	3.97	1.08	1.59	1.82	0.04	0.06	0.06
CV (%)	1.59	0.53	1.01	1.67	0.49	1.23	0.26
Judgement	Good	Good	Good	Good	Good	Good	Good
t-IARV*	318	318	318	318	12.7	12.7	20
St.Dev./t-IARV (%)	1.25	0.34	0.50	0.57	0.31	0.47	0.29
Judgement	Good	Good	Good	Good	Good	Good	Good

* t-IARV: Tentative Injury Assessment Reference Values
 ** Injury assessment items and monitoring items were evaluated.

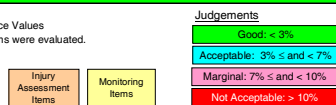


Table 7. Maximum Values and Variations (Test ID: P7-P9, Repeatability: Flex-GTR-proto (SN03)).

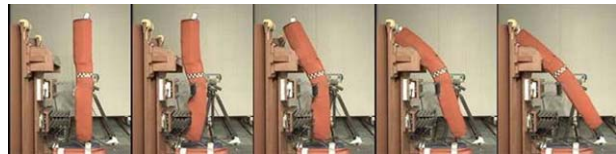
	Max. values**						
	Tibia-1 (Nm)	Tibia-2 (Nm)	Tibia-3 (Nm)	Tibia-4 (Nm)	Knee-ACL (mm)	Knee-PCL (mm)	Knee-MCL (mm)
Flex-GTR-proto. (SN03), P7	235.8	197.7	165.5	105.9	8.09	4.83	22.3
Flex-GTR-proto. (SN03), P8	236.0	198.5	166.3	105.6	7.31	5.57	22.3
Flex-GTR-proto. (SN03), P9	245.1	206.9	173.4	110.8	8.43	4.96	22.7
Avg.	239.0	201.0	168.4	107.4	7.94	5.12	22.4
St. Dev.	5.31	5.10	4.35	2.92	0.57	0.40	0.23
CV (%)	2.22	2.54	2.58	2.72	7.23	7.72	1.03
Judgement	Good	Good	Good	Good	Marginal	Acceptable	Good
t-IARV*	318	318	318	318	12.7	12.7	20
St.Dev./t-IARV (%)	1.67	1.60	1.37	0.92	4.52	3.11	1.15
Judgement	Good	Good	Good	Good	Acceptable	Acceptable	Good

* t-IARV: Tentative Injury Assessment Reference Values
 ** Injury assessment items and monitoring items were evaluated.

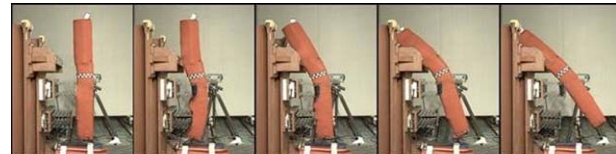


Simplified Car Test Series – Evaluation test results on the repeatability of the Flex-GTR-proto (SN02) in the simplified car test series are shown in Figure 22 through Figure 23 and in Table 8. The Flex-GTR-proto (SN02) shows repeatable kinematics and waveforms. The CV values with regard to the injury assessment or monitoring items are lower than 3.26% (SN02, Tibia-4), with the majority of the CV values being less than 3%. When we see the standard deviation values related to the tentative injury assessment reference levels (St.Dev./t-IARV), all of the values are lower than 1.8 % (SN02, Tibia-1).

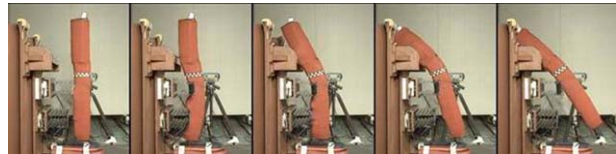
Flex-GTR-proto. (SN02), S2



Flex-GTR-proto. (SN02), S3



Flex-GTR-proto. (SN02), S4



Flex-GTR-proto. (SN02), S5

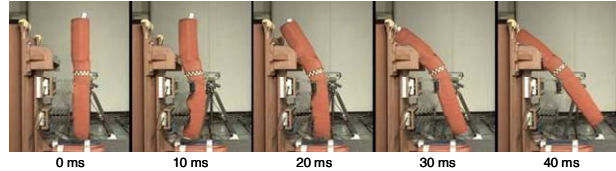


Figure 22. Kinematics (Test ID: S2-S5 Repeatability: Flex-GTR-proto (SN02)).

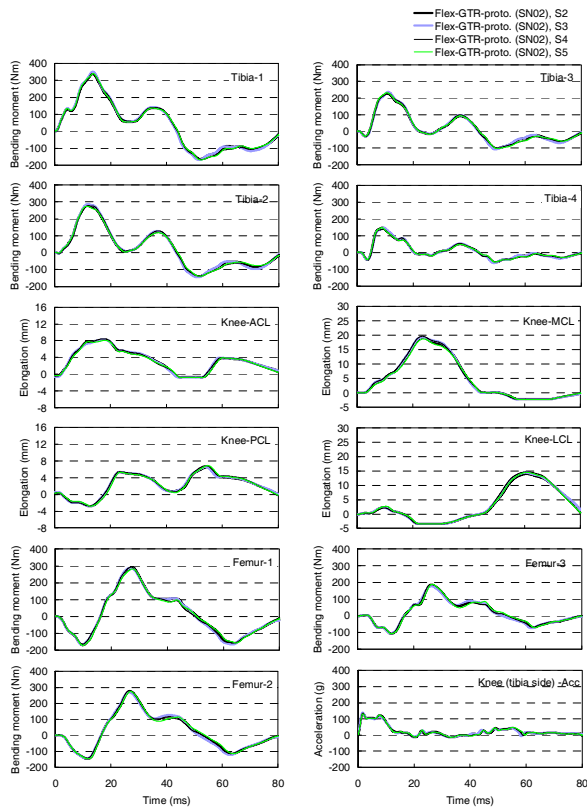
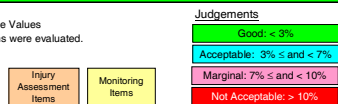


Figure 23. Waveforms (Test ID: S2-S5, Repeatability: Flex-GTR-proto (SN02)).

Table 8. Maximum Values and Variations (Test ID: S2-S5 Repeatability: Flex-GTR-proto (SN02)).

	Max. values**						
	Tibia-1 (Nm)	Tibia-2 (Nm)	Tibia-3 (Nm)	Tibia-4 (Nm)	Knee-ACL (mm)	Knee-PCL (mm)	Knee-MCL (mm)
Flex-GTR-proto. (SN02), S2	338.2	276.3	227.7	147.7	8.32	6.52	19.3
Flex-GTR-proto. (SN02), S3	350.6	285.5	236.5	148.5	8.28	6.61	19.3
Flex-GTR-proto. (SN02), S4	340.1	276.4	228.1	138.4	8.43	6.85	19.6
Flex-GTR-proto. (SN02), S5	339.4	273.5	231.6	147.3	8.08	6.90	18.8
Avg.	342.1	277.9	231.0	145.5	8.28	6.72	19.25
St. Dev.	5.74	5.23	4.08	4.74	0.15	0.18	0.33
CV (%)	1.68	1.88	1.77	3.26	1.77	2.74	1.72
Judgement	Good	Good	Good	Acceptable	Good	Good	Good
t-IARV*	318	318	318	318	12.7	12.7	20.0
St.Dev./t-IARV (%)	1.80	1.64	1.28	1.49	1.15	1.45	1.66
Judgement	Good	Good	Good	Good	Good	Good	Good

* t-IARV: Tentative Injury Assessment Reference Values
 ** Injury assessment items and monitoring items were evaluated.



E2: Reproducibility of the Flex-GTR-proto

Assembly Pendulum Type Calibration Test Series – Evaluation test results on the reproducibility of the Flex-GTR-proto (SN01-SN03) in the assembly pendulum type calibration test series are shown in Figure 24 and Table 9. Each impactor shows very similar waveforms. The Coefficient of Variation (CV) values with regard to the injury assessment or monitoring items are lower than 7.94% (SN01-SN03, Knee-PCL), with the majority of the CV values being less than 3%. When we see the standard deviation related to the tentative injury assessment reference levels (St.Dev./t-IARV), all of the values are lower than 3.0 % (SN03, Knee-PCL), and most of the

values are less than 3 %.

Simplified Car Test Series – Evaluation test results on the reproducibility of the Flex-GTR-proto (SN02) in the simplified car test series are shown in Figure 25 through Figure 26 and in Table 10. The Flex-GTR-proto (SN01-SN03) shows comparable kinematics and waveforms. The CV values with regard to the injury assessment or monitoring items are lower than 6.68% (SN01-SN03, Tibia-4), with the majority of the CV values being less than 4%. When we see the standard deviation values related to the tentative injury assessment reference levels (St.Dev./t-IARV), all of the values are lower than 4.12 % (SN01-SN03, Tibia-3).

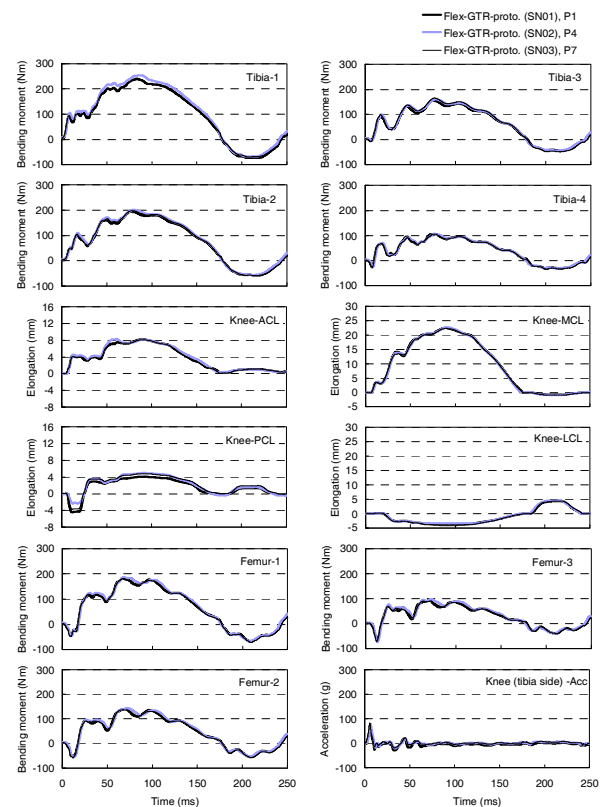


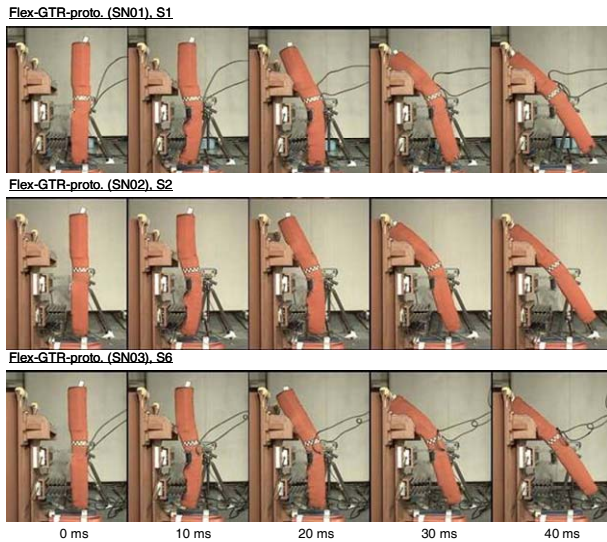
Figure 24. Waveforms (Test ID: P1, P4, P7 Reproducibility: Flex-GTR-proto (SN01-SN03)).

Table 9. Maximum Values and Variations (Data: Avg. of SN01 (P1-P3), S02 (P4-P6), S03 (P7-P9), Reproducibility: Flex-GTR-proto (SN01-SN03)).

	Max. values**						
	Tibia-1 (Nm)	Tibia-2 (Nm)	Tibia-3 (Nm)	Tibia-4 (Nm)	Knee-ACL (mm)	Knee-PCL (mm)	Knee-MCL (mm)
Flex-GTR-proto (SN01), Avg.***	240.9	193.7	153.7	105.0	8.05	4.38	22.4
Flex-GTR-proto (SN02), Avg.***	249.3	202.3	158.5	108.9	8.24	4.91	22.5
Flex-GTR-proto (SN03), Avg.***	239.0	201.0	168.4	107.4	7.94	5.12	22.4
Avg.	243.1	199.0	160.2	107.1	8.08	4.80	22.4
St. Dev.	5.48	4.64	7.50	1.97	0.15	0.38	0.06
CV (%)	2.26	2.33	4.68	1.84	1.88	7.94	0.26
Judgement	Good	Good	Acceptable	Good	Good	Marginal	Good
t-IARV*	318	318	318	318	12.7	12.7	20
St.Dev./t-IARV (%)	1.72	1.46	2.36	0.62	1.20	3.00	0.29
Judgement	Good	Good	Good	Good	Good	Acceptable	Good

* t-IARV: Tentative Injury Assessment Reference Values
 ** Injury assessment items and monitoring items were evaluated.
 *** Flex-GTR-proto (SN01), Avg.: Average data of P1-P3
 Flex-GTR-proto (SN02), Avg.: Average data of P4-P6
 Flex-GTR-proto (SN03), Avg.: Average data of P7-P9





**Figure 25. Kinematics (Test ID: S1, S2, S6
Reproducibility: Flex-GTR-PROTO (SN01-SN03)).**

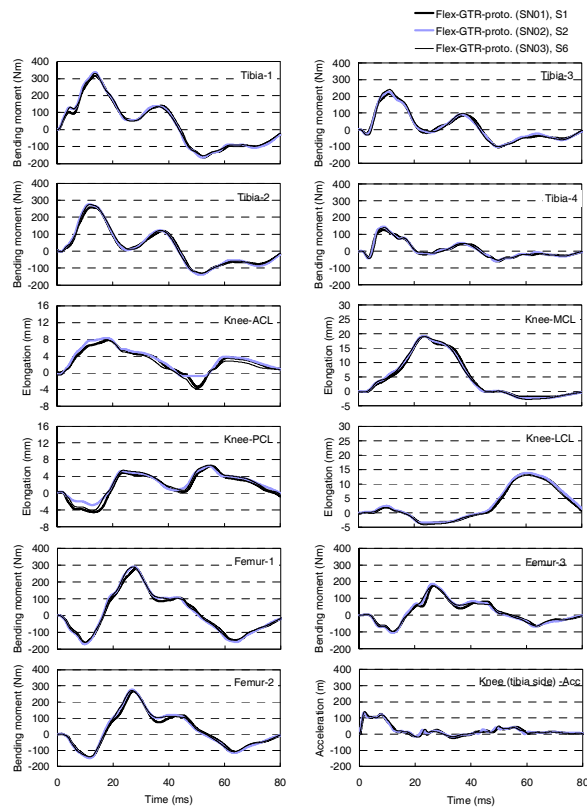


**Figure 26. Waveforms (Test ID: S1, S2, S6
Reproducibility: Flex-GTR-PROTO (SN01-SN03)).**

Table 10. Maximum Values and Its variations (Data: S1, Avg. of SN02 (S2-S5), S6, Reproducibility: Flex-GTR-PROTO (SN01, SN02, SN03)).

	Max. values**						
	Tibia-1 (Nm)	Tibia-2 (Nm)	Tibia-3 (Nm)	Tibia-4 (Nm)	Knee-ACL (mm)	Knee-PCL (mm)	Knee-MCL (mm)
Flex-GTR-PROTO (SN01), S1	317.2	258.5	214.7	127.7	7.81	6.54	19.2
Flex-GTR-PROTO (SN02), Avg.***	342.1	277.9	231.0	145.5	8.28	6.72	19.3
Flex-GTR-PROTO (SN03), S6	330.9	275.6	240.6	140.8	7.80	6.71	19.1
Avg.	330.1	270.7	228.8	138.0	7.96	6.66	19.2
St. Dev.	12.47	10.60	13.09	9.22	0.27	0.10	0.10
CV (%)	3.78	3.92	5.72	6.68	3.44	1.52	0.52
Judgement	Acceptable	Acceptable	Acceptable	Acceptable	Acceptable	Good	Good
TIARV*	318	318	318	318	12.7	12.7	20
St.Dev./TIARV (%)	3.92	3.33	4.12	2.90	2.16	0.80	0.50
Judgement	Acceptable	Acceptable	Acceptable	Good	Good	Good	Good

* TIARV: Tentative Injury Assessment Reference Values
 ** Injury assessment items and monitoring items were evaluated.
 *** Flex-GTR-PROTO (SN02), Avg.: Average data of S2-S5



E3: Comparability between the Flex-GT and Flex-GTR-PROTO

Assembly Pendulum Type Calibration Test Series – Evaluation test results on the comparability between the Flex-GT and the Flex-GTR-PROTO in the assembly pendulum type calibration test series are shown in Figure 27 and Figure 28. Several measurement values of the Flex-GTR-PROTO are slightly higher than the Flex-GT (SN03), however, most of the Flex-GTR-PROTO outputs are within the Flex-GT corridor [9], which is tentatively settled to calibrate the Flex-GT by using the assembly pendulum type calibration test method (Type 1).

The average ratio of the measurement values of the Flex-GTR-PROTO to the Flex-GT corridor (center) are shown in Figure 29. All of the average ratios are lower than 1.36 (Knee-PCL, Avg.), and most of the average ratios are less than 1.1.

Simplified Car Test Series – Evaluation test results on the comparability between the Flex-GT and the Flex-GTR-PROTO in the simplified car test series are shown in Figure 30 through Figure 32. Several measurement values of the Flex-GTR-PROTO are slightly higher than the Flex-GT (SN03).

The average ratio of the measurement values of the Flex-GTR-PROTO to the Flex-GT (SN03) are shown in Figure 33. All of the average ratios are lower than 1.16 (Femur-3, Avg.), and most of the average ratios are less than 1.1.

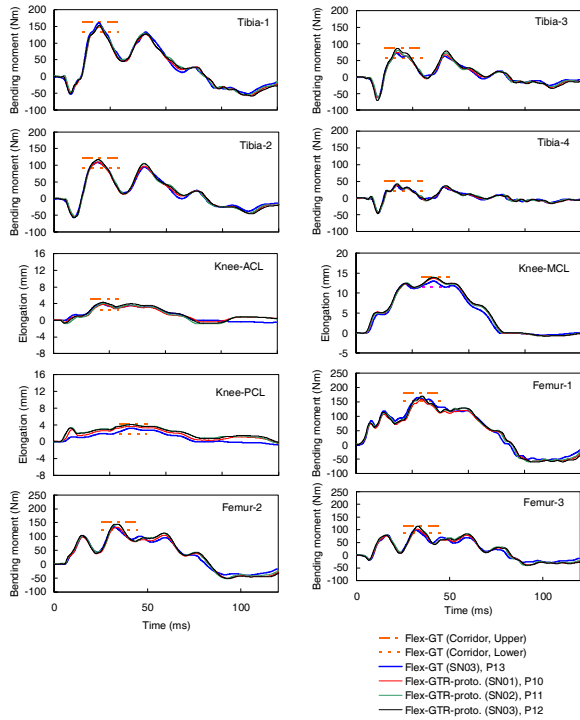


Figure 27. Waveforms with Flex-GT Corridor (Test ID: P13, P10-P12, Comparability: Flex-GT and Flex-GTR-proto).

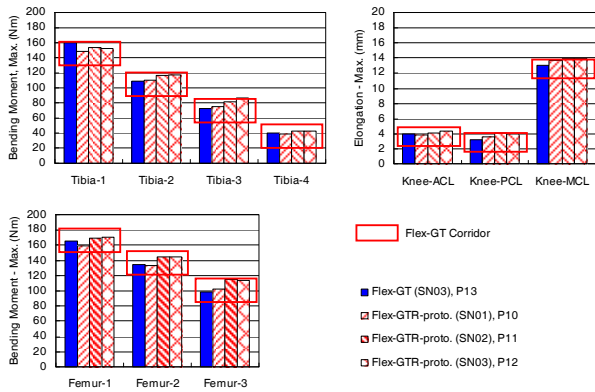


Figure 28. Maximum Values with Flex-GT Corridor (Test ID: P13, P10-P12, Comparability: Flex-GT and Flex-GTR-proto).

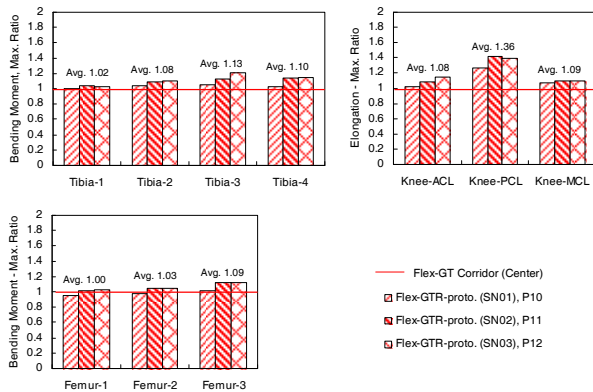


Figure 29. Maximum Value Ratio to the Flex-GT Center Corridor (Test ID: P10-P12, Comparability: Flex-GT and Flex-GTR-proto).

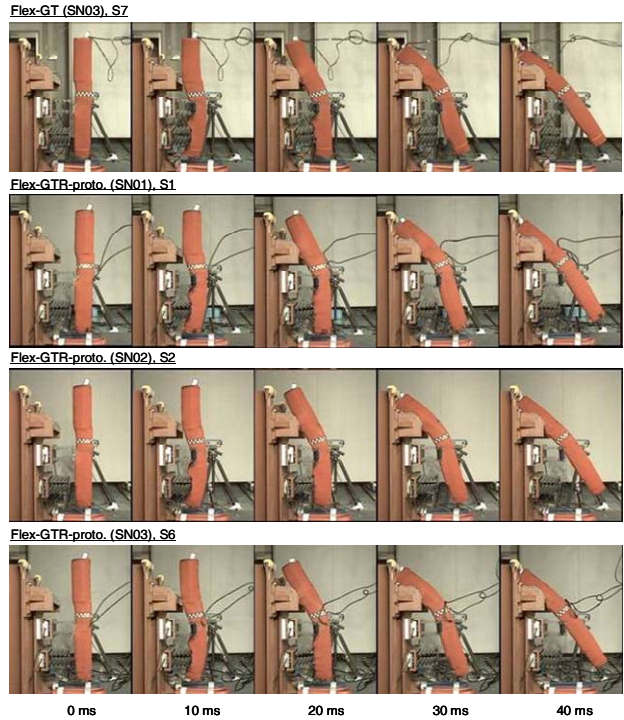


Figure 30. Kinematics (Test ID: S7, S1, S2, S6, Comparability: Flex-GT and Flex-GTR-proto).

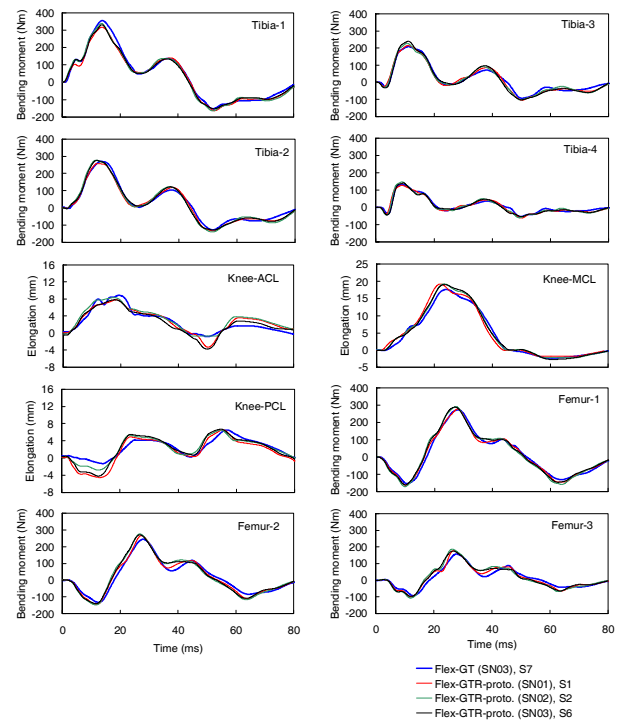


Figure 31. Waveforms (Test ID: S7, S1, S2, S6, Comparability: Flex-GT and Flex-GTR-proto).

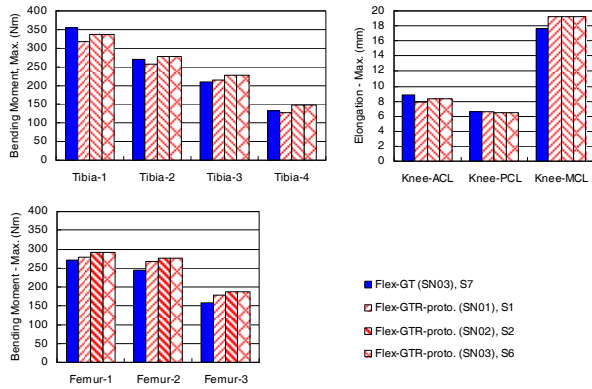


Figure 32. Maximum Values (Test ID: S7, S1, S2, S6, Comparability: Flex-GT and Flex-GTR-proto).

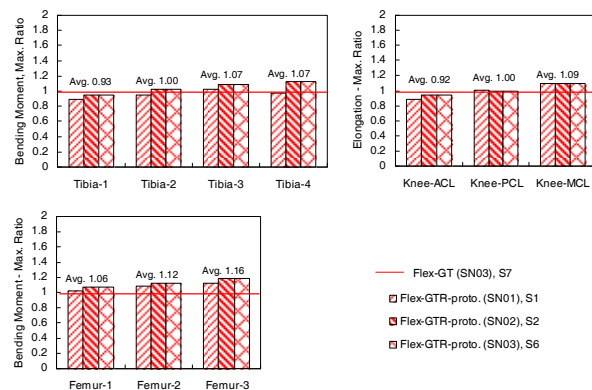


Figure 33. Maximum Value Ratio to the Flex-GT (SN03) (Test ID: S7, S1, S2, S6, Comparability: Flex-GT and Flex-GTR-proto).

E4: Comparability of the Flex-GTR-prototype output under the symmetric right and left bumper corner impacts

Evaluation test results on the comparability of the Flex-GTR-proto (SN03) output under the symmetric right and left bumper corner impacts are shown in Figure 34, Figure 35, and Table 11. The Flex-GTR-proto shows comparable kinematics and waveforms under the symmetric right and left bumper corner impacts. The Coefficient of Variation (CV) values with regard to the injury assessment or monitoring items are lower than 4.94% (Knee-PCL), with the majority of the CV values being less than 3%. When we see the standard deviation values to the tentative injury assessment reference values (St.Dev./t-IARV), all of the values are lower than 2.98 % (Knee-PCL).

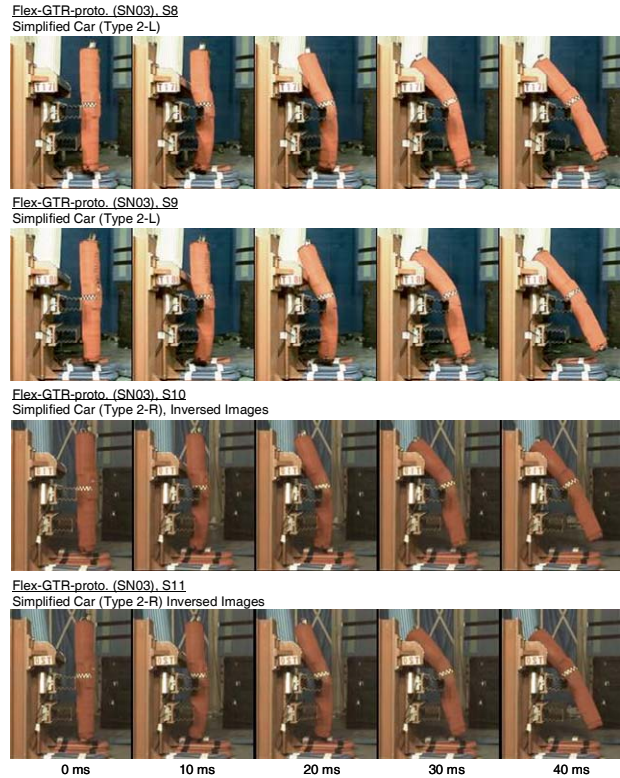


Figure 34. Kinematics (Test ID: S8-S11, Comparability: Flex-GTR-proto output under Symmetric Right and Left Bumper Corner Impact).

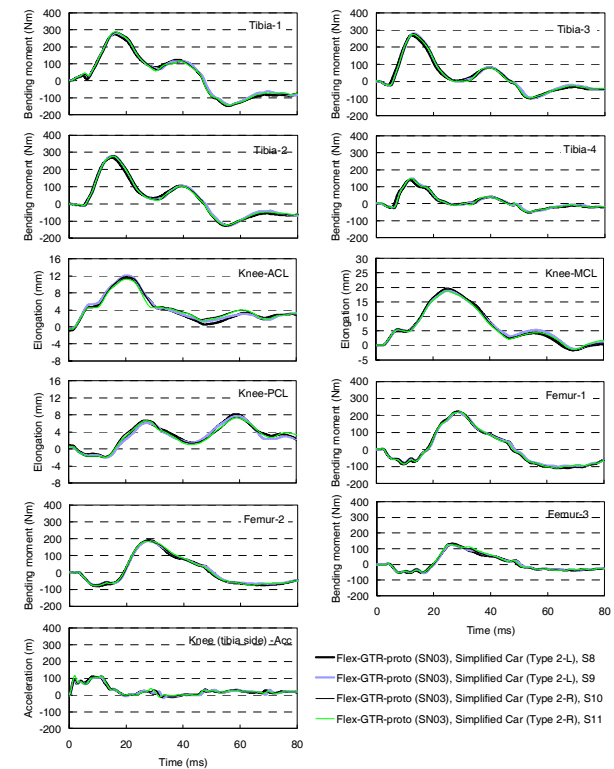


Figure 35. Waveforms (Test ID: S8-S11, Comparability: Flex-GTR-proto output under Symmetric Right and Left Bumper Corner Impact).

Table 11. Maximum Values and Variations (Test ID: S8-S11, Comparability: Flex-GTR-proto output under Symmetric Right and Left Bumper Corner Impact).

	Max. values**						
	Tibia-1 (Nm)	Tibia-2 (Nm)	Tibia-3 (Nm)	Tibia-4 (Nm)	Knee-ACL (mm)	Knee-PCL (mm)	Knee-MCL (mm)
Flex-GTR-prot. (SN03), S8	273.7	269.6	269.6	139.5	11.61	6.16	19.3
Flex-GTR-prot. (SN03), S9	282.1	280.0	281.1	149.2	12.11	7.72	18.8
Flex-GTR-prot. (SN03), S10	285.6	281.5	278.7	146.5	11.81	7.38	19.8
Flex-GTR-prot. (SN03), S11	285.6	281.5	278.7	146.5	11.81	7.38	19.8
Avg.	281.8	278.2	277.1	145.4	11.84	7.67	19.43
St. Dev.	5.61	5.74	4.98	4.15	0.21	0.38	0.48
CV (%)	1.99	2.06	1.80	2.85	1.74	4.94	2.46
Judgement	Good	Good	Good	Good	Good	Acceptable	Good
t-IARV*	318	318	318	318	12.7	12.7	20.0
St.Dev./t-IARV (%)	1.77	1.81	1.57	1.31	1.62	2.98	2.39
Judgement	Good	Good	Good	Good	Good	Good	Good

* t-IARV: Tentative Injury Assessment Reference Values

** Injury assessment items and monitoring items were evaluated.



DISCUSSIONS

In this research the following items were evaluated.

- E1: Repeatability of the Flex-GTR-proto
- E2: Reproducibility of the Flex-GTR-proto
- E3: Comparability between the Flex-GT and Flex-GTR-proto
- E4: Comparability of the Flex-GTR-proto output under the symmetric right and left bumper corner impacts

The evaluation results of each item are discussed below.

E1: Repeatability of the Flex-GTR-proto

Technical evaluations on the repeatability of the Flex-GTR-proto were conducted in the assembly pendulum type calibration test series as well as in the simplified car test series. As a result, the Coefficient of Variation (CV) values with regard to the injury assessment or monitoring items are lower than 7.72% (SN03, Knee-PCL, Assembly pendulum type test series), with the majority of the CV values being less than 3%. When we see the standard deviation values to the tentative injury assessment reference values (St.Dev./t-IARV), all of the values are lower than 4.52 % (SN03, Knee-ACL, Assembly pendulum type test series), with the majority of the values being less than 3 %.

The acceptance level of the CV values for a regulatory tool is less than 10% based on a BASt proposal [10]; therefore, the test results show fairly good repeatability of the Flex-GTR-proto relative to the proposed acceptance level.

E2: Reproducibility of the Flex-GTR-proto

Technical evaluations on the reproducibility of the Flex-GTR-proto were conducted in the assembly pendulum type calibration test series as well as in the simplified car test series. As a result, the Coefficient of Variation (CV) values with regard to the injury

assessment or monitoring items are lower than 7.94% (SN03, Knee-PCL, Assembly pendulum type test series), with the majority of the CV values being less than 3%. When we see the standard deviation values to the tentative injury assessment reference values (St.Dev./t-IARV), all of the values are lower than 4.12 % (Tibia-3, Simplified car test series), and most of the values are less than 3 %.

The results of the CV value evaluations show fairly good reproducibility of the Flex-GTR-proto relative to the proposed acceptance level.

E3: Comparability between the Flex-GT and Flex-GTR-proto

Technical evaluations on the comparability between the Flex-GT and Flex-GTR-proto were conducted in the assembly pendulum type calibration test series as well as in the simplified car test series. As a result, the maximum measurement values of the Flex-GTR-proto are slightly higher than the Flex-GT in general. The ratios of the maximum measurement values of the Flex-GTR-proto to the Flex-GT are lower than 1.36 (Knee-PCL, Avg., Assembly pendulum type test series), and the majority of the ratios are less than 1.1.

In particular, the difference of the Knee-PCL output under the assembly pendulum type test series, 1.36, is larger than the differences of the other outputs. This is because the absolute Knee-PCL output during the test is very small, 4 mm or less, therefore, even a very small difference of 1 mm or less (the differences are within the Flex-GT corridor, besides its t-IARV is 12.7 mm, i.e. relative difference to the t-IARV is very small), appears exaggerated when expressed in ratio.

E4: Comparability of the Flex-GTR-proto output under the symmetric right and left bumper corner impacts

Technical evaluations on the comparability of the Flex-GTR-proto output under the symmetric right and left bumper corner impacts were conducted in the simplified car test series. As a result, the Coefficient of Variation (CV) values with regard to the injury assessment or monitoring items are lower than 4.94% (Knee-PCL), and the majority of the CV values is less than 3%. When we see the standard deviation values to the tentative injury assessment reference values (St.Dev./t-IARV), all of the values are lower than 2.98 % (Knee-PCL).

The results of the CV value evaluations show fairly good comparability of the Flex-GTR-proto output under the symmetric right and left bumper corner impacts relative to the proposed acceptance level.

Overall

Technical evaluations on the Flex-GTR-PROTO were conducted in this research. As a result, fairly good evaluation results were obtained. The results were led by the improvement of the knee construction from an asymmetric construction of the Flex-GT to symmetric construction of the Flex-GTR-PROTO. The symmetric construction prevents the knee twist motion around the longitudinal axis of the impactor, which leads to stable outputs and a comparable output at the symmetric right and left bumper corners. Additionally, from the Flex-GTR-PROTO version, FTSS, a company specialized in manufacturing crash dummies, joined the development to assure that the Flex-GTR is produced under high quality control conditions.

The difference between the Flex-GT and Flex-GTR-PROTO outputs may alter appropriate threshold values for each injury criterion; therefore a following research has been investigating the threshold values for the Flex-GTR-PROTO using ratios of the Flex-GT and Flex-GTR-PROTO outputs in this study, and/or using the correlation between the Flex-GTR-PROTO and human lower extremities which can be obtained from a computer simulation analysis.

CONCLUSIONS

In this research, the following items were evaluated.

- Repeatability of the Flex-GTR-PROTO
- Reproducibility of the Flex-GTR-PROTO
- Comparability between the Flex-GT and Flex-GTR-PROTO
- Comparability of the Flex-GTR-PROTO output under the symmetric right and left bumper corner impacts

As a result, fairly good repeatability and reproducibility of Flex-GTR-PROTO, and comparability of the Flex-GTR-PROTO output under the symmetric right and left bumper corner impacts were observed (majorities of CV values are less than 3%).

As for the comparability between the Flex-GT and Flex-GTR-PROTO, some differences were observed between them. Most of the maximum value ratios of the Flex-GTR-PROTO relative to the Flex-GT are less than 1.1.

The difference between the Flex-GT and Flex-GTR-PROTO has a chance to affect the injury threshold values; therefore, a following research has been investigating the threshold values for the Flex-GTR-PROTO using the ratios of the Flex-GT and Flex-GTR-PROTO outputs and/or using the correlations between the Flex-GTR-PROTO and human lower

extremities which can be obtained from a computer simulation analysis.

The Flex-TEG members have been conducting further technical evaluation after our initial technical evaluations. The results are going to be put together and used for the Flex-GTR finalization.

REFERENCES

- [1] European Enhanced Vehicle-safety Committee: EEVC Working Group 17 report, 1998. "Improved test methods to evaluate pedestrian protection afforded by passenger cars".
- [2] Konosu A. and Tanahashi M. 2003. "Development of a biofidelic pedestrian legform impactor: Introduction of JAMA-JARI legform impactor ver. 2002.", Proc. 18th ESV, Paper No. 378.
- [3] Konosu A. and Tanahashi M. 2005. "Development of a Biofidelic Flexible Pedestrian Leg-form Impactor (Flex-PLI 2004) and Evaluation of its Biofidelity at the Component Level and at the Assembly Level", SAE paper No. 2005-01-1879.
- [4] UN/ECE/WP29/GRSP/INF-GR-PS/Flex-TEG 2008. "First Technology Safety Systems Design Freeze Status FLEX PLI GTR Development Mechanical Design", TEG-054-Rev.1.
- [5] Been B., Burleigh M. et. al. 2009. "Development of a Biofidelic Flexible Pedestrian Legform Impactor Type GTR prototype, Part 2: Technical Details", Proc. 21th ESV, Paper No. 09-0145.
- [6] UN/ECE/WP29/GRSP/INF-GR-PS/Flex-TEG 2008. "Injury Threshold for the Flex-PLI Medial Collateral Ligament (MCL), JAMA proposal", TEG-076.
- [7] UN/ECE/WP29/GRSP/INF-GR-PS/Flex-TEG 2008. "Injury Threshold for the Flex-PLI Tibia Bending Moment, JAMA proposal", TEG-077.
- [8] UN/ECE/WP29/GRSP/INF-GR-PS/Flex-TEG 2008. "Flex-GTR: Open questions and proposals for ACL, PCL and MCL injury thresholds, BAST", TEG-078.
- [9] UN/ECE/WP29/GRSP/INF-GR-PS/Flex-TEG 2006. "Information on the Flexible Pedestrian Legform Impactor GT Alpha (Flex-GT α)", TEG-021.
- [10] UN/ECE/WP29/GRSP/INF-GR-PS/Flex-TEG 2008. "Dynamic full assembly certification test procedure (inverse test setup) in conjunction with functional test, BAST and BGS", TEG-075.

THE SCATTER OF PEDESTRIAN UPPER-LEG IMPACTOR

Christian Pinecki,
Céline Adalian,
Richard Zeitouni
PSA Peugeot Citroën
France
Paulin Kazumba,
UTAC
France
Paper number 09-0262

ABSTRACT

The pedestrian protection given by a vehicle is assessed according to four independent impact test procedures, related to different body segments. Four impactors were developed specifically: leg, femur (or upper-leg), child head and adult head. These impactors, which are thrown against specific zones of the front face of the vehicle, allow the measurements of biomechanical criteria simulating the injury risk during the impact. Such test procedures are used by Euro NCAP and by the European regulation on pedestrian protection.

Concerning the upper-leg impactor, two biomechanical criteria are analysed: the sum of force and the three femur bending moments. A specific study has been carried out on the scatter of upper-leg tests by PSA Peugeot Citroën in cooperation with UTAC in order to assess the scatter of this set of biomechanical criteria in different laboratories.

In order to reduce the number of parameters of scatter and to isolate those linked to the upper-leg impactor, these tests have not been made on a full vehicle but on a simplified sub-system which permits to obtain biomechanical criteria very close to those obtained with a complete vehicle.

Tests conditions of the upper-leg impactor (weight and speed) vary in protocols (Euro NCAP as well as regulation) according to the vehicle style. About forty tests have been carried-out in each laboratory according to two different impact energies and with two different upper-leg impactors.

Results of those tests have enabled us to better understand and to quantify the scatter of the upper-leg impactor and to improve the design of our vehicles for the pedestrian protection.

INTRODUCTION - AIM OF THE STUDY

Every year, approximately 8,000 pedestrians and cyclists are killed and 300,000 others injured in road accidents in Europe. The accidents are particularly frequent in urban zones. Even when cars are driving at relatively reduced speeds, very severe injuries can occur.

Below a speed of approximately 40 km/h, it is nevertheless possible to considerably reduce the gravity of injury with modifications of the frontal parts of vehicles

So, since 2005, a new European Directive [1] (called “phase 1”) requires the car manufacturers to treat their new vehicles for pedestrian protection.

Moreover, the consumerist organization Euro NCAP assesses the pedestrian protection offered by a new car through component tests [2], [3]. The level of pedestrian protection is then ranked by attributing the vehicle a given number of stars.

The assessment of pedestrian protection offered by a vehicle is made through three different and independent component test procedures corresponding to different body segments:

- the first one is related to the assessment of the protection of the leg. The test is called “legform to bumper test”
- the second one is related to the upper leg. The test is called “upper legform to bonnet leading edge”
- the last one is related to the head, adult head impact and child head impact. The tests are called “Adult and Child headforms to bonnet and windscreen test”

Four specific body form impactors are used in these tests. They are propelled against the front part of the vehicle (from the bumper up to the windscreen depending on the type of test) and they are equipped with several sensors in order to measure biomechanical criteria that are used to assess the risk of injuries (see Figure 1).

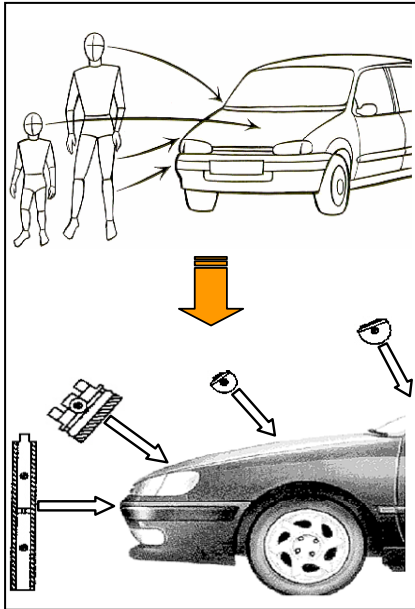


Figure 1. Euro NCAP Pedestrian tests made of body form impactors propelled against the car front-end.

The leg and head impactors have already been discussed in a previous paper [4].

The upper leg impactor requirements are only present in the Euro NCAP assessment (a maximum of 6 points is given to the upper leg test performance). Whereas, the European Directive only asks the upper leg tests to be carried out for monitoring purpose. The reason is that this test has not been proved to be relevant to real world pedestrian accident and because the results of this test are highly scattered.

Because of the increasing requirements on the pedestrian protection performance in the Euro NCAP new rating (overall rating), predicting the performance of upper leg tests becomes more and more sensible.

This paper aims to assess the scattering measured on the upper leg impactor tests.

THE UPPER LEG IMPACTOR TEST PROTOCOL

Euro NCAP Test Protocol [2]

The upper leg impactor aims to represent the adult femur. It is made of a rigid frame on which a metallic tube (the femur) is fixed. This tube is surrounded by a specific foam which behaviour represents the muscles and the skin. The link between the rigid frame and the femur is made of two load cells. Three extensometric gages are present in the central part

The upper leg impactor tests consist in propelling the femur impactor against the front part of the car (hood). The impact test parameters (angle, velocity and mass) depend on the geometry of the car front (see Figure 2).

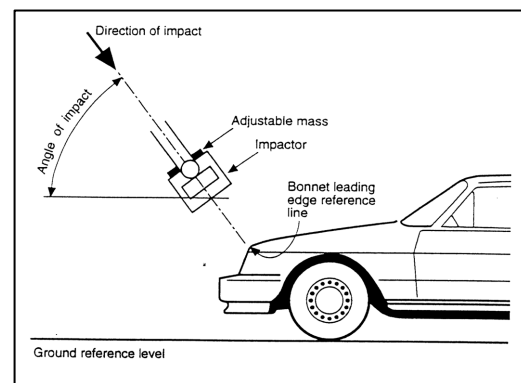


Figure 2. Upper-Leg impactor test.

The impact zone is named “Bonnet Leading Edge”.

Definitions

In order to define the impact test conditions, we first need to know the following definitions.

- **The Bonnet Leading Edge Reference Line:**
The Bonnet Leading Edge Reference Line is defined as the geometric trace of the points of contact between a straight edge 1000mm long and the front surface of the bonnet, when the straight edge, held parallel to the vertical longitudinal plane of the car and inclined rearwards by 50° and with the lower end 600mm above the ground, is traversed across and in contact with the bonnet leading edge (see Figure 3).

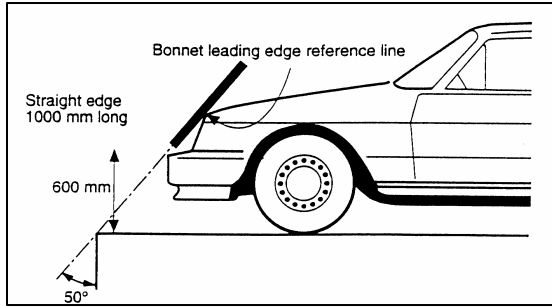


Figure 3. Definition of the Bonnet Leading Edge Reference Line.

- The Upper Bumper Reference Line:

The Upper Bumper Reference Line is defined as the geometric trace of the upper most points of contact between a straight edge and the bumper, when the straight edge, held parallel to the vertical longitudinal plane of the car and inclined rearwards by 20°, is traversed across the front of the car whilst maintaining contact with the upper edge of the bumper (see Figure 4).

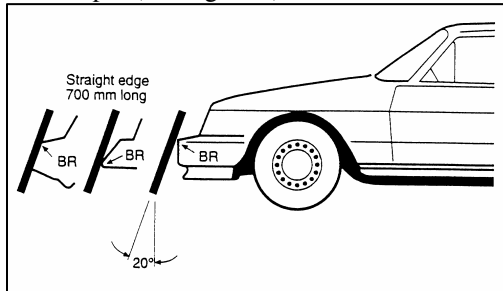


Figure 4. Upper Bumper Reference Line.

- The Bumper Lead:

This is defined as the horizontal distance between the Bonnet Leading Edge Reference Line and the Upper Bumper Reference Line. Please note that the vehicle has to be in its Normal Ride Attitude

- The Bonnet Leading Edge Height:

This is defined simply as the vertical height above the ground of the Bonnet Leading Edge Reference Line.

Impact Test Conditions

At the time of first contact the impactor centre line shall be midway along the Bonnet Leading Edge.

The shape of the front of the car determines the velocity, angle of incidence and kinetic energy of the impactor. Indeed, these three parameters will be calculated from the Bonnet Leading Edge Height and Bumper Lead.

Therefore, three simple test parameters (velocity, angle of incidence and impactor mass) will vary from:

- mass: from 9.5 to 17.7 kg
- velocity: from 20 to 40 km/h
- angle: from 10° to 47°

Figure 5 presents the total kinetic energy with respect to Bumper Lead and the Bonnet Leading Edge Height.

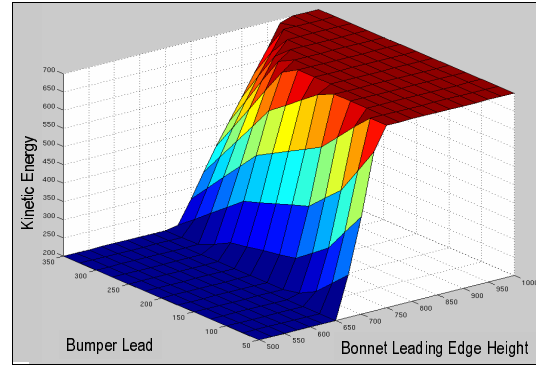


Figure 5. Upper Leg kinetic energy variation depending on the car shape.

Impact Test Measurements

Two type of biomechanical criteria are measured during the Upper Leg impactor tests:

- Force: measured from the two load cells that fix the femur to the rigid frame
- Bending Moment: measured from the three extensometric gages

Table 1 presents the measurements performed of the Upper Leg impactor.

Table 1. Measurements performed of the Upper Leg impactor.

Location	Measurement
Upper femur	Force
Lower femur	Force
Centre of femur	Bending moment
50mm above centre of femur	Bending moment
50mm below centre of femur	Bending moment

The requirements to get the upper leg full score in Euro NCAP [3] are:

- total force < 5kN
- each of the 3 bending moments < 300 N.m

PRESENTATION OF THE STUDY

Presentation Of The Test Rig

To get a relative high number of tests, we decided to carry out simplified test instead of test on a full car. The simplified test is made of a test rig (a rigid frame) that supports two absorbers. These absorbers are made of blocks of polypropylene foam and will be impacted by the upper leg impactor. Figures 6 and 7 present the test rig.

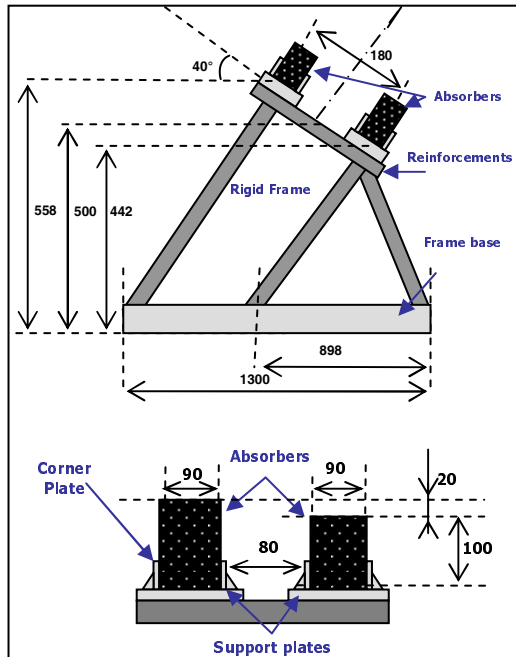


Figure 6. Drawing of the test rig used for characterization of the upper leg impactor scattering.

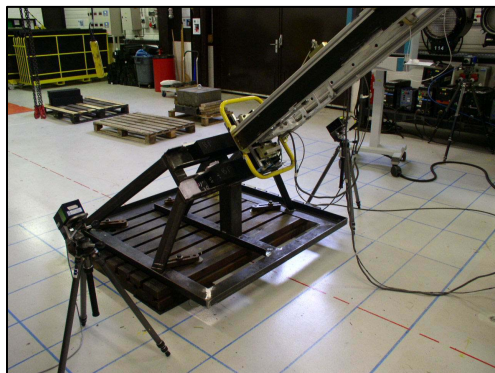


Figure 7. Picture of the test rig used for characterization of the upper leg impactor scattering.

The two blocks of polypropylene foam present a 20 mm of difference in height to reproduce a non symmetrical contact with the upper leg impactor. They have a 90 mm square surface and a 45 g/l density.

For each test, the upper leg impactor is centered midway between the two blocks of foam. (see Figure 7).

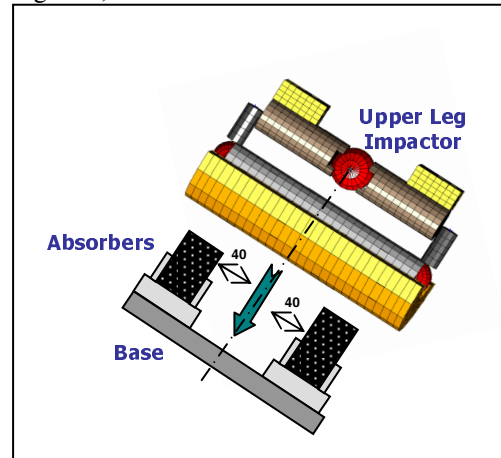


Figure 7. Drawing of the test between the upper leg impactor and the two absorbers.

Presentation Of The Two Test Series

In order to reproduce Euro NCAP test conditions, two test series were carried out. They are described in Table 2.

Table 2.

Test parameters used in the two test series

Test parameters	Test Series 1	Test Series 2
Mass of the Upper Leg impactor (kg)	12.8	10.9
Velocity of the Upper Leg impactor (km/h)	31.0	24.2

For each test series, two laboratories performed the test: Lab 1 and Lab 2.

In each laboratory, up to three different Upper Leg Impactors were used:

- the one of the Lab,
- the one of the other Lab
- and sometimes a third one that belongs to another lab.

These Upper Leg Impactors will be named UL1, UL2 and UL3.

Each impactor was systematically calibrated before the lab test series according to the Euro NCAP test protocol [1].

RESULTS

For each test series, two sets of results will be presented: the one measured in Lab 1 and the one measured in Lab 2.

Results Of Test Series 1 (Mass = 12.8 kg and Velocity = 31.0 km/h)

Results from Lab 1 are presented in Table 3, whereas results from Lab 2 are in Table 4. The analysis of the results will be presented in the next Section: "Analysis Of Test Results".

Table 3.
Results from Lab 1 for Test Series 1

Upper Leg Impacteur	Total femur force (kN)	Maximum bending moment (N.m)
UL1	8.77	393
	8.53	383
	8.44	369
	8.45	372
	8.32	370
UL2	9.31	399
	9.49	413
	9.59	409
	9.56	404
UL3	9.41	402
	9.26	416
	9.36	413
	9.08	401

Table 4.
Results from Lab 2 for Test Series 1

Upper Leg Impacteur	Total femur force (kN)	Maximum bending moment (N.m)
UL1	9.57	414
	9.66	415
	9.75	417
	9.62	415
	9.52	424
UL2	9.60	426
	10.10	450
	9.41	422
	9.56	423
	9.79	431

Results Of Test Series 2 (Mass = 10.9 kg and Velocity = 24.2 km/h)

Results from Lab 1 are presented in Table 5, whereas results from Lab 2 are in Table 6. The analysis of the results will be presented in the next Section: "Analysis Of Test Results".

Table 5.
Results from Lab 1 for Test Series 2

Upper Leg Impacteur	Total femur force (kN)	Maximum bending moment (N.m)
UL1	5.87	316
	5.90	279
	6.02	289
	5.85	286
	5.86	283
UL2	5.80	272
	6.15	293
	5.68	271
	6.00	281
	6.20	295

Table 6.
Results from Lab 2 for Test Series 2

Upper Leg Impacteur	Total femur force (kN)	Maximum bending moment (N.m)
UL1	5.31	274
	5.22	268
	5.25	269
	5.41	276
	5.63	287
UL2	5.24	278
	5.24	280
	5.22	283
	5.37	285
	5.36	286

ANALYSIS OF TEST RESULTS

Concerning the total femur force, we can notice that:

- The average femur force obtained during the first trial series is 9.27 kN.
- The average femur force obtained during the second trial series is 5.63 kN.

Concerning the total maximum bending moment, we can notice that:

- the average maximum bending moment obtained during the first trial series is 407 N.m.
- the average maximum bending moment obtained during the second trial series is 262 N.m.

Analysis Of The Total Femur Force With Regards To The Recorded Trial Speeds

Forces obtained during the first series according to the recorded trials speeds are shown in Figure 8. Whereas Figure 9 presents the total femur force obtained during the second test series according to the recorded trials speeds.

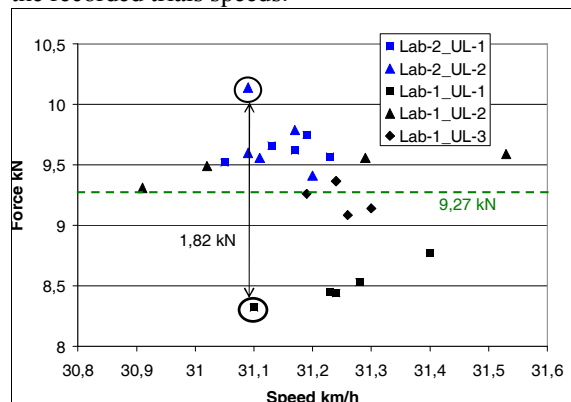


Figure 8. Force vs impact speed for the first test series

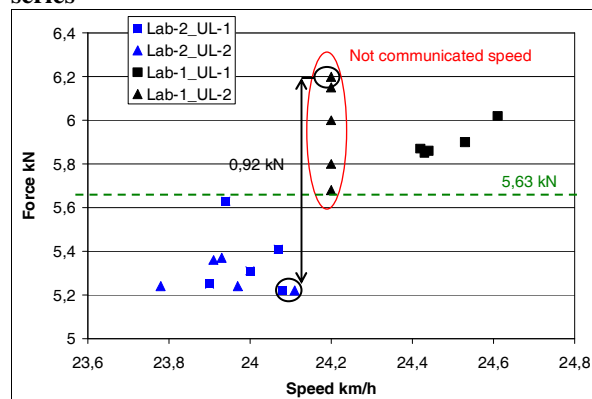


Figure 9. Force vs impact speed for the second test series

The Euro NCAP protocol imposes to comply with the impact speed with a tolerance of 2 %, this means 0.62 km/h in the first test series and 0.48 km/h in the second test series.

In the first test series, a maximum scattering of 1.82 kN was measured. This means a scattering of almost 20% of the 9.27 kN global average value for this test series.

In the second test series, a maximum scatter of 0.92 kN was measured. This means a scatter of almost 18% of the 5.63 kN global average value for this test series.

Therefore, we can conclude that for the two test series where impact parameters are close to Euro NCAP requirements, the maximum scatter can go up to 20% of the average femur force value.

Analysis Of The Average Femur Force Values Obtained With The Same Upper-Leg Impactor And At The Same Laboratory

Average femur forces obtained with the same upper-leg impactor and same laboratory for the first test series are presented in Figure 10.

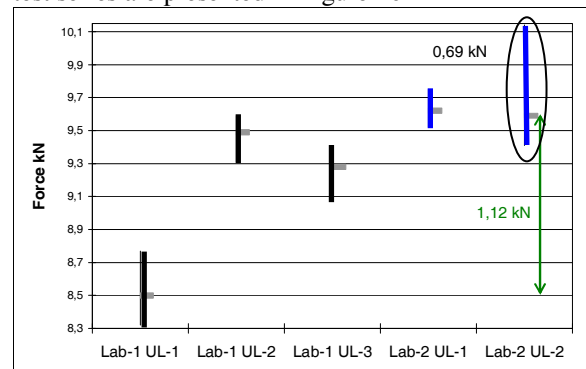


Figure 10. Comparison of femur forces (average and scatter) measured in the same lab and with the same upper leg impactor for the first test series

Average femur forces obtained with the same upper-leg impactor and same laboratory for the second test series are presented in Figure 11.

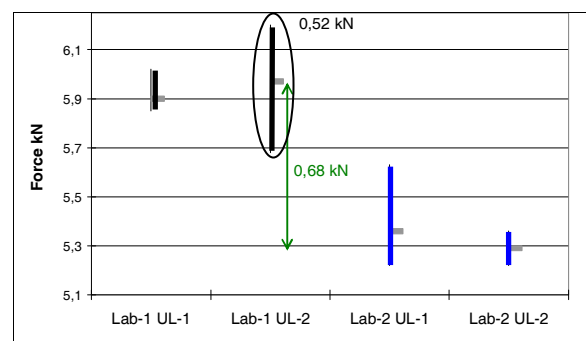


Figure 11. Comparison of femur forces (average and scatter) measured in the same lab and with the same upper leg impactor for the first test series

The maximum scattering measured for a same lab and a same upper leg impactor (what can be called repeatability scattering) is 0.69 kN for the first test series and 0.52 kN for the second one.

If we take into account all the different combinations of lab and upper leg (what can be called reproducibility scattering), we can derive an average scattering.

This average scattering, for the first test series is equal to:

$$(0.23 + 0.69 + 0.33 + 0.38 + 0.28) / 5 = 0.38 \text{ kN.}$$

And for the second test series the average scattering is equal to:

$$(0.40 + 0.17 + 0.15 + 0.52) / 4 = 0.31 \text{ kN.}$$

First of all, this means that there is no significant decrease of the femur force scattering with the impact energy.

Then, if we look at the average values obtained for the different lab and different upper-leg impactor combination, we get a scattering of 1.12 kN (which is 12% of the average value, 9.27 kN) for the first test series and 0.68 kN (which is 12% of the average value, 5.63 kN) for the second test series.

In conclusion, we can say that the reproducibility scattering (scattering between average values of different test configurations) is two times or three times higher than the average repeatability scattering (scattering measured inside a same test configuration: same lab and same impactor).

Analysis Of The Average Values Of Bending Moment, Obtained With The Same Upper-Leg Impactor And At The Same Laboratory

Average bending moments obtained with the same upper-leg impactor and same laboratory for the first test series are presented in Figure 12.

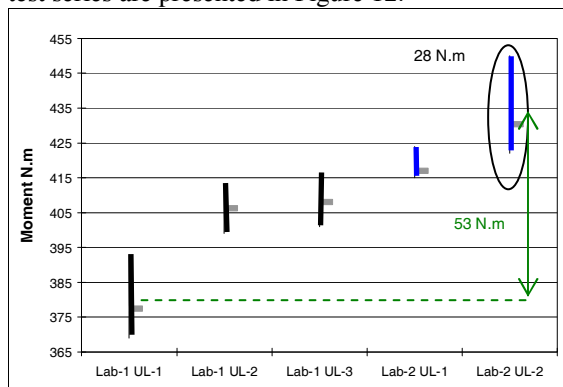


Figure 12. Comparison of femur forces (average and scatter) measured in the same lab and with the same upper leg impactor for the first test series

Average bending moments obtained with the same upper-leg impactor and same laboratory for the second test series are presented in Figure 13.

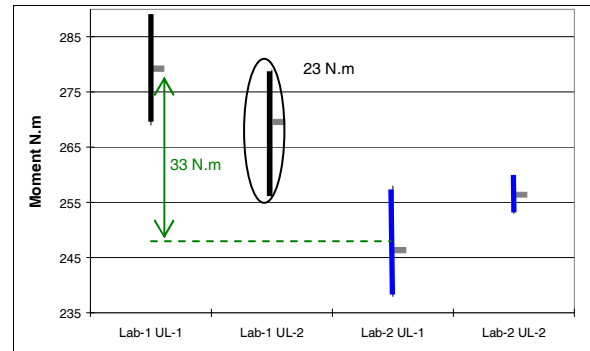


Figure 13. Comparison of bending moments (average and scatter) measured in the same lab and with the same upper leg impactor for the first test series

The maximum scattering measured for a same lab and a same upper leg impactor (what can be called repeatability scattering) is 28 N.m for the first test series and 23 N.m for the second one.

If we take into account all the different combinations of lab and upper leg (what can be called reproducibility scattering), we can derive an average scattering. This average scattering, for the first test series is equal to:

$$(24 + 14 + 15 + 9 + 28) / 5 = 18 \text{ N.m}$$

And for the second test series the average scattering is equal to:

$$(20 + 23 + 20 + 7) / 4 = 17.5 \text{ N.m}$$

First of all, this means that there is no significant decrease of the bending moment scattering with the impact energy.

Then, if we look at the average values obtained for the different lab and different upper-leg impactor combination, we get a scattering of 53 N.m (which is 13% of the average value, 407 N.m) for the first test series and 33 N.m (which is 12% of the average value, 262 N.m) for the second test series.

In conclusion, we can say that the reproducibility scattering (scattering between average values of different test configurations) is 1.5 to 2 times higher than the average repeatability scattering (scattering measured inside a same test configuration: same lab and same impactor).

CONCLUSIONS

We assessed the scattering of the upper-leg impactor through tests carried out in two laboratories with up to three different impactors. The tests we made were close to the Euro NCAP impact energies applied to current cars. Therefore

we can assess the scattering of the Euro NCAP upper leg impactor tests.

We measured we can be called repeatability scattering and reproducibility scattering. As expected, the repeatability scattering is always smaller than the reproducibility scattering.

These strong scatterings can be bound to the choice of the impactor, to the choice of the laboratory, the temperature, the impacted element, or the hygrometry.

By taking as an hypothesis that by increasing the number of tests, the Gaussian centre would be close to the calculated average values, we found that the maximum scattering between 2 pairs (laboratory / impactor) is 12 % of each of the two biomechanical criteria average.

Then, we can apply this scattering value in the Euro NCAP pedestrian rating. We recall that the maximum of points in the pedestrian upper-leg Euro NCAP protocol is given when the total femur force is lower than 5 kN, and the maximum bending moment lower than 300 N.m. We also recall that the femur zone is divided into 3 parts, each of them receive a maximum of 2 points in the Euro NCAP rating.

Therefore, a 12% scattering of the biomechanical criteria level, will give a difference of $1.2*3=3.6$ points for the total femur force and $0.9*3=2.7$ points for the maximum bending moment, out of 6 in the pedestrian upper-leg Euro NCAP rating. So, we can lose a maximum of 3.6 points out of 6, for a target from 5kN and 300 N.m.

As a final conclusion it should be stressed that this assessment of the upper-leg scattering will be added to other scatterings such as the difference in car behaviour or the scatter in the impact points.

ACKNOWLEDGMENTS

The authors wish to thank all the laboratories involved in this study as well as the PSA research team. A special thank to:

- Jean Claude Leclerc from PSA
- Francois Minne from UTAC
- Cyrille Edon from Renault SA

REFERENCES

- [1] European Directive 2003/102/EC of the European Parliament and of the Council relating to the protection of pedestrians and other vulnerable road users before and in the event of a collision with a motor vehicle
- [2] Euro NCAP Pedestrian Testing Protocol - Version 4.3
- [3] Euro NCAP Assessment Protocol And Biomechanical Limits - Version 4.3
- [4] Technical solutions for enhancing the pedestrian protection. C. Pinecki et al - ESV 2007 - Paper number 07-0307

EVALUATION OF A FLEXIBLE PEDESTRIAN LEGFORM IMPACTOR (FLEX-PLI) FOR THE IMPLEMENTATION WITHIN LEGISLATION ON PEDESTRIAN PROTECTION

Oliver Zander

Federal Highway Research Institute (BASt)
Germany

Dirk-Uwe Gehring

Peter Leßmann

BGS Böhme & Gehring GmbH
Germany

Jens Bovenkerk

ika - Institut für Kraftfahrzeuge RWTH Aachen University
Germany
Paper Number 09-0277

ABSTRACT

A flexible pedestrian legform impactor (FlexPLI) with biofidelic characteristics is aimed to be implemented within global legislation on pedestrian protection. Therefore, it is being evaluated by a technical evaluation group (Flex-TEG) of GRSP with respect to its biofidelity, robustness, durability, usability and protection level (Zander, 2008). Previous studies at the Federal Highway Research Institute (BASt) and other laboratories already showed good progress concerning the general development, but also the need for further improvement and further research in various areas (Zander et al., 2007). This paper gives an overview of the different levels of development and all kinds of evaluation activities of the Flex-TEG, starting with the Polar II full scale pedestrian dummy as its origin and ending up with the latest legform impactor built level GTR that is expected to be finalized by the end of the year 2009. Using the latest built levels as a basis, the paper reveals gaps that are recommended to be closed by future developments, like the usage of an upper body mass (UBM), the validation of the femur loads, injury risk functions for the cruciate knee ligaments and an appropriate certification method. A recent study on an additional upper body mass being applied for the first time to the Flex-GT is used as means of validation of the lately proposed modified impact conditions by Konosu et al. (2007-2). Therefore, two test series on a modern vehicle front using an impactor with and without upper body mass are being compared. A test series with the Flex-GTR will be used to study both the comparability of the impact behavior of the GT and GTR built level as well as the consistency of test results. Recommendations for the implementation within legislation on pedestrian protection are made.

INTRODUCTION

After being adopted by the World Forum for Harmonisation of Vehicle Regulations (WP.29) and the Executive Committee of the Agreement on Global Technical Regulations from 1998 (AC.3), the Global Technical Regulation on Pedestrian Safety (GTR No. 9) has been published in January 2009 (UNECE, 2009). Its preamble considers the flexible pedestrian legform impactor (FlexPLI), which is deemed to have high biofidelic characteristics along with an excellent leg injury assessment ability to replace the currently used rigid EEVC WG 17 pedestrian legform impactor (EEVC, 2002) in the future. Therefore, the Working Party on Passive Safety (GRSP) of UNECE has tasked the Flexible Pedestrian Legform Impactor Technical Evaluation Group (Flex-TEG) with the technical evaluation of the FlexPLI and a recommendation on the date on which the FlexPLI could replace the EEVC impactor within legislation. Subsequent to a summary of the history of the FlexPLI, the present study gives an overview of the activities carried out by the FlexTEG. The injury criteria and currently proposed, tentative threshold values are briefly discussed. The recently introduced inverse certification method will be used to assess the repeatability and reproducibility of test results of the final impactor built level. In a test series with the Flex-GTR the protection potential of two modern car frontends are assessed and a comparison between the built levels GT and GTR is made afterwards. An additional series of tests evaluates the effect of a missing upper body mass on the assessment of two modern vehicle front shapes representing the categories SUV and Sedan. Finally, still existing gaps of the final built level GTR are revealed and recommendations for implementation within legislation and future improvements are given.

FLEX-PLI HISTORY

Subsequent to the development of the POLAR-II Pedestrian dummy, the Japanese Automobile Research Institute (JARI) developed the “New JARI legform impactor” in the year 2000. This antecessor of the FlexPLI with a knee joint derived from the POLAR-II leg and rigid aluminium tubes representing the femur and tibia sections of the human leg already showed a higher biofidelity within PMHS tests (Wittek et al, 2001). The next built level called “JAMA-JARI legform impactor ver. 2002” with flexible femur and tibia bones had a more compact design and further improved biofidelic properties on component as well as on assembly level (Konosu et al., 2003). In the years 2003 and 2004 the first two built levels of the FlexPLI were released. Main changes were a further improved biofidelity on component level in version 2003 and improvements w.r.t. the impactor robustness, usability and biofidelity on assembly level in version 2004. Besides, a biofidelity rating system was introduced (Konosu et al., 2005). The subsequent impactor built level Flex-G showed a good repeatability and reproducibility of test results under idealized test conditions, but a comparatively low robustness (Zander et al., 2006). This impactor level was followed in the year 2006 by the Flex-GT α with modified specifications, a higher knee stiffness and knee bending angle limitation. Besides, an increased impact height was meant to improve the injury assessment ability of the impactor (Konosu et al., 2007). Built level GT then revealed moderate changes only, having a continuous outer neoprene skin and symmetrical bones with a smaller diameter (Konosu et al., 2007), which were found to have no significant influence on the impactor output (Zander, 2007).

FLEX-GTR

The final built level Flex-GTR (Figure 1) that has been released as prototype version at the end of 2008 and that is currently assessed by the Flex-TEG shows further improvements like the avoidance of dissymmetric sensitivities and twist in the knee area, an optional on-board data acquisition system and internal wiring. Furthermore, a tibia accelerometer as well as a potentiometer for the acquisition of the lateral collateral ligament elongation are added with the purpose of obtaining additional information during the pendulum function test (Been, 2008). All design changes are intended not to have any influence on the test results. However, the very first validation tests at BASt experienced an inconsistent tibia acceleration signal caused by high vibration during the impact. Due to that reason, the acceleration output will not be examined further within this study.

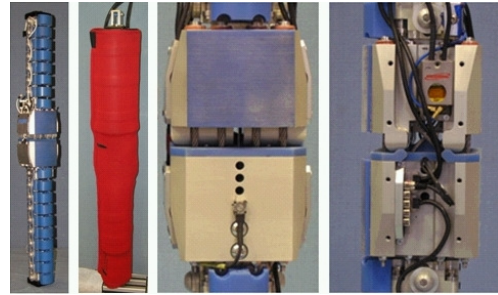


Figure 1. Flex-GTR impactor and knee detail.

INJURY CRITERIA AND TENTATIVE THRESHOLD VALUES

The Flex-GTR is aimed by the Flex-TEG to assess pedestrian leg injuries by the maximum bending of the tibia section measured by four strain gauges and the maximum elongations of the medial collateral ligament and the anterior and posterior cruciate ligaments acquired by three string potentiometers.

The current tentative threshold values for the maximum tibia bending moments of the Flex-GTR have been derived from previous studies on the 50% injury risk of the 50th AM (Nyquist et al., 1985 and Kerrigan et al., 2003). Those injury risk levels have been transformed by Konosu (2007) into the upper and lower performance limits for the tibia bending moment of the human model, the Flex-GT model and the Flex-GT impactor. The Japan Automobile Manufacturers Association (JAMA, 2008) lately proposed an average value between the lowmost and upmost limit as injury threshold for the Flex-GTR tibia bending moment.

The tentative threshold values for the medial collateral ligament have been derived by Konosu (2007) transforming the 50% injury risk levels for the 50th AM found by Ivarsson et al. (2004) into the lowmost and upmost limits for the human model knee bending angle and the elongation of the medial collateral ligament (MCL), the Flex GT model MCL elongation and finally into the Flex-GT impactor MCL elongation. JAMA lately proposed a more relaxed threshold value taking into account high bumper vehicles and the effect of muscle tension (2008). On the other hand, BASt proposed new tentative threshold values based on the dynamic response corridor found out by Ivarsson et al. (2004) and the injury risk curve of Konosu et al. (2001), pointing out that high bumper vehicles still have to be taken into account (Zander, 2008-2).

In terms of the threshold values for the cruciate ligaments, no injury risk curve has been developed so far. Therefore, and as the cruciate ligaments are estimated being sufficiently protected by the MCL thresholds, the International Harmonised Research

Activities Pedestrian Safety Working Group (IHRA-PS) suggested 10 mm maximum elongation of the anterior cruciate ligament (ACL) / posterior cruciate ligament (PCL) taking the risk of cruciate ligament rupture sufficiently into account (IHRA, 2004). Meanwhile, BASt tried to derive an injury threshold from impact tests with the Flex-PLI and the EEVC WG 17 PLI on identical impact locations of different vehicles representing a modern vehicle fleet (1box, Sedan, SUV). By linear regression it was found that the assessment of cruciate ligament protection provided by car front shapes using the FlexPLI ACL/PCL elongation readings is not comparable to the assessment using the WG 17 PLI shearing displacement results and vice versa. Therefore, BASt proposed to stick with PMHS knee shearing results evaluated by Bhalla et al. (2003) for knee shear displacement of the 50th AM as the tentative threshold value, even though the timing of injury could not be clearly identified and the common injury mechanisms still have to be better understood. (Zander, 2008-2).

Due to the missing effect of an upper body mass on the impactor kinematics and test results, the loadings of the femur sections are currently not considered as injury criteria for the assessment of pedestrian leg injuries. However, the knee and tibia injury assessment ability were found within a computer simulation study to be improved by lifting up the impactor by 75 mm above ground level when impacting the vehicle bumper (Konosu et al., 2007-2). The actual effects of an upper body mass on the femur, tibia and knee loadings are discussed later within this study.

An overview of the currently proposed Flex-GTR injury threshold values based on the 50% injury risk for the 50th AM is given in Table 1.

Table 1.
Proposed Flex-GTR injury threshold values based on the 50% injury risk of the 50th AM (Zander et al., 2009)

Leg region	50% injury risk level for 50 th AM	Flex-GTR thresholds (tentative)
Tibia	312 - 350 Nm	318 Nm
MCL	16 - 20°	16 - 23 mm
ACL	12,7 mm	12,7 mm
PCL	12,7 mm	12,7 mm

FLEX-TEG EVALUATION ACTIVITIES

The Flex-TEG of GRSP that had been tasked with the technical evaluation of the FlexPLI started its work in 2005. Previous activities included the technical evaluation of built levels G and GT by means of a technical review of the impactor and its

calibration methods, an analysis of the so far applied certification methods by carrying out inverse and pendulum tests, and an analysis of the injury assessment ability by performing simplified vehicle tests and real car tests. In this context, the repeatability and reproducibility of test results were found as good in most cases respect to the tibia and MCL values, while a partly high scatter was found in the cruciate ligament test results. From the simplified vehicle tests no direct correlation between the impact height and the test results could be derived. Furthermore, only the loadings on the medial collateral ligament were found critical when modern shaped vehicle frontends were tested with the Flex-GT, while good test results obtained with the rigid legform impactor according to EEVC WG 17 were in line with good results with the Flex-GT/GT α (Zander, 2008). Besides, first studies related to the application of an upper body mass to the FlexPLI were performed, showing already to some extent comparable results of a Flex-GT legform model and a MADYMO full pedestrian dummy (Mallory et al., 2008). Moreover, the injury risk functions were reviewed and the tentative threshold values modified as discussed before. Finally, a first evaluation of the pedestrian protection level provided by the FlexPLI was done, estimating 2797 lower extremity injuries being prevented by the introduction of the FlexPLI, which is equal to 40% addressed by the GTR (JAMA/JARI, 2007).

Currently ongoing Flex-TEG activities related to the final built level GTR as the finalization of the inverse certification test procedure, repeatability and reproducibility (r&R) assessment, real car tests and a comparison of the impactor output to the GT version will be discussed in the following chapters as well as the introduction of an upper body mass for future improvement of the injury assessment ability and impact kinematics.

INVERSE CERTIFICATION TEST

An inverse test setup, having its origin in the assessment of the repeatability and reproducibility of tests results with the EEVC WG 17 legform impactor (Zander et al., 2005) is proposed to be introduced as the certification procedure for the FlexPLI. In this test, the stationary FlexPLI is impacted by a linearly guided aluminium honeycomb impactor having its upper edge in line with the impactor knee joint, causing bending of the bones and shearing and bending of the knee in a soft impact (Figure 2).



Figure 2. Flex-GTR inverse certification test.

Pass/fail parameters of the inverse certification test are the outputs of the four tibia strain gauges and the ACL, PCL and MCL potentiometer. As exemplarily shown by means of the traces for ligaments and tibia bending moments (Figure 3), this procedure is found to mirror the loadings of the FlexPLI during a real car impact in a realistic way with respect to the timing, the kinematics and the maxima. Besides, the impactor rotation as well as the high influence of the impactor mass and the location of its center of gravity on real car test results are appropriately taken into account.

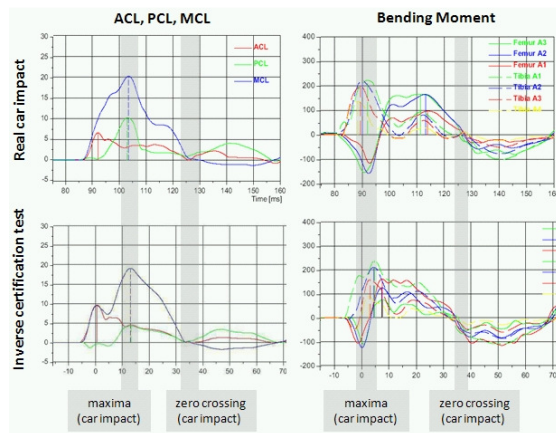


Figure 3. Comparison of the traces in real car and inverse certification test (Zander et al., 2008).

Currently, the FlexTEG is discussing the type of honeycomb material used for the inverse test w.r.t. properties and dimensions. The material so far used was of 5052 alloy type with a crush strength of 75 PSI, a density of 3.1 lb/ft³ and a cell size of 3/16 inches. The honeycomb dimensions were 250*160*60 mm.

ASSESSMENT OF REPEATABILITY AND REPRODUCIBILITY OF TEST RESULTS

In a joint project with the European Automobile Manufacturers' Association (ACEA) BAST has carried out a series of inverse certification tests with the first prototypes of the Flex-GTR in order to assess the repeatability and reproducibility of test results. By using the inverse test setup idealized impact conditions with identical test parameters kept the focus on the impactor output itself.

Test results under idealized impact conditions

Three GTR impactors, one of these equipped with the conventional external Data Acquisition System (DAS) (SN01) and two with different on-board DAS, the MESSRING M-BUS (SN02) and the DTS Slice system (SN03) were each tested three times at an impact speed of 40 km/h. The results for the tibia bending moments and knee elongations (ACL, PCL and MCL) being the currently by the Flex-TEG proposed pass/fail parameters are given in Figures 4 and 5.

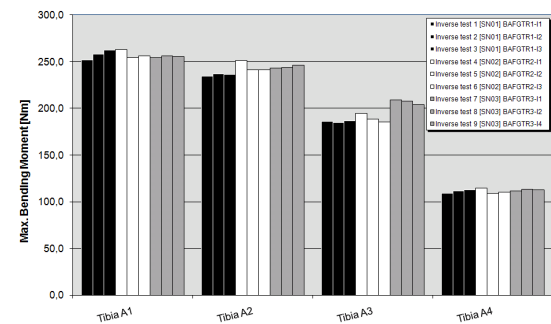


Figure 4. Tibia bending moment results of Flex-GTR inverse certification tests.

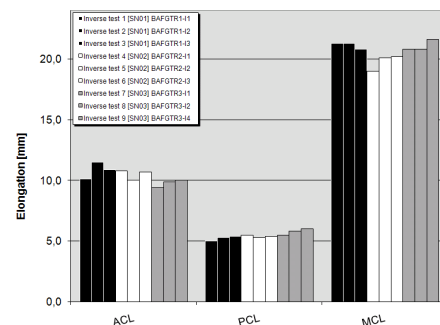


Figure 5. Knee ligament elongation results of Flex-GTR inverse certification tests.

The impactor output of all three prototypes showed very comparable results with the maximum values in a range being expected for real car test results as well.

Repeatability

The repeatability (r) of test results was studied using the best practice guidelines for crash test dummies. Here, the coefficients of variation (CV) of the three impactors are assessed according to Table 2.

Table 2.
Assessment of repeatability of test results

Ranking	Criterion
Good	$0\% \leq CV \leq 3\%$
Acceptable	$3\% < CV \leq 7\%$
Marginal	$7\% < CV \leq 10\%$
Not acceptable	$10\% < CV$

Figure 6 gives an overview of the coefficients of variation of all tibia bending moment and knee ligament elongation results of the three impactors. Thus, the repeatability of all tibia bending moments is assessed good, while the repeatability of the ligament elongations is between good and acceptable. Even though the repeatability was, most likely by the symmetrical knee design, significantly improved being compared to impactor built level GT, the cruciate ligament elongations still produce the highest coefficients of variation. However, all results are in an at least acceptable range.

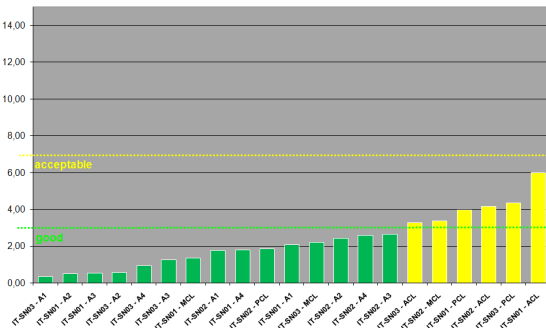


Figure 6. Repeatability of GTR impactor test results under idealized impact conditions.

Reproducibility

The reproducibility (R) of test results is assessed by drafting a reproducibility corridor which is based on the pooled means (MV) of all segments with a coefficient of variation lower than 5% according to Mertz (2004):

Table 3.
Assessment of reproducibility of test results

Ranking	Criterion
Not acceptable	$x < 0,9 * MV$
Acceptable	$0,9 * MV \leq x \leq 1,1 * MV$
Not acceptable	$x > 1,1 * MV$

According to this assessment method, all tibia segments and knee ligaments gave reproducible test results with their pooled means within the reproducibility corridor. Only the ACL results of the impactor with external DAS (SN01) were outside the reproducibility corridor (CV = 6%).

REAL CAR TESTS

Aim of performing impact tests with the Flex-GTR on modern vehicle fronts was to obtain information on the feasibility of the current requirements as well as a verification of the impactor output of built level GTR that was required to stay in line with the previous results.

Flex-GTR tests on Sedan #1

A modern vehicle with Sedan front shape and a borderline to green bumper area according to the Euro NCAP requirements (Euro NCAP, 2009) was tested three times on two different impact locations with the same impactor (SN02) at 40 km/h and the currently proposed impact height of 75 mm above ground level. The test results are given in Figures 7 and 8.

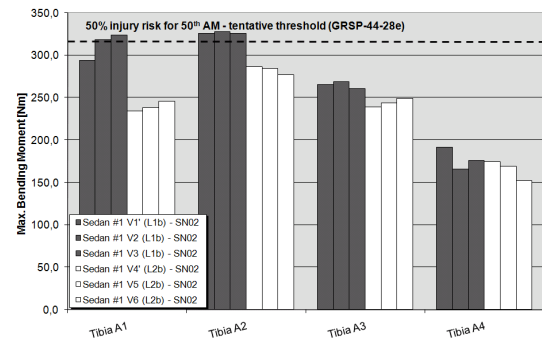


Figure 7. Tibia bending moment results of Sedan #1 tests.

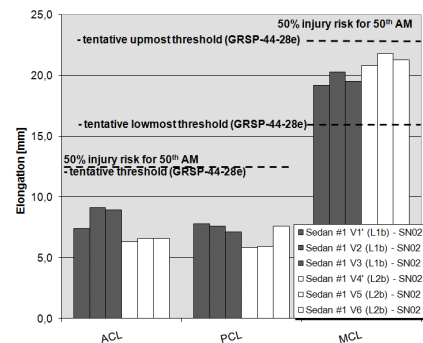


Figure 8. Knee ligament elongation results of Sedan #1 tests.

Both impact locations fulfilled the tentative requirements for most of the tibia segments except impact location #1 for the two tibia segments that

were at height of the vehicle cross beam. The tentative thresholds for the cruciate ligaments were clearly met by both impact locations. In terms of the medial collateral ligament, all results were found in between the lowmost and upmost tentative threshold. Thus, the marginal Euro NCAP knee bending angle results were confirmed by the MCL test results with the Flex-GTR.

The tests showed a high repeatability of the MCL and most tibia segments while the coefficient of variation of the cruciate ligaments was partly not acceptable (Figure 9). This was, to some extent, according to the results of the previous built level GT.

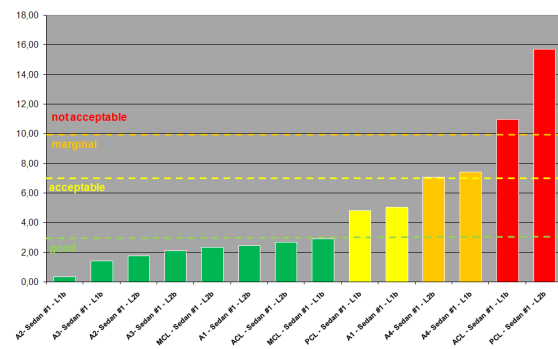


Figure 9. Repeatability of impactor test results with Sedan #1.

Flex-GTR tests on Sedan #2

In a tests series on a second Sedan shaped vehicle front within this joint project between ACEA and BASt two impact locations were tested, the first one with all three impactors three times each, the second one three times with Flex-GTR SN02.

Figure 10 gives an overview of the tibia peak results. At the first impact location impactor SN03 obviously gave a significantly higher output at segment A3 in all three tests.

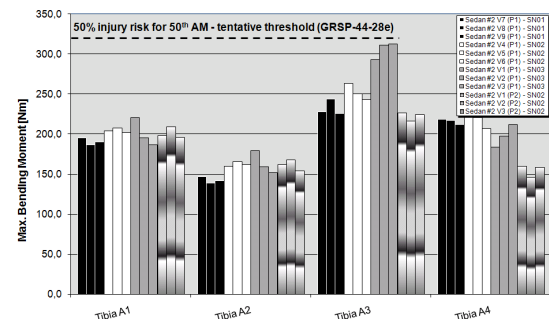


Figure 10. Tibia BM results of Sedan #2 tests.

The peak knee ligament elongation results are summarized in Figure 11. The output of all three impactors at impact location #1 is comparable

except in the first test of SN03. The test results at impact location #2 were similar as well.

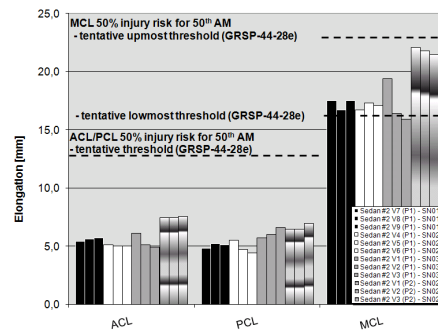


Figure 11. Knee EL results of Sedan #2 tests.

In terms of repeatability of test results, the cruciate ligament output was still partly not acceptable (Figure 12). The high coefficient of variation of SN03 MCL was found due to the detachment of a fixation in the first test. Altogether, Flex-GTR SN03 showed the lowest repeatability of test results. However, the majority of results was good or acceptable.

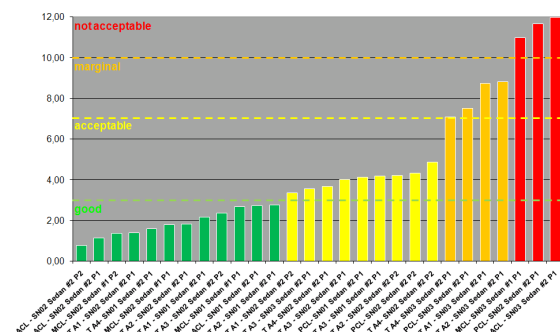


Figure 12. Repeatability of impactor test results with Sedan #2.

COMPARISON OF THE OUTPUT OF BUILT LEVELS GT AND GTR

A comparison of the impactor output of the final built level GTR with the previous one (Zander, 2007-2) was meant by the FlexTEG to ensure a consistent level of biofidelity. As the tests under idealized conditions focusing on the impactor only were generally found to have a higher repeatability than tests on real cars they were examined more in detail.

Most tibia segments of impactor level GTR gave an output that was about 10 to 15 percent higher than that of built level GT. Only segment A1 showed comparable results with both built levels. This trend was confirmed by real car tests on Sedan #1 that had been conducted within a previous study with the Flex-GTα. Also the Sedan #2 tests confirmed the higher results obtained with the

Flex-GTR at both impact locations. On the other hand, in latter case it has to be taken into account that only one test on each impact location had been carried out with the Flex-GT α (Zander, 2007).

A comparison of the ligament elongation results of the two impactor built levels showed a higher output of the medial collateral ligament potentiometer of the latest built level GTR. This trend was in line with the real car tests of Sedan #1 with Flex-GTR and Flex-GT α w.r.t. the second impact location. Here, the Flex-GTR gave an output that was 10 to 20 percent higher for all ligament elongations. At the first impact location, the real car tests did not show any clear tendency.

In a comparison of the coefficients of variation it was found out that built level GT still had segments with a repeatability in a marginal or even not acceptable range only, especially with respect to the cruciate ligaments, while at GTR level, the repeatability of test results was generally further improved. This improvement most likely had been addressed by the new symmetrical knee design.

On the other hand, the repeatability improvement of the cruciate ligament elongation results was only partly mirrored by the real car tests on both Sedans. However, the MCL and most of the tibia car test results showed a significantly improved repeatability.

EFFECTS OF AN UPPER BODY MASS

The Flex-TEG had been tasked by GRSP to evaluate the FlexPLI with the aim of its introduction into global legislation on pedestrian protection and, after a certain transition time, replacing the rigid legform impactor according to EEC WG 17. However, as the FlexPLI in its final built level is missing an upper body mass (UBM), the output of the femur strain gauges is currently not considered for the assessment of femur injuries and therefore is used for monitoring purposes only. On the other hand, computer simulation studies carried out by JARI found that vertically lifting the impactor by 75 mm in relation to ground level would compensate best the missing effect of an upper body mass with respect to impact kinematics and impactor tibia and knee loadings (Konosu et al., 2007-2).

Based on simulation results with the Pedestrian Total Human Model for Safety (THUMS) on a generic SUV front, a pedestrian upper body mass was developed and applied to the flexible legform impactor built level GT within the European FP6 research project on Advanced Protection Systems (APROSYS). In tests against a real SUV front shape the effects of this upper body mass on the

impact kinematics and test results were studied in detail. SUV front shapes were found to have a greater influence on the impact kinematics of a pedestrian in a collision. The isolated legform impacted above its center of gravity in most cases results in overrunning the legform. This impact behaviour is not according to a real pedestrian impact because its torso mass causes the pedestrians' body to wrap around the vehicle even when being impacted above the center of gravity of the leg (Bovenkerk et al., 2009).

Besides, the effect of the pedestrian upper body mass was also studied by BAST within additional tests on a Sedan shaped vehicle in order to verify the proposed impact conditions for lower bumper vehicles as well.

Upper body mass development

THUMS simulations of a collision between a pedestrian and a large SUV carried out by Compigne et al. (2009) found optimum parameters for an upper body mass to be applied to the FlexPLI in a total mass of 6 kg, an adjustable location of the center of gravity w.r.t. height and offset and an inclination of the leg by 6° taking into account the orientation of the human leg. According to these recommendations an upper body mass of 6.8 kg with four adjustable positions was developed and manufactured (Figure 13).

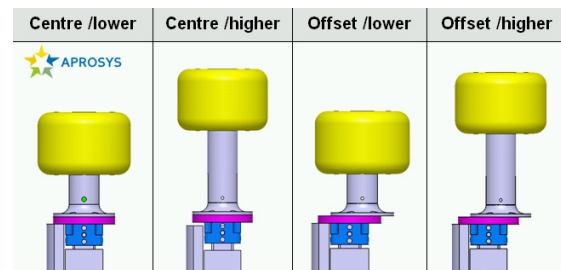


Figure 13. Development of an upper body mass for the Flex-GT (Bovenkerk et al., 2009).

For feasibility and comparability purposes it was decided to carry out the real car tests at the center lower position of the UBM (CoG at 110 mm, no offset) without leg inclination angle.

SUV test matrix and impact kinematics

In a first series of tests an SUV with a soft nose design and a consistently green rated bumper area according to Euro NCAP was tested at two different impact locations three times with the Flex-GT with and without UBM (Table 4).

Table 4.
SUV Test matrix for Flex-GT and Flex-GT UBM

Impact location	Lateral vehicle position [mm]	Impactor setup	Impact height [mm]	No. of tests
1	-350	GT Standard	75	3
		GT UBM	25	3
2	128	GT Standard	75	3
		GT UBM	25	3

As test positions the most likely worst impact locations according to the European New Car Assessment Programme (Euro NCAP, 2009) pedestrian testing protocol were selected (Figure 14).



Figure 14. Test setup Flex-GT UBM against SUV and impact locations.

An exemplary evaluation of the high speed film sequences of impact location #2 already revealed the significant differences of the impact kinematics of the Flex-GT Standard and the UBM version (Figure 15).

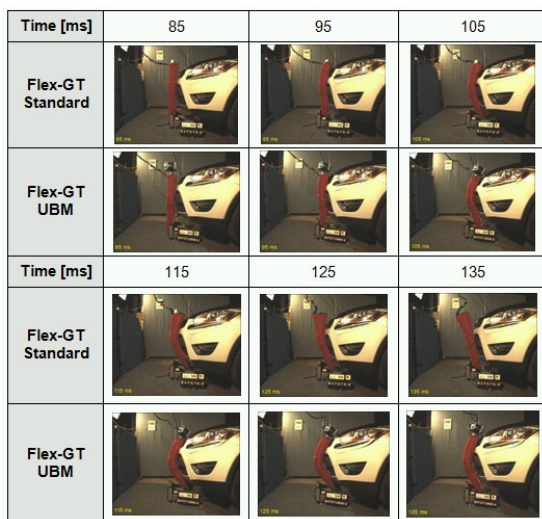


Figure 15. Effects of the upper body mass on the SUV impact kinematics (t_0 = impactor release).

In the first flight phase up to 100 ms from impactor release the kinematics of the standard impactor and the one with applied upper body mass were quite similar. Having reached its maximum knee bending the Flex-GT Standard passed over into the rebound phase while the UBM version reached its highest

bending level at a significantly later time at around 125 ms, likely due to the forces induced by the additional mass.

A comparison of the time of maximum loads of the femur segments of the Flex-GT Standard and the Flex-GT UBM showed the standard impactor being loaded with the maximum femur bending moments at an earlier stage than the UBM version. In the latter one, the peak value of segment A1 being the closest one to the vehicle cross beam occurred at a later time, i.e. that the additional mass was suspected to have the highest influence on the impact kinematics of this segment.

Like for the femur bending moments, the maximum loads of the tibia section of the standard impactor version occurred earlier than those of the UBM version. The maximum values for segment tibia A1 of the UBM impactor were reached at a later time than those for the other segments. This effect could have been caused by the decreased impact height in relation to the standard impactor version along with a possibly different influence of the lower stiffener on that area of the legform.

A comparison of the ligament elongations confirmed the different impact kinematics of both impactors w.r.t. the time and maximum loading. The maximum ligament elongations of the UBM version all occurred at a later time. Despite the modified impact height for the UBM version the additional mass showed its highest influence on the medial collateral ligament and the cruciate ligaments.

Analysis of SUV traces

In Figures 16 and 17 the traces for the femur and tibia segments of both impactor versions are exemplarily given for the respectively first test of impact location #2.

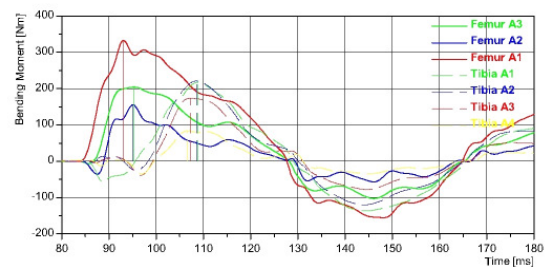


Figure 16. Femur and tibia test results of Flex-GT Standard at impact location #2 (Test V4).

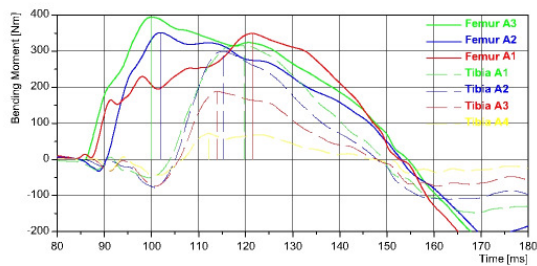


Figure 17. Femur and tibia test results of Flex-GT with UBM at impact location #2 (Test V4).

The traces show the femur and tibia segments of the UBM version being longer loaded than those of the standard impactor.

All three femur segments of the standard GT impactor reached their maximum values at almost identical times in all three tests of impact location #2. Femur segment A1 showed the highest bending. The time interval for the maximum femur bending moments of the Flex-GT with UBM was within 22 ms. In the UBM version of the impactor segment A3 showed the highest results. Besides the application of the upper body mass, the changed impact height (25 mm with UBM vs. 75 mm w/o UBM) was expected to have an influence on the femur test results as well. In addition, the UBM version of the impactor showed a significantly higher negative bending of the femur segments after the zero-crossing.

In terms of the tibia section, all segments of the standard GT impactor reached their highest loads in a time interval of 5 ms in all three tests, again in each test at almost identical times. Tibia segment A2 showed the highest bending moments, closely followed by segment A1. The maximum tibia bending moments of the UBM equipped legform at impact location #2 occurred in a time interval of 9 ms, and to some extent at a later time than with the standard impactor. Tibia segment A1 showed in all three tests the highest bending moments, closely followed by segment A2. An explanation for this reciprocal order was assumed by the changed impact height along with a modified distance of the segments to the vehicle main cross beam and the body mass having an effect on the peak results.

A comparison of the femur and tibia traces of the impactor with and without upper body mass gave clear evidence that especially the loads on the femur parts and the upper tibia segments (A1 and A2) increase significantly with a additional mass induction. In other words, the higher load transmission due to the upper body mass is not proven to be sufficiently compensated by an increase of the impact height by 50 mm compared to GTR level when related to SUV fronts.

Finally, the tibia A1 load measured by the Flex-GT with applied UBM was comparable to its bending moment simulated by the weighted impactor model w.r.t. to time and curve progression. On the other hand, the result was not comparable to that produced by the THUMS model.

The ligament traces for both impactors are exemplarily given as well for the respectively first test of impact location #2 (Figures 18 and 19).

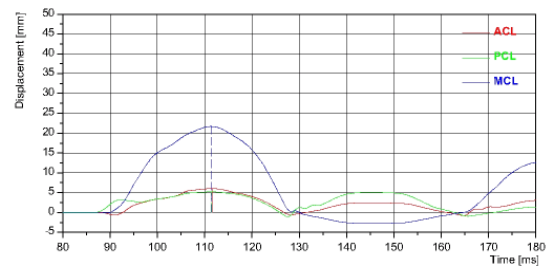


Figure 18. Ligament test results of Flex-GT Standard at impact location #2 (Test V4).

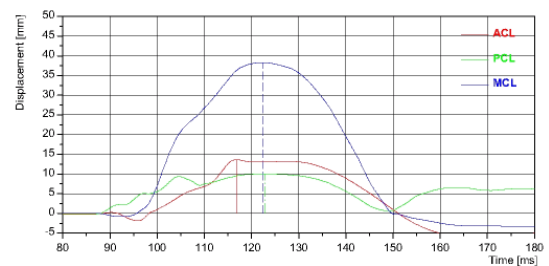


Figure 19. Ligament test results of Flex-GT UBM at impact location #2 (Test V4).

The peak values for the ACL, PCL and MCL elongation of the standard impactor occurred at almost identical times with very similar ACL and PCL maxima. Only the maximum PCL value in the last test was observed at a later time. The cruciate ligament characteristics are very similar to each other before the zero-crossing of the MCL elongation. After 130 ms measured from impactor release, the ACL output was significantly lower than that of the posterior cruciate ligament.

In the tests with Flex-GT UBM, the MCL and PCL maxima occurred almost simultaneously. The cruciate ligament traces diverged to a higher extent than in the standard tests which was more related to the structure of the impact location than to the effect of the upper body mass because at impact location #1 this divergence could not be observed. On the other hand, after the zero-crossing of MCL, the ACL output stayed always lower than that of PCL.

A comparison of the ligament elongation traces of the Flex-GT standard and Flex-GT UBM again

revealed the significant influence of the upper body mass on the test results. The potentiometer output of all ligaments was increased by nearly 100 percent in all tests at impact location #2. The difference in ACL/PCL results at impact location #1 showed similar tendencies. As already with the femur and tibia loads, the increase of impact height by 50 mm doesn't seem to compensate the mass effect when testing an SUV shaped vehicle front.

Finally, a comparison of the Flex-GT UBM traces with the output of the THUMS and 6 kg UBM impactor model confirmed the produced MCL values around or beyond 40 mm elongation. Anyway, it has to be stated that those loads were far beyond the biomechanical limits of the human knee.

SUV test results

Tentative threshold values for the maximum tibia bending moments of the Flex-GTR had been derived from a previous study on the 50% injury risk of the 50th AM (Kerrigan et al., 2003). As the femur bending moments of the FlexPLI had not been taken into account by the Flex-TEG for the assessment of leg injuries, for the time being those limits were withdrawn. For the introduction of an upper body mass and the corresponding assessment of femur injuries, those thresholds were tentatively introduced again. Thus, the 50 % risk of femur fracture for the 50th AM was estimated at a bending moment between 372 and 447 Nm.

Figure 20 shows the peak femur bending moment results on impact location #1 when tested with the Flex-GT with and without upper body mass.

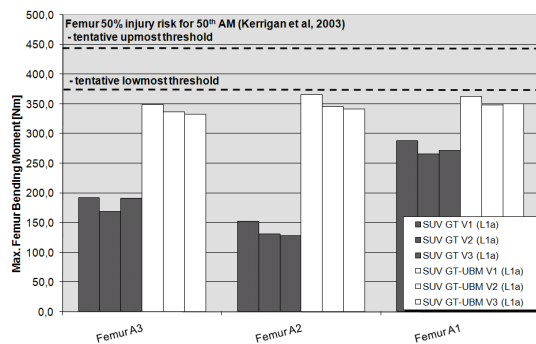


Figure 20. Femur bending moment results of impact location #1 (SUV).

It can be easily seen that the peak values for the femur loads increased significantly when the impact location was loaded with the UBM-equipped legform. The vertical distance between the vehicle cross beam and the particular femur strain gauge seemed to have an influence on the effect of the upper body mass. However, test results

obtained with UBM were more homogeneous over the whole femur length. Altogether, all test results obtained with this configuration still fulfilled the tentative upper performance limits.

The results of the tibia bending moments for impact location #1 are shown in Figure 21.

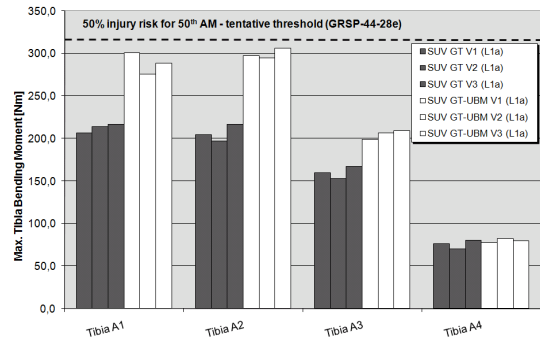


Figure 21. Tibia bending moment results of impact location #1 (SUV).

The tibia results for segments A1-A3 were significantly higher when the impact location was tested with the Flex-GT with UBM. In this context it also had to be taken into consideration that the height of the segments A1 and A2 was close to that of the vehicle main cross beam; therefore these loads were by trend higher than those of the two lower tibia segments. For segment A4, no difference in test results between standard and UBM legform could be observed.

Figure 22 shows the ligament elongation results of impact location #1.

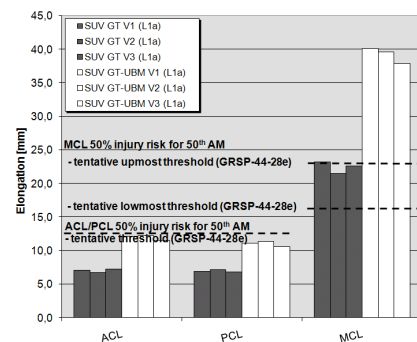


Figure 22. Knee ligament elongation results of impact location #1 (SUV).

As already seen with most of the bending moment results, the upper body mass also had a significant influence on the test results of the cruciate and medial collateral ligaments. While the cruciate ligament elongation requirements could just be fulfilled by impact location #1 when being impacted with the Flex-GT with UBM, the currently discussed MCL threshold values were

exceeded by almost 100 percent, i.e. as well that the MCL results obtained with the Flex-GT with UBM clearly exceeded the biomechanical limits of the human knee.

No evidence was given that the Flex-GT Standard being lifted up by 50 mm in relation to the UBM version could compensate the missing mass effect on the tibia and knee loads when testing an SUV shaped vehicle front.

The peak femur bending moment results of impact location #2 are given in Figure 23.

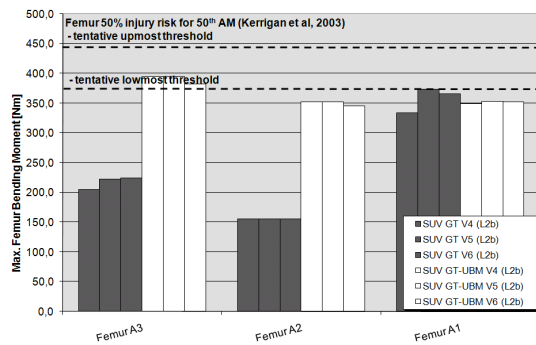


Figure 23. Femur bending moment results of impact location #2(SUV).

For the femur segments A3 and A2 the same tendencies as for impact location #1 could be observed: the test results obtained with Flex-GT and UBM were significantly higher than those without UBM. Again, latter ones were more homogeneous over the whole femur length. Besides, this impact location did not meet the upper performance limit at femur A3 when tested with UBM. At femur segment A1, the UBM did not have any influence on the peak values.

The tibia test results at impact location #2 showed the same tendencies as at impact location #1 (Figure 24).

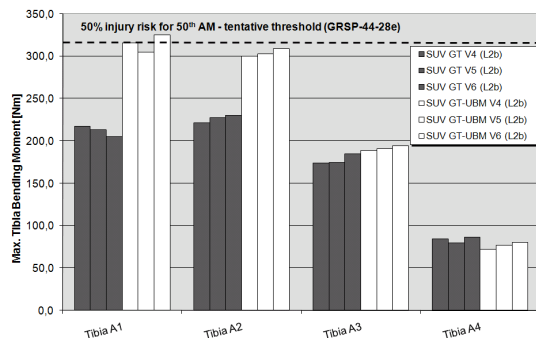


Figure 24. Tibia bending moment results of impact location #2 (SUV).

On the tibia segments A1 and A2 the applied UBM had a significant influence on the test results. For

segment A3 the difference was marginal, while for segment A4 no influence of the UBM could be observed.

The test results of the crucial and medial collateral ligaments of impact location #2 are given in Figure 25.

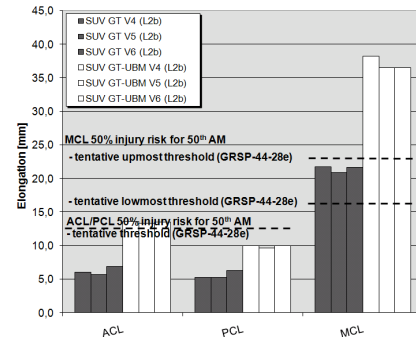


Figure 25. Knee ligament elongation results of impact location #2(SUV).

Again, the application of the upper body mass was of significant influence on all ligament test results. In case of the ACL results, the UBM signed responsible for the exceedence of the currently proposed threshold values. In case of the MCL results, latter ones clearly missed the tentative upmost threshold and were almost twice the results obtained without UBM. Once again, the elongations of the medial collateral ligament measured by the Flex-GT equipped with UBM clearly exceeded the biomechanical limits of the human knee which is expected to suffer from ligament rupture at an earlier stage of the accident already.

Influence of upper body mass on repeatability of test results (SUV)

As for the Flex-GTR inverse and Sedan tests, in order to gain additional information on the repeatability of test results, the influence of the upper body mass on the coefficient of variation for each of the segments was examined.

Figure 26 summarizes the repeatability of all ligament elongation results as well as all tibia and femur bending moment results for both impact points when impacted with the Flex-GT standard version.

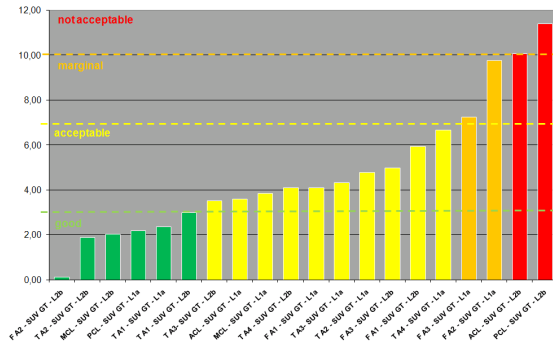


Figure 26. Repeatability of Flex-GT standard test results on SUV front.

As it can be seen, the repeatability of test results was at least in an acceptable range for most of the segments. Only the femur loads of segments A3 and A2 were in a marginal range when testing impact location #1. Besides, the repeatability of the cruciate ligament elongation results when testing impact location #2 was not acceptable. This was, to some extent, a confirmation of previously made observations w.r.t. the repeatability of the ACL/PCL results of impactor built level GT. The partly high scatter was found due to the play in the knee area and the dissymmetrical design of the knee in combination with impactor rotation caused by the design of particular impact areas (Zander et al., 2007 and 2008).

The repeatability of test results obtained with the Flex-GT with applied upper body mass is shown in Figure 27.

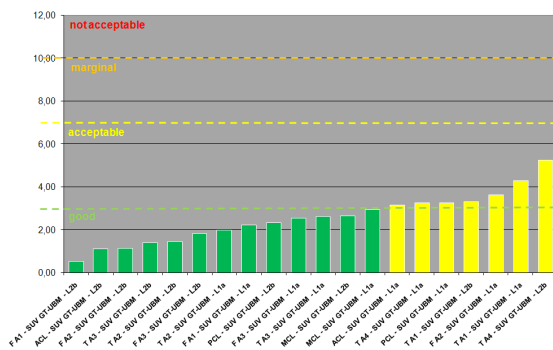


Figure 27. Repeatability of Flex-GT UBM test results on SUV front.

All test results were in a good or at least acceptable range ($CV < 5.5\%$). The influence of the applied upper body mass seemed to some extent the cause for this improved repeatability such that the knee dissymmetries and possible knee twist at the point of impact appeared to be negligible.

Study of UBM effects on Sedan test results

An additional test series carried out by BAST was meant to study the effect of an applied upper body mass on test results of a Sedan shaped vehicle. The influence was expected to be lower in comparison to that on SUV fronts due to the center of gravity of the isolated legform at or above bumper height in most of the cases.

Therefore, three tests with the Flex-GT with UBM were performed at the proposed impact height of 25 mm on a Sedan shaped car at an impact location formerly being tested with the rigid EEVC WG 17 legform impactor and assessed borderline to green according to Euro NCAP (Figure 28). The results were compared to tests with the Flex-GT α Standard at 25 as well as 75 mm impact height carried out by Zander et al. (2007).



Figure 28. Test setup Flex-GT UBM against Sedan and impact location.

The high speed sequence for the respectively first test of the Flex-GT α at 75 mm and the Flex-GT UBM is given in Figure 29.

Time [ms]	85	95	105
Flex-GT Standard			
Flex-GT UBM			
Time [ms]	115	125	135
Flex-GT Standard			
Flex-GT UBM			

Figure 29. Effects of the upper body mass on the Sedan impact kinematics (t_0 = impactor release).

As for the SUV, the first flight phase up to 100 ms from impactor release the kinematics of both impactors were comparable. Having reached its maximum knee bending the Flex-GT α standard impactor turned over into its rebound phase while the UBM version was loaded with a high bending moment during a significantly longer time interval. Thus, the second flight phase in its entirety was different due to the induced upper body mass.

Figure 30 shows the curve progressions of the respectively first test carried out with each test setup.

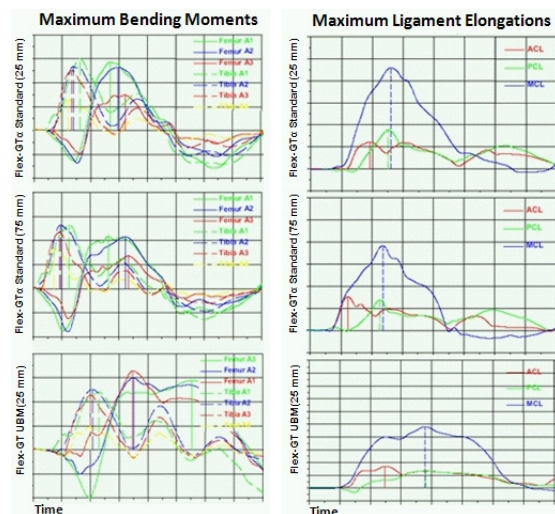


Figure 30. Femur, tibia and knee test results of Flex-GT α Standard at 25 and 75 mm and Flex-GT with UBM (Test V1).

While the traces of the Flex-GT α at 25 and 75 mm impact height showed to some extent a comparable behavior for the tibia segments and ligament elongations, the Flex-GT α femur output in the tests at an impact height of 75 mm w.r.t. its shape went more in line with the UBM version. The Flex-GT UBM showed an entirely different behavior of the knee ligaments w.r.t. shape and time interval. Altogether, the loadings measured by the UBM version were significantly higher for the femur part and occurred during a longer time interval. The traces for the tibia section were in line with those acquired by the standard impactor regardless its impact height.

A comparison of the peak femur results acquired with all three test setups is given in Figure 31.

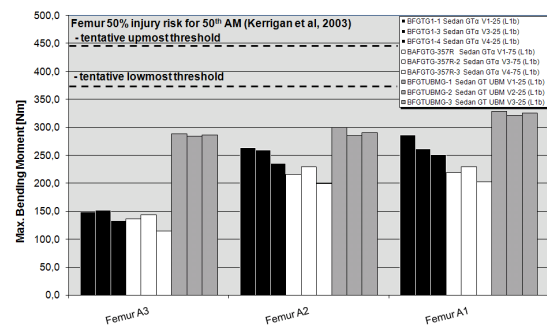


Figure 31. Femur bending moment results of Flex-GT α Standard (25 and 75 mm) and Flex-GT with UBM.

The results give evidence of the modified impact height not having any effect on the maximum femur loads compensating a missing upper body mass. Far from it, the peak results acquired by the UBM version went more in line with the results when using the original test setup. However, the tentative upper performance limit was met in tests with all three test setups.

In Figure 32, the maximum tibia bending moments are given.

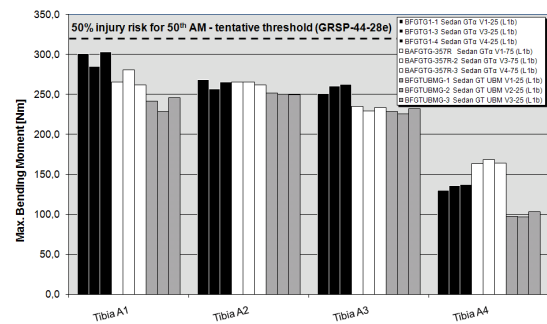


Figure 32. Tibia bending moment results of Flex-GT α Standard (25 and 75 mm) and Flex-GT with UBM.

Only in terms of tibia segments A1 and A3 the upper body mass effect was meant to be compensated by an increased impact height of the standard impactor. For segment A2, no effect could be observed, the peak results of segment A4 using the UBM impactor version were closer to the standard test setup at 25 mm impact height. Again, the tentative threshold was met in all three cases.

The knee elongation peak results are summarized in Figure 33.

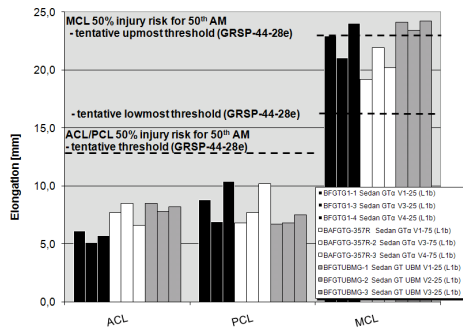


Figure 33. Knee elongation results of Flex-GT α Standard (25 and 75 mm) and Flex-GT with UBM.

Again, no justification for the increased impact height of the standard impactor could be found in the maximum output of the ligaments during the Sedan testing.

Figure 34 shows the coefficients of variation for the assessment of the repeatability of test results.

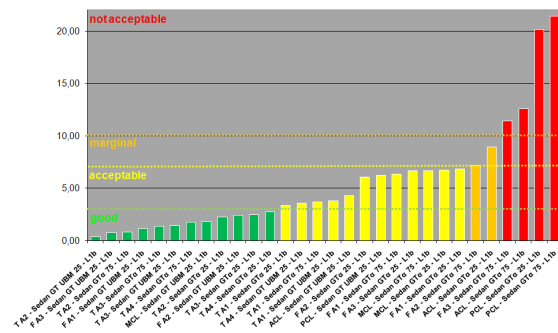


Figure 34. Repeatability of Flex-GT test results on Sedan front.

As during the SUV tests, the repeatability of the Sedan test results was significantly improved using the UBM impactor. All results were in a good or acceptable range. Concerning the standard impactor version, the cruciate ligament results gave as expected the highest scatter regardless the selected impact height.

DISCUSSION

In the present study, tests with the final built level of the FlexPLI were carried out on two Sedan shaped vehicles with pedestrian-friendly bumpers according to Euro NCAP. Once again it could be confirmed that pedestrian protection packages that pass the Euro NCAP criteria are as well in line with the Flex-GTR requirements. On the other hand, in the current tests the impactor output of built level GTR was observed in most cases to be 10 to 20 percent higher than that of the Flex-GT while showing an improved repeatability especially for the cruciate ligament elongation results.

The developed inverse certification method gives an output that is in the range of real car tests w.r.t. traces and maxima and is therefore proposed as the Flex-GTR certification method.

New threshold values for the ligament elongations and the tibia bending moments were proposed. However, no injury risk curves for the cruciate ligaments are available due to the fact that ACL / PCL rupture is expected to be prevented as well by the protection of MCL. On the other hand, high bumper vehicles as well as the effect of muscle tension still need to be included when transforming the human knee bending angles into impactor model elongation results.

A comparative test series with built level GT and upper body mass against an SUV shaped car front revealed the effects of an applied upper body mass on the impact kinematics and test results of the FlexPLI. This effect cannot be compensated by just an increase of the impact height of the standard impactor by 75 mm in relation to ground level as recommended by Konsou et al. (2007). In the tests against a modern SUV with green rated bumper according to Euro NCAP, the loads on the medial collateral ligament increased by almost 100 percent. Furthermore, the femur loads showed significantly different characteristics w.r.t their traces and maximum values. Despite of the different impact heights, a comparison of the kinematics between the Flex-GT UBM version and the Flex-GT UBM model gave quite similar results until maximum loading. Therefore, the influence of impact height compared to the mass effect is concluded to be marginal. All in all it has to be stated that the pedestrian protection packages of modern SUV frontends that fulfill regulatory as well as the biomechanical requirements assessed by the FlexPLI do not necessarily take sufficiently into account the influence of the upper body mass during a pedestrian vehicle collision. It is therefore recommended to aim for the introduction of an upper body mass for the assessment of leg injuries caused by SUV frontends.

Testing a Sedan front shape also revealed the very limited effect of an increased impact height in comparison to the application of an upper body mass. Therefore, the UBM effect on Sedan shaped car fronts needs to be investigated further.

CONCLUSIONS

In the present study the final built level of the FlexPLI foreseen for the implementation within global legislation on pedestrian protection was evaluated. The robust impactor shows an output that is mostly 10 to 20 percent higher than that of the previous built level. An extension of the test

series to vehicles with different front shapes is recommended. The repeatability and reproducibility of test results has been improved especially by eliminating the previously dissymmetrical knee design along with possible knee twist. Due to an inconsistent tibia acceleration signal caused by high vibration during the impact it is recommended to remove the tibia accelerometer because the output value is not found to give any usable additional information.

A new impactor certification method is recommended to be introduced for the Flex-GTR and new tentative injury threshold values are derived.

For an improved assessment ability of cruciate ligament injuries and a development of ACL/PCL injury risk functions, further research on the knee injury mechanisms is needed.

Gaps regarding the assessment of the risk of femur fracture are proposed to be closed by the introduction of an upper body mass developed in the FP 6 project APROSYS rather than by an increased impact height because latter one does not compensate the effects of a missing upper body mass of the FlexPLI. However, further research in this field is needed. It is therefore recommended to extend the study on the influence of the upper body mass to more vehicle frontend shapes in order to generate a classification of vehicles to be tested with the FlexPLI with upper body mass.

ACKNOWLEDGEMENT

The Federal Highway Research Institute (BAST) would like to thank Ford-Werke GmbH and Volkswagen AG for the provision of vehicles and spare parts, JARI/JAMA for the loan of the Flex-GT and GTR impactors, ika for the provision of the upper body mass and the FP6 project APROSYS for the contribution of results.

REFERENCES

Been B. 2008. „Design freeze status Flex-PLI-GTR development: Mechanical and electrical design.” Docs TEG-054 and TEG-055 of 6th Meeting of the GRSP Flex PLI Technical Evaluation Group. Bergisch Gladbach, March 31st.

Bhalla K., Bose D., Madeley N., Kerrigan J., Crandall J. 2003. „Evaluation of the response of mechanical pedestrian knee joint impactors in bending and shear loading.“ Paper no. 429 of ESV conference proceedings.

Bovenkerk J., Zander O. 2009. “Evaluation of the extended scope for FlexPLI obtained by adding an

upper body mass.” Deliverable D333H of the European FP6 research project on Advanced Protection Systems (APROSYS).

Compigne S., Martinez L. 2009. “New or improved test methods to address lower and upper leg impacts.” Deliverable D333B of the European FP6 research project on Advanced Protection Systems (APROSYS).

European New Car Assessment Programme. 2009. “Pedestrian Testing Protocol Version 4.3.”

EEVC Working Group 17. 2002. „Improved test methods to evaluate pedestrian protection afforded by passenger cars.“ December 1998 report with September 2002 updates.

International Harmonised Research Activities (IHRA). 2004. Draft Meeting Minutes for the 16th Expert Meeting of IHRA Pedestrian Protection. Australia.

Ivarsson J., Lessley D., Kerrigan J., Bhalla K., Bose D., Crandall J., Kent R. 2004. „Dynamic response corridors and injury thresholds of the pedestrian lower extremities.“ IRCOBI conference proceedings.

Japan Automobile Manufacturers Association (JAMA). 2008. “Injury threshold for the Flex-PLI tibia bending moment (JAMA-Proposal).” Doc TEG-077 of 7th Meeting of the GRSP Flex PLI Technical Evaluation Group. Bergisch Gladbach, December 8th.

Japan Automobile Manufacturers Association (JAMA) and Japanese Automobile Research Institute (JARI). 2007. “Evaluation of pedestrian lower extremity protection level provided by the FlexPLI (for discussion).” Doc TEG-049 of 5th Meeting of the GRSP Flex PLI Technical Evaluation Group. Bergisch Gladbach, November 29th.

Kerrigan J., Bhalla K., Madeley N., Funk J., Bose D., Crandall J. 2003. „Experiments for establishing pedestrian-impact lower limb injury criteria.“ SAE World Congress, SAE paper no. 2003-01-0895

Konosu A. 2007. “Review of injury criteria and injury thresholds for Flex-PLI.” Doc TEG-048 of 5th Meeting of the GRSP Flex PLI Technical Evaluation Group. Bergisch Gladbach, November 29th.

Konosu A. 2008. “Status Report on Flexible Pedestrian Legform Impactor Technical Evaluation Group (Flex-TEG) Activities.” Inf. Doc GRSP-44-

28 of 44th Meeting of GRSP. Geneva, December 10th – 13th.

Konosu A., Ishikawa H., Tanahashi M. 2001. „Reconsideration of injury criteria for pedestrian subsystem legform test - problems of rigid legform impactor -.“ Paper no. 01-S8-O-263 of ESV conference proceedings.

Konosu A., Issiki T., Suzuki H. 2007. „Information on flexible pedestrian legform impactor type GT (Flex-GT).“ Doc TEG-033 of 4th Meeting of the GRSP Flex PLI Technical Evaluation Group. Bergisch Gladbach, April 2nd.

Konosu A., Issiki T., Tanahashi M. 2005. „Development of a biofidelic flexible pedestrian leg-form impactor (Flex-PLI 2004) and evaluation of its biofidelity at the component level and at the assembly level. SAE World Congress paper no. 2005-01-1879.

Konosu A., Issiki T., Tanahashi M., Suzuki H. 2007-2. “ Development of a biofidelic flexible pedestrian legform impactor Type GT (Flex-GT).“ Paper no. 07-0178 of 20th ESV conference proceedings.

Konosu A., Tanahashi M. 2003. “Development of a biofidelic pedestrian legform impactor - introduction of JAMA-JARI legform impactor Ver.2002.” Paper no. 378 of 18th ESV conference proceedings.

Mallory A., Stammen J. 2008. „Design of a proposed upper body mass (UBM).“ Doc TEG-065 of 6th Meeting of the GRSP Flex PLI Technical Evaluation Group. Bergisch Gladbach, March 31st.

Mertz, H. 2004.: “Calculation methods & acceptance levels for assessing repeatability and reproducibility (R & R).“ ISO/TC22/SC12/WG5 Document N751.

Nyquist G., Cheng R., El-Bohy A., King A. 1985. “Tibia bending: strength and response.” Proceedings of the 29th Stapp Car Crash Conference, SAE paper no. 851728.

United Nations Economic Commission for Europe. 2009. “Global Registry: Agreement concerning the establishing of global technical regulations for wheeled vehicles, equipment and parts which can be fitted and/or be used on wheeled vehicles (ECE/TRANS/132 and Corr.1) – Addendum: Global technical regulation No. 9 Pedestrian Safety.” ECE/TRANS/180/Add.9 and ECE/TRANS/180/Add./Appendix 1, 26 January.

Wittek A., Konosu A., Matsui Y., Ishikawa H., Sasaki A., Shams T., McDonald J. 2001. “A new legform impactor for evaluation of car aggressiveness in car-pedestrian accidents.” Paper no. 184 of 17th ESV conference proceedings.

Zander O. 2007. ”Bewertung des Schutzpotentials moderner Fahrzeugfronten mit dem flexiblen Beinprüfkörper (FlexPLI).“ Proceedings of Praxiskonferenz Fußgängerschutz.

Zander O. 2007-2. ” Flex-GT: Repeatability and reproducibility of assembly certification and inverse test results.” Doc TEG-051 of 5th Meeting of the GRSP Flex PLI Technical Evaluation Group. Bergisch Gladbach, December 7th.

Zander O. 2008. “Current status of the FlexPLI evaluation.” APROSYS SP3 Workshop on initial concepts for new or improved vulnerable road user test methods. Brussels, Belgium.

Zander O. 2008-2. ”Flex-GTR: Open questions and proposals for ACL, PCL and MCL injury thresholds.” Doc TEG-078 of 7th Meeting of the GRSP Flex PLI Technical Evaluation Group. Bergisch Gladbach, December 8th.

Zander O., Gehring D., Leßmann P. 2009. „Future pedestrian protection requirements for modern vehicle fronts with respect to the introduction of the flexible pedestrian legform impactor (FlexPLI)“ crash.tech Conference Proceedings.

Zander O., Leßmann P., Gehring D. 2008. „Dynamic full assembly certification test procedure (inverse test setup) in conjunction with functional test.” Doc TEG-075 of 7th Meeting of the GRSP Flex PLI Technical Evaluation Group. Bergisch Gladbach, December 8th.

Zander O., Lorenz B. 2006. “ Assessment of the flexible pedestrian legform impactor (FlexPLI-G) as a test tool for legislation on pedestrian protection.” IRCOBI conference proceedings.

Zander O., Lorenz B., Gehring D., Leßmann P. 2007. “Prediction of lower extremity injury risks during an impact on modern car fronts with a flexible pedestrian legform impactor and the pedestrian legform impactor according to EEVC WG 17.” Paper no. 07-0206 of 20th ESV conference proceedings.

Zander O., Lorenz B., Leßmann P., Gehring D. 2005. “The pedestrian legform impactor according to EEVC WG 17 - results of an actual research and possibilities for the implementation within regulations on pedestrian protection.” IRCOBI conference proceedings.

EVALUATION OF THE EFFECTIVENESS OF PEDESTRIAN PROTECTION SYSTEMS THROUGH IN-DEPTH ACCIDENT INVESTIGATION, RECONSTRUCTION AND SIMULATION

José Manuel Barrios

Andrés Aparicio

Arturo Dávila

IDIADA Automotive Technology SA (1)

Spain

Juan Luis de Miguel

Sara Modrego

Ana Olona

Centro Zaragoza, Accident Research and Traffic Safety (2)

Spain

Alexandro Badea

Arturo Furones

Francisco Javier Páez

INSIA- UPM Accident Research and Vehicle Dynamics (3)

Spain

José María Martín

SERNAUTO (4)

Spain

Paper Number 09-0376



ABSTRACT

Around 15% of traffic accident casualties in Europe are pedestrians. To date, most of the studies carried out only provide statistical information on the problem and few in-depth studies provide countermeasures which might correct it.

There are many studies concerning pedestrian protection, which can be grouped into 'pedestrian modelling', 'biomechanical limits for pedestrians' and 'statistical analysis for pedestrian accidents'. Despite these studies, there is no predictive analysis of the benefits of pedestrian protection systems based on their intrinsic capabilities applied to a real accident sample.

This paper describes a methodology for the evaluation of pedestrian protection systems based on the analysis of a wide sample of urban pedestrian accidents. All of them are analysed in-depth and reconstructed with PC-Crash®. The effects of the frontal structure of the vehicles and several active systems, such as BAS and Pedestrian Detection Systems are evaluated.

The paper includes the description of the methodology followed for a sample of approximately 140 pedestrian urban accidents in three cities of Spain (Madrid, Barcelona and Zaragoza) and the corresponding reconstructions generated with PC-Crash®. Then, a methodology to simulate the passive and active improvements (including pedestrian friendly structure, BAS and Pedestrian Detection Systems) is defined and applied to all sample accidents. The results of these

new simulations are used to evaluate the benefits of these systems. The main conclusions are discussed, accounting for the limitations of the study, which basically lie in the modelling of the Pedestrian Detection Systems.

The methodology proposed in this paper can be applied to other vehicle safety devices to evaluate their effectiveness, based on the analysis of real accidents. All the results presented here come from a project partly funded by the Spanish Ministry of Industry.

In-depth Analysis of a Sample of Pedestrian Accidents

The following general methodology was used for the pedestrian accident analysis:

- Accident Scenario Information
 - Accident description
 - Sketch
 - General photographs
 - Pedestrian Data
- Analysis and information process
 - Damage to the vehicle
 - Pedestrian injuries
 - Injury description
 - Injury mechanism
- Virtual reconstruction of the accident
 - Vehicle parameters and profile definition
 - Pedestrian model
 - Simulation with PC-Crash®
 - Tyre-road adherence
 - Impact velocity

- Previous phase to the pedestrian accident

Definition of the Simulation Methodology with PC-CRASH® and Parameter Adjustment

Once the initial phase of information compilation from the accident scenario is complete, and after having carried out the complete analysis of that information, a series of input data is obtained for simulation with PC-Crash®.

The first step in the reconstruction of the pedestrian accident is the definition of a complete, scaled sketch of the accident scenario (street geometry and configuration, vehicles involved in their initial, intermediate and final positions, manoeuvres, pedestrian trajectory, obstacles, distances, comments, etc). In the complete project, all sketches and accident analyses can be found for each case.

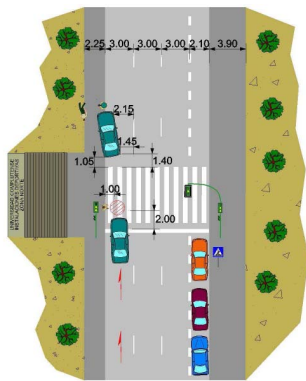


Figure 1. Sketch of the accident scenario.

The next step and according to the real situation, vehicle properties and parameters (make & model, manufacturing year, version, engine, weight, etc.) are chosen from the PC-Crash® data base. Some of these parameters can be modified according to the real case.

Related to this topic, the real geometry of the frontal profile of the vehicles involved has been measured in the available cases, as it is shown in the following figure. This geometry has been used during the virtual reconstructions.

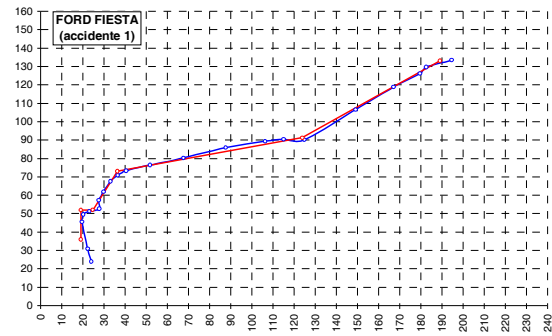


Figure 2. Real geometry of the frontal profile of the vehicles.

Once the vehicle and its parameters have been adjusted properly, the pedestrian model is defined by using a multi-body model created for this project, where height, weight, age and gender are taken into consideration.

Next, the adherence conditions are defined by adjusting the pedestrian-vehicle and pedestrian-ground friction coefficients, adding the dynamic adherence of the tyres.

Finally, the pedestrian accident is simulated. All the information about the parameters involved, driver manoeuvres before the accident, reactions, events, initial speed, etc. are included and adjusted for the simulation. In order to simplify and standardize the simulations, some basic criteria were established:

- Driver reaction time is always 1 second.
- The time reaction for a conventional brake system is 0.25 second.
- The possible perception point (PPP) is the point where the pedestrian invades the lane where the vehicle was driving.
- Just before the accident and according to the case, the vehicle can drive with constant speed (without reaction), brake with medium intensity (pre-established value) or brake with maximum intensity (skid marks were seen on the accident place).

Analysis of the Sample of Studied Accidents

A data base for 139 pedestrian accidents from three representative cities in Spain (Madrid, Barcelona and Zaragoza) was created. It includes information on the vehicle, person (anthropomorphic variables, injury codification), scenario and pedestrian accident kinematics. This data base constitutes one of the most complete data bases for pedestrian protection studies in Europe. In general, the studied

cases are frontal accidents involving touring cars inside urban areas.

The following characteristics have been analyzed:

- Time when the pedestrian accident happened
- Characteristics and geometry of the vehicle involved in the accident
- Pedestrian parameters:
 - Gender
 - Age
 - Height and weight (when available).
 - Walking velocity.
 - Relative to vehicle orientation before the accident.
- Injuries produced during the accident
 - Severity of pedestrian injuries

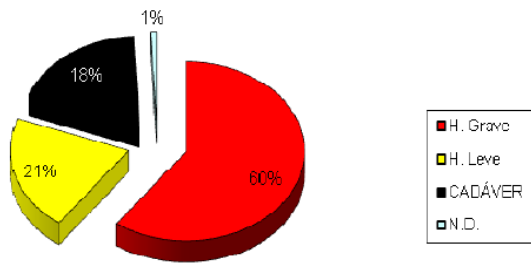


Figure 3. Severity of pedestrian injuries.

- Location and kind of injury

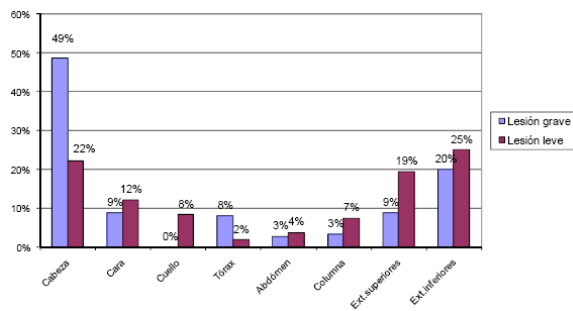


Figure 4. Body location and severity of injury.

- Distribution of the main injury mechanisms
- Driver manoeuvres before the accident

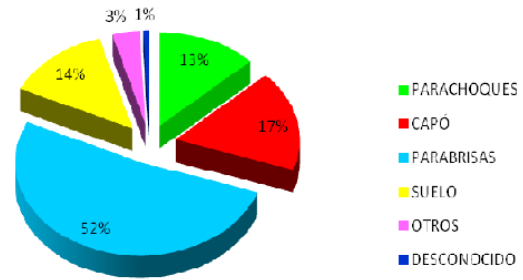


Figure 5. Principal Injury Mechanism Distribution.

According to the analyzed pedestrian sample accidents, the majority of them occurred in broad daylight. 93% of the vehicles involved in these accidents were passenger cars and most of them small cars. In almost half of the cases (49%) the vehicle was equipped with ABS, but only 8% of the total incorporated BAS. In 71% of the cases, the driver of the vehicle involved in the pedestrian accident tried to do a braking manoeuvre before the accident. 34% of the pedestrians were older than 60 years old, and 21% were younger than 20. 60% of the persons were seriously injured and 18% accounted as fatalities.

The majority of serious injuries occur in the head (49%) and lower extremities (20%). The most frequent injury mechanism is the vehicle (82%), for which the most important element is the windscreen (52%), followed by the bonnet (17%) and the bumper (13%). In 14% of the cases the most important injury for the pedestrian was produced when impacting against the ground.

Primary Safety Technologies Effectiveness Evaluation Methodology

PC-CRASH® Simulation Methodology for the Chosen Systems - Parameter adjustment and the simulation methodology for the primary safety systems subject to study (ABS+BAS System and pedestrian DETECTION + Automatic Brake system) are detailed in the entire project. Nevertheless, some of the most important aspects are emphasized in this paper.

Simulation Parameters - The parameters under simulation, bearing in mind the different performance of both braking systems (ABS+BAS and pedestrian DETECTION + Automatic brake systems) are:

ABS+BAS System:

- Pedestrian reaction time: pre established at 1 second.
- Brake System with BAS reaction time: pre-established at 0.1 second.

- ABS Action Frequency: in general 10 Hz.
- Adherence coefficient: general value.
- Tyre adherence curve (one of the four predefined models): implies the definition of the μ_{max} , μ_d , F_{max} , F_d values.
- Maximum deceleration possible depending on the chosen adherence model and the ABS performance.

Pedestrian DETECTION + Automatic Brake System:

- Detection range with risk sector division, remarking especially automatic system actuation area.

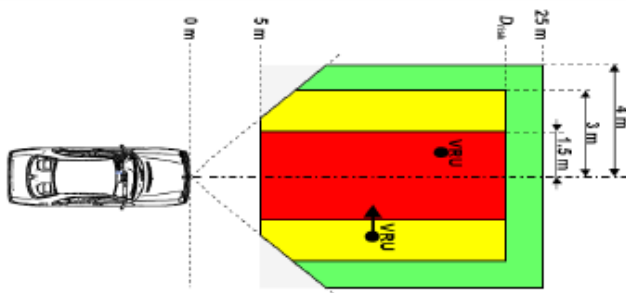


Figure 6. Division of the risk areas for the pedestrian DETECTION + Automatic Brake system.

- All parameters from the BAS+ABS system mentioned above, apply for the Automatic brake system

In both cases, simulations provide a series of parameters which can be used for the evaluation of the vehicle’s dynamic performance in each case. Some of these parameters are:

- Braking distance (S_f), by measuring directly in the simulation.
- Medium deceleration (a_k) from the resultant graphics.
- Brake time (t_f), directly from the simulation.

Simulation Algorithms

Simulation with ABS+BAS - Having previously defined the adherence model and tyre performance, ABS is activated in the vehicle options, the system reaction time is reduced from 0.25 seconds to 0.1 seconds and the brake force is amplified to the maximum (pedal position).

Simulation with BAS and Pedestrian Detection Systems - With the same configuration used before, the driver reaction time is eliminated and the entry moment for the BAS function is chosen based on the scope ratio established for the detection system.

Pedestrian Injury Risk Evaluation

Development of a Software Tool for Head Injury Risk Evaluation - A software tool for determining head injury risk values was developed in this project. After all possible impact points in the frontal part of a standard vehicle have been mapped; a bench test rig simulating the front part of a standard vehicle was built and validated by means of correlating the results with those of Euro NCAP tests.

By these means, a software tool for the determination of head injury risk values in different areas of the frontal part of the vehicle was developed in this project. As an example, some of the results for a speed of 30 km/h are shown in the next figure:

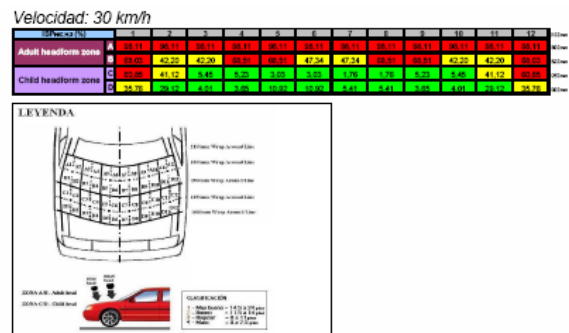


Figure 7. Head Injury Risk Value Evaluation by means of the developed software tool.

Methodology for Software Tool Application in PC-CRASH® Simulations - The software tool for determining head injury risk values developed in this project is applied to the simulations done with PC-Crash®, following the next algorithm:

As a result of the simulations, the value of the run over speed (V_k or V_{at}) is known; this is one of the input data in the application. Next, the head impact point with the vehicle has to be determined. This step lies in the application of the impact area matrix to the frontal part of the vehicle and the location of the pedestrian head contact cell.

Simulation is stopped when the pedestrian head impacts against the vehicle, instant in which two images are taken (cross-section and elevation). In the cross-section of the vehicle used during the

simulation, a wrap-around measurement is done and the contact line in the matrix is determined, as shown in **Figure 8**. The head impact column is also determined using the elevated view, as shown in **Figure 9**.

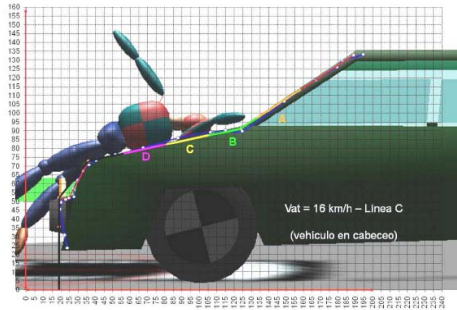


Figure 8. Head impact line determination.

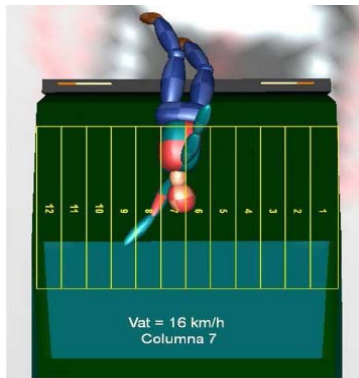


Figure 9. Head impact column determination.

The next step consists of choosing the vehicle make and model from the application data base and calculates the ISP (head injury risk index) value for the respective cell. In those cases in which the vehicle make and model were not included in the software application database, another similar model (with similar frontal cross-section) was chosen.

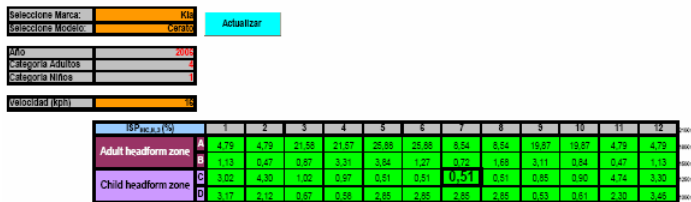


Figure 10. Head injury risk index ISP calculation (C7 cell, $V_{at} = 16$ km/h, ISP = 0.51).

RESULTS AND EVALUATION OF SYSTEM EFFECTIVENESS

In this section the results of the new simulations are used to evaluate the benefits of the systems. The main conclusions are discussed, taking into account

the limitations of the study, which basically lie in the modelling of Pedestrian Detection Systems.

Their efficiency, capacity for reducing run over speed, avoiding the accident or reducing the severity of the injuries produced are some of the aspects analysed in this section.

Many investigations discuss, from a general point of view, the reduction of distance and brake time by using BAS systems, concluding that the number of accidents can be reduced; but until now the benefits of the system as a primary safety tool for avoiding pedestrian accidents have not been looked at.

Even more interesting are the results obtained for the Pedestrian Detection Systems. In this case, the results obtained based on real accidents represent, a priori, an evaluation of the potential benefits of this kind of system. This information could be very appreciated for evaluating the cost/benefit ratio in case of implementation.

Efficacy and Influence on Run over Speed

According to the simulations, 48% of the pedestrian accidents analysed could have been avoided with a system of pedestrian detection and automatic brake. The brake system ABS+BAS would have helped the driver to avoid the accident in 11% of the cases. 44% of the accidents could not have been avoided with any of the analysed systems. See **Figure 11**:

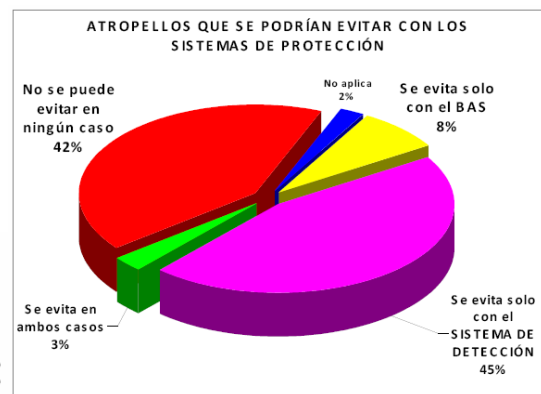


Figure 11. Pedestrian accidents that could be avoided by means of the use of the protection systems.

In the next figure, pedestrian accident reduction tendency with each of the two systems is shown.

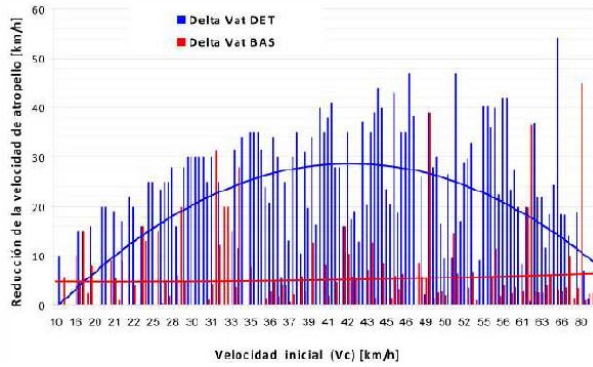


Figure 12. Reduction of the run over speed.

The blue curve represents the speed reduction obtained with the pedestrian DETECTION + automatic brake system and it reaches its peak value at about 42 km/h. In contrast, with the BAS system, the speed reduction remains practically constant (red line) at about 5-7 km/h.

In only 21% of the cases, the BAS system would have reduced vehicle speed in the moment of the accident to less than half of its initial driving speed. On the other hand, with the DETECTION+ Automatic Braking System this reduction would have happened in 74% of the cases.

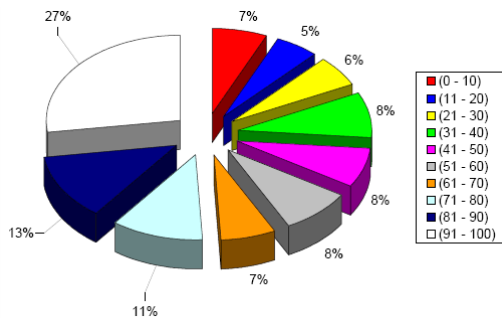


Figure 13. Percentage reduction of the pedestrian accident speed with the BAS system.

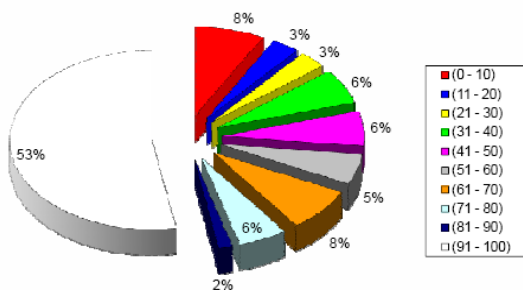
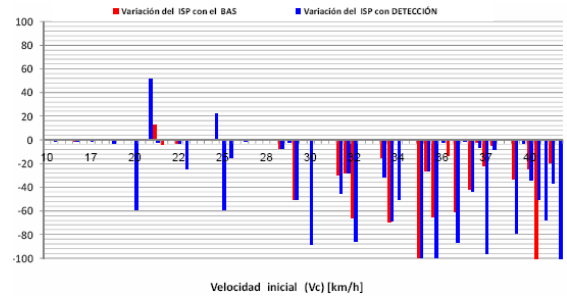


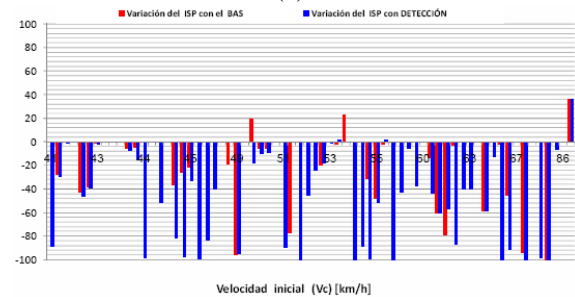
Figure 14. Percentage reduction of the pedestrian accident speed with the DETECTION + Automatic Brake system.

Influence of the Systems in Head Injury Risk

In the following figures the ISP (index that represents the probability of a serious head injury) based on driving speed is shown for both systems: BAS system and DETECTION + Automatic brake system.



(a)



(b)

Figure 15. Absolute variation of the ISP. (a) $V_c = 0 - 41$ km/h (b) $V_c = 41 - 87$ km/h.

In the following figure, the reduction (in percentage) of the ISP with the vehicle equipped with ABS+BAS in comparison to the ISP value in real life accidents is shown. It is observed that the ISP would be reduced by more than 80% in 18% of the cases.

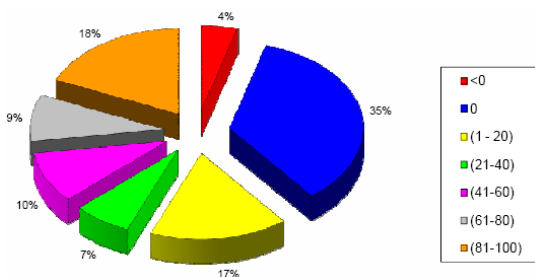


Figure 16. Relative reduction of the ISP with ABS+BAS.

As shown in the next figure, by equipping the vehicle with a DETECTION + Automatic Brake System the ISP is reduced by the same amount in 66% of cases.

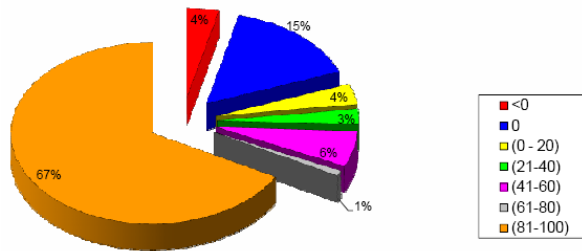
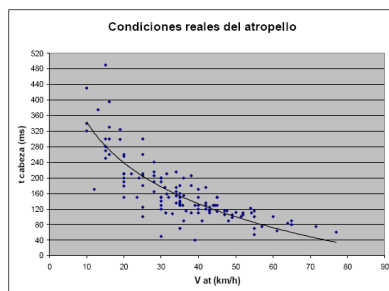


Figure 17. Relative reduction of the ISP with DETECTION + automatic brake.

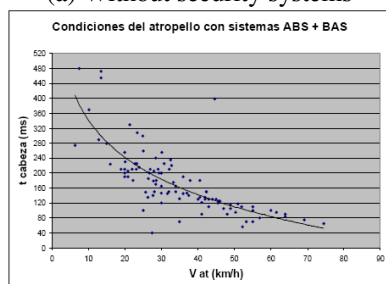
Influence on Parameters from Secondary Safety Devices

An important factor related to the actuating time of pedestrian protection devices installed in the frontal part of some vehicles, is the impact time of the pedestrian head on the vehicle from the moment in which the pedestrian lower extremities came in contact with the frontal part of the vehicle.

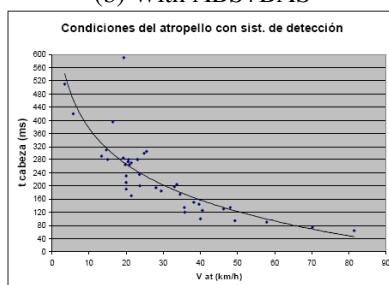
The impact time of the pedestrian head on the vehicle, according to the pedestrian accident speed, is shown in the following three graphics: (a) *without security systems* (b) *with ABS+BAS* (c) *with DETECTION + automatic brake system*.



(a) Without security systems



(b) With ABS+BAS



(c) With DETECTION + automatic brake system

Figure 18. Head impact time.

It is observed that the dot clusters for both systems (b) and (c) is displaced to the left and upwards compared to the real accident conditions (a). This fact is due to the lower pedestrian accident speed achieved with these systems and the increase of the pedestrian impact time with the vehicle

These times are used as a reference for pedestrian secondary protection systems which are activated once the pedestrian has impacted against the frontal bumper, such as, for example, an active bonnet and pedestrian protection external airbags installed in the bonnet and on the lower part of the windscreen.

CONCLUSIONS

This project is the result of collaboration between Spanish Research Institutes such as SERNAUTO (coordinator), Applus+IDIADA (participant), Centro Zaragoza (participant) and INSIA (subcontractor), and Local Traffic Authorities (Madrid, Zaragoza and Barcelona councils) who will have at their disposal a common methodology for pedestrian accident investigation.

A database for 139 pedestrian accidents was created, in which information of the vehicle, person (anthropomorphic variables, injury codification); scenery and pedestrian accident kinematics were included. This database constitutes one of the most complete databases for the study of pedestrian protection in Europe.

According to the analyzed pedestrian sample accidents, the majority of them occurred in broad daylight. 93% of the vehicles involved in these accidents were passenger cars with the majority of them being small cars. In almost half of the cases (49%) the vehicle was equipped with ABS, but only 8% of the total incorporated BAS. In 71% of the cases the driver of the vehicle involved in the pedestrian accident tried to do a braking manoeuvre before the accident. 34% of the pedestrians were older than 60 years old, and 21% were younger than 20 years old. 60% of the persons were seriously injured and 18% were fatalities.

The majority of serious injuries occur in the head (49%) and lower extremities (20%). The most frequent injury mechanism is the vehicle (82%), for which the most important element is the windscreen (52%), followed by the bonnet (17%) and the bumper (13%). In 14% of the cases the most important injury for the pedestrian was produced when impacting against the ground.

The compiled information has been used for the evaluation of the effectiveness of two primary

security systems: BAS (brake assistance system) and the Pedestrian Detection Systems. The performance of these two systems has been simulated during reconstructions done with PCCrash©, analyzing their capacity for reducing severity of run over accidents or for avoiding them.

A new software tool was developed for calculating head injury risk values based on the runover speed and the head impact point over the frontal part of the vehicle.

Both analyzed systems (BAS and Pedestrian Detection Systems) proved efficient for reducing severity of pedestrian accidents in the majority of cases. BAS is being progressively incorporated in the current fleet. Nevertheless, Pedestrian Detection Systems are still being investigated as a prototype.

Pedestrian Detection Systems would avoid run over cases by at least half and greatly reduce falling speed in the rest of the cases, which reduces the head injury risk. The brake assistance system (BAS) presents lower effectiveness in the prevention of pedestrian accidents compared to Pedestrian Detection Systems.

REFERENCES

[1] Applus+IDIADA, Centro Zaragoza, INSIA, 2007. "Investigación Industrial en la Protección de Peatones a partir del Estudio en Profundidad de Accidentes de Tráfico en Madrid, Zaragoza y Barcelona.", Proyecto FIT - 370100 - 2007 -51.

[2] Páez Ayuso, F. J y otros. "Avances en la seguridad pasiva de los vehículos para la protección de peatones". Revista DYNA. Vol. 84 nº2. Marzo 2009.

[3] Páez Ayuso, F. J y otros. "Problemas de la protección de peatones en accidentes de atropello". STA: revista de la Sociedad de Técnicos de Automoción. Vol. 163. 2004.

DEVELOPMENT OF FLEXIBLE PEDESTRIAN LEGFORM IMPACTOR FE MODEL AND COMPARATIVE STUDY WITH LEG BEHAVIOR OF HUMAN FE MODEL THUMS

Hiroshi Miyazaki
Yuichi Kitagawa
Tsuyoshi Yasuki
Masaaki Kuwahara
Fumio Matsuoka

Toyota Motor Corporation
Japan
Paper Number 09-0112

ABSTRACT

The current legform impactor in pedestrian safety tests uses a steel shaft connected to metal plates to represent the femur and tibia. It evaluates leg fracture risk based on tibia acceleration, and knee ligament rupture risk based on knee bending angle and shear displacement. However, the impactor does not generate the tibia deflection that occurs when a vehicle impacts a pedestrian. The new flexible pedestrian legform impactor (Flex-PLI) currently under development is designed to simulate the impact behavior of the human leg, reproducing tibia deflection with flexible shafts and representing the knee ligaments using wires. As a result, it can be used to help assess injury based on deformation by estimating the risk of tibia fracture from the bending moment of the tibia shaft and the risk of knee ligament rupture from the elongation of the wires.

In this study, a finite element (FE) model of the Flex-PLI was developed to examine the impact test protocol for pedestrian leg injury assessment, comparing the impactor behavior and response with that of a whole human FE model. The Flex-PLI FE model was created by reverse engineering that reproduced the shape and mechanical properties of each part. The impact velocity of the impactor was set to 40 km/h based on accident data. An impact height of 75 mm above the ground has been proposed for the Flex-PLI in contrast to the current protocol, which specifies an impact height of 0 mm. The study compared results at the base impact height of 75 mm with those obtained at different heights. It also investigated the effect of adding mass to simulate the upper body of a pedestrian. Vehicle-to-pedestrian impact simulations were conducted with the Total Human Model for Safety (THUMS) to estimate the behavior and response of a human leg for comparison with the results from the impactor model. The bending moment of the tibia and the elongation of the knee ligament wires in an impact varied depending on the impact height and additional mass. Impactor behavior was closest to THUMS at a height of 0 mm, but a closer response to THUMS for bending moment and

ligament elongation was obtained at 75 mm. It was also found that adding a mass of 6 kg to the upper end of the impactor in SUV impacts created a closer response to THUMS.

INTRODUCTION

In 2007, 5,744 fatalities occurred as a result of traffic accidents in Japan, roughly 30% of which were pedestrians. Pedestrians also accounted for 17% of serious injuries. 58% of the pedestrian fatalities sustained head injuries, while the lower extremities were the most frequently injured (37%) in all cases of injury.[1]

In 2003, the Japan New Car Assessment Program (JNCAP) began to assess pedestrian safety performance. Currently, only a head safety test is conducted, but another test protocol for lower leg injury assessment will be introduced in 2010. A proposal has also been drawn up to integrate a leg test into the Global Technical Regulations (GTR) that are observed as a set of international standards for vehicle safety in various countries around the world.[2] This proposal includes a new flexible pedestrian legform impactor (Flex-PLI) that is currently under development.[3] Whereas the current leg impactor uses rigid steel parts to simulate the femur and tibia, the new impactor expresses these portions with bendable flexible materials. It also uses wires to represent the ligaments in the knee joints. Development of the Flex-PLI began in 2000,[4] and a proposal for its final specifications was announced in 2008.

Studies into the conditions for the leg test have continued during the development of the Flex-PLI. It is currently proposed to collide the Flex-PLI with a vehicle at a height of 75 mm from the ground. It has been reported that the results for leg bone deflection and knee ligament elongation obtained from the impactor at a height of 75 mm are close to the response of a pedestrian's leg.[5] However, since this setting results in the initial knee joint being positioned higher than the knee of an actual pedestrian, it must be verified whether the effect of the shape of the front edge of the vehicle can be adequately evaluated.

It has also been pointed out that the mass of the pedestrian's upper body has an effect on leg behavior.[6] Behavior is also thought to be affected by the fact that legs are inclined inward from the vertical while walking.

The study focused on the following three factors using an FE model of the Flex-PLI. Comparing the impact behavior and mechanical response of this model with a human FE model, this paper discusses the optimal test conditions for predicting and assessing full-body pedestrian behavior and injury criteria.

- Impact height
- Additional mass for simulating the upper body
- Impactor inclination angle

The Flex-PLI FE model was created by reverse engineering from the actual Flex-PLI. The Total Human Model for Safety (THUMS) FE model was used for the comparison.

METHODS

Human FE Model

Outline of THUMS - THUMS is a human FE model jointly developed by Toyota Central R & D Labs., Inc. and Toyota Motor Corporation. Figure 1 shows a standing THUMS model simulating a pedestrian crossing a road. THUMS has a height of 175 cm and a mass of 77 kg to simulate a 50th percentile American male (AM50). In its walking pose, the left leg is inclined 22 degrees forward of the body and the right leg is inclined 7.2 degrees to the rear, based on the standard acetabulum angles. Both arms are hanging downward and both hands are positioned slightly in front of the torso. Parts for simulating shoes have also been added to the soles of the feet. As a result, the inferior surface of the calcaneus is positioned at a height of 29 mm from the ground. THUMS includes the major skeletal and soft tissue that form the interior of the body. The skeleton is divided into cortical and cancellous bones, which are modeled using shell and solid elements, respectively. The cortical bones are modeled with elasto-plastic properties, and bone fractures are simulated by eliminating elements where strain exceeds a threshold. The physical properties of the bones were defined in reference to the values described by Yamada et al.[7] The threshold value for bone fracture strain was assumed to be 3%, based on the study by Burstein et al.[8] The joints are modeled with bone-to-bone contacts and ligament connections, without using artificial joint elements provided in FE codes. In the same way as bone fracture, ligament rupture is simulated by eliminating elements where strain exceeds a threshold. The physical properties of ligament tissue were defined in reference to the

values described by Abe et al. (1996). Kerrigan et al. reported a range of approximately 11 to 20% as the critical stretch for ligament rupture.[9] The study assumed an elongation of 15% as the threshold. Subcutaneous fat, muscle, organs, and other soft tissue were modeled with solid elements. However, neck and leg muscles are modeled with bar elements to reproduce only their resistance force when forcibly extended. THUMS contains approximately 80,000 elements and has approximately 60,000 nodes.



Figure 1. Pedestrian THUMS (AM50).

Validation of Leg Model - The validity of the THUMS leg was examined by comparing its mechanical response with test data reported in literature using post mortem human subjects (PMHS). Figure 2 shows a comparison between force-deflection curves calculated using the THUMS leg model and test data obtained by Yamada et al.[7] for mechanical response to static 3-point bending of the femur, tibia, and fibula bones. In the calculations, the tests were simulated by

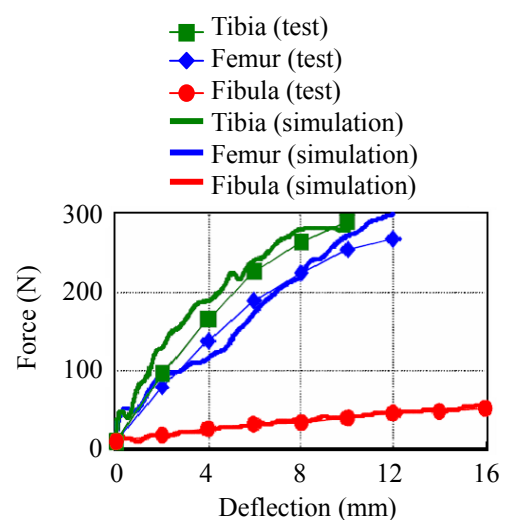


Figure 2. Comparison of force-deflection curves for THUMS response and test results.

removing each bone model from THUMS. The bones were then supported at both ends before being contacted in the center by an impactor. In the figure, the solid lines show the test results and the lines marked with symbols show the calculation results. The force curves obtained from the models correspond closely with the force curves obtained from the tests.

Figure 3 shows the relationship between knee bending angle and knee bending moment when a knee ligament ruptures. The data is obtained from 3-point bending tests performed by Kajzer et al.,[10],[11] Levine et al.,[12] and Ramet et al.[13] on PHMS knees. The results are mainly distributed within the dotted line circle. Previous studies have reported that the medial collateral ligament (MCL) is likely to be ruptured in a vehicle-to-pedestrian impact. The MCL of THUMS is modeled to rupture when the bending moment around the knee joint exceeds approximately 200 Nm. This condition is close to the center of the data distribution in this figure.

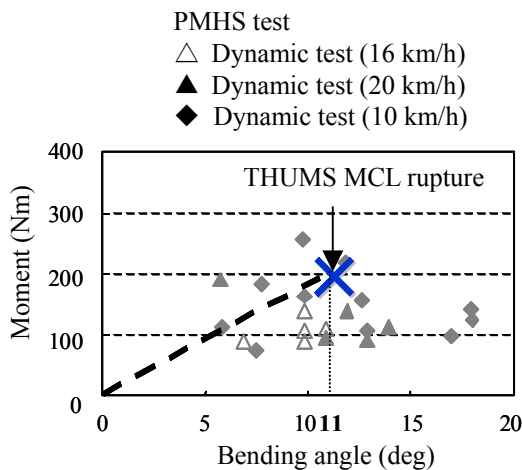


Figure 3. Comparison of knee bending moments.

The comparative verification described above shows that the mechanical response of the femur, tibia, fibula, and knee ligaments (MCL) in THUMS corresponds closely with that of the human body (PHMS).

Development of Flex-PLI FE Model

Flex-PLI - Figure 4 shows the exterior of the Flex-PLI and Table 1 lists its dimensions. The Flex-PLI was created using the values of a 50th percentile American male. It has a body portion consisting of a femur, knee joint, and tibia, and an exterior flesh portion.

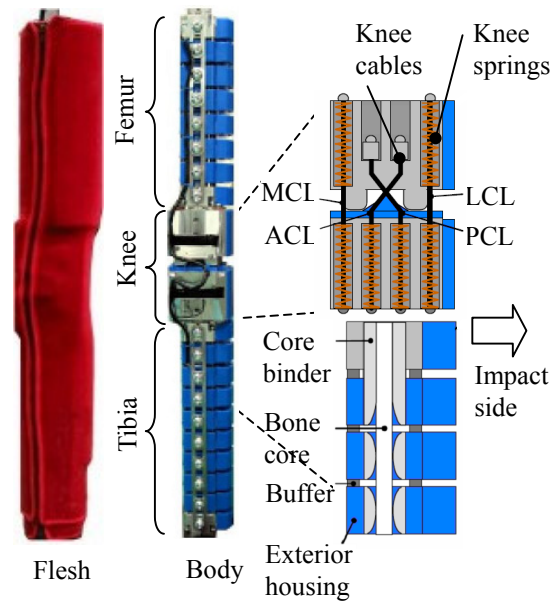


Figure 4. Flex-PLI.

Table 1. Dimensions of AM50 and Flex-PLI

	AM50[14]	Flex-PLI
Femur length (mm)	428	434
Tibia length (mm)	493	494
CG of thigh* (mm)	218	202
CG of tibia* (mm)	233	216
Total mass (kg)	13.4	13.5
Femur mass (kg)	8.6	7.4
Tibia mass (kg)	4.8	6.1

* from the knee joint center

The femur and tibia are each constructed from multiple divided block portions, through the center of which a glass fiber reinforced plastic (GFRP) core runs from top to bottom. The tibia and femur cores are joined to the lower and upper knee joint blocks, respectively. Leg bone deflection is reproduced using the flexure of the core. To prevent breakage in excessive bending deformation, four stopper cables are inserted in the block parts.

The knee joint is constructed from the tibia- and femur-side blocks and wires connecting the blocks. The wires are connected to springs inside the knee blocks that are used to simulate the elongation of ligaments. As shown in Figure 4, the knee is provided with crossed wires to simulate the cruciate ligaments. The wires are designed to extend when the knee joint bends.

Rubber sheeting and neoprene are wrapped around the exterior of the impactor from the femur to the tibia. As the rubber sheeting is designed to simulate

the shape of the femur and calf, the role of the neoprene is to hold the parts in place and alleviate the impact. The upper end of the impactor is also provided with a suspension jig that is used for performing the tests.

The Flex-PLI measures bending moment to assess the risk of leg bone fracture and injury. As shown in Figure 5, bending moment is evaluated at three locations along the femur, and four locations along the tibia. Bending moment is calculated from the output values of strain gages attached to the bone core.

The risk of knee ligament rupture is assessed based on the elongation amount of the wires representing each ligament. There are a total of four wires, representing the anterior cruciate ligament (ACL), posterior cruciate ligament (PCL), MCL, and lateral collateral ligament (LCL). The elongation of each knee ligament is output from the potentiometers provided in the Flex-PLI.

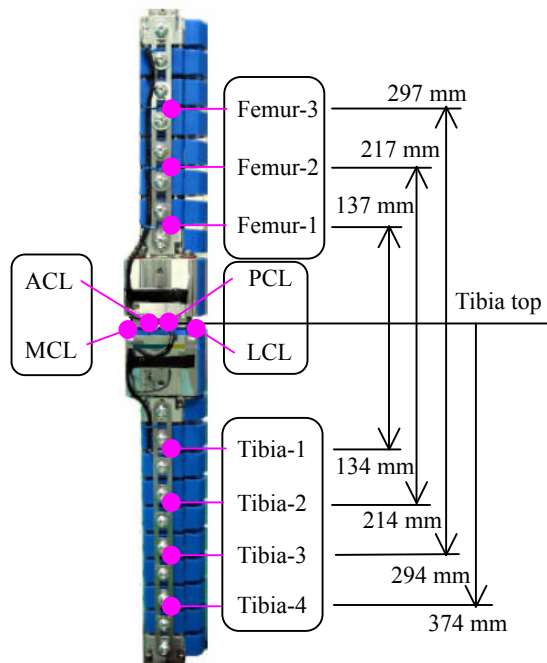


Figure 5. Measurement points.

Development of FE Model by Reverse Engineering - The FE model development process consisted of three stages: measurement of the actual geometry of the Flex-PLI, 3D reconstruction of the geometry data, and the generation of an FE mesh. Non-contact X-ray computerized tomography (CT) was used to measure the surface and internal shapes of the Flex-PLI. Using X-ray CT scans of an assembled Flex-PLI enabled the actual shapes of the component parts to be obtained, as well as positional information of these parts in an assembled state. First, an actual Flex-PLI was scanned at a pitch of 0.5 mm to express the whole

of the impactor including its internal structure as point group data. The point group data was filtered while adjusting the CT values to specify and read the steel, aluminum, and non-metallic parts. This data was converted to stereolithography (STL) format 3D polygon data, which was then used as the basis to prepare the surface data for FE mesh creation. In generating the FE mesh, the element size was controlled to 2 to 3 mm so that the bone core was divided into five sections in the thickness direction.

Figure 6 shows the created FE model and Table 2 lists the number of nodes and elements in the model. Parts with a thickness of 1 mm or more were modeled using solid elements and parts with a thickness of less than 1 mm were modeled using shell elements. The springs, stopper cables, and ligaments in the knee blocks were modeled from beam elements and the rotatable pin joints were modeled from joint elements.

The mechanical properties of the materials of the bone core, flesh rubber, neoprene, cushion rubber, wire cables, internal knee block springs, and other parts that are thought to have a major impact on impactor response were measured, and the obtained values were input into the FE model. These input values were validated by subjecting the FE model to the same analysis as performed in materials tests. The other parts were treated as rigid bodies. The mass of the individual parts was set to the same values as the actual Flex-PLI.

It should be noted that the structure and shape of the created Flex-PLI are identical to the Flex-GT impactor announced in 2007.[15]

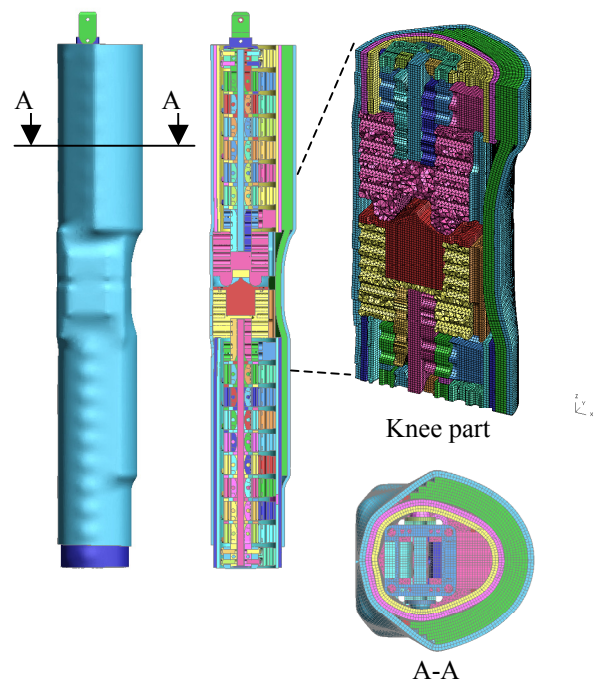


Figure 6. Flex-PLI FE model.

Table 2.
Description of Flex-PLI FE model

		Nodes	Elements
Whole model		1,330,000	1,900,000
Part	Femur	220,000	290,000
	Knee	80,000	270,000
	Tibia	260,000	360,000
	Flesh	770,000	980,000

Injury Criteria Assessment Using Flex-PLI FE Model - Strain was measured in the FE model by elements representing the strain gages in the actual Flex-PLI. Knee ligament elongation was calculated from the elongation of the beam elements simulating the wires.

The injury criteria judgment conditions were set to 299 Nm for the tibia bending moment threshold and 18 mm for the MCL elongation threshold.[16]

Model Validation

The Flex-PLI was tested using quasi-static 3-point bending tests on each of the femur, tibia, and knee joint sub-assemblies, and dynamic pendulum tests on the body assembly.[15]

First, the FE model was validated under the conditions of the quasi-static 3-point bending tests for each sub-assembly.

The tibia test was performed by fixing both ends of the tibia sub-assembly on cylindrical supports with a radius of 75 mm. The distance between the supports was 410 mm. A round block was attached on the impact side of the force application point to the outside of the bone form, and a neoprene pad with a thickness of 5 mm was placed between the block and the load cell. A force of 1.33 mm/s was applied from the impact side to the center of the supports using a 40 mm diameter cylindrical impactor.

In the FE model, the supports at both ends were simulated using rigid bodies and connected to the ends of the tibia. The force was applied at 133 mm/s. (100 times of experiment)

Figure 7 compares the actual Flex-PLI in its bent form (deflection: 26 mm) with the FE model. It also shows the graph that compares the bending moment-deflection curves of the FE model and actual Flex-PLI. The bending moment generated at the force application point (Equation 1) is plotted on the vertical axis and the deflection is plotted on the horizontal axis. The moment was calculated using Equation 1 as follows.

$$M = \frac{F}{2} \times \frac{D}{2} \tag{1}$$

where,

M: 3-point bending moment (Nm)

F: Force (N)

D: Deflection (m)

The curve for the Flex-PLI is shown as a corridor calculated from multiple experiment results. The bending moment curve for the FE model fits inside the Flex-PLI corridor. The same comparison was performed for the femur and it was verified that the moment response of the FE model fitted inside the corridor calculated for the Flex-PLI.

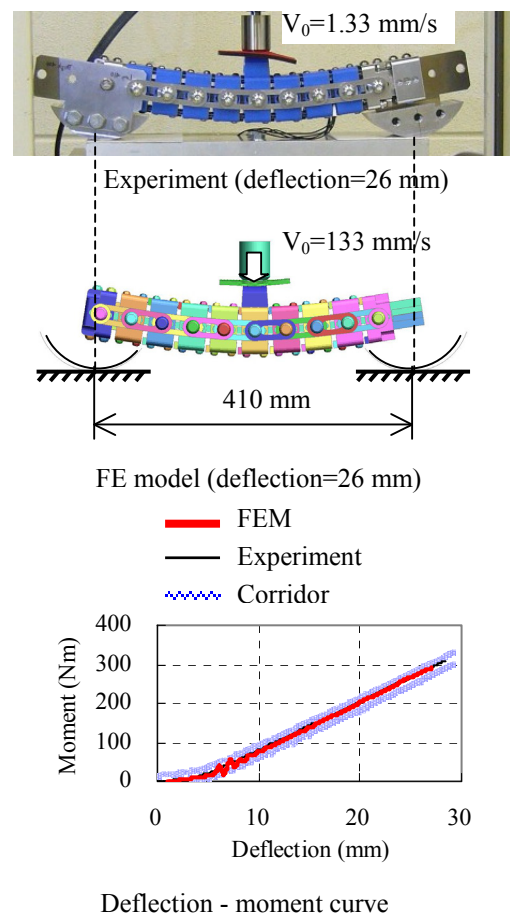


Figure 7. Quasi-static 3-point bending test of tibia sub-assembly.

Figure 8 shows the knee sub-assembly of the Flex-PLI FE model simulating the knee bending test and compares the MCL force-elongation curves obtained by the FE model and in the actual tests. In the testing, both ends of the knee joint were fixed on cylindrical supports with a radius of 75 mm to create a distance between the supports of 400 mm. A neoprene pad with a thickness of 5 mm was placed at the force application point and a force of

1.0 mm/s was applied from the impact side using a cylindrical impactor with a radius of 50 mm. A response corridor was generated from multiple test data.

In the FE model, the supports at both ends were simulated using rigid bodies and connected to the knee blocks. The force was applied at 500 mm/s. (500 times of experiment)

It was confirmed that the results of the FE model closely reproduced the MCL elongation characteristics and fell within the test corridor. The same comparison was performed for the elongation of other ligament wires and the bending moment of the knee joint. The elongation values of the FE model were also confirmed to be within the response corridor of the Flex-PLI.

The FE model was then validated with respect to the dynamic pendulum test applied to the body assembly. The test was conducted by suspending it by the jig at the upper end. Then, using this point as a reference, the Flex-PLI was raised 15 degrees from the horizontal and released, causing the femur-side knee block to impact the fixed stopper on the test device. A rubber and neoprene pad (width: 100 mm, height, 100 mm, thickness: 25 mm) was attached to the surface of the stopper. The bending moment at each part of the Flex-PLI and elongation of each ligament on impact were

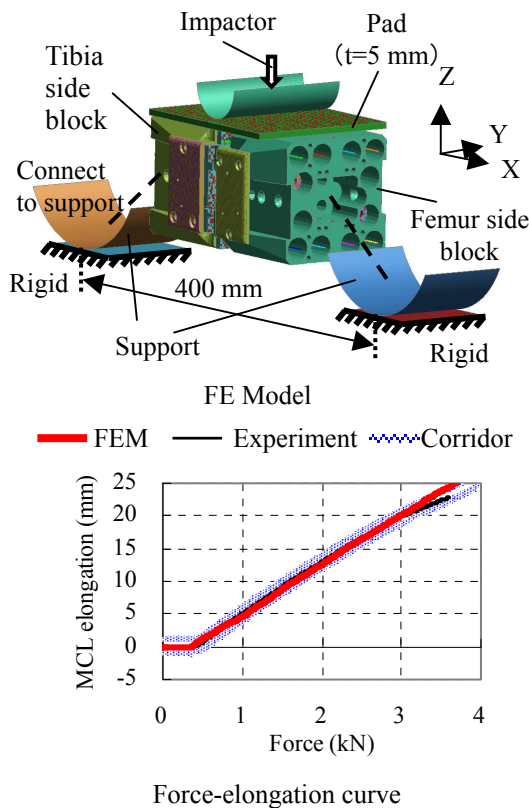


Figure 8. Quasi-static 3-point bending test of knee sub-assembly.

measured.

In the FE model, the support conditions of the Flex-PLI were reproduced and calculation started after applying an angular velocity from a position immediately prior to impact.

Figure 9 shows the deformed shape of the Flex-PLI at 22 ms, when the tibia bending moment was greatest. It also shows the deformed shape of the FE model at the same time, and as an example of the results, the time history of the bending moment at the tibia-1 measurement position and MCL

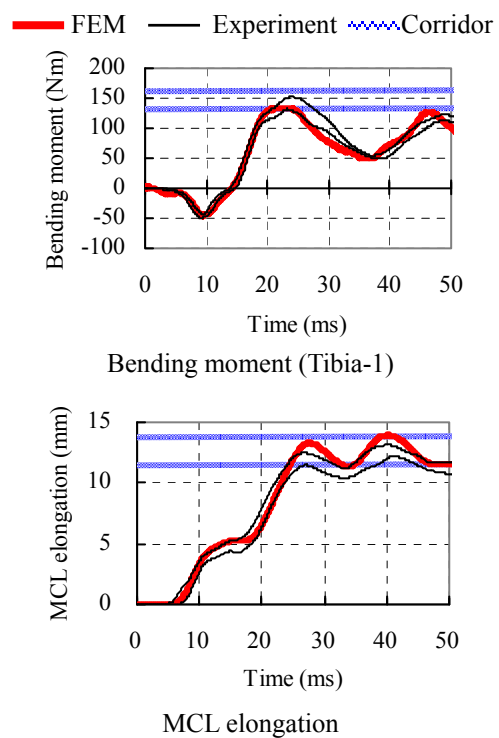
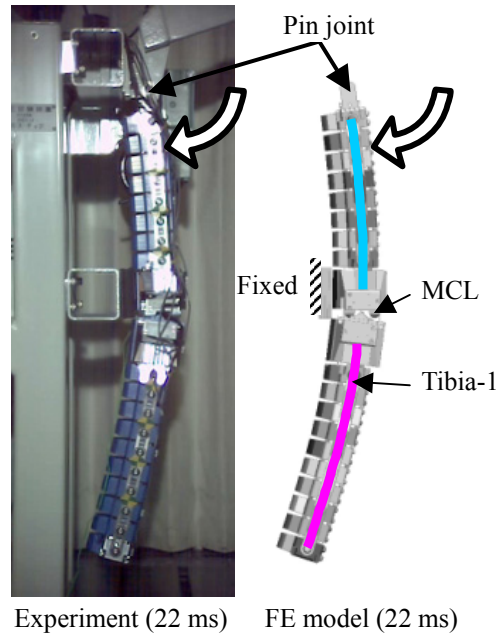


Figure 9. Flex-PLI assembly dynamic pendulum test.

elongation. The way that the Flex-PLI bodies bend, the movement of the lower portion, and the waveforms for bending moment and MCL elongation indicate a close correlation between the FE model and the test results. In the test, response was deemed acceptable if the peak moment fell within the test corridor. As the peak moment of the FE model was calculated to be within the corridor, the test conditions were judged to be satisfied. The bending moment at measurement positions other than tibia-1 and the elongation for knee ligaments other than MCL also showed a close correlation with the waveforms obtained in tests. The values of the FE model were confirmed to be within the test corridors.

Vehicle Models

Two models representing the front end of a sedan and a SUV, as adopted by Yasuki et al. were used in this study.[17],[18]

The bumper cover of the sedan model is made from polypropylene (PP) and the internal structure is provided with two absorbers, one in the upper portion and the other in the lower. The upper absorber is fixed in front of the bumper reinforcement and has properties corresponding to polyurethane with an expansion ratio of 40 at thickness of 65 mm. The lower absorber is connected rigidly with the body at its rear end and has properties corresponding to polyurethane with an expansion ratio of 10 at a thickness of 150 mm. The hood is aluminum and an acrylonitrile butadiene styrene (ABS) grille is provided between the hood and the bumper cover. The vehicle mass is 1.7 tons and the model includes approximately 145,000 elements and approximately 150,000 nodes.

The bumper cover of the SUV model is PP and one internal bumper absorber is provided. This absorber is fixed in front of the bumper reinforcement and has properties corresponding to polyurethane with an expansion ratio of 40 at a maximum thickness of 65 mm. The hood is steel and the grille is made from ABS. The vehicle mass is 2.9 tons and the model includes approximately 320,000 elements and approximately 330,000 nodes. The SUV model includes drive train components such as the suspension, tires, and engine, but these parts are regarded as having only a small impact on legform impactor conditions.

Impact Simulations

Figure 10 shows the study model. The center sections of the vehicle models are displayed and the positions of the upper and lower absorbers are highlighted. The impact simulation with THUMS

assumed a pedestrian-to-vehicle impact at 40 km/h where the vehicle model collided against a stationary THUMS in walking pose from the left side. Friction between the soles of the shoes and the ground was ignored. In the Flex-PLI simulation, a stationary vehicle was impacted at 40 km/h to simulate the actual assessment test. The impact point in both simulations was at the center of the vehicle front in the lateral direction. Gravitational acceleration was applied to the entire model in the vertically downward direction. Calculation was performed over 40 ms. For impactor measurement, the knee and tibia bending angles were added to the injury criteria described above. To compare the injury criteria for the Flex-PLI and THUMS, the following items were measured in THUMS: the bending moment of the tibia and femur bones at the same heights as the bending moment measurement positions of the Flex-PLI, the elongation of each knee ligament, and the knee bending angle. The impact simulations used the general-purpose finite element code LS-DYNA TM V971.

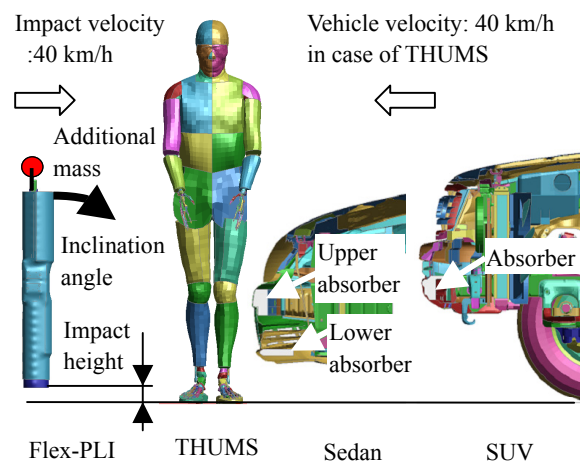


Figure 10. Study model.

Evaluation Matrix

Table 3 shows the evaluation matrix. The impact height of the Flex-PLI was adjusted to the following three levels: 0 mm, 25 mm, and 75 mm above the ground. At a height of 0 mm, the knee joint position is close to that of THUMS. The 25 mm condition simulates the thickness of shoe soles, and 75 mm is the value proposed by Matsui et al.[19] The height of the knee joint in THUMS while wearing shoes is 498 mm, whilst that of the Flex-PLI is 494 mm. Therefore, an impact height of 0 mm is the closest condition to the height of the knee.

Additional mass was set to four levels: 0 kg (no additional mass), 6 kg, 10 kg, and 14 kg. The 6 kg case was added because, although the mass of the pelvis portion of THUMS is approximately 10 kg,

and approximately 14 kg in combination with the abdomen, it is possible that the effective mass that is applied to each leg individually may be less. The additional mass was positioned at the top end of the Flex-PLI and set as a mass point. The inclination

angle of the Flex-PLI was set to 0 degrees from the vertical as a reference and a case with an inclination angle of 6 degrees from the external line of the THUMS leg was also performed.

Table 3.
Evaluation matrix

Case No.	Subject		Impact height (mm)			Additional mass (kg)				Inclination angle (deg)	
	THUMS	Flex-PLI	0	25	75	0	6	10	14	0	6
1	O		O								
2		O	O			O				O	
3		O	O				O			O	
4		O	O					O		O	
5		O	O						O	O	
6		O		O		O				O	
7		O			O	O				O	
8		O			O		O			O	
9		O	O						O		O
SUV	THUMS	Flex-PLI	0	25	75	0	6	10	14	0	6
10	O		O								
11		O	O			O				O	
12		O	O				O			O	
13		O	O					O		O	
14		O	O						O	O	
15		O		O		O				O	
16		O			O	O				O	
17		O			O		O			O	
18		O	O						O		O

RESULTS

This section first compares the impact behavior of THUMS and the Flex-PLI in a typical case. Figure 11 shows the behavior of the THUMS and impactor skeletons at every 10 ms in the collision with the sedan. Case 1 is shown for THUMS and case 7 for the Flex-PLI (impact height: 75 mm).

The vehicle first contacted the THUMS leg at the knee, followed by the tibia, and femur, causing bending deformation. The tibia was in contact with the bumper cover from 10 to 20 ms. After 30 ms, the lower leg rebounded. The femur contacted the hood after 30 ms. Bending deformation of the knee joint continued to increase until 40 ms. The MCL ruptured at 28 ms, but rupture did not occur in any of the other ligaments. The tibia and fibula bones did not fracture.

The lower portion of the Flex-PLI began to rebound at 20 ms after bending deformation of the tibia

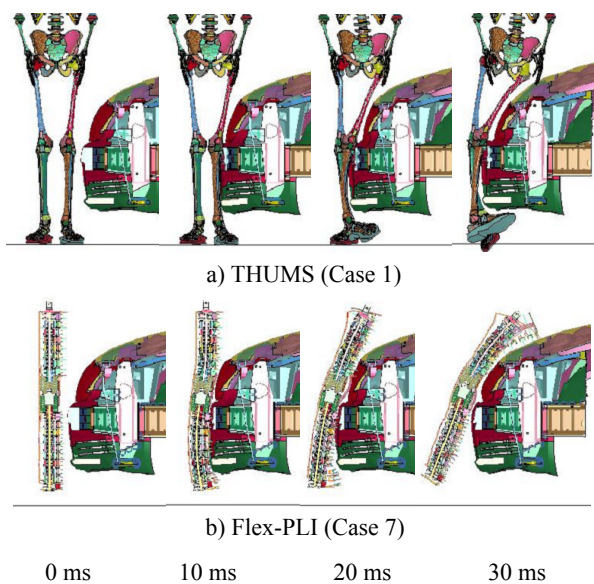


Figure 11. Behavior of a) THUMS (Case 1) and b) Flex-PLI (Case 7).

occurred. After bending briefly, bending of the knee joint decreased because the tibia rebounded upward.

Figure 12 shows the results of impacts with the SUV. Case 10 is shown for THUMS and case 16 for the Flex-PLI. The vehicle contacted THUMS close to the knee joint and comparatively less bending deformation of the femur, tibia, and fibula bones occurred than with the sedan impact. In contrast, the knee joint was bent toward the rear of the vehicle after 20 ms, and the MCL and ACL ruptured at 19 ms and 20 ms, respectively. The tibia, fibula, and femur bones did not fracture.

In the case of the Flex-PLI, the tibia was bent toward the rear of the vehicle. The knee joint flexed after 20 ms, but bending decreased after 30 ms due to the rebounding femur. Femur rebound occurred after it contacted the grille.

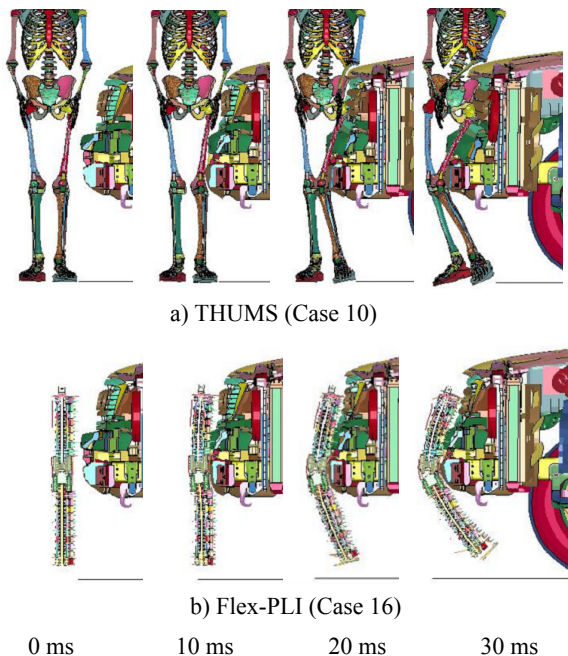


Figure 12. Behavior of a) THUMS (Case 10) and b) Flex-PLI (Case 16).

The next section discusses the comparative results for THUMS with respect to the effect of the Flex-PLI test conditions on impact behavior and response.

Effect of Impact height

Figure 13 compares the behavior of THUMS and the Flex-PLI at impact heights of 0 mm (case 2) and 75 mm (case 7) after collision with the sedan. The behavior shown in the graph occurred at 15 ms, the point at which the maximum bending moment of the tibia was generated. The distance to the knee center is plotted on the vertical axis and the X-direction displacement at each point of the

THUMS tibia and impactor bone core is plotted on the horizontal axis. The origin of the graph is the center of the knee joint. The black line indicates the behavior of THUMS, the red line that of the Flex-PLI at an impact height of 0 mm, and the green line that of the Flex-PLI at an impact height of 75 mm.

Regardless of the impact height, the Flex-PLI generated a bending deformation mode corresponding to that of the THUMS leg. However, there was a discrepancy in the amount of tibia deformation. The X-direction displacement of the inferior end was approximately 50 mm from the knee center toward the impact side in THUMS. In comparison, the lower end of the Flex-PLI displaced toward the opposite side of the impact at 75 mm, but to the impact side at 0 mm. Thus, the Flex-PLI behavior at 15 ms was closer to THUMS when the impact height was adjusted to 0 mm.

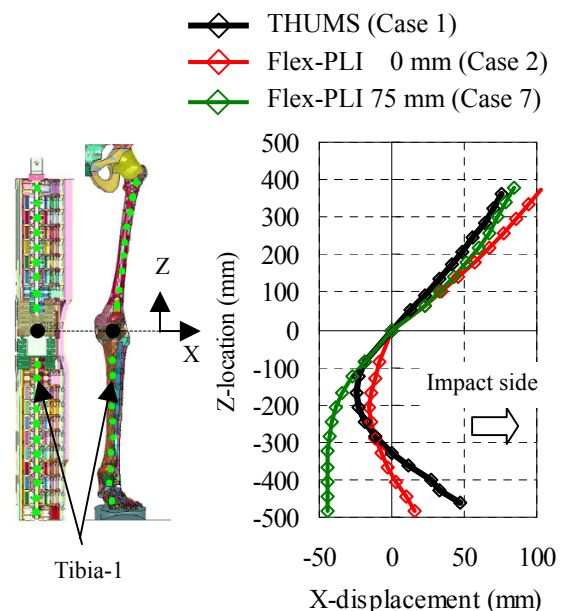


Figure 13. Effect of impact height: behavior of THUMS and Flex-PLI (sedan, 15 ms).

Figure 14 compares the time history curves of the tibia bending moment (measurement position: tibia-1) between THUMS and the Flex-PLI. The graph also shows the moment criterion of 299 Nm. In either case, moment began to increase from approximately 3 ms, reaching a maximum peak at around 14 ms, before falling to around zero at approximately 25 ms. Regardless of the impact height, the moment response waveforms of the Flex-PLI corresponded well with THUMS. However, the maximum moment peak for the Flex-PLI was 230 Nm at an impact height of 0 mm and 270 Nm at an impact height of 75 mm. Both values are higher than the maximum moment peak of approximately 200 Nm in THUMS.

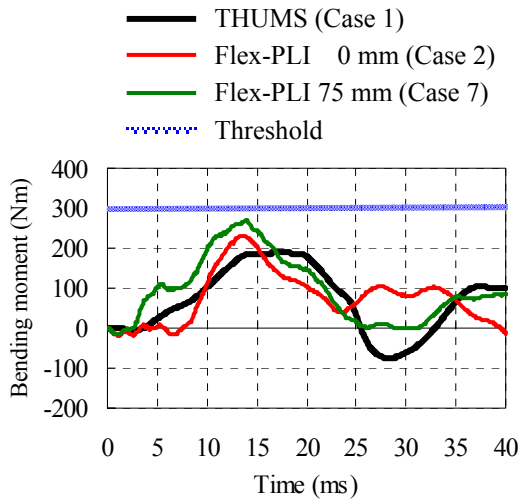


Figure 14. Effect of impact height: tibia bending moment (sedan).

Figure 15 shows the time history curves of the knee bending angle for the same cases. The knee bending angle of THUMS continued to increase, which is attributable to the MCL rupture at 10 degrees, after which the rate of increase continued to rise. Because the knee ligament wires in the Flex-PLI do not rupture, ligament elongation decreased after reaching a peak. At an impact height of 75 mm, although the start of bending was later than in THUMS, the peak value and timing was close to the point of MCL rupture in THUMS. In contrast, at an impact height of 0 mm, the knee started to bend at a timing similar to THUMS, but then increased rapidly after 12 ms. It reached a peak of 17 degrees, which is larger than the bending angle when MCL rupture occurred in THUMS. At this height, the knee bending angle decreased after 28 ms due to the rebound of the lower tibia. Therefore, the ligament rupture risk assessment is closer to THUMS when the impact height is set to 75 mm.

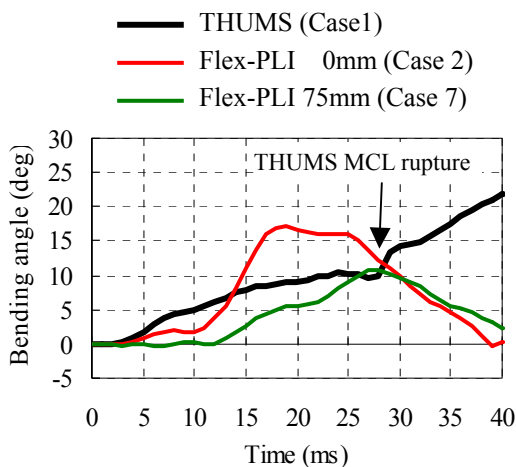


Figure 15. Effect of impact height: knee bending angle (sedan).

Effect of Additional Mass

This section compares THUMS with the results when 6 kg was added to the upper end of the Flex-PLI in the cases of SUV impact. Figure 16 compares the behavior of THUMS and the Flex-PLI at 20 ms. The condition of THUMS is equivalent to the state immediately after rupture of the MCL. The figure shows results with an impact height of 0 mm and additional mass of 0 kg (case 11) and 6 kg (case 12). The black line indicates the behavior of THUMS, the red line that of the Flex-PLI with an additional mass of 0 kg, and the brown line that of the Flex-PLI with an additional mass of 6 kg. The behavior of the femur with mass added to the Flex-PLI was closer to the behavior of THUMS. In contrast, no significant difference was observed in tibia behavior.

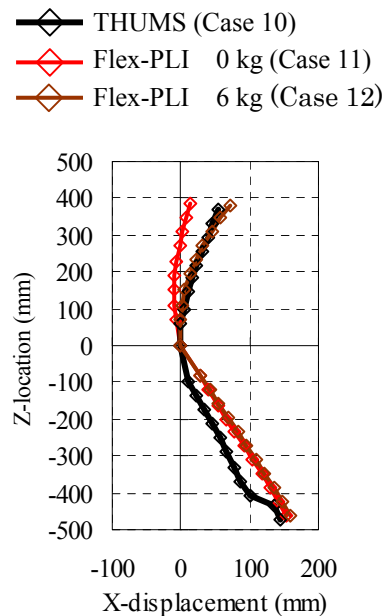


Figure 16. Effect of additional mass: behavior of THUMS and Flex-PLI (SUV).

Figure 17 shows the time history curves of the tibia bending moment (measurement position: tibia-1) between THUMS and the Flex-PLI. In THUMS, an initial negative moment was generated, which became positive moment at 15 ms after the impact. The MCL ruptured at 19 ms, after which, bending became concentrated in the knee joint due the rupture of the ACL at 20 ms, and the tibia bending moment did not increase. For the cases with the Flex-PLI, negative bending moment appeared at the beginning, but the bending moment continued to increase after 20 ms in both conditions. Since the ligament wires in the Flex-PLI do not rupture, knee bending is restricted within a certain range. As a result, the bending moment continued to act on the knee joint side of the tibia bone. In other

words, the moment generated in the Flex-PLI after 20 ms cannot be used for comparison.

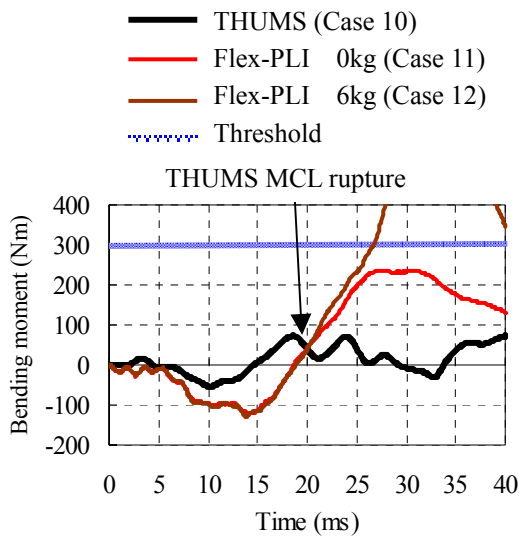


Figure 17. Effect of additional mass: tibia bending moment (SUV).

Figure 18 shows the time history curves of the knee bending angle for the same cases. In THUMS, the knee bending angle increased rapidly after the rupture of the MCL and ACL at 20 ms, and then continued to increase. In contrast, the bending angle of the Flex-PLI started at 10 ms, which was earlier than THUMS. With an additional mass of 0 kg, the maximum bending angle of 25 degrees was reached at 32 ms, and with an additional mass of 6 kg, the maximum bending angle increased to 38 degrees. According to Bose et al., the knee ligaments rupture at a bending angle of approximately 15 degrees.[20] The criterion for knee bending angle in Euro NCAP is also 15 degrees. In both conditions, the knee bending angle of the Flex-PLI exceeded 15 degrees, indicating the possibility of ligament rupture. It should be noted that in THUMS, the MCL ruptured

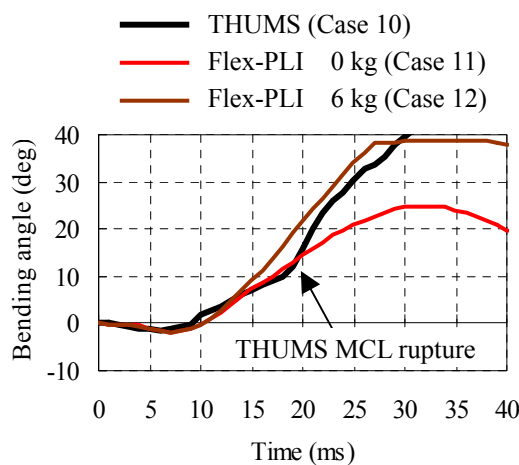


Figure 18. Effect of additional mass: knee bending angle (SUV).

at a knee bending angle of 10 degrees. Under this condition, local elongation of the MCL occurred, causing the rupture at a small angle.

These results suggest that additional mass has little effect in terms of injury assessment. However, in the case of SUV impact, impactor behavior is closer to THUMS when an additional mass is applied. A mass of 6 kg is considered to be sufficient to create such a correlation.

Effect of Impactor Inclination Angle

Figure 19 compares the behavior of THUMS and the Flex-PLI at impactor inclination angles of 0 degrees (case 5) and 6 degrees (case 9) 15 ms after impact. The impact vehicle was the sedan and an additional mass of 14 kg was applied to the upper end of the Flex-PLI. The black line indicates the behavior of THUMS, the blue line that of the Flex-PLI at an inclination angle of 0 degrees, and the green line that of the Flex-PLI at an inclination angle of 6 degrees.

It shows that femur behavior was closer to THUMS when impacted at an angle of 6 degrees. X-direction displacement of the lower tibia was also closer to THUMS when the Flex-PLI was inclined at 6 degrees.

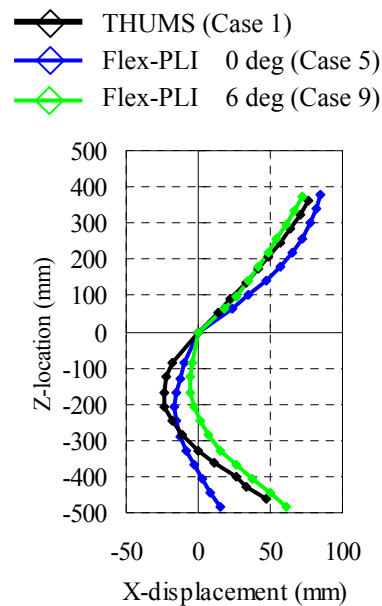


Figure 19. Effect of impactor angle: behavior of THUMS and Flex-PLI (sedan, mass: 14 kg).

Figure 20 shows the time history curves of the tibia bending moment (measurement position: tibia-1) in the above cases. Bending moment was generated at 8 ms when the inclination angle was 0 degrees, but at 3 ms at 6 degrees. This latter value was closer to THUMS. There were no major changes in

maximum moment.

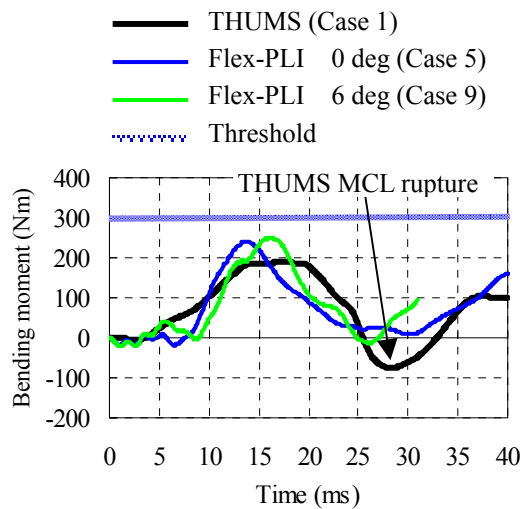


Figure 20. Effect of impactor angle: tibia bending moment (sedan, mass: 14 kg).

Figure 21 shows the time history curves of the knee bending angle for the same cases. The MCL in THUMS ruptured at approximately 10 degrees, immediately after which the bending angle increased suddenly. The bending angle continued to increase after MCL rupture. When the Flex-PLI was inclined at 6 degrees, the bending angle closely followed THUMS until 15 ms. After this point, however, the bending angle increased, greatly exceeding that of THUMS. When there was no inclination, the overall trend of the knee bending angle was closer to that of THUMS, despite the localized peak that occurred between 15 and 25 ms.

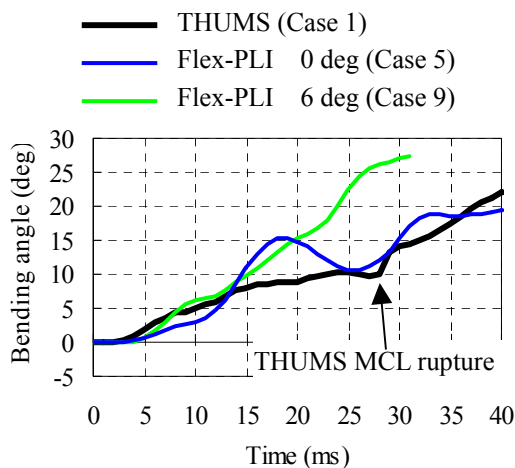


Figure 21. Effect of impactor angle: knee bending angle (sedan, mass: 14 kg).

DISCUSSION

Effect of Impact Height

Figure 22 compares the Flex-PLI behavior in the cases with the sedan at impact heights of 0 mm and 75 mm. The figure shows the degree of deformation 20 ms after the impact in each case. When the impact height was adjusted to 0 mm, the knee block on the tibia part (A) was positioned at the same height as the upper bumper absorber, meaning that the load of the vehicle bumper was mostly applied to the knee block. Since the knee block is made of highly rigid steel, bending deformation was exclusively concentrated in the knee joint and the tibia part did not deform greatly. In contrast, when the impact height was set to 75 mm, since the upper absorber contacted both the tibia and the knee block, bending deformation was generated at both the tibia part and the knee joint. In this case, bending was not concentrated only at the knee joint. Although a human tibia bone also widens proximally, in an impact with a sedan, bending deformation does not concentrate only at the knee joint. Therefore, it is preferable to set the impact height to 75 mm in order to simulate realistic bending deformation of the human tibia-knee complex, which is essential for injury assessment.

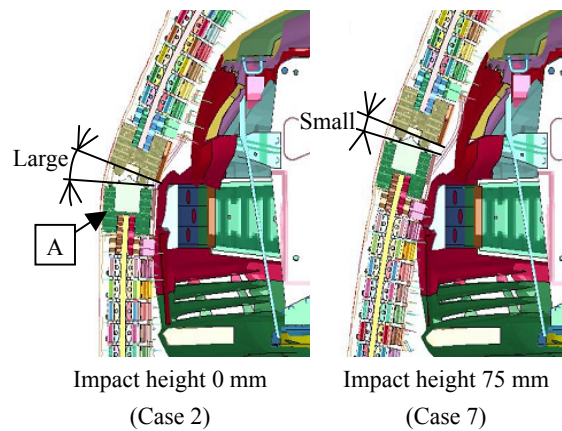


Figure 22. Deformation of Flex-PLI in impact with sedan (20 ms).

Figure 23 compares the knee and tibia bending angles in each model. The tibia bending angle is defined as the difference between the inclination angle of the knee lower block from the vertical axis and the inclination angle of the lower end of the tibia.

In THUMS, although the knee bending angle showed a simple increasing trend, the tibia bending angle became extremely large before decreasing. With the Flex-PLI, both the knee and tibia bending angles decreased after reaching extremely high

values. As stated above, the Flex-PLI knee bending angle is closer to THUMS at an impact height of 75 mm. The maximum impactor tibia bending angle is lower than THUMS and reached at an earlier timing at both impact heights. However, the time history curves in both cases are close to THUMS. Therefore, to assess the risk of ligament rupture related to the knee bending angle, it is preferable to set the impact height to 75 mm.

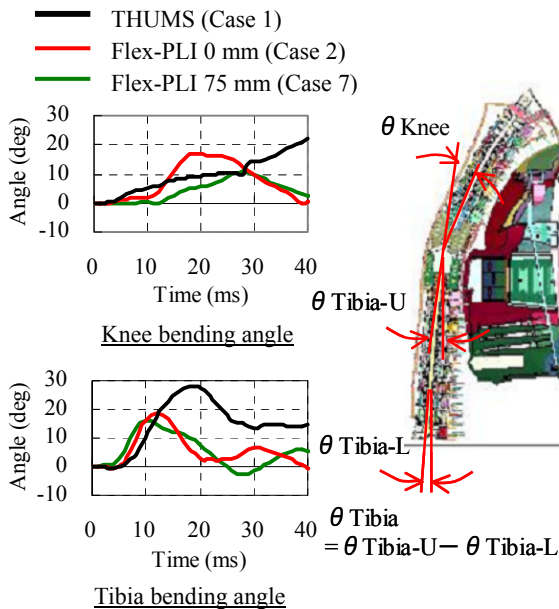


Figure 23. Tibia and knee bending angles.

Appropriate Additional Mass

Figure 24 compares the behavior of THUMS and the Flex-PLI with different additional masses applied to the top end of the Flex-PLI. The figure shows the degree of deformation at 20 ms after impact with the SUV in all cases. When no additional mass was set, X-direction displacement of the femur diverged from THUMS. In contrast, in all cases with an additional mass, X-direction displacement was closer to THUMS and there was little change based on the amount of mass.

The effect of the additional mass was considered by focusing on the leg center of gravity (CG). Figure 25 shows the CG of the THUMS leg and the Flex-PLI. In THUMS, the femur CG is located 227 mm from the knee joint. Including the femur and the pelvis, the CG of the THUMS leg becomes 310 mm from the knee joint. The femur CG of the Flex-PLI is 202 mm from the knee joint, which is closer to that of THUMS. With additional masses of 6 kg, 10 kg, and 14 kg, the CG from the knee joint is 306 mm, 358 mm, and 380 mm, respectively. Although the CG moves upward as the amount of mass is increased, the closest value to that of

THUMS when the femur and pelvis are considered is with an additional mass of 6 kg. Therefore, it appears that the addition of more mass did not cause discrepancies in femur behavior because the addition of 6 kg created a CG closer to that of THUMS. Thus, an additional mass of 6 kg is considered to be sufficient for injury criteria assessment.

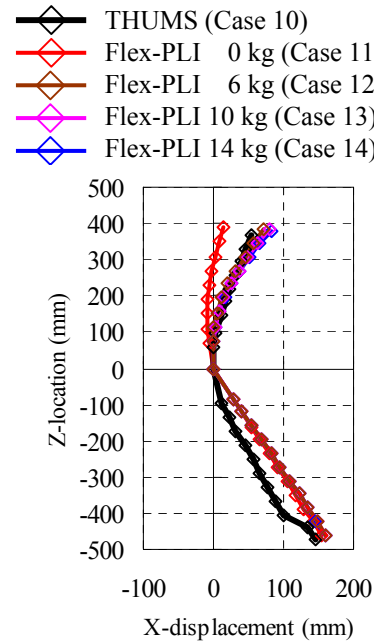


Figure 24. Effect of additional mass: behavior of THUMS and Flex-PLI (SUV, 20 ms).

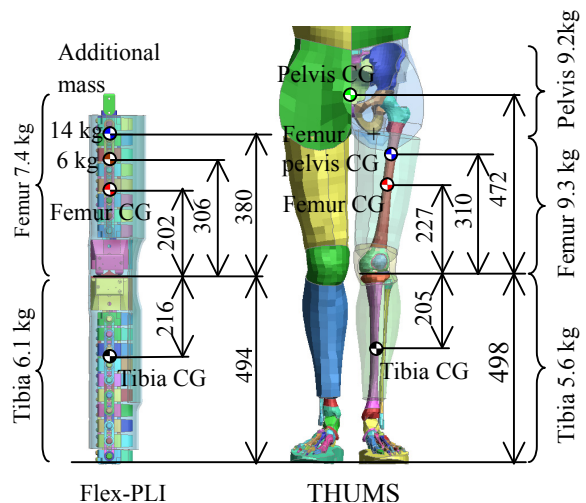


Figure 25. Centre of gravity of THUMS and Flex-PLI.

Effect of Impactor Inclination Angle

As shown in Figure 25, the skeletal structure of the human leg generally inclines inward when walking. Additionally, the external shape of the leg becomes

thinner from the base of the femur to the ankle. In a sedan impact, there is contact between the vehicle and the tibia, but the lower the part downward along the tibia, the later the contact occurs. In this study, when the Flex-PLI was inclined at 6 degrees to match the leg shape of THUMS, the trend for the timing of tibia bending moment was closer to that of THUMS. Therefore, adjusting the timing of contact with the vehicle at each leg position to reflect impact with an actual person is likely to be more effective for assessing injury criteria.

In contrast, since the results with a knee bending angle of 0 degrees were closer to THUMS than with an angle of 6 degrees, this is thought to be better for more accurate assessment.

The present results do not conclude which impactor inclination angle is better for injury criteria assessment of the leg as a whole. This is one possible area for study in the future.

CONCLUSIONS

(1) An FE model of the Flex-PLI was created by reverse engineering. X-ray CT scans were used to faithfully recreate the shape of the actual Flex-PLI, and the mechanical response of each component part was investigated before being input into the model.

(2) The Flex-PLI FE model was validated against actual impactor behavior and response in static 3-point bending tests on the femur, tibia, and knee joint, and dynamic pendulum tests in an assembled state. The results revealed that the impact behavior of the FE model closely correlated with that of the actual Flex-PLI, and that the mechanical response for moment and the like was within the test data corridors.

(3) The impact behavior and mechanical response of the Flex-PLI FE model and the THUMS full-body pedestrian FE model were compared to investigate suitable test conditions for assessing pedestrian leg injury. The following three test conditions were studied.

- Impact height above the ground
- Additional mass for simulating the upper body
- Impactor inclination angle

It was found that impact behavior at an impact height of 0 mm was closer to that of THUMS, but that 75 mm was closer in terms of injury response. For the effect of adding mass, it was found that the addition of 6 kg enabled a response closer to that of THUMS for an impact with an SUV. It was also discovered that the timing of tibia bending moment was closer to the response of THUMS at an impactor inclination angle of 6 degrees, but that the results with a knee bending angle of 0 degrees were closer.

In conclusion, these findings indicate that the

recommended conditions for assessing leg safety performance with the Flex-PLI are an impact height of 75 mm above the ground, an additional mass of 6 kg for SUV impacts, and an inclination angle of 0 degrees.

ACKNOWLEDGMENTS

The authors would like to express their gratitude to everyone at Toyota Motor Corporation and Toyota Technical Development Corporation for their support and guidance for completion of this technical paper.

REFERENCES

- [1] Institute for Traffic Accident Research and Data Analysis (ITARDA). 2007. "Traffic accident statistics annual report."
- [2] UN/ECE/WP29/GSRP/2006/2, 2006. "Proposal for a global technical regulation on uniform provisions concerning the approval of vehicles with regard to their construction in order to improve the protection and mitigate the severity of injuries to pedestrians and other vulnerable road users in the event of a collision."
- [3] Konosu, A., and Tanahashi, M. 2007. "Development of a Biofidelic Flexible Pedestrian Legform Impactor type GT (Flex-GT)." Proc. 20th ESV Conference, Paper No. 07-0178
- [4] Wittek, A., Konosu, A., Matsui, Y., Ishikawa, H., Sasaki, A., Shams, T., McDonald, J. 2001. "A new legform impactor for evaluation of car aggressiveness in car-pedestrian accidents." Proc. 17th ESV Conference, Paper No. 174
- [5] UN/ECE/WP29/GSRP/INF-GR-PS/Flex-TEG 2007. "Flex-GT development." TEG-032
- [6] Matsui, Y., Takabayashi, M. 2004. "Effects of Upper Body Mass on Dynamic Behavior of Legform Impactor for Pedestrian Subsystem Tests." Transaction of Society of Automotive Engineers of Japan, Vol. 35; No. 2; pp. 211-216
- [7] Yamada, H. 1970. "Strength of Biological Materials." FG. Evean, Ed., The Williams & Wilkines Company, Baltimore.
- [8] Burstein AH et al. 1976. "Aging of bone tissue : mechanical properties." J. Bone Joint Surg. 58(A):pp. 82-86

- [9] Kerrigan, J., Bhalla, K., Madeley, N., Funk, J., Bose, D., Crandall, J. 2003. "Experiments for establishing pedestrian-impact lower limb injury criteria." Society of Automotive Engineers World Congress, SAE Paper No. 2003-01-0895
- [10] Kajzer J. et al. 1999. "Shearing and Bending Effects at the Knee Joint at Low Speed Lateral Loading." Society of Automotive Engineers World Congress, SAE Paper No. 1999-01-0712
- [11] Kajzer J. et al. 1997. "Shearing and Bending Effects at the Knee Joint at High Speed Lateral Loading." Society of Automotive Engineers World Congress, SAE Paper No. 973326
- [12] Levine R. S., Vegeman P.C., King A. I. 1984. "An Analysis of the Protection of Lateral Knee Bracing in Full Extension Using a Cadaver Simulation of Lateral Knee Impact." American Academic of Orthopedica Surgical
- [13] Ramet, M., Bouqut R., Bermond F., Caire Y., Bouallegue M. 1995. "Shearing and Bending Human Knee Joint Tests in Quasi-Static Lateral Load." IRCOBI Conference Proceedings, pp. 93-105
- [14] Robbins, D.H. 1985. "Anthropometry of Motor Vehicle Occupants." Vol.2, NHTSA Contract DTNH22-80-C-07502 Pub.
- [15] UN/ECE/WP29/GSRP/INF-GR-PS/Flex-TEG 2007. "Flex-GT information.", TEG-033
- [16] UN/ECE/WP29/GSRP/INF-GR-SP/Flex-TEG 2007. "Review of Injury Criteria and Injury Thresholds for Flex-PLI.", TEG-048
- [17] Yasuki T., Yamamae Y. 2005. "A Study on Behavior of Legform Impactor." Transaction of Society of Automotive Engineers of Japan, Vol. 36, No. 6, pp. 219-223
- [18] Yasuki T. 2005. "A Survey on the Biofidelity of the Knee Bending Angle of the TRL Lower Leg Impactor." Proc. 19th ESV Conference, Paper No. 05-0101
- [19] Matsui Y., Ishikawa H., Sasaki A., Kajzer J., Schroeder G. 1999. "Impact Response and Biofidelity of Pedestrian Legform Impactors." IRCOBI Conference Proceedings, pp.343-354
- [20] Bose, D., Bhalla, K., van Rooji, L., Millington, S., Studley, A., Crandall, J. 2004. "Response of the knee joint to the pedestrian impact loading environment." Society of Automotive Engineers World Congress, SAE Paper No. 2004-01-1608
- [21] Konosu A., Ishikawa H., et al. 2001. "Reconsideration if injury criteria for pedestrian subsystem legform test - Problem of rigid legform impactor -." Proc. 17th ESV Conference, Paper No. 01-0263
- [22] Maeno T., Hasegawa J. 2001. "Development of a Finite Element Model of the Total Human Model for Safety (THUMS) and Application to Car-Pedestrian Impacts." Proc. 17th ESV Conference, Paper No. 494.
- [23] Bhalla K., Bose D., et al. 2003. "Evaluation of the Response of Mechanical Pedestrian Knee Joint Impactors in Bending and Shear Loading." Proc. 18th ESV Conference, Paper No. 429

PERFORMANCE OF VEHICLE BUMPER SYSTEMS WITH THE EEVC/TRL PEDESTRIAN LOWER LEGFORM

Ann Mallory

Transportation Research Center Inc.

Jason Stammen

National Highway Traffic Safety Administration
United States of America

Paper No. 09-0318

ABSTRACT

In U.S. pedestrian crashes, serious lower extremity injuries are second only to head injuries in frequency. The Global Technical Regulation (GTR) for pedestrian safety uses the EEVC/TRL pedestrian lower legform to evaluate the risk of these injuries from bumper impact. In order to evaluate the level of pedestrian lower extremity protection offered by front bumpers in the U.S. fleet, NHTSA's Vehicle Research and Test Center (VRTC) conducted 40 pedestrian lower legform impact tests on 9 vehicles. These vehicles were selected to represent the U.S. fleet, with a focus on light trucks and vans. The goal was to generate an overall picture of current U.S. vehicle performance with respect to lower extremity protection requirements in the regulation. Results showed that pedestrian lower extremity protection was poor overall, with no vehicle meeting the GTR injury limits in all locations tested. One vehicle was able to meet the requirements by a wide margin in all but one impact location. Two other vehicles each had a single passing impact location. Results are consistent with prior results from legform testing on U.S. passenger cars.

INTRODUCTION

In U.S. pedestrian crashes in the Pedestrian Crash Data Study (PCDS), injuries to the lower extremity are more frequent than injuries to any other body region (Mallory and Stammen 2006). Among serious pedestrian injuries, lower extremity injuries are second in frequency only to head injuries (Figure 1). Approximately 80% of the vehicle impact injuries to the thigh, knee, and lower leg are caused by bumper contact.

To evaluate lower extremity protection in pedestrian impacts, the Global Technical Regulation (GTR) for pedestrian safety includes front bumper testing with the EEVC/TRL lower legform or the upper legform depending on the height of the bumper. The EEVC/TRL lower legform is manufactured by TRL Limited and conforms to EEVC (European Enhanced

Vehicle-safety Committee) requirements. According to the GTR, at locations where bumpers have a LBRL (Lower Bumper Reference Line) below 425 mm, the lower legform test is required. At locations where the LBRL is greater than or equal to 500 mm, the bumper is subjected to the upper legform test. At locations where the LBRL is between these two limits, the manufacturer may choose either test. As shown in Figure 2, PCDS bumper height data indicates that the majority of pedestrian-involved vehicles in the PCDS data set would be required to use the lower legform under GTR requirements (Mallory and Stammen 2006). Although the PCDS cases were collected between 1994 and 1998, they represent the most current U.S. pedestrian crash data available.

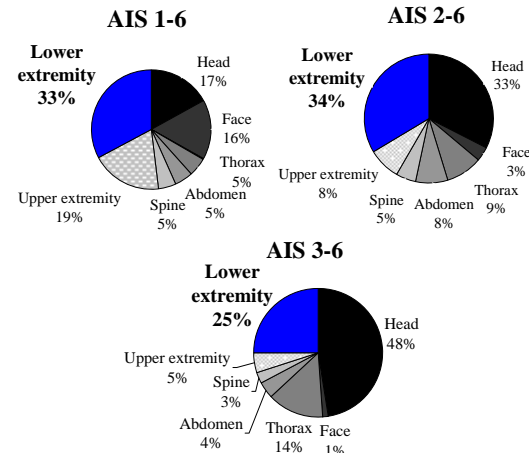


Figure 1. Distribution of injuries in the PCDS by body region (Mallory and Stammen 2006).

The performance of the U.S. fleet relative to the GTR lower legform test requirements has not previously been reported. In 2005, VRTC reported on the performance of five U.S. passenger cars in tests with the EEVC/TRL legform under EuroNCAP pedestrian test conditions (Mallory, Stammen et al. 2005). However, the EuroNCAP test conditions differ from those defined in the GTR. Furthermore, since the nature and risk of lower extremity injuries is affected by vehicle type (Ballesteros, Dischinger et al. 2004; Matsui 2005) the prior study of passenger cars may not reflect the level of pedestrian protection offered

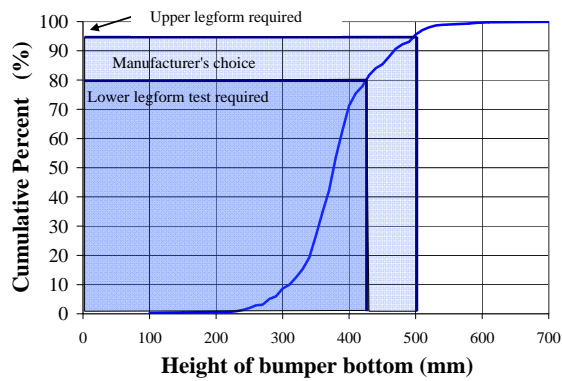


Figure 2. Lower bumper reference line height (Mallory and Stammen 2006).

by the rest of the U.S. fleet, which includes a large proportion of light trucks and vans.

In order to evaluate the performance of the current fleet relative to the GTR requirements, NHTSA's Vehicle Research and Test Center (VRTC) has conducted 40 pedestrian lower legform impact tests on 9 vehicles from the U.S. fleet with a focus on light trucks and vans. One vehicle from the previous series of testing done according to EuroNCAP test procedures was re-tested in the current series of tests according to GTR lower legform test procedures. If the results from the two sets of tests were similar enough, the prior test results with passenger cars could be combined with the current results to generate a more comprehensive picture of the current level of US vehicle performance.

METHODS

Testing was performed according to the lower legform procedures in the Proposal for a Global Technical Regulation (GTR) for the Protection of Pedestrians (GRSP 2006).

Vehicles Tested

The vehicles were selected to represent a range of vehicle types and sizes, including three sport utility vehicles (SUV), two pickups (PU) of different sizes, one minivan (MV), one full-size van (VAN), and two passenger cars (PC) as shown in Table 1.

Of the vehicles listed, only the Mazda Miata had been tested previously in lower extremity component tests under EuroNCAP conditions (Mallory, Stammen et al. 2005). The Passat, Wrangler, Durango, CR-V, Tacoma, and E-350 van had been previously tested in VRTC's evaluation of the U.S.

fleet relative to the head test requirements in the GTR (Mallory, Stammen et al. 2007). The Silverado tested in the current series was a different vehicle than the Silverado used in the previously-reported head test series. The Sienna had not previously been used in pedestrian testing at VRTC.

Table 1. Vehicles tested

Year	Vehicle	VIN
2002	Mazda Miata	JM1NB353320228887
2006	VW Passat	WVGK73C56P171110
2002	Jeep Wrangler	1J4FA39S42P744167
2006	Dodge Durango	1D8HD38K66F118432
2005	Honda CR-V	JHLRD68585C000383
2006	Toyota Tacoma	5TENX22N16Z291865
2005	Chevy Silverado	1GCHC23U05F921031
2006	Toyota Sienna	5TDZA23C365448521
2003	Ford E-350 Van	1FBSS31L03HB67515

Bumper measurements made on each vehicle included the height of the Upper Bumper Reference Line and the Lower Bumper Reference Line, the width of the Bumper Test Area, and the distance from the vehicle centerline to the Corner of the Bumper. The maximum and minimum LBRL heights for each vehicle are documented in Table 2. Part of the Dodge Durango test zone is in the mandatory lower legform height range and part is in the manufacturer's option height range. The Jeep Wrangler test zone is entirely in the manufacturer's choice height range. The Silverado test zone has portions in all three ranges.

Table 2. Range of LBRL height across width of test zone, color-coded by required test procedure

		LBRL Minimum (mm)	LBRL Max. (mm)
SUV	Dodge Durango	405	452
	Jeep Wrangler	451	481
	Honda CR-V	410	415
PU	Chevy Silverado	420	505
	Toyota Tacoma	378	378
MV	Toyota Sienna	260	264
VAN	Ford E350 Van	348	408
PC	VW Passat	219	230
	Mazda Miata	200	218
Color Legend: Test procedure required in GTR based on LBRL Height		Upper Leg > 500 mm	
		Manufacturer Choice	
		Lower Leg < 425 mm	

Impact Point Locations

Five impacts were planned for each vehicle. All impacts were within the test zone defined in the GTR. Assuming symmetry, these tests are equivalent to a center impact, an outboard impact, and three impacts between. In order to maximize the number of tests per bumper, the impacts were performed on both sides of the test zone as shown in Figure 3. The impacts are spaced at intervals proportional to 1/8 of the width of the bumper test zone, with the exception of the far outboard impact which was moved inboard from the edge of the test zone by 5 mm to ensure it was within the test zone. The intention of the test location selection was to represent the range of typical bumper performance. A maximum of three impacts were planned per bumper, before replacement of all bumper system parts. Damage was inspected following each impact. If post-test damage was identified that could have an effect on subsequent tests, the damaged parts were replaced prior to additional testing, or subsequent tests were cancelled. Subsequent tests were also cancelled if a vehicle produced damage to the legform in multiple tests. As a result, two vehicles underwent only four tests, and one vehicle was tested only twice. The test locations for each vehicle are listed in Table 3.

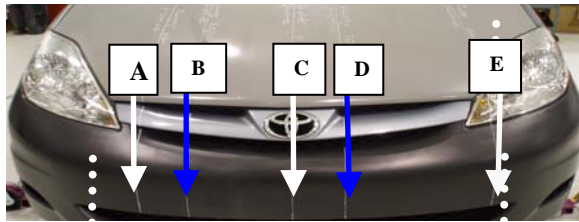


Figure 3. Example of five test locations on Toyota Sienna. Dashed boundaries show limits of test area and solid lines are impact locations. White and blue arrows indicate impacts performed on different bumper systems.

Table 3. Location of each impact in mm from centerline of vehicle, positive toward driver’s side

	A	B	C	D	E
Durango	-540	-360	0	--	715
Wrangler	-545	-364	0	182	722
CR-V	-347	-232	0	116	458
Silverado	-590	-394	0	197	782
Tacoma	--	--	0	--	503
Sienna	-404	-269	0	135	533
E350 Van	-596	-398	0	--	790
Passat	-361	-241	0	120	476
Miata	-368	-245	0	123	485

Test Procedure

Temperature and humidity were maintained within GTR-defined corridors for testing and during pre-test soaking. Impact speed in the GTR is required to be 11.1 m/s (+/- 0.2 m/s). Test speed was measured by an Aries laser speed meter (Model SM-2BL/F). During initial testing the speed meter was positioned at the approximate height of the CG of the legform. After testing demonstrated negligible pitch rotation in the legform during flight, the speed meter was moved down to allow a better lateral view of the legform-to-bumper impact. Integration of the upper tibia accelerometer was also performed to track velocity in case the speed meter failed to measure the speed. Deviations from the required speed range are documented.

The bottom of each vehicle tire was positioned 25 mm below the level of the bottom of the legform at impact.

Between tests, the ligaments and foam flesh on the EEVC/TRL legform were replaced. Legform inspection was performed and any necessary repairs were made, including replacement of the neoprene skin if needed.

The GTR specifies that the axis of the legform shall be perpendicular to the horizontal with a tolerance of +/- two degrees in the lateral and longitudinal plane, and the rotation about the vertical axis will have a tolerance of +/- five degrees. Initial video analysis of legform flight without a vehicle in place showed that legform alignment in the lateral and longitudinal planes were consistently within tolerance, but that orientation about the vertical axis showed variation. Therefore, overhead video was recorded during all vehicle testing and reviewed following each test. Any test that appeared to approach the five degree limit on rotation underwent video analysis using TEMA motion analysis software (Version 2.6, Image Systems AB).

The EEVC/TRL lower legform was instrumented as specified in the GTR. A uniaxial accelerometer (7264-2000) was mounted on the non-impact side of the upper tibia. The legform was equipped with rotary potentiometers located in the upper tibia and lower femur (Contelec, Type GL 60) to measure knee bending angle and knee shearing displacement. The knee bending angle and shear displacement are calculated based on the potentiometer angles as specified in the TRL Legform User’s Manual (TRL, 2007).

Static and dynamic certification of the legform was performed after not more than 20 vehicle impacts, following GTR defined procedures.

RESULTS

Results are presented separately for each vehicle, followed by a comparison of peak measures across all vehicles. Peak injury measurements are compared to GTR requirements which limit peak knee bending angle to 19 degrees and shear displacement to 6 mm. Over most of the test area upper tibia acceleration is limited to 170 g, but the limit is relaxed to 250 g over areas totaling up to 264 mm of the width of the bumper. The location of the relaxed bumper area is designated by the vehicle manufacturer.

Mazda Miata - Time histories for injury measures on all tests are shown in Figure 4 and peak values are tabulated in Table 4. The Mazda Miata was below GTR limits for the impact to the center bumper (Impact C) only. In impact C, peak bending angle was within 0.3 degrees of the GTR limit of 19 degrees. In all other impacts, the bending angle limit was exceeded. Impact A, which was close to the bumper support location, resulted in the highest shear displacement, bending angle, and tibia acceleration of any of the Miata test locations.

As indicated in Table 4, impact B was slower than the required impact speed range of 10.9 -11.3 m/s and impact D was faster than the required speed.

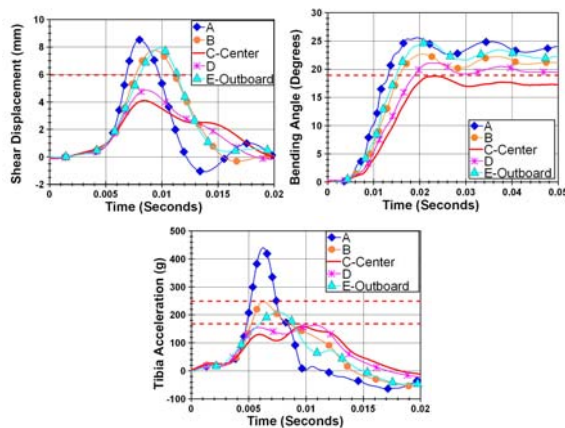


Figure 4. Time histories for shear displacement, knee bending angle, and tibia acceleration for Mazda Miata, with GTR limits shown in red.

Table 4. Peak results for each Mazda Miata impact, with passing impact (C) shaded green

	GTR Limit	Impact Location				
		A	B*	C	D**	E
Bending angle (degrees)	19	25.7	22.9	18.7	20.9	24.9
Shear displacement (mm)	6	8.6	7.8	4.2	4.9	7.9
Tibia acceleration (g)	170 (250)	440	247	159	163	210

* Location B impact speed was 10.87 m/s

** Location D impact speed was 11.39 m/s

A video frame showing the legform in the center impact (C) at the moment of peak bending angle is shown in Figure 5. In all impacts, the tibia segment of the legform was supported by the lower bumper structures on the Miata while the femur segment wrapped forward toward the hood.



Figure 5. Legform at time of maximum bending angle in Mazda Miata center impact (C).

Volkswagen Passat - None of the impacts to the Volkswagen Passat met the GTR requirements, as shown by the time histories in Figure 6 and the peak values in Table 5. Peak bending angle exceeded the 19 degree limit in every test. Shear displacement exceeded the GTR limit only in impact A. Tibia acceleration was over 170 g centrally, and exceeded 250 g in the more outboard test locations.

Figure 7 shows the legform at the moment of peak bending deformation in the center impact. At all impact locations, the legform conformed with the vehicle front by the time of maximum bending with the tibia segment essentially vertical against the bumper structures and the femur segment wrapped around the grille structures.

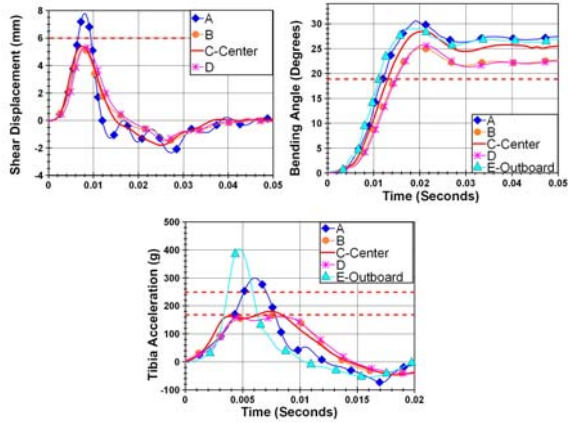


Figure 6. Time histories for shear displacement, knee bending angle, and tibia acceleration for Volkswagen Passat, with GTR limits shown in red.

Table 5.

Peak results for each Volkswagen Passat impact

	GTR Limit	Impact Location				
		A	B	C	D	E
Bending angle (degrees)	19	30.5	25.1	28.5	25.8	29.0
Shear displacement (mm)	6	7.8	5.2	5.4	5.4	--*
Tibia acceleration (g)	170 (250)	300	166	181	161	405

* Shear pot wire broken – data invalid.



Figure 7. Legform at time of maximum bending angle in Volkswagen Passat center impact (C).

Jeep Wrangler - In four of the five Jeep Wrangler impacts, all three injury measures were above the GTR limit (Figure 8, Table 6). In the fifth impact, the outboard-most point tested, the injury measures were well below the GTR limits. The negative shear displacement documented in the Wrangler tests indicates that, relative to the femur, the tibia segment moved toward the vehicle. Figure 9

shows a video frame from the moment of maximum bending angle in impact C.

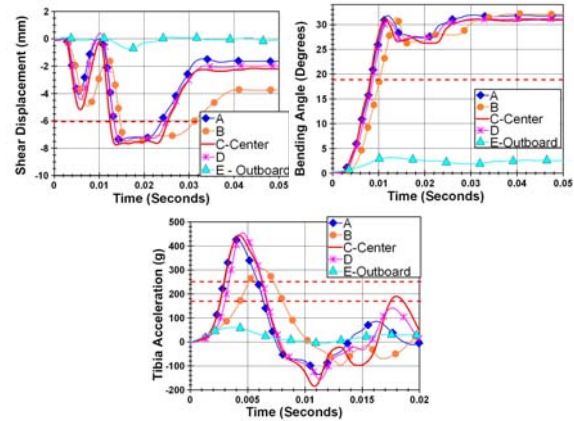


Figure 8. Time histories for shear displacement, knee bending angle, and tibia acceleration for Jeep Wrangler, with GTR limits shown in red.

Table 6.

Peak results for Jeep Wrangler each impact, with passing impact (E) shaded green

	GTR Limit	Impact Location				
		A	B	C	D	E
Bending angle (degrees)	19	31.9	32.2	31.3	31.2	3.2
Shear displacement (mm)	6	-7.5	-7.6	-7.8	-7.5	-0.75
Tibia acceleration (g)	170 (250)	427	305	445	455	60



Figure 9. Legform at time of maximum bending angle in Jeep Wrangler center impact (C).

Video showed that there was little to no bumper deformation in the four failed impacts, but there was significant deformation of the bumper end in the passing outboard impact. The end cap of the bumper bent rearward, allowing the legform to move into the front surface of the tire and fender, supporting the

legform along its full length to limit bending and shear.

Dodge Durango - The Dodge Durango was tested in only four locations because legform damage was sustained in three of the first four impacts. The Durango exceeded the bending angle limit by a wide margin in three impacts, and by a narrow margin in the outboard-most impact (Figure 10 and Table 7). Tibia acceleration limits were exceeded by all but the outboard-most impact. Shear limits were exceeded at points B and C. The negative shear values indicate that, relative to the femur, the tibia moved toward the car in all impacts.



Figure 11. Legform at time of maximum bending angle in Dodge Durango center impact (C).

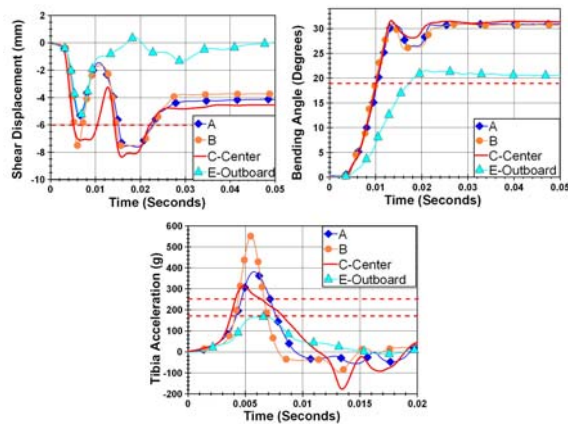


Figure 10. Time histories for shear displacement, knee bending angle, and tibia acceleration for Dodge Durango, with GTR limits shown in red.

Table 7.

Peak results for each Dodge Durango impact

	GTR Limit	Impact Location			
		A	B	C	E
Bending angle (degrees)	19	31.0	30.9	31.6	21.5
Shear displacement (mm)	6	-8.4	-7.6	-8.4	-5.3
Tibia acceleration (g)	170 (250)	314	552	314	167

A video frame from the moment of maximum displacement (Figure 11) shows that the upper leg and lower leg both rotate toward the car around the bumper. In the outboard-most impact at location E, the legform has started to rotate outboard by the time of maximum bending.

Honda CR-V - In four of the five impacts, the Honda CR-V was well below GTR limits in all measures. The exception was the outboard-most impact, where the tibia acceleration exceeded even the relaxed limit of 250 g, and the bending angle exceeded the 19 degree limit (Figure 12, Table 8). Shear displacement in the outboard impact E was negative, indicating that the tibia displacement was toward the vehicle relative to the femur, rather than away from the vehicle relative to the femur as was seen in the other four tests.

As indicated in Table 8, the rotation about the Z axis exceeded the GTR limit of 5 degrees in the impacts at locations D and E. Table 8 also shows the higher peak bending angle in outboard impact E, compared to the much lower peak bending angles in the remaining tests. The outboard impact E also shows dramatically less bumper and vehicle-front deformation than the inboard, passing impacts.

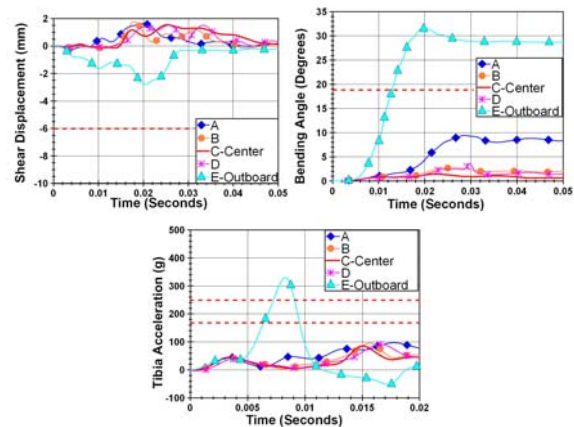


Figure 12. Time histories for shear displacement, knee bending angle, and tibia acceleration for Honda CR-V, with GTR limits shown in red.

Table 8.
Peak results for each Honda VR-V impact, with passing impacts shaded green

	GTR Limit	Impact Location				
		A	B	C	D*	E**
Bending angle (degrees)	19	9.5	2.8	1.5	3.6	31.5
Shear displacement (mm)	6	1.6	1.8	1.8	1.5	-2.8
Tibia acceleration (g)	170/250	97	96	85	91	329

* Location D rotation about Z axis exceeded 5 degrees.
** Location E rotation about Z axis exceeded 5 degrees.



Figure 13. Legform at time of maximum bending angle in Honda CR-V impact (C).

Toyota Tacoma - Only two tests were performed on the Toyota Tacoma due to vehicle damage. After two tests there was extensive unforeseen damage to the grille, the grille surround and to the headlamp mounts. With no replacement parts available, subsequent testing was suspended because these structures could potentially have been limiting the peak bending angle and shear displacement of the legform. Therefore, testing with damaged structures may not have been valid. Figure 14 and Table 9 show that all injury limits were exceeded in both tests. Figure 15 shows that the upper leg tended to rotate into the grille structures while the tibia segment of the legform rotated much less.

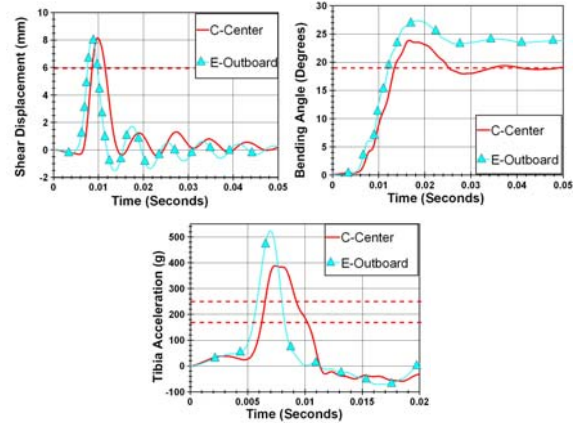


Figure 14. Time histories for shear displacement, knee bending angle, and tibia acceleration for Toyota Tacoma, with GTR limits shown in red.

Table 9.
Peak results for each Toyota Tacoma impact

	GTR Limit	Impact Location	
		C	E
Bending angle (degrees)	19	23.9	27.4
Shear displacement (mm)	6	8.2	8.1
Tibia acceleration (g)	170 (250)	388	523



Figure 15. Legform at time of maximum bending angle in Toyota Tacoma center impact (C).

Chevrolet Silverado - None of the Chevrolet Silverado impacts met the GTR requirements. In contrast to other vehicles, two of the failing impacts did meet bending angle requirements (Figure 16 and Table 10). Shear displacement limits were exceeded in every test. Tibia acceleration was over 170 g in all tests, but below the relaxed limit of 250 g in one test.

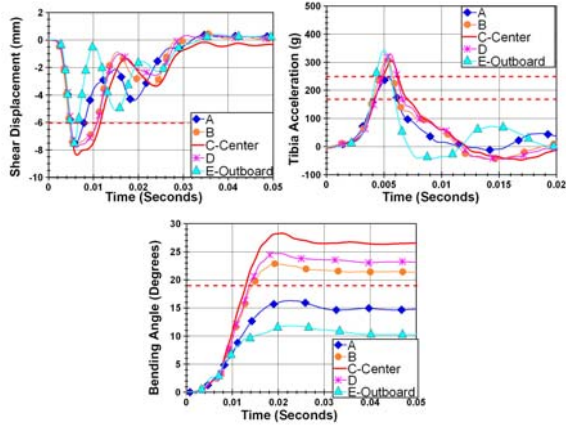


Figure 16. Time histories for shear displacement, knee bending angle, and tibia acceleration for Chevrolet Silverado, with GTR limits shown in red.

Table 10. Peak results for each Chevrolet Silverado impact

	GTR Limit	Impact Location				
		A	B*	C	D	E
Bending angle (degrees)	19	16.3	22.9	28.3	24.8	11.8
Shear displacement (mm)	6	7.6	7.8	8.4	7.8	7.5
Tibia acceleration (g)	170 (250)	245	311	306	330	342

* LBRL higher than 500 mm at location B.

As indicated in Table 10, impact location B was tested with the lower legform in spite of the fact that the Lower Bumper Reference Line at this test location put it in a zone where upper legform testing would have been required per the GTR requirements.

Figure 17 illustrates the interaction of the legform with the bumper at peak bending angle, with the lower leg bending under the bumper and the upper leg supported almost vertically by the bumper structures.



Figure 17. Legform at time of maximum bending angle in Chevrolet Silverado center impact (C).

Toyota Sienna - All impacts to the Toyota Sienna failed to meet GTR requirements. Although the center impact (C) was below the shear displacement limit and impact D was below the 170 g limit on tibia acceleration, bending angle was well over the 19 degree limit in all tests (Figure 18 and Table 11). The video frame at the moment of maximum bending angle show that the top of the bumper contacts the legform near the knee and the upper portion of the legform wrapped down to the hood of the Sienna in all impacts (Figure 19).

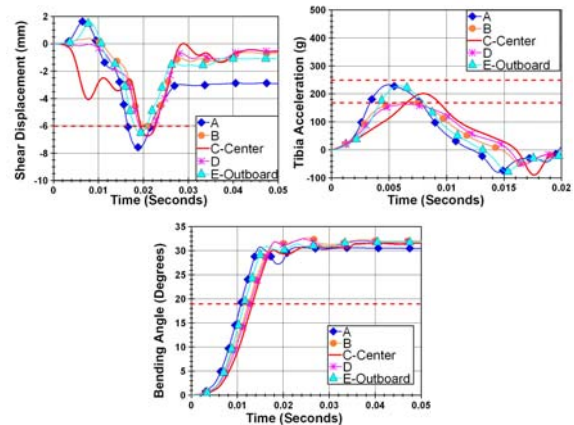


Figure 18. Time histories for shear displacement, knee bending angle, and tibia acceleration for Toyota Sienna, with GTR limits shown in red.

As indicated in Table 11., the rotation about the vertical axis exceeded the GTR limit of 5 degrees in the impact at location B.

Table 11.
Peak results for each Toyota Sienna impact

	GTR Limit	Impact Location				
		A	B*	C	D	E
Bending angle (degrees)	19	30.8	32.7	31.0	32.5	31.4
Shear displacement (mm)	6	-7.6	-6.0	-6.7	-6.8	-6.5
Tibia acceleration (g)	170 (250)	233	172	202	162	228

* Location B rotation about vertical axis exceeded 5 degrees.



Figure 19. Legform at time of maximum bending angle in Toyota Sienna center impact (C).

Ford E-350 Van - The first four impacts to the Ford E-350 bumper exceeded injury limits by a wide margin with bending angle over 31 degrees in all tests and tibia acceleration exceeding 350 g's in three tests (Figure 20 and Table 12). In the center impact (C), acceleration data was not collected due to wire damage. In the fourth impact (B) the pot arm of the potentiometer sustained damage. Due to a limited number of replacement pot arms, and the assumption that point D results would be similar to points B and C, testing was suspended prior to testing point D. Figure 21 shows that the femur segment tended to rotate into the grille while the tibia segment rotated under the bumper in all impacts. The knee was approximately centered over the height of the bumper.

As indicated in Table 12, the rotation about the vertical axis exceeded the GTR limit of 5 degrees in the impact at location C.

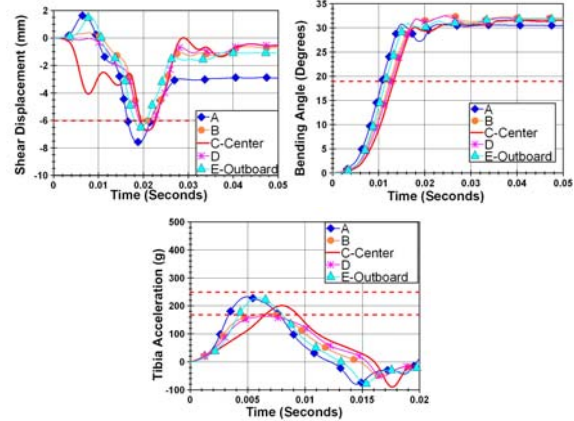


Figure 20. Time histories for shear displacement, knee bending angle, and tibia acceleration for Toyota Sienna, with GTR limits shown in red.

Table 12.
Peak results for each Ford E-350 impact

	GTR Limit	Impact Location			
		A	B	C*	E
Bending angle (degrees)	19	31.8	31.7	32.0	32.7
Shear displacement (mm)	6	-7.5	-7.5	-7.6	-7.5
Tibia acceleration (g)	170/250	516	592	--*	379

* Location C rotation about vertical axis exceeded 5 degrees.



Figure 21. Legform at time of maximum bending angle in Ford E-350 center impact (C).

Comparison of results among vehicles

Peak results for tibia acceleration are shown for all vehicles in Figure 22. The acceleration limit of 170 g and the relaxation limit of 250 g are indicated in red.

Only five of 39 (13%) test locations met the 170 g limit with a wide margin: the four passing CR-V impacts and the outboard Wrangler impact. The remaining impacts were all either very close to, or in excess of, 170 g. Some tests exceeded the acceleration limits dramatically and six vehicles exceeded 400 g in at least one test location.

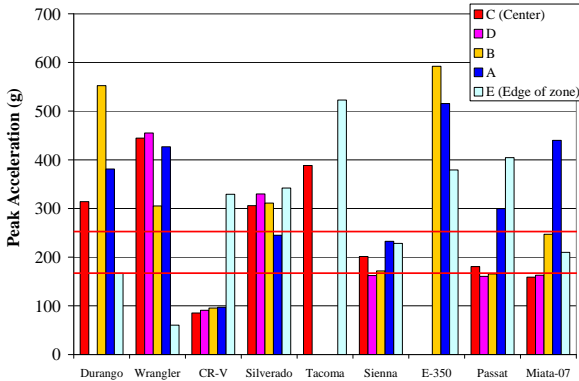


Figure 22. Peak acceleration for all impacts by vehicle and impact location.

Peak magnitude of shear displacement is shown in Figure 23. This peak is an absolute value, representing the peak magnitude. The GTR shear displacement limit of 6 mm is indicated in red. Only the CR-V passed shear limits in all tests, but six of the nine vehicles were able to pass the shear requirement in at least one test location.

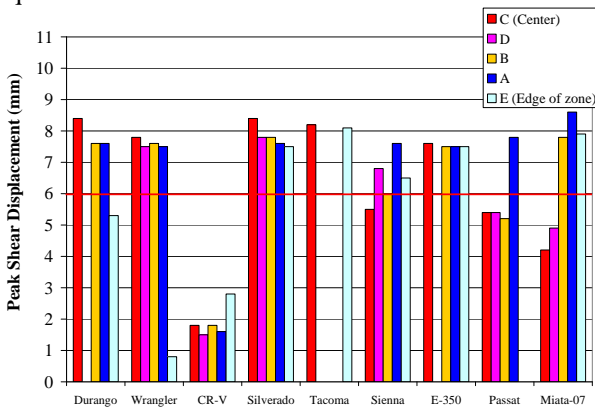


Figure 23. Peak shear displacement for all impacts, by vehicle and impact location.

Peak knee bending angle is shown in Figure 24. Only 8 of 40 (20%) impacts resulted in bending angle peaks below the injury limit of 19 degrees, which is shown in red. The majority of the failing impacts showed bending angles in excess of 30 degrees.

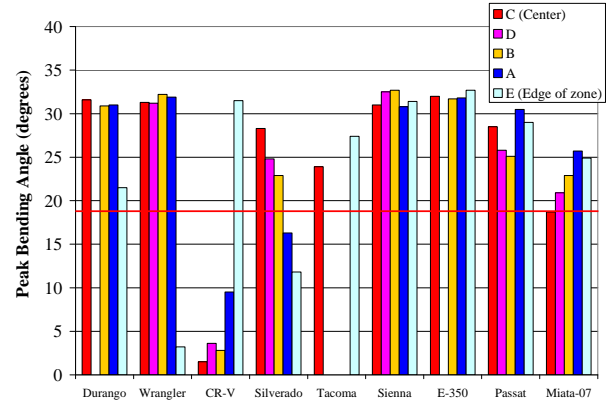


Figure 24. Peak bending angle for all impacts, by vehicle and impact location.

DISCUSSION

Adherence to GTR Testing Requirements

Several tests in the results section are reported as not meeting the test *conditions* required by the GTR. The test parameters that were “failed” in those tests will be discussed in this section, along with implications for interpreting the results of those tests.

In four tests, axial rotation about the vertical axis exceeded the 5 degree limit listed in the GTR: locations D and E on the Honda CR-V, location B on the Toyota Sienna, and location C on the E-350. In all of these tests axial rotation was 7 degrees or less. It is likely that the injury measures were the same or lower than they would have been had the axial rotation been less than 5 degrees. Since acceleration is a single-axis measurement in the direction of impact, pre-impact rotation would reduce the acceleration measured. Based on trigonometry, a rotation of up to 7 degrees would be expected to lead to a drop in measured acceleration of less than 1% compared to a perfectly aligned impact. Similarly, the EEVC/TRL legform is designed to measure shear and bending angle in only one direction. If the measured shear displacement and knee bending angle are affected by rotation of the legform off its normal design direction, the rotation would be expected to lead to lower measured shear displacement and knee bending angle.

Two tests on the Mazda Miata were not within the impact speed requirements of the GTR, which are 11.1 m/s +/- 0.2 m/s. The test at impact location B was slow at 10.87 m/s and the test at location D was fast at 11.39 m/s. It is assumed that impact D produced higher injury measures than those expected

had the test been within the speed range, and the impact B produced lower injury measures than those expected had the test been within the speed range. In the case of the impact at location D, the higher-than-allowed impact speed may have been responsible for the failing bending measurement, which was only 1.9 degrees beyond the injury limit. Had the impact been in the correct speed range, impact D may have met GTR requirements. In the case of impact location B, the lower-than-allowed impact speed did not have an effect on its failure to meet GTR requirements.

Impact B on the Silverado (Figure 25) deviated from the requirements of the GTR in that it was performed at a location where the Lower Bumper Reference Line exceeded 500 mm and therefore was not subject to lower legform testing. Shear and bending measurements may have been affected by LBRL height, as these measures were lower for impacts C and D in the lower central portion of the bumper. However, all tests on the Silverado failed the GTR limits by a wide margin. The height of the LBRL at location B was not believed to have been the cause of the failure at this test location.



Figure 25. Chevy Silverado bumper showing Lower Bumper Reference Line (LBRL) in white and impact location B in yellow, where LBRL is greater than 500 mm.

The tests listed above were not tested in strict accordance with the GTR procedures. These should not therefore be used directly to evaluate compliance with the GTR. The results are reported here because they are not expected to be significantly different from the expected result had the GTR test procedure requirements been met. With the exception of location D on the Miata, all of the impacts that failed would still have been expected to fail had the GTR test requirements been met. Location D on the Miata,

which was impacted too fast and exceeded injury measures by a narrow margin, may have passed had it been tested within the GTR test procedure limits.

Relative Difficulty of Injury Measures

Six of the nine vehicles tested met the 170 g limit on *upper tibia acceleration* in at least one test location. Of the 39 impacts where acceleration was measured, 20 indicated upper tibia acceleration over 250 g, and 8 were above 170 g but below the relaxed limit of 250 g (Figure 22). Of the 11 impacts that were below 170 g, only 5 impacts met the requirement with a margin wider than 10 g. The relaxed GTR acceleration limit of 250 g applies only to a width of bumper equal to approximately 2 widths of the legform, which is equivalent to one test location on each side of the car. In the current series, it is assumed that a vehicle could potentially pass the requirements if it has only one test over 170 g (but under the relaxed limit of 250 g) with the remainder of the tests under 170 g. The CR-V came closest to achieving those requirements with four of five tests under 170 g, but exceeded the limits with a fifth test over the relaxed limit of 250 g. The Sienna was able to remain under 250 g for all tests, but exceeded the 170 g limit in four out of five tests; given that there is not enough relaxation zone to cover all four of those impact locations, this vehicle would not meet the GTR acceleration requirement.

As shown in Figure 22, whether acceleration was higher in inboard locations or outboard locations was design-specific. The highest measures of acceleration were often measured near the bumper support, suggesting that tibia acceleration is more sensitive to stiffness of structures under the bumper than to the gradual changes in profile shape that occur across the front of the vehicle. Among vehicle types, the pickup trucks and the full-size van showed consistently high levels of acceleration, with all impacts close to or in excess of the 250 g limit.

Six of nine vehicles tested passed the *knee shear displacement* limit in at least one location, and one vehicle (CR-V) passed the shear requirement in all locations tested (Figure 23). Fourteen impact locations were at or below the shear limit of 6 mm, and 25 impact locations exceeded the knee shear limit of 6 mm. Many of the tests that exceeded 6 mm indicated shear displacements in the range of 7.5 mm to 8.5 mm suggesting a possible physical limit on the magnitude of shear displacement allowed by the EEVC/TRL legform. If this injury measure is bottoming-out, estimates of injury risk based on this level of shear may be underestimated.

Knee shear measures appeared to be related to inboard/outboard position on the vehicle. Most vehicles either showed a trend toward increased or decreased shear displacement as the impacts moved outboard, suggesting that shape change across the front of the vehicle may have more effect on shear displacement than the stiffness of under-bumper structures.

The *knee bending angle* limit appeared to be the most challenging to meet for the vehicles tested. Only four of the nine vehicles tested met the 19 degree bending angle limit in at least one location, and only 8 impacts in the series passed this limit. Many of the failing impacts showed peak bending angle clustered between 30 and 32 degrees, suggesting a physical limit on knee bend in this range. It is likely that the legform is physically bottoming out so estimates of injury risk based on this level of bending may be underestimated.

Peak bending angle tended to either increase or decrease as the impacts moved outboard, suggesting that, as with knee shear, the shape change across the front of the vehicle had more effect on bending angle than did stiffness of under-bumper structures.

To summarize the relative difficulty of the injury measures, bending angle was the most frequently failed injury criterion. Shear and bending angle appeared related to the change of shape across the front of the vehicle while acceleration seemed more linked to stiffness of the underlying structures. Measurements of knee shear and bending angle may be bottoming out, leading to potential underestimation of injury risk.

Results by Vehicle Type

Based on the vehicles tested in this series, the passenger vehicles (Miata and Passat) and minivan (Sienna) showed relatively better results in acceleration and peak shear displacement compared to the full-size van (E-350) and pickup trucks (Silverado and Tacoma). Results for the SUVs were mixed, with the CR-V performing better than other vehicles in all three injury measures, and the Wrangler and Durango performing relatively poorly.

Characteristics of Passing Impacts

There were a total of six passing impacts in the current series, four for the CR-V, one for the Wrangler, and one for the Miata.

In the passing impacts, video showed visibly more bumper deformation than there was in impacts that exceeded acceleration limits. Passing and failing CR-V impacts (Figure 26), Miata impacts (Figure 27), and Wrangler impacts (Figure 28) are compared below to illustrate that deformation appears to be associated with better performance relative to upper tibia acceleration. In all three passing impacts illustrated below, there was visible deformation of the bumper, resulting in varying degrees of damage. In the CR-V center impact (C), the CR-V sustained permanent deformation to the bumper cover, the underlying bumper support, and adjacent grille and air conditioning structures. The Miata center impact (C) resulted in damage to the ribbed energy absorber immediately adjacent to the impact point but showed no external evidence of damage. On the Wrangler, the end-cap on the bumper snapped off at impact allowing the legform to move into the front face of the fender and the tire tread. The fender, which is parallel to the bumper in its undeformed state, then deformed to absorb additional energy from the impact. In the passing impacts, the bumper and underlying structures absorbed energy and reduced the levels of deceleration in the legform by deforming during impact.



Figure 26. Passing CR-V center impact C on left (acceleration 85.3 g) and failing CR-V outboard impact E on right (acceleration 329 g).

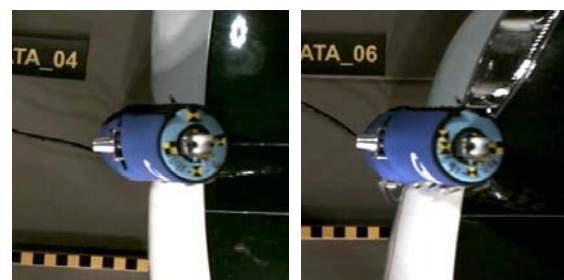


Figure 27. Passing Miata center impact C on left (acceleration 159 g) and failing Miata impact A on right (acceleration 40 g).



Figure 28. Passing outboard Wrangler impact E on left (acceleration 60 g) and failing Wrangler impact center impact C on right (acceleration 445 g).

Another characteristic of passing impacts appears to be the distribution of impact forces over a large area on the legform above *and* below the knee. In passing CR-V tests, the load is applied over a relatively tall bumper that makes contact above and below the knee of the legform (Figure 29). In the Miata passing impact C, the top of the bumper is adjacent to the lower femur, and tibia loads are shared by a lower spoiler. On the passing Wrangler test, the failure of the bumper end-cap allowed the femur to move into the vertical fender and the tibia to move into the tire tread, sharing the loads over a large portion of the legform.



Figure 29. Bumper contact area in passing impacts CR-V (C), Miata(C), and Wrangler(E).

It should be noted that the low injury measures indicated in passing Wrangler impact E do not account for the potential injury risk posed by striking the tread of a tire on a moving vehicle.

Comparison to Prior Testing of U.S. Vehicles using EuroNCAP Test Procedures

Testing was performed previously with the EEVC/TRL legform in a collaborative study with Transport Canada (Mallory, Stammen et al. 2005). That initial series of testing was done using EuroNCAP procedures. Those EuroNCAP procedures were similar to, but not the same as, GTR

lower legform test procedures. Each vehicle underwent impacts to the center of the bumper and over the bumper support. The following North American vehicles were tested:

- 1999 Ford Focus,
- 2001 Honda Civic,
- 2002 Mazda Miata MX5,
- 1999 VW Beetle, and
- 1997 Volvo S40.

The 2005 series of tests performed according to EuroNCAP procedures and the current series of GTR tests both used the EEVC/TRL legform at an impact speed of 40 km/h. The primary difference between the tests defined in the EuroNCAP procedure and the GTR procedure, and between the two series of tests run at VRTC, is the height of the bottom of the legform, which is at ground reference level in the EuroNCAP procedure/VRTC's 2005 series and 2.5 cm above ground reference level in the GTR test series being reported in this paper.

Test data from the Mazda Miata was compared for the two series in order to evaluate whether the passenger car results from the first series of EuroNCAP testing at VRTC could be combined with the results from the currently reported GTR testing. Figure 30 shows the location of comparable impacts in the two series. Each series had at least one test at the center of the bumper that can be compared directly. The 2005 EuroNCAP tests included an impact directly over the bumper support that can be compared to tests adjacent to the bumper support in 2007 GTR testing. Figure 31 compares the test results for impacts in the center of the bumper for both series, and Figure 32 compares the results for impacts near the bumper support.

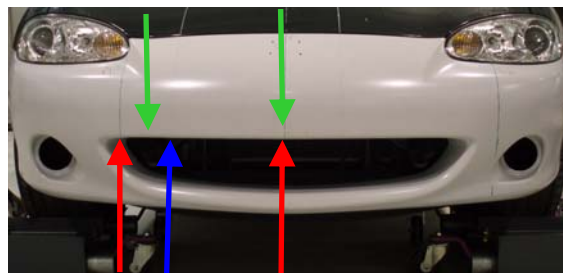


Figure 30: Photograph of Mazda Miata showing comparable impact locations in 2005 EuroNCAP testing (green, upper arrows) and in 2007 GTR testing (red and blue, lower arrows).

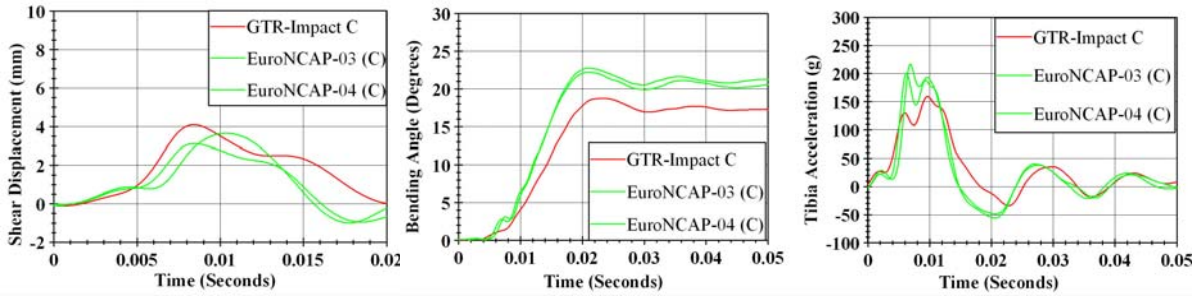


Figure 31: Shear displacement, bending angle and tibia acceleration for center impact using GTR procedure in 2007 VRTC testing (red) compared to prior testing at the center bumper according to 2005 EuroNCAP testing (green).

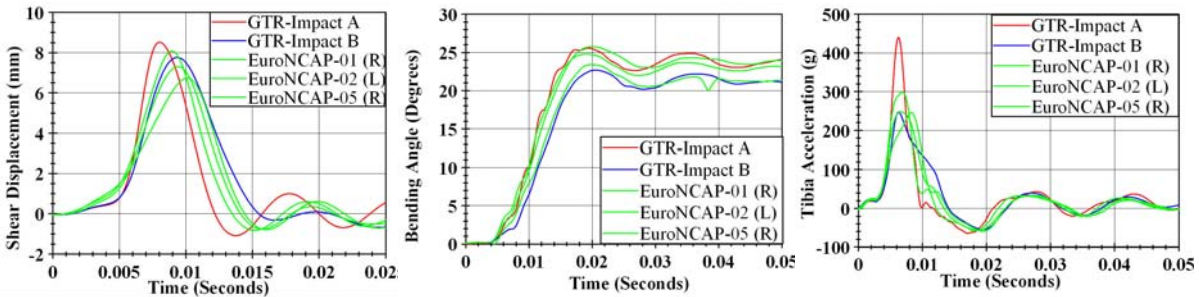


Figure 32: Shear displacement, bending angle and tibia acceleration for impacts adjacent to bumper support 2007 GTR testing (red, blue) compared to prior testing over left and right bumper support according to 2005 EuroNCAP testing (green).

Figure 31 and Figure 32 show that the differences between the peak values from 2005 EuroNCAP testing and 2007 GTR testing do not appear significantly greater than the differences in peak results among repeats of individual 2005 EuroNCAP tests over the lateral bumper in spite of difference in leg-to-ground-reference height. However, it should be noted that the difference in test results at the center bumper location in Figure 32 are important, in that the 2005 tests failed the acceleration and bending angle requirements in the current GTR (175 g and 19 degrees, respectively), while the 2007 tests passed.

In spite of the differences in results between the 2005 series of tests and the 2007 series, data from the 2005 offer pedestrian performance information on four U.S. passenger cars, in addition to the two tested in the 2007 series, even if results must be considered approximate relative to the requirements in the GTR (Table 13).

Table 13.
Peak measures in 2005 test series (Mallory, Stammen et al. 2005), average values for tests at center bumper and over bumper support

		Tibia Acceleration (g)	Bending Angle (degrees)	Shear Displ. (mm)
Ford Focus	Center	195	33.4	-4.9
	Support	209	32.3	-3.8
Honda Civic	Center	221	31.0	4.7
	Support	369	30.7	7.7
Mazda Miata	Center	209	24.7	3.4
	Support	264	25.1	7.4
VW Beetle	Center	462	34.7	8.3
	Support	264	29.1	8.2
Volvo S40	Center	263	31.1	8.2
	Support	246	30.2	6.2

As with the larger vehicles that were the focus of the current study, all of the U.S. passenger cars tested exceeded the GTR limits. The best performing

vehicle in the 2005 EuroNCAP series, the Mazda Miata, was only able to pass GTR requirements in one test location when retested to GTR conditions. Given the wide margin by which most of the passenger car test locations exceeded the injury limits, it is assumed that these vehicles would not have met the requirements even had they been run under GTR conditions. Average values for all impact locations exceeded the 19 degree bending limit and the 170 g upper tibia acceleration limit. Four of five vehicles showed higher acceleration in impacts over the support, while four of five vehicles showed higher bending values in the central bumper area. These passenger car results are consistent with the performance of the vehicles in the currently reported series of tests.

CONCLUSIONS

The results from the current series of tests, along with tests previously reported, can be used to provide a snapshot of the level of pedestrian lower extremity protection provided by the current U.S. fleet.

Relative to GTR requirements, pedestrian lower extremity protection was poor overall in the U.S. vehicles tested. No vehicle was able to meet GTR injury limits in all locations tested, although the CR-V came closest by meeting the requirements by a wide margin in all but one of the impact locations tested. Two other vehicles each had a single passing impact location.

Knee bending angle limits were the most difficult requirement for the tested U.S. vehicles to meet. Only 8 impacts in the current series were below the 19 degree limit, and only 4 vehicles met that requirement in any location. Bending angle appeared to be most associated with the shape of the front of the vehicle. Upper tibia acceleration limits were also challenging for the vehicles tested, with only 11 impacts meeting the 170 g limit and 8 more over 170 g but below the relaxed limit of 250 g. Acceleration appeared to be associated with the stiffness and deformation of structures under the bumper, and tended to be highest in the area of the bumper support.

Impacts that passed all injury measures tended to be associated with deformation of bumper structures at the impact point and distribution of loads over a large area on the legform, both above and below the knee.

ACKNOWLEDGEMENTS

The authors acknowledge Transportation Research Center Inc.'s David Hyder and Patrick Biondillo who performed the testing reported in this paper.

REFERENCES

- Ballesteros, M., P. Dischinger, et al. (2004). "Pedestrian injuries and vehicle type in Maryland, 1995-1999." Accident Analysis and Prevention **36**: 73-81.
- GRSP (2006). Proposal for a Global Technical Regulation on Uniform Provisions Concerning the Approval of Vehicles with Regard to their Construction in Order to Improve the Protection and Mitigate the Severity of Injuries to Pedestrians and Other Vulnerable Road Users in the Event of a Collision". **TRANS/WP.29/GRSP/2006/2**.
- Mallory, A. and J. Stammen (2006). "Lower Extremity Pedestrian Injury in the U.S.: A Summary of PCDS Data", NHTSA Vehicle Research and Test Center:<http://www.unece.org/trans/doc/2008/wp29/WP29-144-03e.pdf>
- Mallory, A., J. Stammen, et al. (2007). Pedestrian GTR Testing of Current Vehicles. 20th International Technical Conference on the Enhanced Safety of Vehicles (ESV). Lyon, France.
- Mallory, A., J. A. Stammen, et al. (2005). Component Leg Testing of Vehicle Front Structures. 19th International Technical Conference on the Enhanced Safety of Vehicles (ESV). Washington, DC.
- Matsui, Y. (2005). "Effects of vehicle bumper height and impact velocity on type of lower extremity injury in vehicle-pedestrian accidents." Accident Analysis and Prevention **37**: 633-640.

Characteristics of the TRL Pedestrian Legform and the Flexible Pedestrian Legform Impactors in Car-front Impact Tests

Yasuhiro Matsui
Shunsuke Takagi
Yoshitomo Tanaka
Naruyuki Hosokawa
Fujine Itoh
Hideto Nakasato
Noriaki Watanabe
Hideki Yonezawa
National Traffic Safety and Environment Laboratory
Japan

Paper Number 09-0206

ABSTRACT

Pedestrian protection is one of the key topics of discussion in the area of vehicle safety legislation in Europe and Japan. Leg injuries are the most common injuries found in nonfatal pedestrian accidents. The EC regulation and Euro NCAP are evaluating pedestrian leg protection performance in current vehicles. The TRL legform impactor is specified by the EC regulation, where Phase 1 took effect during 2005 and a draft phase 2 is scheduled to take effect in 2013. The global technical regulation (GTR) pedestrian protection test protocol was made basically using the TRL legform impactor. However, a flexible legform impactor has been under development. When the flexible legform impactor development is fully completed and evaluated, it is possible that both legform impactors may be determined to be useful in the GTR. Thus, the objective of this study is to investigate the characteristics of pedestrian leg protection performance of the frontal area of current vehicles using the TRL legform impactor and the flexible legform impactor. Different types of vehicles (sedan, sport utility vehicle (SUV), height wagon, and 1 box car) were used. The center of the bumper and center of the side members (i.e., the vehicles main longitudinal beams) were selected as impact locations for the legform impactors tests. This paper discusses an equivalence of injury assessment between the TRL legform impactor and flexible legform impactor.

INTRODUCTION

Every year, around 78,000 pedestrians are injured in traffic accidents in Japan [1]. Pedestrian protection is one of the key topics of discussion in the area of vehicle safety legislation in Europe and Japan. Leg injuries are the most common injuries found in nonfatal pedestrian accidents [1]; therefore, this investigation focuses on evaluating the protection provided by the

bumpers of eight typical cars found in Japan. The basis of the test procedure used in this study for evaluation of bumper performance was developed by the European Enhanced Vehicle-safety Committee (EEVC)/WG17 [2]. The Transport Research Laboratory (TRL) legform impactor [3] approved by the EEVC/WG17 is employed by the EC regulation, where Phase 1 [4] took effect during 2005 and a draft Phase 2 [5] is scheduled to take effect in 2013. The global technical regulation (GTR) pedestrian protection test protocol was made basically using the TRL legform impactor.

On the other hand, a flexible legform impactor which has a greater biofidelic level has been under development [6]. The flexible legform impactor has been evaluated for its technical level as a test tool by the pedestrian legform impactor technical evaluation group (TEG) of GRSP. When the flexible legform impactor development is completed and evaluated, both legform impactors have a possibility to be used in the GTR. Thus, the objective of this study is to investigate the characteristics of the pedestrian leg protection performance of the frontal area of current vehicles using the TRL legform impactor and the flexible legform impactor.

METHOD

Set-up

The current model (2000) of the TRL legform impactor [3] and the flexible legform impactor type GT (2007) [6] were propelled into a stationary vehicle (Figure 2), respectively. The target impact velocity of the legform impactor was 11.1 m/s (40 km/h). The bottom surface of the TRL legform impactor was set to be the same level as the ground line at the moment of contact moment between the legform and bumper surface. The bottom surface of flexible legform impactor was set to be 75 mm higher level from the

ground line at the moment of contact, in order to have the flexible legform behavior became similar to that observed in the human body model simulations [6].

The tire pressure in each tested vehicle was adjusted to the pressure recommended by the vehicle manufacturer. To simulate two adult front seat occupants, 75-kg weights were placed on each seat. The temperature in the test facility during the test program was maintained in the range 20 to 21 degrees Celsius. The motion of the legform impactor during its impact with the vehicle was recorded by means of a high-speed digital camera (1000 frames/second).

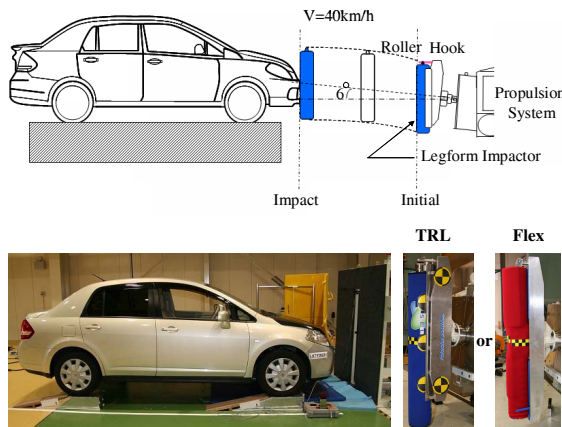


Figure 1. Legform impactor to vehicle bumper impact test setup

Eight different vehicles were tested from the following four categories: sedan, sport utility vehicle (SUV), height wagon, and 1 box car. Their specifications are summarized in Table 1. The height wagon and 1 box car used in this study were classified into the K-car (less than or equal to 660 cc of engine displacement) in Japan.

Table 1. Vehicle specifications

Vehicle type		All length*all width *all height (mm)	Net weight (kg)	Displacement (cc)	Bumper material
Sedan	A	4410*1695*1460	1130	1496	resin
	B	4670*1695*1505	1390	1990	resin
	C	4395*1695*1535	1120	1498	resin
SUV	A	4420*1785*1710	1550	2354	resin
	B	4455*1765*1675	1400	1998	resin
Height wagon	A	3395*1475*1645	840	658	resin
1Box	A	3395*1475*1870	940	658	resin
	B	3395*1475*1880	920	656	resin

The center of the bumper and the center of the side members (i.e., the vehicles main longitudinal beams) were selected as an impact location for both legform impactors tests as shown in Figure 2. The center of the bumper was defined to be on the line of the bonnet lock. It should be noted here that the bonnet lock of the height wagon A was slightly off-set from the vehicle's

center line as shown by CI in Figure 2 (6). The location of CII of the height wagon A was 295 mm away from CI.

SI of SUV A is the most outer location in the impact area defined by EC regulation [5]. SII of SUV A is the location in front of the main longitudinal beam.

In front of the 1box A car, there are two cross beams. SI of the 1 box A is the location in front of the main longitudinal beam which is connected to the lower cross beam. SII of the 1box A is the location in front of the longitudinal beam connecting to the upper part of the cross beam. A total of 19 locations from eight vehicles were impacted by the TRL and flexible legform impactors, respectively.

Injury Measures

TRL legform impactor

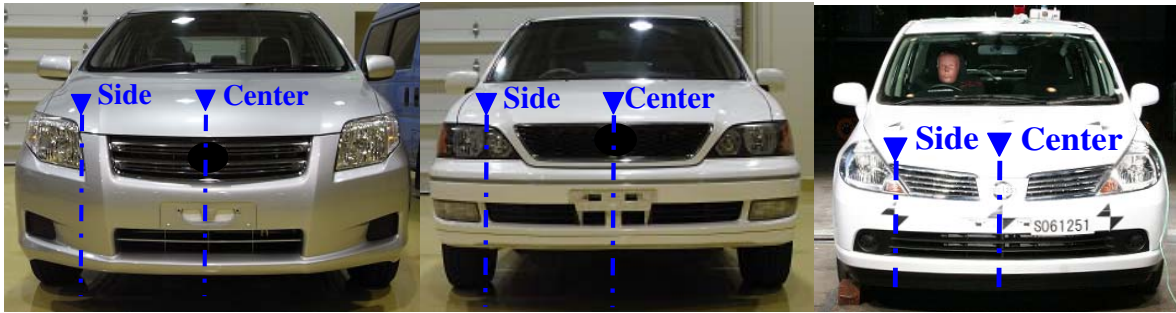
The lower leg acceleration was used to evaluate tibia fracture risk. The knee shearing displacement (i.e., relative displacement between the leg and thigh at the knee joint level in the lateral direction) was measured to evaluate the cruciate ligament injury risk. The knee bending angle (i.e., angular displacement of the knee joint) was measured to evaluate the collateral ligament injury risk. Each data channel was sampled at 10 kHz, and data processing was done with an SAE Class 180 filter. In this study, the measured criteria were compared to the injury assessment reference values (IARVs), which will be employed by EC regulation phase 2 [5].

Flexible legform impactor

The bending moment was used to evaluate the tibia fracture risk. The anterior cruciate ligament (ACL) elongation and posterior cruciate ligament (PCL) elongation were measured to evaluate each cruciate ligament injury risk. The medial collateral ligament (MCL) elongation was measured to evaluate collateral ligament injury risk. Each data channel was sampled at 10 kHz, and data processing was done with an SAE Class 180 filter. Since the IARVs of flexible legform have not been decided to date, this study used the lowest values employed in the paper [7]. The IARVs used in this study are summarized in Table 2.

Table 2. Injury assessment reference values

	Tibia	Knee ligament		
		ACL	PCL	MCL
TRL	Acceleration	Shear displacement		Bending angle
	170 G ⁵⁾	6 mm ⁵⁾		19 degrees ⁵⁾
Flex	Bending moment	Elongation		
	312 Nm (312-350) ⁷⁾	11.2 mm (11.2 mm) ⁷⁾	11.2 mm (11.2 mm) ⁷⁾	19.5 mm (19.5-21.6 mm) ⁷⁾



(1) Sedan A

(2) Sedan B

(3) Sedan C



(4) SUV A



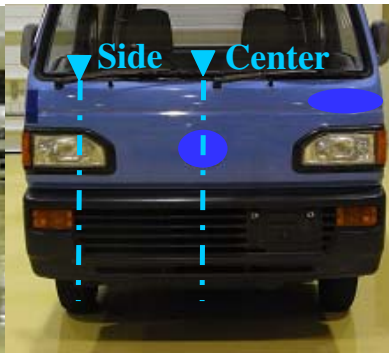
(5) SUV B



(6) Height wagon A



(7) 1 Box A



(8) 1 Box B

Figure 2. Impact locations on bumper of tested vehicles

RESULTS

Fitting Ratio

The measured injury criteria utilized by the TRL and legform impactors are listed in Table 3. The measured criteria which exceed the IARVs shown in Table 2 are indicated by the yellow shading. The TRL legform impactor impact results which exceed the IARVs [5] did not match the flexible legform impactor impact results which exceed the IARVs [7].

The measured injury criteria of the TRL and flexible legform impactors, together with the zone indicating whether the measures fulfilled the IARVs, are also shown in Figure 3. For the assessment of the tibia fracture risk, the relation between the acceleration measured by the TRL legform impactor and the bending moment by flexible legform impactor are summarized in Figure 3 (1). For the assessment of the ACL injury risk, the relation between the shear displacement measured by the TRL legform impactor and the ACL elongation measured by the flexible legform impactor are summarized in Figure 3 (2). For the assessment of the PCL injury risk, the relation between the bending angle measured by the TRL legform impactor and the PCL elongation measured by flexible the legform impactor are summarized in Figure 3 (3). For the assessment of the MCL injury risk,

the relation between the bending angle measured by the TRL legform impactor and the MCL elongation measured by the flexible legform impactor are summarized in Figure 3 (4). The red shaded areas indicate that the measured criteria exceeded both requirements for the TRL and the flexible legform impactors. The blue shaded areas indicate that the measured criteria met both requirements for the TRL and the flexible legform impactors. For the assessment performance and the injury risk level of the IARVs between the TRL and flexible legform impactors to be completely the same for each injury, the measured criteria both have to be either in the blue area or both in the red area. However, all measured criteria were not in the blue or red area.

In this study, the fitting ratio was defined as the number in the blue or red area divided by the number in the all impact locations (n=19). The fitting ratios corresponding to each injury are listed in Table 4. The fitting ratio for the tibia fracture risk assessment was 63%. On the other hand, the fitting ratios for the ACL, PCL, and MCL injury risk assessments were 84%, 79%, and 84%, respectively. Therefore, the knee ligament injury risk assessment was at a higher level compared to the tibia fracture risk assessment between the TRL and flexible legform impactors.

Table 3. List of measured injury criteria

Vehicle type	Impact location	Impact test result using TRL					Impact test result using Flex				
		Velocity (km/h)	Tibia fracture assessment	Knee ligament injury assessment		Velocity (km/h)	Tibia fracture assessment	Knee ligament injury assessment			
			Acceleration (G)	Shear displacement (mm)	Bending angle (deg)		Bending moment (Nm)	ACL	PCL	MCL	
		Elongation (mm)		Elongation (mm)							
Sedan	A	Center	39.7	138	2.8	4.8	40.7	232	4.2	4.0	11.3
		Side	39.7	291	2.0	20.3	40.5	311	7.7	13.0	25.0
	B	Center	39.8	224	3.7	28.9	39.4	349	9.7	8.5	31.0
		Side	39.9	371	3.9	25.6	40.2	339	17.2	10.2	31.0
	C	Center	40.1	198	1.7	12.6	40.2	178	6.2	4.1	15.4
		Side	39.8	307	3.0	24.3	39.9	307	7.3	8.8	23.2
SUV	A	Center	40.0	81	2.0	2.8	40.1	221	3.7	0.6	9.5
		Side I	40.1	97	2.6	12.6	40.5	238	6.0	5.4	18.1
		Side II	39.9	383	7.5	25.3	40.2	433	13.8	8.7	31.0
	B	Center	40.0	126	1.1	16.5	40.0	356	10.5	6.0	23.5
		Side	40.5	342	6.8	25.3	40.0	435	20.8	9.5	31.1
Height Wagon	A	Center I	40.3	129	1.3	4.0	40.0	279	2.6	1.9	5.6
		Center II	40.3	142	1.7	3.0	40.1	321	2.7	4.1	4.2
		Side	40.4	545	7.8	24.0	40.4	377	10.0	6.7	13.9
1Box	A	Center	39.7	178	2.0	1.6	40.4	236	2.6	5.0	1.4
		Side I	40.1	453	4.0	19.3	40.2	329	9.5	8.3	15.4
		Side II	40.0	399	7.6	24.4	40.3	286	7.2	17.9	27.5
	B	Center	40.3	97	1.8	4.7	39.9	268	4.1	2.7	13.1
		Side	39.9	159	3.0	10.9	39.9	267	6.2	3.8	17.8

: Over injury assessment reference value (IARV)

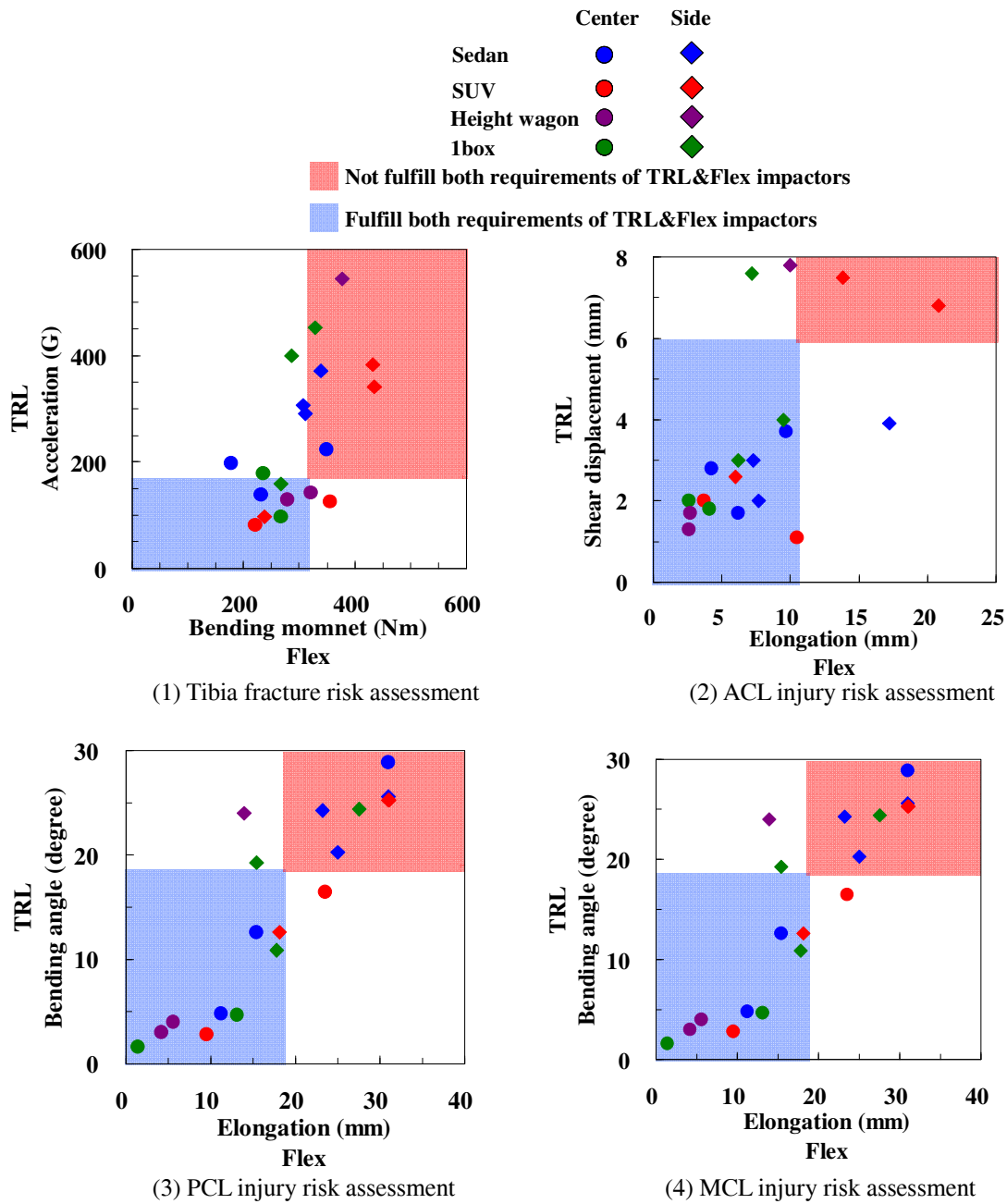


Figure 3. Measured injury criteria

Table 4. Fitting ratio

Injury type	(1) Tibia	(2) ACL	(3) PCL	(4) MCL
Fitting ratio	12/19	16/19	15/19	16/19
	63%	84%	79%	84%

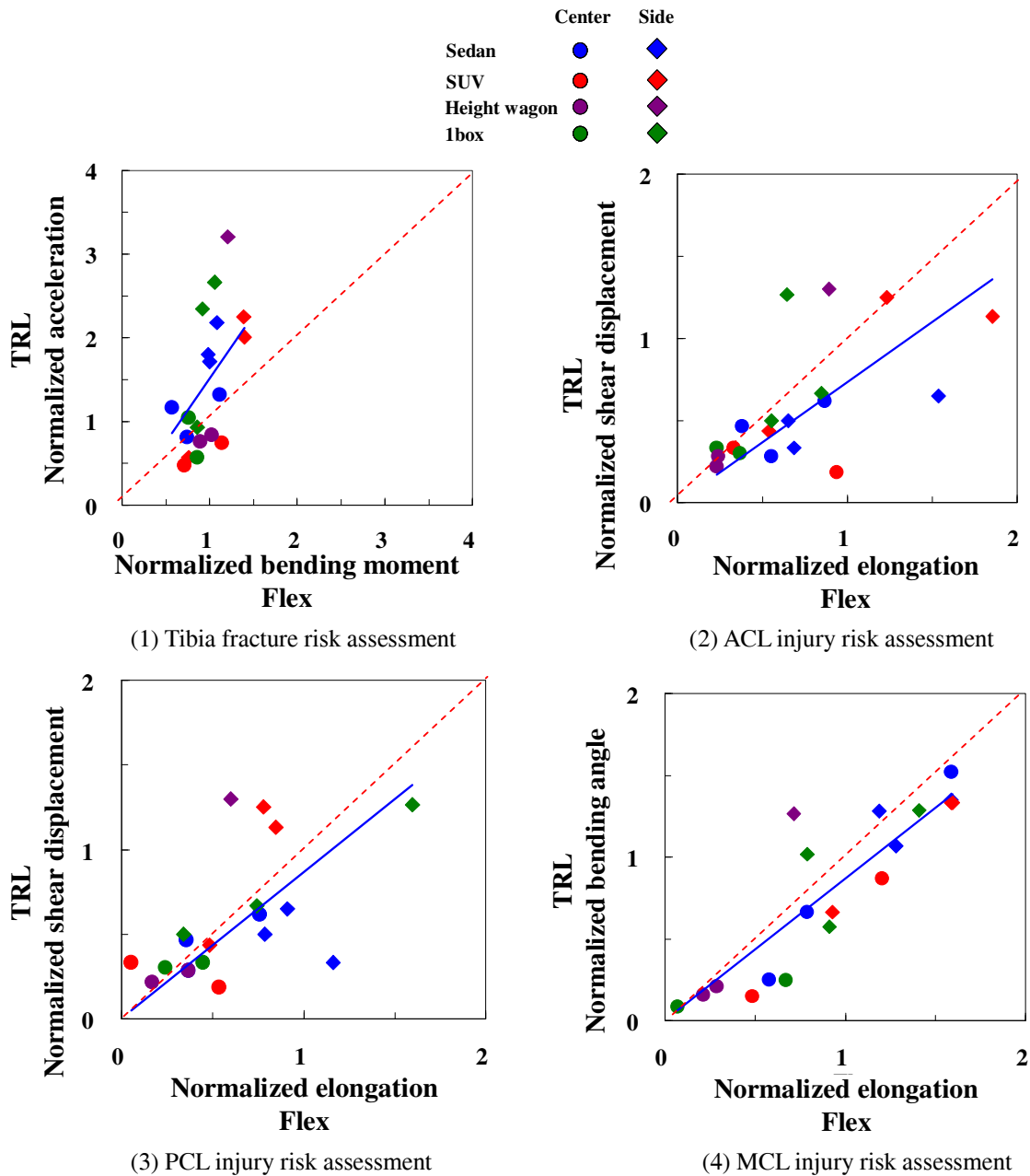


Figure 4. Injury measures normalized by IARVs

Comparison of Injury Measures Normalized by IARV between TRL and Flexible Legform Impactors

The investigation of an equal possibility of using both the TRL and flexible legform impactors for injury risk estimation is necessary. To assess the injury severity when evaluating the bumper aggressiveness by means of the TRL and flexible legform impactors, the

maximum values obtained by both impactors were expressed as injury measures normalized by IARVs (normalized injury measures). The IARVs of the TRL and flexible legforms listed in Table 2 were used. The relationship between the normalized measures of the TRL and the flexible legforms are summarized in Figure 4. The regression line starting from the coordinate origin between the two normalized injury measures was indicated by a blue solid line. The

dashed line, corresponding to an 1:1 ratio indicated that the injury risk assessment between the TRL and the flexible legforms is exactly the same. The risk assessment of the tibia fracture using the TRL legform impactor is more severe than that using the flexible legform impactor [see Figure 4 (1)]. The risk assessments of the knee ligament injuries (i.e., the ACL, PCL, and MCL) using the flexible legform impactor are more severe than those using the TRL legform impactor [see Figures 4 (2), 4(3), and 4(4)].

The coefficients of linear regression and the correlation coefficients are listed in Table 5. The correlation coefficient between the normalized injury measures of the TRL legform and the normalized injury measures of the flexible legform were over 0.51 for all injury types. Specifically, the correlation coefficient between the normalized bending angle of the TRL legform and the normalized MCL elongation of the flexible legform was 0.89. The coefficient of linear regression between the two normalized injury measures was 0.87. These coefficients indicate that both normalized injury measures could predict a similar risk of medial collateral ligament injury.

Table 5. Coefficient of linear regression and correlation coefficient

Injury type	(1) Tibia	(2) ACL	(3) PCL	(4) MCL
Coefficient of linear regression	1.50	0.73	0.87	0.87
Correlation coefficient	0.57	0.52	0.51	0.89

DISCUSSION

In this study, the criteria measured by TRL legform impactor and the criteria measured by flexible legform impactor were compared. Ideally, when comparing both results, the impact conditions such as impact velocity should be completely same. However, in this study, the impact velocity ranged 39.7 km/h to 40.7 km/h. One of the limitations of this study is that the analyzed results might be affected by the variation in impact velocity. In the future, the effect of impact velocity on the injury measures should be investigated. Then, the current results possibly could be improved by the elimination of the velocity effect.

The measured injury criteria in each tested vehicle were shown in Figure 3. When focusing on the tibia for its fracture risk assessment against a vehicle center impact, all tested vehicles except three cases fulfilled the requirements for both legform impactors [see

Figure 3(1)]. In contrast, for the tibia fracture risk assessment against a vehicle side member, the measured injury criteria indicated extremely high levels compared to those obtained at the vehicle center impact. The stiffness of the bumper in front of the main longitudinal vehicle beam in current vehicles is relatively high, and the distance between the inner surface of the bumper cover and frontal edge of the main longitudinal vehicle beam is too short to allow absorption of the impact energy exerted by the legform impactor. Some countermeasures, including attachment of energy absorbing structures in front of main longitudinal vehicle beam, might be necessary in terms of providing future pedestrian leg protection.

When focusing on the MCL injury risk assessment, the measured bending angles of an 1 box car by the TRL legform impactor were relatively smaller than those of a sedan or an SUV [see Figure 3(4)]. The frontal shape of the 1 box car could contribute to the reduction of the possibility of an MCL injury.

In this study, eight different vehicles including two 1 box cars were used. The 1 box cars were classified into the K-car (less than equal to 660 cc of engine displacement) in Japan. On the other hand, larger 1 box cars (such as more than or equal to 2000 cc engine displacement) are also popular in Japan. Since the difference in the car front design between the K-car and the relatively large engine displacement car is not understood, the pedestrian lower leg safety performance of the large engine displacement 1 box car should be investigated.

In Figure 4, linear regression was applied by the least square method for the injury measures normalized by the IARVs. The distances between each injury measure data point and the linear regression line are summarized in Table 6. The distances over 0.5 are marked by the yellow shaded areas. Table 6 indicates that the distances were over 0.5 in all injury types at the side of the height wagon. It implies that there is a possibility that the car front structure at the side of the height wagon is different than the structure of other vehicles.

Table 6 The distances between injury measures and the linear regression line

Vehicle type		Distance from linear regression line			
		Tibia fracture	ACL injury	PCL injury	MCL injury
Sedan A	Center	0.21	0.26	0.18	0.29
	Side	0.13	0.23	0.78	0.05
Sedan B	Center	0.25	0.03	0.05	0.17
	Side	0.35	0.65	0.16	0.03
Sedan C	Center	0.20	0.17	0.04	0.02
	Side	0.21	0.03	0.21	0.29
SUV A	Center	0.39	0.12	0.33	0.32
	Side I	0.39	0.06	0.02	0.16
	Side II	0.10	0.47	0.67	0.05
SUV B	Center	0.65	0.69	0.32	0.20
	Side	0.07	0.31	0.46	0.06
Height wagon	Center I	0.39	0.06	0.08	0.04
	Center II	0.48	0.15	0.04	0.03
	Side	0.90	0.88	0.90	0.74
1Box A	Center	0.07	0.22	0.06	0.03
	Side I	0.70	0.06	0.03	0.38
	Side II	0.63	1.08	0.13	0.07
1Box B	Center	0.48	0.04	0.11	0.39
	Side	0.24	0.13	0.24	0.25

The time history of the MCL elongation for the flexible legform impactor impacting against the center of Sedan A and the behavior of the flexible legform impactor at the time of maximum elongation are shown in Figures 5 and 6, respectively. According to Figure 5, 31.7 ms is the time when the maximum elongation was observed; however, the legform impactor was not in complete contact with the car front at this time (see Figure 6). Since the injury measures should be evaluated during the contact to the car front, the duration for the injury risk evaluation due to contact to a car front should be investigated in the future.

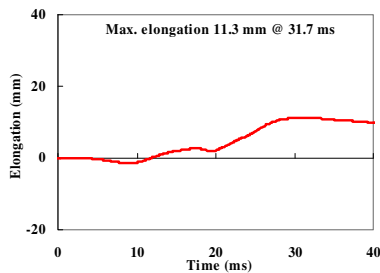


Figure 5 Time history of MCL elongation



Figure 6 Flexible legform behavior at 32 ms

For the assessment of tibia fracture, the TRL legform impactor has a simplified design such that it can measure the acceleration at 66 mm below the knee level. In contrast, strain gauges were attached at four different levels in vertical locations on the tibia of the flexible legform to measure bending moments. An analysis of the maximum bending moment was employed for this study. If the lower part of the bumper in a tested car is more rigid, the measured bending moment at the corresponding location of the flexible legform could be the highest. Thus, there is a possibility to have lower correlation coefficients when comparing the relationship between the normalized acceleration of the TRL legform and the normalized bending moment of the flexible legform at the similar level to 66 mm below the knee.

CONCLUSIONS

This study investigated the equal possibility of injury risk estimation using both the TRL and the flexible legform impactors. Nineteen locations of eight different Japanese vehicles (including sedan, sport utility vehicle (SUV), height wagon, and 1 box cars) were impacted by the TRL and the flexible legform impactors, respectively.

In this study, the fitting ratio was defined as the number in an area where the measured criteria either fulfilled both requirements or exceeded both requirements of the TRL and the flexible legform impactors divided by the number in the all test cases (n=19). The fitting ratio for the tibia fracture risk assessment was 63%. In contrast, the fitting ratios for the ACL, PCL and MCL injury risk assessments were 84%, 79% and 84%, respectively. Therefore, the knee ligament injury risk assessment was at a higher level as compared to the tibia fracture risk assessment between the TRL and the flexible legform impactors.

The measured injury criteria were normalized by the injury assessment reference values (IARVs) (normalized injury measures). In this study, the IARVs which are to be employed by EC regulation Phase 2 were used for the normalized criteria for the TRL legform impactor. Since the IARVs of the flexible legform have not been decided to date, this study used the values employed in an ESV paper. The relationship between normalized measures of the TRL and the flexible legforms were investigated. The risk assessment of tibia fracture using the TRL legform impactor is more severe than that using the flexible legform impactor. The risk assessments of knee ligament injuries (ACL, PCL, MCL) using the flexible legform impactor are more severe than those using the TRL legform impactor. The coefficients of linear regression and correlation coefficients were investigated. The correlation coefficients between the

normalized injury measures of the TRL legform and normalized injury measures of the flexible legform were over 0.51 for all injury types. Specifically, the correlation coefficient between the normalized bending angle of TRL legform and the normalized MCL elongation of the flexible legform was 0.89. The coefficient of linear regression between the two normalized injury measures was 0.87. These coefficients indicate that both normalized injury measures could predict a similar risk of medial collateral ligament injury.

REFERENCES

- [1] Institute for Traffic Accident Research and Data Analysis of Japan, *Annual Traffic Accident Report in 2006 (in Japanese)*, Tokyo, 2007.
- [2] European Enhanced Vehicle-safety Committee, *Improved Test Methods to Evaluate Pedestrian Protection Afforded by Passenger Cars*, EEVC Working Group 17 Draft Report, 1998.
- [3] Transport Research Laboratory, *TRL Pedestrian Legform Impactor User Manual. version 2.0*, 2000.
- [4] Commission of the European Communities : Pedestrian Protection: Technical Prescriptions Concerning Test Provisions for Pedestrian Protection, DG Enterprise Working Document 2003.
- [5] Commission of the European Communities : Proposal for a Regulation of the European Parliament and of the Council on the Protection of Pedestrians and other vulnerable road users Protection, 2007.
- [6] A Konosu, T Issiki, M Tanahashi and H Suzuki 'Development of a biofidelic flexible pedestrian legform impactor type GT (Flex-GT)', Paper number 07-0178, Proceeding of 20th International Technical Conference on the Enhanced Safety of Vehicles (CD), 2007
- [7] Oliver Zander et al., 'Prediction of lower extremity injury risks during an impact on modern car fronts with a flexible pedestrian legform impactor and the pedestrian legform impactor according to EEVC WG17' Paper number 07-0206, Proceeding of 20th International Technical Conference on the Enhanced Safety of Vehicles (CD), 2007

THE CAUSES OF PEDESTRIANS' HEAD INJURIES FOLLOWING COLLISIONS WITH CARS REGISTERED IN 2000 OR LATER

David Richards
Rebecca Cookson
Richard Cuerden

TRL

Gareth Davies

Helicopter Emergency Medical Service
United Kingdom
Paper Number 09-0459

ABSTRACT

Injury and collision data from London's Helicopter Emergency Medical Service (HEMS) and the UK's Police fatal files were used to quantify and describe the nature of pedestrian head injury and investigate the causes.

The HEMS data relating to all pedestrian accidents since 2000 was analysed with respect to their injuries, and the cost of these injuries was estimated using the time they spent on the ward and/or in intensive care. In addition to the HEMS data, Police fatal files containing details of fatal pedestrian impacts with the front of cars registered in 2000 or newer were analysed. These included post-mortems, which were coded using the Abbreviated Injury Scale. Although the fatal file sample was limited in size, it had the advantage of containing photographs of the accident and many other pertinent details. This enabled the causes of individual injuries to be determined. The head injuries seen in the HEMS data were then compared to the injuries in the fatal files .

The HEMS dataset contained 746 pedestrians struck by motor vehicles, with 2,974 recorded injuries. 34 fatal pedestrian accidents were analysed using the Police fatal files.

The analysis of the HEMS data showed that the most frequent and costly injuries were to the head and legs. Head injuries of fatally injured adults were found to be principally caused by contact with the windscreen and surrounding structure.

This research highlights the potential of hospital data to be an important tool in accident research, as the injury information can provide evidence of the effects of the changing vehicle fleet, and what injuries should be prioritised in the future. The paper also begins to quantify the proportion of the most serious head injuries (suffered by fatalities) which are caused directly by the vehicle, compared with secondary impacts with the ground or other objects.

INTRODUCTION

Pedestrian injuries

In 2007 in Great Britain there were 646 pedestrian deaths and 6,924 seriously injured pedestrian casualties in traffic accidents [1]. The majority of pedestrian impacts are with the front of the car. Pedestrians are usually hit from the side, and are 3 to 4 times more likely to be crossing the path of the vehicle than travelling in a parallel direction to it. Cases where the vehicle runs over the pedestrian (where the wheels travel over the pedestrian) are rare, with estimates varying between 2 % and 10 % [2] of pedestrian casualties.

Previous studies have seen that the body parts with the highest risk of injury for a pedestrian struck by a vehicle are the head, followed by the lower extremities, the thorax, and the pelvis [2]. For non-fatal injuries, the lower extremities have been seen as the most frequently injured.

The head is often subject to two impacts, the first with the car itself, and the second with the ground as the pedestrian is thrown from the car. In relation to the relative severity of these two impacts, the literature is divided. Some observe that the primary impact (with the car) is the most severe impact [2]. This is in line with papers suggesting that the injuries caused by secondary impact are fewer and less serious than those caused by primary impact [3]. However, others claim that the secondary impact is often a source of injury comparable to the primary impact [4].

At-the-scene studies [5] have shown that contact with the vehicle was responsible for more life-threatening or fatal head injuries than contact with the ground, and also that the windscreen frame was more likely to give a serious head injury than contact with the windscreen glass or the bonnet. There were other trends in the type of injuries suffered: head injuries were the most frequent injury sustained by those

having non-minor injuries, with leg injuries being the second most common. As the overall injury severity of the pedestrians increased, the likelihood of injury for the individual body regions also increased: more severely injured pedestrians had more injuries in more regions.

Supported by the European Commission (EC), the European Enhanced Vehicle-safety Committee Working Group 10 (EEVC WG10) and 11 developed testing methods and standards for pedestrian protection in frontal impacts with cars. These new standards have been introduced in a 2-stage approach, the first of which was the EC Directive 2003/102/EC [6]. This directive introduced a number of tests, including limits on the results of impacts between a lower leg form and the bumper and a head form to the bonnet top.

In addition to the pedestrian regulation, Euro NCAP undertakes pedestrian sub-system impactor tests. Leg forms impact with the bumper and the bonnet leading edge and the head forms strike the bonnet at a variety of locations. As of 2009, the pedestrian tests have become an integral part of the new overall score given by Euro NCAP for any new car [7].

Much of the previous accident research performed in the area of pedestrian injury has been based on pedestrian impacts with relatively old cars. Since these studies car geometry, stiffness and mass has altered such that previous conclusions may no longer be valid for the modern car fleet. The purpose of this paper is to explore how a new source of data, collected by medical professionals, can add to the knowledge of the injuries received by pedestrians in traffic accidents. The causes of these injuries in pedestrian impacts with new cars (registered in 2000 or later) will also be explored for a selection of fatally injured pedestrians using Police fatal files.

London's Helicopter Emergency Medical Service

A report was produced in the 1980s by the Royal College of Surgeons which documented cases of patients dying unnecessarily because of the delay in receiving prompt and appropriate medical care. London's Air Ambulance was established to address the findings of this report and to find a way to respond quickly in London's increasingly congested roads. London's Air Ambulance began operations in 1989 from a temporary base at Biggin Hill Airport and in 1990 moved to a permanent base in central London. This is at the Royal London hospital, which was the only multidisciplinary hospital with a site where it would be safe to build a rooftop helipad. The

Helicopter Emergency Medical Service (HEMS) began to fly from the rooftop at the Royal London on 30 August 1990 and to date has flown over 17,000 missions.

Two trauma teams are available to attend major trauma incidents seven days a week from 7am to sunset. At night the poor visibility makes flying around the city dangerous, therefore the teams are grounded and rapid response cars are used instead. These cars can also be used if the emergency occurs whilst the helicopter is away on another mission.

The HEMS primarily deals with major trauma accidents of all varieties including serious road traffic accidents. The patient is then seen as quickly as possible by a specialist trauma doctor and paramedic team to provide the greatest chance of survival. The paramedic team at the London Ambulance Service control room decides which of the 3,500 calls they receive a day are appropriate for the HEMS to attend. The paramedic team can also request for the HEMS to attend if they require further medical resources in the field. The helicopter's medical team are equipped with a substantial range of drugs, emergency surgical kits, monitors and other equipment so that they can begin treatment straightaway. A doctor is part of the HEMS team and is able to perform life saving medical procedures that a paramedic is not qualified to undertake. They can also take the patients to the hospital best suited for the patient's needs rather than the closest Accident and Emergency (A&E) department.

Police fatal files

Police fatal file accident reports are recognised as an important source of information for accident research. They can provide detailed information on the events leading up to an accident, as well as giving details of driver errors and/or vehicle defects which may have contributed to the accident and to the injuries that resulted in the fatality.

These fatal accident reports cost a great deal to produce both in terms of police and pathologists' time. The reports are produced, even where no criminal prosecution is envisaged, for presentation in evidence at the Coroner's inquest.

In 1992, TRL was commissioned by the UK's Department for Transport (DfT) to set up and manage the police fatal road traffic accident reports project. The purpose of this project was to institute a scheme whereby police forces in England and Wales would routinely send fatal road traffic accident reports to

TRL when they were no longer of use for legal purposes.

The fatal reports provide a valuable insight into how and why fatal accidents occur and offer an opportunity to learn from these tragic accidents, so that future incidents may be prevented. The current archive contains over 34,000 police fatal accident reports.

METHOD

The types of injuries sustained by pedestrians in traffic accidents were explored using data collected by HEMS. This data was also used to estimate the cost of these pedestrian casualties to the hospital. The causes of the head injuries of a sample of fatally injured pedestrians were determined using information present in Police fatal files.

HEMS pedestrian data

The data from the accidents attended by the HEMS team is entered into a database which is then primarily used for various analyses aimed at improving patient care and trauma management. This database holds information on the age and gender of the patient as well as their injuries and the treatment they received both on route to the hospital and during their stay. This includes information on operations, who treated them, outcome (i.e. whether they lived and if not then the area of the hospital in which they died) and their length of stay in hospital (both on wards and in Intensive Care Unit).

The HEMS database is a medical database, and as such it has detailed information on the injuries sustained by pedestrian casualties. Each injury is coded using the International Statistical Classification of Diseases and Related Health Problems, Ninth Revision (ICD-9). This is a coding system developed by the World Health Organisation, where each possible injury has a unique four character ICD-9 code associated with it. There are dictionaries of ICD-9 codes freely available on the internet [8]. This code describes what the injury is, but does not include a measure of the severity of the injury.

The severity of the injuries is recorded by the HEMS team using the Abbreviated Injury Scale (AIS 1998). Each injury description is assigned a unique six digit numerical code in addition to the AIS severity score. The AIS severity score is a consensus-derived anatomically-based system that classifies individual injuries by body region on a six point ordinal severity scale ranging from AIS 1 (minor) to AIS 6

(practically untreatable), shown in Table 3 [9]. This paper concentrates on injuries with an AIS score of 2 or greater.

Table 1.
Possible values of AIS.

AIS Score	Description
1	Minor
2	Moderate
3	Serious
4	Severe
5	Critical
6	Maximum
9	Unknown

MAIS denotes the maximum AIS score of all injuries sustained by a particular occupant. It is a single number that attempts to describe the seriousness of the injuries suffered by that occupant.

The analysis of the HEMS data was carried out at two levels: the casualty level (of 746 pedestrians), and the injury level (of 2,974 injuries). To investigate injuries at the more meaningful casualty level, the maximum AIS in different body regions was calculated for each pedestrian. The body regions were:

- H – Head (includes Neck)
- L – Lower limb
- U – Upper limb
- A – Abdominal region (includes abdomen, lower back, lumbar spine and pelvis)
- T – Thorax (includes thoracic spine)
- M – Multiple and Not specified regions

The “Multiple and Not specified regions” category was used for injuries such as external burns, which are a single injury but affect more than one region.

The cost of these pedestrian casualties to the hospital was estimated, by considering the different cost of a day on a normal ward and a day in an intensive care unit (ICU). The Intensive Care Society state that the cost of a day in an ICU is approximately six times as costly to the hospital as a day spent on a ward [10]. Christensen et al [11] cites the Department of Health statistics [12] which say that the mean cost per patient per day on a general ward is £281, and the mean cost per patient per day in a critical care unit is £1,328 (approximately 4.7 times more costly than the

ward). The information in the HEMS database includes the number of days spent by each patient on the ward and in the ICU, so this was used to calculate a cost of each patient to the hospital.

It should be noted that this cost only accounts for the length of time each pedestrian was in hospital, and does not account for the differing costs of surgical operations and procedures carried out during their stay or other pertinent factors. This is partially because this information could not readily be provided by the HEMS for this study, but also because the length of stay in hospital makes up a large proportion of the cost for each patient. In a study of blunt trauma patients, Christensen et al [11] calculated that approximately 75% of the total costs were accounted for by the length of stay in hospital.

The distributions of some variables, for example the body regions injured for different age groups, were compared using a chi-squared test of significance to determine whether any differences were statistically significant. Where this was performed the p-value given by the test has been quoted. For example, a p-value of 0.05 means that the probability that the distributions being compared are different is 95 %.

Police fatal files

The fatal file archive was searched to find and extract any files containing fatal pedestrian accidents involving a car registered in 2000 or later. These files were then searched through in order to identify whether they included photographs of the vehicle damage and a post mortem. This was required as the aim of looking at the files was to correlate the damage on the vehicles to the injuries the pedestrians received.

In the time available, 34 fatal files were analysed with details obtained on the circumstances of the accident (i.e. the location, time, date, contributory factors etc.), the driver of the vehicle, the vehicle itself and its damage, and the pedestrian and their injuries. The details were filled out on forms and input into a database for analysis. The injuries detailed in the post mortems were coded into AIS 2005 codes [13].

The location of damage on the cars which were involved in collisions with pedestrians was described using a 70 zone grid, shown in Figure 1. The AIS 2+ injuries received by each pedestrian were attributed to the various zones on the vehicle that were damaged or to other causation factors such as the ground, walls or acceleration injuries. This was done using a

combination of the evidence from the photographs, scene plans, the post-mortems, and other aspects of the Police report (e.g. the direction of travel of the pedestrian, the speed and action of the car and the rest position of the pedestrian).

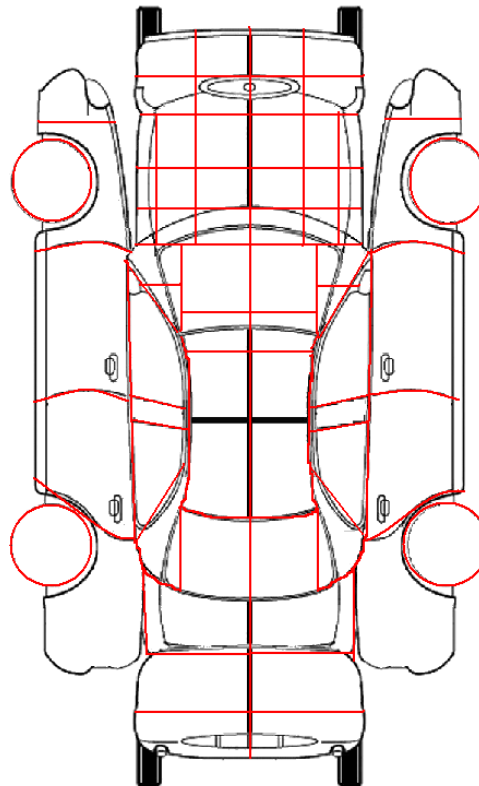


Figure 1. Zones on vehicle used for injury causation

RESULTS

An overview of the injuries received by pedestrians, and the costs associated with these injuries, was provided using the data recorded in the HEMS dataset. This also provided an overview of the head injuries received by pedestrians. The causes of pedestrian head injuries in impacts with cars registered in 2000 or later were investigated using the information present in Police fatal files.

Overview of HEMS pedestrian injuries

In total, the HEMS dataset used in this paper consisted of 746 pedestrians struck by motor vehicles between 2000 and 2007; with 2,974 injuries received in total. Of the 746 pedestrians, 616 survived (83%).

Figure 2 shows the proportion of the pedestrians in each of three age groups who received at least one

AIS 2+ injury to one of the six different body regions.

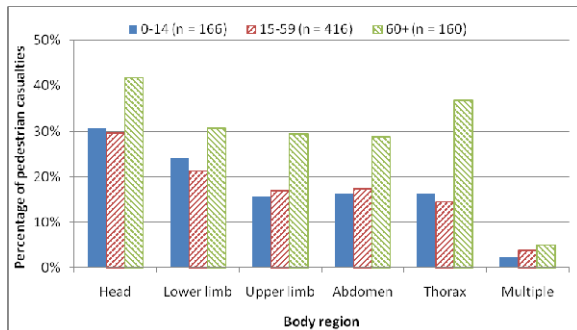


Figure 2. Injury regions by age group.

Head injuries were the most frequent AIS 2+ injuries for pedestrians in all age groups. Like all injury regions, head injuries were proportionally more frequent in pedestrian casualties aged 60 or older. The differences in the injury distributions for the different age groups were statistically significant ($p < 0.01$).

Selecting only fatally injured pedestrians gave a different injury distribution, shown in Figure 3. In this figure, head injuries are no longer the most frequently injured region: the abdomen and thorax both received more AIS 2+ injuries. Also, thorax and injuries to multiple or non specified body regions were most frequent for the youngest age group. The differences in the injury distributions for the different age groups for these fatalities are significant ($p < 0.1$).

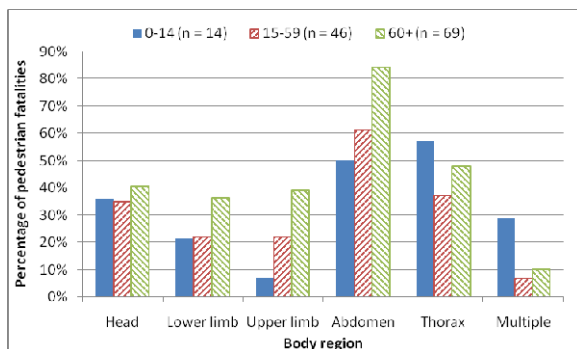


Figure 3. Injury regions by age group for fatally injured pedestrians

Table 2 shows the most frequent combinations of AIS 2+ injuries received by the pedestrians in the HEMS dataset, where 'H' is head, 'L' is lower limb, 'U' is upper limb, 'A' is abdomen, 'T' is thorax and 'M' is injury to multiple or non specific regions. There were 330 pedestrians who had injuries recorded, and for whom the highest AIS in each of these body regions

were known. This table shows the injury combinations received by at least 10 pedestrians.

Table 2. Most frequent combinations of AIS 2+ injuries

H	L	U	A	T	M	Freq.
X						92
	X					40
X				X		16
		X				14
X	X					13
	X		X			12
X		X				10
X	X			X		10
X	X		X	X		10

The most frequent combination of serious injuries was an AIS 2+ injury to the head only, a combination received by 28% of the pedestrians in the dataset. AIS 2+ injuries to the lower extremities only were the next most frequent, accounting for 12% of the pedestrians. Other combinations of injuries made up the remaining 60%, although no other single combination accounted for more than 5% of the casualties.

Of the 2,974 recorded injuries to the pedestrians in the HEMS dataset, 1,857 were known to be AIS 2+ injuries. Table 3 shows the ten most frequent AIS 2+ injuries received by the pedestrian casualties.

Table 3. Most frequent AIS 2+ injuries

Injury description	Freq.
Cerebral contusion closed	158
Generalized SAH IVH	133
Cerebral subdural haematoma	93
Fracture of ribs closed	92
Fracture of base of skull, closed with intracranial injury	81
Pneumothorax, without wound into thorax	73
Injury to lung without wound into thorax	70
Fracture of malar and maxillary bones closed	67
Fracture of pelvis, pubis closed	54
Fracture of clavicle, closed	53

The list of the most frequent AIS 2+ injuries is dominated by head injuries. The three most frequent AIS 2+ injuries were head injuries, which made up five of the ten most frequent.

Cost of pedestrian injuries (HEMS dataset)

Figure 4 shows the mean cost of the pedestrian injuries in the HEMS dataset, calculated using the method based on the duration of stay of the casualties in hospital. Figure 5 shows the cumulative annual cost for these pedestrians by body region injured. These figures show the cost of the pedestrians who had AIS 2+ injuries in the given body region.

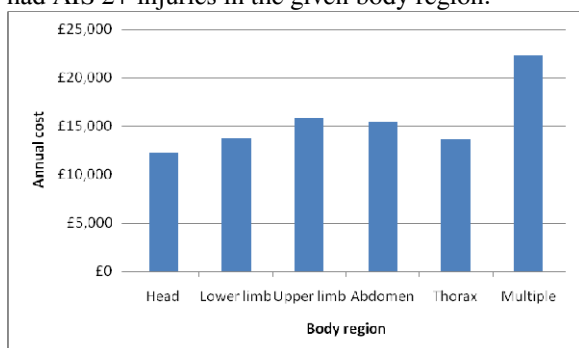


Figure 4. Mean cost per patient in HEMS dataset by injury region.

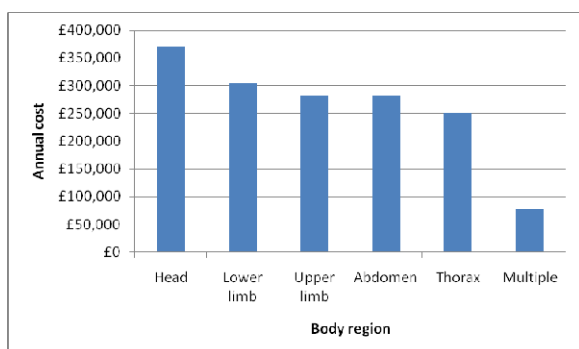


Figure 5. Annual cost of pedestrian casualties in HEMS dataset by injured region.

Although the average cost of head injuries was relatively low compared to other body regions, the large number of head injuries meant that pedestrians with AIS 2+ head injuries had a larger cumulative cost than pedestrians with AIS 2+ injuries in other regions.

Pedestrian head injuries

The analysis of the HEMS dataset has shown that head injuries were the most frequent serious injuries received by these pedestrians. Table 4 shows the ten most frequent AIS 2+ head injuries received by the pedestrians in the HEMS dataset.

Table 4. Most frequent head injuries in HEMS dataset

Injury description	Freq.
Cerebral contusion closed	158
Generalized SAH IVH	133
Cerebral subdural haematoma	93
Fracture of base of skull, closed with intracranial injury	81
Fracture of malar and maxillary bones closed	67
Intracranial injury of unspecified nature closed	39
Fracture of other facial bones, closed	36
Cerebral haemorrhage extradural closed	35
Fracture of vault of skull, closed with intracranial injury	30
Fracture of base of skull, closed without intracranial injury	29

These injuries are split between injuries involving the brain, and fractures of the surrounding bones. Brain injuries dominated, especially the two most frequent AIS 2+ head injuries: cerebral contusion, and generalised SAH IVH (subarachnoid haemorrhage and intraventricular haemorrhage).

In comparison, Table 5 shows the most frequent AIS 2+ head injuries received by the fatalities in the HEMS pedestrian dataset.

Table 5. Most frequent head injuries of fatally injured pedestrians in HEMS dataset

Injury description	Freq.
Generalized SAH IVH	64
Cerebral contusion closed	44
Cerebral subdural haematoma	41
Fracture of base of skull, closed with intracranial injury	33
Intracranial injury of unspecified nature closed	26
Fracture of malar and maxillary bones closed	12
Fracture of vault of skull, closed with intracranial injury	11
Other or unspec. intracranial haem.	8
Fracture of other facial bones, closed	6
Cerebral haemorrhage extradural closed	5

The types of head injuries received by the fatalities were very similar to the head injuries received by the pedestrian dataset as a whole: nine of the ten most frequent pedestrian head injuries for all casualties

were also present in the ten most frequent pedestrian head injuries of fatalities.

Causes of pedestrian head injuries (In-depth review of Police fatal files)

Figure 6 shows the causes of the AIS 2+ head injuries sustained by the 27 pedestrians in the Police fatal files who received at least one AIS 2+ head injury. This figure is at the pedestrian level.

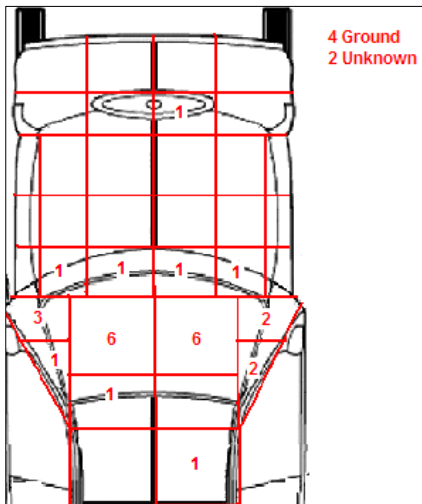


Figure 6. Causes of pedestrian head injuries.

Impacts to the windscreen caused AIS 2+ head injuries for 12 of the pedestrians, more than any other area of the vehicle. Impacts to the A-pillars caused 8 pedestrians' AIS 2+ head injuries, and impacts at the base of the windscreen caused 4 pedestrians' AIS 2+ head injuries. The remaining head injuries were caused by the header rail, the roof, the leading edge of the bonnet, the ground, or had an unknown cause. It should be noted that the head injury caused by the leading edge of the bonnet was to a 7 year old child, in an impact with a large 4x4 vehicle. With the exception of this impact, no head injuries were caused by any point of the bonnet below the base of the windscreen.

The severity of the head injuries caused by these different parts of the vehicle are summarised in Figure 7.

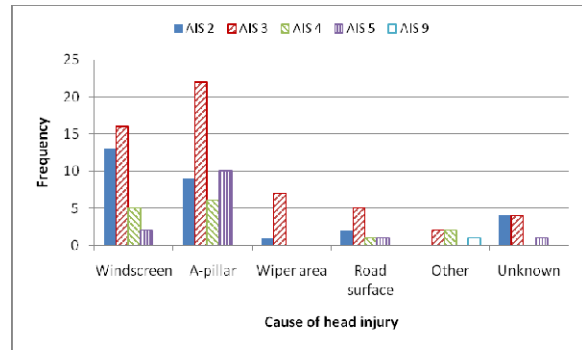


Figure 7. Severity of head injuries by cause.

Although more pedestrians (at a casualty level) had head injuries caused by the windscreen, the greatest number of serious head injuries (at an injury level) was caused by impacts with the A-pillar. Impacts with the A-pillar also caused proportionally more AIS 4+ head injuries than the windscreen.

Table 6, Table 7, Table 8, Table 9, Table 10, and Table 11 list the AIS 2+ injuries which were recorded for pedestrian impacts with the windscreen, A-pillars, wiper area, other parts of the vehicle, the road surface, and those with an unknown cause respectively. The injury descriptions are abbreviated versions of those recorded using the AIS injury coding system.

Table 6.
AIS 2+ head injuries caused by impacts with windscreen

AIS	Description	Freq
5	Brain stem compression	1
	Cerebellum: haematoma, epidural or extradural, large	1
4	Cerebellum: haematoma, subdural, small	1
	Cerebrum: haematoma, subdural, small, bilateral	1
	Cerebrum, brain swelling, moderate	1
	Base (basilar) fracture, complex	1
	Vault fracture, complex	1
3	Cerebrum: brain swelling NFS	4
	Base (basilar) fracture NFS	3
	Cerebrum: contusion, multiple, at least one on each side but NFS	2
	Cerebrum: haematoma, subdural NFS	2
	Cerebrum, contusion, single NFS	1
	Cerebrum: contusion, multiple NFS	1
	Cerebrum: contusion, multiple, on same side but NFS	1
	Cerebrum: brain oedema NFS	1
	Cerebrum: NFS	1
2	Cerebrum: subarachnoid haemorrhage	4
	Cerebellum: subarachnoid haemorrhage	3
	Vault fracture NFS	3
	Cerebrum: intraventricular haemorrhage	1
	Vault fracture, closed	1
	Maxilla fracture	1
Total		36

Table 7.
AIS 2+ head injuries caused by impacts with A-pillars

AIS	Description	Freq.
5	Brain stem NFS	3
	Brain stem compression	2
	Brain stem: injury involving haemorrhage	2
	Cerebrum: contusion, single, extensive	1
	Cerebrum: contusion, multiple, extensive	1
	Diffuse axonal injury LOC > 24 hours NFS	1
4	Base (basilar) fracture, complex	2
	Sinus: sigmoid sinus, thrombosis, occlusion	1
	Sinus, transverse sinus, thrombosis.	
	Occlusion	1
	Cerebrum: intraventricular haemorrhage, associated with coma > 6 hours	1
	Vault fracture, complex	1
3	Cerebrum: contusion, multiple, at least one on each side, small	3
	Cerebrum, haematoma, NFS	3
	Cerebrum, brain swelling NFS	3
	Cerebellum: brain swelling/oedema NFS	2
	Intracranial vascular injury	1
	Cerebellum: haematoma NFS	1
	Cerebellum, haematoma, subdural NFS	1
	Cerebellum NFS	1
	Cerebrum: contusion NFS	1
	Cerebrum: brain oedema NFS	1
	Cerebrum: laceration NFS	1
	Cerebrum: subarachnoid haemorrhage, associated with come > 6 hours	1
	Cerebrum: NFS	1
	Base (basilar) fracture NFS	1
	Vault fracture comminuted	1
2	Cerebrum: subarachnoid haemorrhage	3
	Vault fracture NFS	2
	Orbit, fracture, closed or NFS	2
	Cerebellum: subarachnoid haemorrhage	1
	Vault fracture, closed	1
Total		47

Table 8.
AIS 2+ head injuries caused by impacts with wiper area

AIS	Description	Freq.
3	Cerebrum: haematoma, subdural NFS	2
	Cerebrum: brain oedema NFS	2
	Cerebrum: contusion, multiple, at least one on each side but NFS	1
	Cerebrum, haematoma, NFS	1
	Cerebrum: brain swelling NFS	1
2	Cerebrum: subarachnoid haemorrhage	1
Total		8

Table 9.
AIS 2+ head injuries caused by impacts with other parts of vehicle

AIS	Description	Freq.
Unknown	Unknown	1
4	Base (basilar) fracture, complex	1
	Base (basilar) fracture, complex	1
3	Cerebrum: contusion, single, small	1
	Cerebrum: brain swelling NFS	1
Total		5

Table 10.
AIS 2+ head injuries caused by impacts with road surface

AIS	Description	Freq.
5	Brain stem: injury involving haemorrhage	1
4	Base (basilar) fracture, complex	1
3	Cerebrum: contusion NFS	1
	Cerebrum: laceration, <2cm	1
	Cerebrum: laceration NFS	1
	Base (basilar) fracture NFS	1
	Vault fracture comminuted	1
2	Cerebrum: subarachnoid haemorrhage	1
	Vault fracture NFS	1
Total		9

Table 11.
AIS 2+ head injuries with unknown cause

AIS	Description	Freq.
5	Cerebrum: haematoma, subdural, large	1
3	Cerebrum: haematoma, subdural NFS	1
	Cerebrum: brain swelling NFS	1
	Base (basilar) fracture NFS	1
	Vault fracture comminuted	1
2	Cerebellum: subarachnoid haemorrhage	1
	Cerebrum: intraventricular haemorrhage	1
	Cerebrum: subarachnoid haemorrhage	1
	Vault fracture NFS	1
Total		9

The 12 pedestrians who received AIS 2+ head injuries caused by impacts with the windscreen received a total of 36 AIS 2+ injuries - an average of 3 injuries each. The 8 pedestrians who received AIS 2+ head injuries from impacts with the A-pillars received a total of 47 AIS 2+ head injuries – an average of almost 6 per pedestrian. So although more pedestrians received fatal injuries caused by the windscreen, the total number of injuries was greater for the pedestrians in impacts with the A-pillars.

The head injuries received by the pedestrians were largely made up of haematomas, haemorrhages, and contusions of various areas of the brain. Of the 113 known head injuries, 74 % were various brain injuries, while the other 26 % were fractures to various parts of the skull. The proportion of fractures compared to other injuries caused by the windscreen was 28 %. This proportion for the A-pillar was 21 %.

DISCUSSION

This project has set out the nature and pattern of the injuries received by pedestrian road traffic casualties attended by London's HEMS team between 2000 and 2007. It is recognised that this dataset typically represents the most seriously injured pedestrians, but nonetheless the sample size presents a useful overview of the types of injuries received. Injuries to the head were identified as the most costly based on an annual summation of the cost to the treating hospital, calculated from length of stay multiplied by injury frequency.

Injuries to the head were also seen to be the most frequent. A single AIS 2+ head injury was found to be the most frequent combination of serious injuries, and the list of the most frequent injuries (as recorded using ICD-9) was dominated by head injuries. The

cumulative cost of head injuries was also seen to be greater than the cost of injuries to any other body region.

The nature of the injuries to the head recorded in the HEMS dataset were investigated and compared with injuries observed in the Police fatal files. Similar trauma was noted. Forensic investigation of the evidence available in the Police fatal files allowed the AIS 2+ head injury mechanisms to be investigated.

Head injuries have been seen to be the most frequent type of pedestrian injury in other studies of pedestrian casualties [2,5]. Head injuries may also be expected to be more frequent in the HEMS dataset, as these pedestrians are likely to have been involved in relatively serious crashes compared to the population of pedestrian casualties as a whole. However, comparing the most frequently injured body regions of all casualties and fatalities only shows that the pedestrians who were killed suffered a higher proportion of abdomen and thorax injuries than head injuries, for all age groups. The analysis of the cost of injuries also showed that, although head injuries were the most frequent in the HEMS dataset, they accounted for the lowest average cost of all the body regions. Assuming that the cost (based on the duration of stay) is related to the severity of the injury, this suggests that serious head injuries are not as severe for pedestrians as severe injuries to other parts of the body.

When the causes of the pedestrians' head injuries were investigated in the sample of fatal casualties, the most frequent cause was an impact with the windscreen. The second most frequent cause was an impact with the A-pillar. However, a large number of injuries were caused by impacts with the A-pillar, suggesting that impacts to the A-pillar are more severe than impacts with the windscreen. The severity of the impacts with the A-pillar was also greater, making up the majority of the AIS 4+ head injuries.

Comparing the causes of these head injuries with the EuroNCAP and European pedestrian directive shows that, with the possible exception of the head impact of a small child with a large 4x4, not one of the impact zones are tested and acceptable limits applied. Testing of pedestrian head impacts currently focuses on impacts with the bonnet only. On the evidence of these fatally injured pedestrians, areas further up the car, especially the A-pillars and windscreen, should also be tested, or interventions applied to prevent head strikes to these areas.

The number of pedestrians with serious head injuries caused by secondary impacts was much fewer than the number whose head injuries were caused by the primary impact with the vehicle. Of the 32 pedestrians receiving AIS 2+ injuries, only four pedestrians had serious head injuries caused by secondary impacts with the ground. In comparison, Otte and Pohlemann [3] saw that 33 % of pedestrian injuries were caused by secondary impacts. The method used to determine the cause of the injuries – using photographs, statements and post mortems contained in Police fatal files – was perhaps more likely to attribute injuries to the vehicle rather than to secondary impacts. This is because the evidence of impacts to the vehicle is more obvious and more likely to be collected than evidence of secondary impacts. For example, a head may have struck a windscreen and the road surface, but the windscreen is the most visually obvious contact. Secondary impacts are likely to have been recorded as a cause when there was no evidence of an impact to the vehicle, or if the location of the injuries did not match the nature of the impact with the vehicle.

This study has looked at pedestrian impacts with the front of cars only. It is likely that other impact configurations, such as impacts with the side of cars, would produce different injuries and different causes of injury. For example, it might be expected that the proportion of the head injuries caused by secondary impacts with the ground would be larger for these types of accident, as the pedestrian would be less likely to contact the vehicle with their head before they were thrown to the ground.

Both of the datasets used in this paper contained more severely injured people than the national population of pedestrian accidents. For this reason, it is likely that the average costs of the pedestrian injuries calculated using the HEMS dataset is higher than the national average. However, it is likely that due to the rapid response provided by the HEMS and the specialized trauma care provided, that pedestrians suffering some of these serious injuries may have better outcomes than other pedestrians suffering the same injuries. However, there is data available which could be used to weight these costs – for example the national Hospital Episode Statistics – and performing this weighting would be a natural extension of this study.

With respect to the mechanisms of injury, the severity bias of the selection of fatally injured pedestrians is more pronounced, and it is likely that less severely injured pedestrians receive a different distribution of injuries from different causes.

Another limitation of the Police fatal files is that the post-mortems are often not consistent in the amount of information they record for the injuries. This may lead less specific, lower severity injuries to be recorded using AIS if the information was not available (e.g. amount of blood loss, exact location of fractures) to code a more severe injury. Further, the sample size is relatively small.

The costing model, based on the duration of stay of pedestrians on the ward and in intensive care, is an example of one method which can be used to prioritise injuries using medical information. The costs of individual injuries could be refined if other information was considered, such as the operations and procedures performed on the patient while they were in hospital. Costing road traffic injuries in a similar way is already carried out in the USA [14] and is used when considering the cost-benefit of countermeasures designed to increase road safety.

Finally, the analysis of pedestrian injuries using the HEMS dataset and Police fatal files is not limited to what has been presented here. For example, it is possible to focus on one particular cause of pedestrian injuries in more detail. The precise location of impacts on the windscreen could be investigated, and injuries caused by impacts near the edge of the screen could be compared with the impacts in the centre of the screen. The changes over time of the type of pedestrian injuries could be analysed using the HEMS dataset, to determine if changes in car design or other factors over time have changed the epidemiology of pedestrian injury. The costing model could also be developed, incorporating the cost of the operations and procedures carried out on the pedestrians in the hospital, and weighting the costs to be more representative of the national population of pedestrian casualties (using, for example, the nationally recorded Hospital Episode Statistics).

CONCLUSIONS

Using London's HEMS dataset, serious head injuries are more frequent, and have a higher total cost, than serious injuries to any other body region.

More fatally injured pedestrians had serious head injuries caused by impacts with the windscreen than any other part of the car. However, a greater number of injuries were caused by the A-pillars, and these tended to have a greater severity.

No fatally injured adult pedestrian head injuries were caused by any part of the car forward of the base of the windscreen. This is in contrast to current pedestrian impact legislation and consumer testing, which concentrate on head injuries caused by impacts with the bonnet.

ACKNOWLEDGEMENTS

The authors would like to thank Alistair Wilson, Gareth Davies, Elizabeth Foster and the rest of the HEMS team at the Royal London Hospital, Whitechapel, for providing data on pedestrian casualties, and their help and support throughout the study.

This project uses accident data from the Police fatal accident reports which are archived and stored for research purposes by a project funded by the Department for Transport.

REFERENCES

- [1] Department for Transport, (2008). Road Casualties Great Britain: 2007. London: The Stationary Office.
- [2] Appel, H; Sturtz, G; Gotzen, L (1975). Influence of Impact speed and vehicle parameter on injuries of children and adults in pedestrian accidents, IRCOBI 1975.
- [3] Otte, D; Pohlemann, T (2001). Analysis and Load Assessment of Secondary Impact to Adult Pedestrians after Car Collisions on Roads, IRCOBI 2001.
- [4] Gavrilu, DM; Marchal, P; Meinecke, MM (2003). Vulnerable Road User Scenario Analysis, SAVE-U Project Deliverable 1-A.
- [5] Ashton, S J; Mackay, G M (1979). Some characteristics of the population who suffer trauma as pedestrians when hit by cars and some resulting implications, Proceedings of the 4th IRCOBI conference 1979.
- [6] Directive 2003/102/EC of the European Parliament and of the Council of 17 November 2003 relating to the protection of pedestrians and other vulnerable road users before and in the event of a collision with a motor vehicle and amending Council Directive 70/156/EEC
- [7] EuroNCAP (2009).

<http://www.euroncap.com> Retrieved on 12th March 2009.

[8] ICD9, (2008).
<http://icd9cm.chrisendres.com/index.php> Retrieved on 12th March 2009.

[9] AAAM, (1998). The Abbreviated Injury Scale. 1998 Revision. Des Plaines, Illinois 60018, U.S.A: Association for the Advancement of Automotive Medicine (AAAM).

[10] Intensive Care Society, (2008). Critical insight: an Intensive Care Society (ICS) introduction to UK adult critical care services, <http://www.ics.ac.uk> Retrieved 20th November 2008

[11] Christensen M C, Ridley S, Lecky F E, Munro V, Morris S, (2008). Outcomes and costs of blunt trauma in England and Wales, Critical Care 2008, 12:R23.

[12] Department of Health. (2005). NHS reference costs 2004. Appendix SRC1 – NHS Trust reference cost index. Retrieved 20 November 2008, from [http://www.dh.gov.uk/en/Publicationsandstatistics/Publications/](http://www.dh.gov.uk/en/Publicationsandstatistics/Publications/PublicationsPolicyAndGuidance/DH_4105545) PublicationsPolicyAndGuidance/DH_4105545 Retrieved 20th November 2008

[13] AAAM, (2005). Abbreviated Injury Scale 2005. U.S.A: Association for the Advancement of Automotive Medicine (AAAM).

[14] Miller, T., Romano, E., Zaloshnja, E., & Spicer, R. (2001). HARM 2000: crash cost and consequence data for the new millennium. 45th annual proceedings Association for the Advancement of Automotive Medicine.

PEDESTRIAN HEAD IMPACT DYNAMICS: COMPARISON OF DUMMY AND PMHS IN SMALL SEDAN AND LARGE SUV IMPACTS

Jason Kerrigan¹

Carlos Arregui²

Jeff Crandall¹

¹University of Virginia Center for Applied Biomechanics
United States

²European Center for Injury Prevention, Universidad de Navarra
Spain

Paper Number 09-0127

ABSTRACT

This study compares head impact dynamics between post mortem human surrogates (PMHS) and the Polar-II pedestrian crash dummy in vehicle-pedestrian impacts with a small sedan and a large SUV. A total of fifteen (8 sedan, 7 SUV) full-scale vehicle pedestrian impact tests were performed at 40 km/h. For each vehicle, two (SUV) or three (sedan) PMHS tests and five dummy tests were performed, with three of the dummy tests in the same configuration to show repeatability, and the other two tests utilizing slightly different configurations. Head linear and angular kinematics were captured from PMHS and dummy head instrumentation, and dummy neck forces and impact forces were calculated from the upper neck load cell data. Differences in head impact locations, timing, and kinematics between the dummy and PMHS were minimized when the dummy was positioned higher above the ground reference level to match the pelvis height of the PMHS. On average, the dummy recorded higher resultant impact forces (2930 N vs. 1862 N) in windshield impacts to the sedan than in hood impacts to the SUV, which resulted in higher HIC15 values and higher peak and averaged angular accelerations. While differences in dummy injury risk metrics both the dummy and PMHS data show that the difference in injury risk metrics predicted by the dummy can be explained by the variation in impact velocity between the sedan (14.1 ± 1.2 m/s) and the SUV (10.7 ± 2.3 m/s), the differences in injury risk predicted by the PMHS is not as clear due to confounding factors. The data and analyses presented in this study also show that neck forces during head impacts contribute a substantial and additive effect to the head impact accelerations (and thus HIC15 values) measured in the dummy, and that for the SUV, neck forces affect head accelerations more than impact forces. Despite analyzing only lateral impacts with two vehicle geometries at 40 km/h, this study provides the only comparison of PMHS and dummy pedestrian head impact kinematics data available.

INTRODUCTION

Head injuries are either the most or second most commonly reported injuries to pedestrians struck by vehicles (Kong et al. 1996, Edwards and Green, 1999, Peng and Bongard, 1999, Chidester and Isenberg, 2001, Mizuno 2003, Toro et al. 2005, Neal-Sturgess et al. 2007). Furthermore, among serious or life-threatening head and brain injuries far outnumber injuries to all other body regions (Chidester and Isenberg, 2001, Fildes et al. 2004). Previous studies have shown that head and neck injuries sustained by pedestrians account for almost 60% of all Harm to pedestrians (Fildes et al. 2004).

In an effort to mitigate the risk of head (and other) injuries to pedestrians, researchers have developed tools, like pedestrian dummies and computational models, to further understand the dynamics of vehicle-pedestrian impact. While the local stiffness of the individual vehicle structures involved in head-to-vehicle impact is a primary concern in decreasing the risk of head injury, impact simulations with pedestrian dummies and computational models allow for examination of other factors that affect head injury risks. For instance, the magnitude of the accelerations sustained by the head in head-to-vehicle impacts is dictated not only by the vehicle stiffness, but by the impact velocity and impact angle, which dictate the magnitude and duration of the impact forces applied to the head. Additionally, Okamoto and Kikuchi (2006), in a study that involved vehicle-pedestrian impacts with the Polar-II pedestrian dummy, used the dummy's neck instrumentation to explore the magnitudes of forces applied to the head through the neck during impact. Since their goal was to compare pedestrian dummy impacts to those of headform impactors, Okamoto and Kikuchi used neck forces to examine similarities and differences between the dummy and the impactor, without examining how neck forces directly affect impact kinematics and estimates of injury risk.

The current study aims to examine how both the impact and neck forces applied to the head during head-to-vehicle impact influence linear and angular impact kinematics. Furthermore, this study uses both the Polar-II dummy, which has been compared to PMHS in previous tests to verify overall kinematic biofidelity (Akiyama et al. 2001, Kerrigan et al. 2005a, Kerrigan et al. 2005b), and PMHS to further examine not only the biofidelity of the dummy but the limitations of the PMHS model. Lastly, this study examines impacts with two vastly different shaped vehicles, a small sedan and a large SUV, to help elucidate the effects vehicle shape has on head impact dynamics.

METHODS

Vehicle-Pedestrian Impact Experiments

A total of 15 vehicle-pedestrian impact tests with a late-model small sedan (n=8) and a late model large SUV (n=7), using both PMHS (n=5) and the Polar-II dummy (n=10) (Table 1). The methodology and some results from 11 of the 15 experiments have been previously presented (Kerrigan et al. 2005a, Kerrigan et al. 2005b, Kerrigan et al. 2008b). Since the current study presents previously unpublished results from these experiments, as well as results from previously unpublished experiments, the following description will provide a general overview of the test methodology, but focus specifically on the methods associated with the previously unpublished results. For a more complete description of all of the methods used to perform the experiments, the previous studies should be referenced.

Table 1. Test matrix.

	Test ID	Subject	Age/ Gender	Mass (kg)	Stature (cm)	Stance/ Support/ Clothing	Ground Level (cm)
Sedan	D1	Dummy		75	173	Dummy	0
	D2	Dummy		75	174	Dummy	0
	D3	Dummy		75	174	Dummy	0
	DA1	Dummy		75	174	PMHS	0
	DA2	Dummy		75	179	PMHS	+5
	P1	PMHS	61/F	80.7	187	PMHS	0
	P2	PMHS	70/M	54.4	179	PMHS	0
	P3	PMHS	62/M	81.6	186	PMHS	0
SUV	D1	Dummy		75	173	Dummy	0
	D2	Dummy		75	172	Dummy	0
	D3	Dummy		75	171	Dummy	0
	DA1	Dummy		75	174	PMHS	0
	DA2	Dummy		75	179	PMHS	+7
	P1	PMHS	75/F	46.7	177	PMHS	0
	P2	PMHS	53/M	104.2	176	PMHS	0

Sled System Drivable production versions of the vehicles were cut just rearward of their B-pillars, their wheels were removed and their suspensions were locked. The vehicles were welded to a sled sub-frame and ballasted up to the vehicle curb weight for the sedan (1176 kg) and to the sled system limit (1600 kg) for the SUV. Computational simulations verified that only negligible differences in vehicle pedestrian impact dynamics resulted from using an SUV mass less than the vehicle's curb weight. Each vehicle buck was attached to the carriage mounted to the deceleration sled system (Via Systems Model 713, Salinas, CA) at the University of Virginia (UVA) Center for Applied Biomechanics (CAB). Damaged or deformed vehicle components were repaired or replaced between each test.

A small, light pedestrian sled that mimicked the vehicle's ground-reference-level was constructed and attached to the sled system to facilitate surrogate positioning prior to each test. Plywood, which has been shown to possess frictional characteristics similar to that of road surfaces (Kam et al. 2005), was used as the shoe-contact surface on the ground-reference-level of the pedestrian sled. A hydraulic decelerator programmed to decelerate the vehicle and pedestrian sled approximately 250 ms after initial vehicle-pedestrian contact was installed at the end of the sled system to provide a constant 6g deceleration. Above the decelerator, an energy absorbing catching mechanism (Kam et al. 2005) was installed to catch the subject, prohibit ground contact, and prevent additional injuries.

Subject Preparation Three male and two female PMHS (Table 1) were selected for this study based on the absence of pre-existing fractures, lesions, or other bone pathology as confirmed by computed tomography (CT) scan. The PMHS were obtained and treated in accordance with the ethical guidelines established by the Human Usage Review Panel of the National Highway Traffic Safety Administration, and all testing and handling procedures were reviewed and approved by the CAB Biological Protocol Committee and an independent Oversight Committee at UVA. Specimens are labeled (Table 1) by the order of testing (with "P" indicating PMHS).

Each specimen was instrumented with a (6) six-degree-of-freedom (6DOF) cube to facilitate head kinematics measurement during the experiments (Kerrigan et al. 2008a). The 6DOF cube contained three linear accelerometers (model 7264B-2000, Endevco Corp., San Juan Capistrano, CA) and three magnetohydrodynamic (MHD) angular rate sensors (model ARS-06, Applied Technology Associates,

Albuquerque, NM). The six sensors were arranged in a specially designed aluminum cube to permit linear acceleration and angular rate measurements about three orthogonal axes (Figure 1). An aluminum plate (44 x 46 x 5 mm) was attached to the posterior-superior aspect of the skull with deep threaded wood screws (Figure 1). Following preparation, each specimen underwent a computed tomography (CT) scan (0.97 mm/pixel, 1.25 mm slice thickness) to document the orientations of the cube mounting hardware (Figure 1).

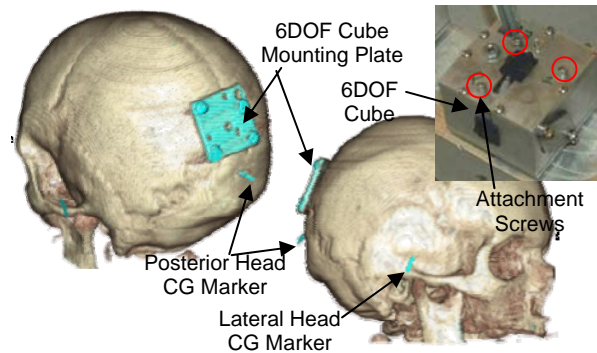


Figure 1. CT scan reconstructions (top) and photograph (bottom) showing 6DOF cube (also inset), cube mounting plate, and markers used to determine head CG. Photograph shows PMHS prone in tray.

The Polar-II dummy was prepared as specified by its developers (e.g. Akiyama et al. 2001). The dummy, which has the head of the Hybrid-III dummy, was instrumented with a nine-accelerometer package (NAP) centered about the head center of gravity using the same geometry as that used in the Hybrid-III. Additionally, the dummy's neck was based on the THOR neck, and thus had a 6-axis upper neck load cell identical to that used in the THOR.

Stance, Support and Clothing Tests were performed in the following order:

- 1) Repeated dummy tests with each vehicle-“D1”, “D2”, and “D3” in Table 1,
- 2) PMHS tests with each vehicle-“P1”, “P2”, and “P3” in Table 1, and
- 3) Adjusted dummy tests-“DA1” and “DA2” in Table 1.

Each of the three series of tests were performed with different stance, support, and clothing of the subject (Figure 2). In the first series of tests (repeated dummy tests) the dummy wore its standard jacket, shorts and shoes as specified by its developers. It was supported for positioning by using a single rope that passed through the dummy's shoulder eyebolts (bilaterally) and through the release mechanism. In positioning the

dummy in mid-stance gait, the following goals were applied (Kerrigan et al. 2005a):

- 1) Both right and left thighs oriented at the same angle relative to the ground and no more than 85 degrees from horizontal,
- 2) Right leg back (struck side) and left leg forward
- 3) Both feet flat on the ground reference level with the back of the right heel and front of the left shoe tip equidistant from the vehicle centerline
- 4) Both knees at 0 degrees flexion.

However, due to limited range of motion of the dummy's right hip (it could not be extended more than 5 degrees from neutral), and that the shoulder eyebolts were anterior to the dummy's CG (and thus the dummy's weight was not supported through its CG), achieving goal #3 was impossible without pushing the pelvis back and creating an angle of the thorax relative to the ground (Figure 2).

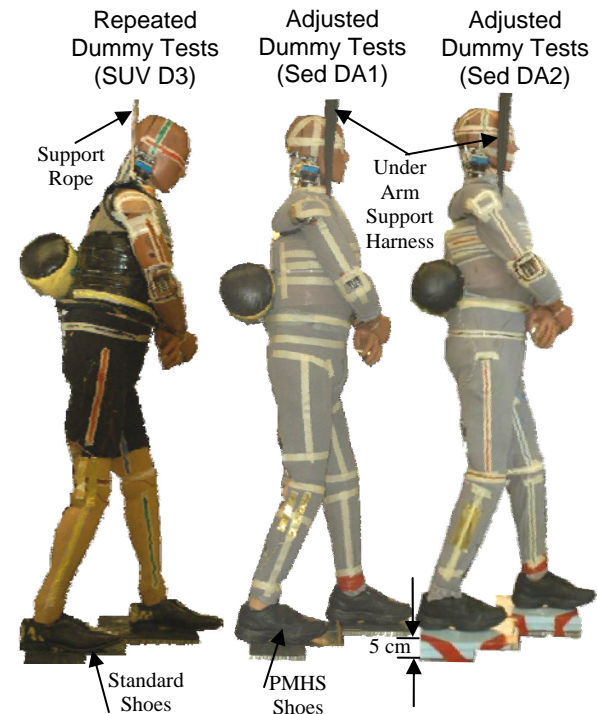


Figure 2. Images from SUV D3 (left), Sed DA1 (middle) and Sed DA2 (right) depicting differences in dummy stance, support and clothing from the three different test series.

The PMHS were outfitted in a TYVEK ® body suit (interior), a cotton/lycra shirt and pants (exterior), a cotton/lycra head cover, and a pair of athletic shoes (Figure 3). The PMHS were supported via a piece of seat belt webbing that passed under the arms anteriorly and across the back posteriorly. Additionally, the PMHS head was positioned with a second piece of

seatbelt webbing that was split and passed under the chin and under the occiput. An attempt was made to position the PMHS like the dummy in the repeated dummy tests, however relatively low stiffness in the hip and knee joints prevented the right hip and right knee from being extended. Gravity drew the right hip and knee into flexion, and the thorax into an orientation perpendicular to the ground.

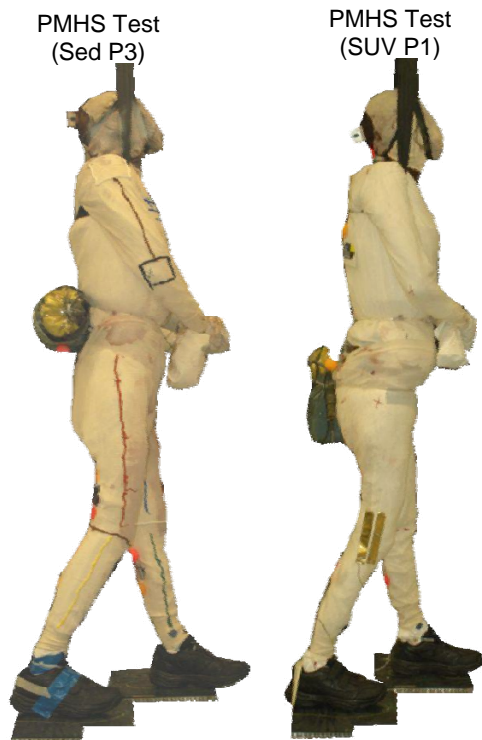


Figure 3. Images from sedan (left) and SUV (right) PMHS tests depicting PMHS stance, support and clothing.

A number of differences between in pedestrian response between the PMHS and dummy were noted (see Results) and thus a subsequent set of tests were performed with the dummy to determine if the differences were related to the differences in stance, support and position. Since the dummy showed repeatable results in the repeated dummy tests (Kerrigan et al. 2005a, Kerrigan et al. 2005b), only single dummy tests ($n=2$ for each vehicle) were performed to examine the sensitivity to stance, support and clothing. In the first test on each vehicle (Sed DA1 and SUV DA1), the dummy was outfitted in the same cotton/lycra shirt and pants, and the same athletic shoes used in the PMHS tests (Figure 2). The dummy was not supported using the shoulder eyebolts, but instead was supported with the seatbelt webbing that passed under the arms anteriorly and across the back posteriorly. This support allowed the dummy to be positioned in the same stance as the PMHS: slight

flexion in the right hip and thorax perpendicular to the ground reference level. These PMHS-like conditions of the stance, support and clothing are indicated in Table 1 as “PMHS”.

In addition to the differences between the PMHS and repeated dummy tests with respect to the stance, support and clothing, all of the PMHS were taller than the dummy (Table 1) as determined by measuring the distance between the top of the head and the ground reference level after positioning each subject. Thus, in an attempt to evaluate how differences in stature affected the response characteristics, in the second of the adjusted dummy tests (Sed DA2 and SUV DA2) the vertical position of the ground reference level was increased using a rigid foam to position the dummy higher up than in the DA1 tests (Figure 2). Since, it has been hypothesized that the height of the pelvis and greater trochanter relative to the vehicle front end components has a larger effect on pedestrian impact kinematics than pedestrian stature (Kerrigan et al. 2005a, Kerrigan et al. 2005b, Kerrigan et al. 2007), the ground reference level height was increased to match the pelvis height of the PMHS. The average height of the PMHS in the sedan tests and SUV tests was approximately 5 cm and 7 cm higher than the height of an analogous point measured on the dummy after positioning in Sed DA1 and SUV DA1, respectively. Thus the ground level for the DA2 tests was adjusted accordingly.

Final Preparation and Test Event Before hoisting PMHS specimens, the 6DOF cube was fixed to the mounting plate, and digitized relative to skull landmarks with a coordinate measurement machine (CMM) (FARO Technologies, Lake Mary, FL). The support harness from each subject was attached to a solenoid release mechanism that supported the weight of the subject until immediately prior to the impact. The subjects were positioned such that the right lateral side facing the vehicle with the support aligned with the vehicle centerline. The upper extremities of the surrogate were bound at the wrist, anterior to the body, with the left wrist closest to the abdomen, to ensure repeatable kinematics and the most severe impact (Kam et al. 2005). Once the final position of the surrogate had been set, the CMM was used to digitize anatomical landmarks used to define the exact position and orientation of the subjects. Additionally, the dummy head and the three attachment screw centers of the PMHS 6DOF cube were digitized to determine the pre-impact global reference frame orientation of the head instrumentation systems.

The test event was initiated by a pneumatic propulsion system that accelerated the vehicle sled to 40 km/h.

The vehicle sled passed an inductive sensor on the track that triggered the release of the surrogate approximately 20 ms before the initial bumper-lower extremity contact. Vehicle-PMHS interaction continued for 250 ms after bumper contact, at which time the vehicle was decelerated (constant ~6 g) and the surrogate was thrown forward into the catching mechanism. All subject-mounted sensor data were sampled at 10 kHz via a wireless data acquisition system (TDAS G5, DTS, Seal Beach, CA). A hardware filter of 3300 Hz was applied during acquisition, and the data were subsequently filtered (CFC 1000) for further processing. The angular rate sensor data were compensated, using a routine specified by the manufacturer (ATA 2008), to extend the effective low frequency corner of the MHD angular rate sensor.

Head Impact Dynamics

Kinematics PMHS head impact kinematics in both the local (body-fixed) and global (inertial) reference frames were calculated at the head CG using established techniques (Rudd et al. 2006, Kerrigan et al. 2008a, Kerrigan et al. 2008b). The location and orientation of the head CG relative to the 6DOF cube was determined by digitizing the cube attachment screws and the posterior and lateral projections of the head CG, which were determined from the Frankfurt plane (based on data from Robbins et al. 1983), prior to positioning the PMHS (Figure 1). Local frame kinematics were determined by first transforming the cube sensor measurements to a reference frame defined by the anatomical axes of the head (adhering to SAE J211), and then by translating cube accelerations first from the surface to the center of the cube, and then to the head CG by applying the rigid body dynamics equation.

The cube's initial global reference frame orientation was determined from the pre-test CMM data. Data from the angular rate sensors were used to update the global frame orientation of the cube at each time step of the impact interaction. By updating the orientation of the cube at each time step, the local sensor data could be expressed in the global reference frame. The components of the global linear velocity vector were determined by integrating the transformed accelerations, and transformed into the vehicle reference frame by using the vehicle velocity time history. Angular acceleration data were determined by differentiating the transformed angular velocity data. To remove the high frequency noise introduced by the numerical differentiation, a 300 Hz (-6 dB cutoff) low-pass second-order Butterworth filter was applied to the angular acceleration data (Rudd et al. 2006).

In the dummy, the components of the local frame angular acceleration vector were calculated from the NAP data (Padgaonkar et al 1975). Angular accelerations were integrated to determine the components of the local frame angular velocity vector. Then the components of the local frame acceleration vector were determined by translating the accelerometer measurements to the head CG using the rigid body kinematics equation. Then, using the same methods as in the PMHS, global reference frame kinematics (linear and angular accelerations, and linear and angular velocities) were calculated.

Impact Forces The time history of the components of the force acting on the dummy head by the vehicle (impact force) can be calculated by applying Newton's second law to the dummy's head (Figure 4). The dummy's head can be modeled as a rigid body with mass m_{head} that accelerates (\mathbf{a}) as a result of the forces acting on it. In vehicle-pedestrian impacts, a force is applied to the dummy's head through its connection to its neck (\mathbf{F}_N), and another force to the head through its contact with the vehicle (\mathbf{F}_I). In some cases, more than one force can act on the head by the vehicle (multiple contact locations), however for the purposes of this analysis, the vector sum of these forces is assumed to be only a single force, acting at a single location.

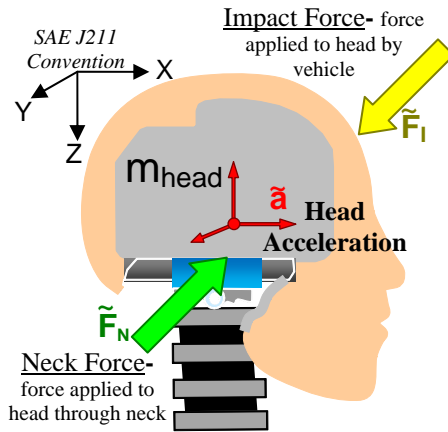


Figure 4. Free body diagram of the dummy's head with component sign convention.

Thus we have the vector relations

$$m_{head} \mathbf{a} = \mathbf{F}_I + \mathbf{F}_N \quad (1), \text{ and}$$

$$\mathbf{F}_I = m_{head} \mathbf{a} - \mathbf{F}_N \quad (2).$$

Time histories of the components of the impact force vector were calculated in each dummy test, using Equation 2 with the neck load cell forces and the components of the local frame acceleration vector.

The neck forces and impact forces were calculated as forces applied to the head and with the SAE J211 sign convention (Figure 4).

RESULTS

Linear Kinematics

All sedan impacts resulted in head impact with the vehicle's windscreen and all SUV impacts resulted in head impact with the vehicle's hood (Figure 5). Subjects that were taller, or raised off the ground

reference level (both DA2 tests), experienced head contacts farther up the vehicle than shorter subjects. In other words, while the relationship is clearly a function of vehicle geometry, specimen stature was positively (generally) correlated with wrap-around-distance (WAD) to the location of head impact for each vehicle (Table 2 and Figure 6). WAD measurements were made using the standard method of measuring vertically from the ground up to the vehicle bumper, and then along the contour of the vehicle to the head impact location.

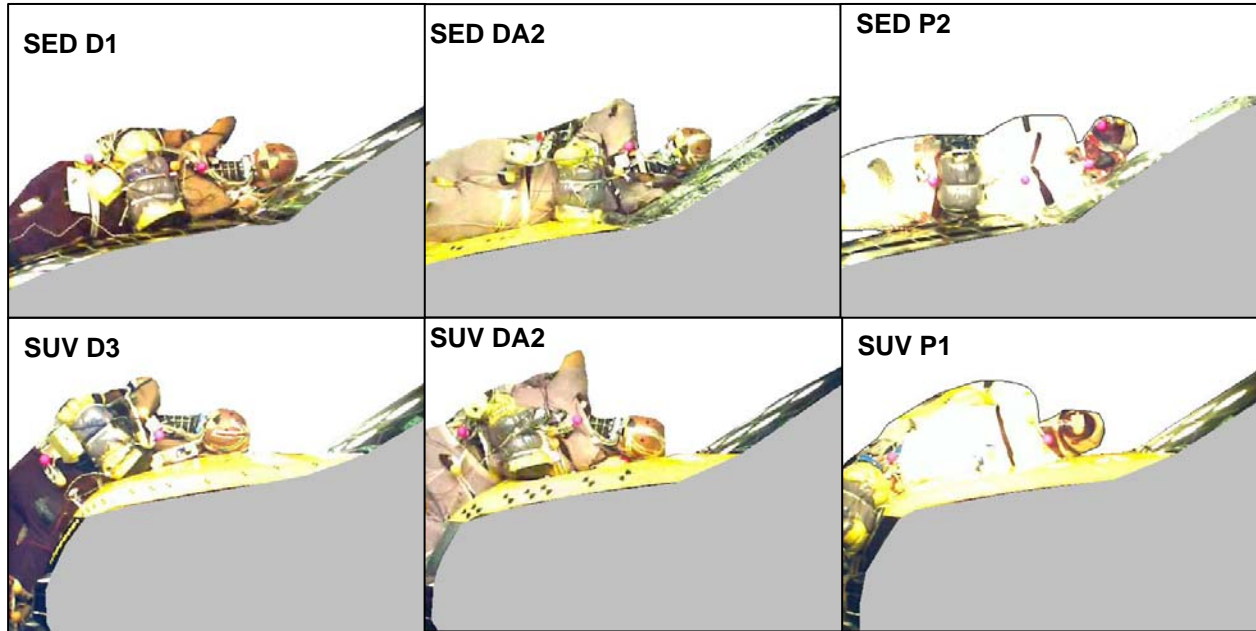


Figure 5. High speed video images depicting the imager frame just prior to impact (HC1) from six of the tests.

Table 2. Head impact parameters for each subject.

Test	Impact		t1- HIC15	t1- HIC15	t2- HIC15	HC1	HC2
	WAD (mm)	Velocity (m/s)					
Sed D1	1930	14.69	1437	123.6	138.6	124	125
Sed D2	1940	13.30	1447	122.3	137.3	123	124
Sed D3	1970	13.88	1321	125.4	140.4	127	128
Sed DA1	1970	15.89	1749	122.6	137.6	122	123
Sed DA2	2130	15.31	1091	131.4	146.4	133	134
Sed P1	2410	13.56	824	147.3	162.3	151	152
Sed P2	2200	14.48	3647	135.3	139.4	134	135
Sed P3	2320	11.80	511	138.8	153.8	141	142
SUV D1	1685	9.29	577	92.4	107.4	98	99
SUV D2	1660	10.45	826	85.2	100.2	93	94
SUV D3	1665	9.29	752	84.7	99.7	93	94
SUV DA1	1700	11.39	1704	87	102	93	94
SUV DA2	1850	12.03	1642	94.8	109.8	99	100
SUV P1	1860	12.11	3694	96.8	101.8	95	96
SUV P2	1845	10.64	745	85.9	100.9	91	92

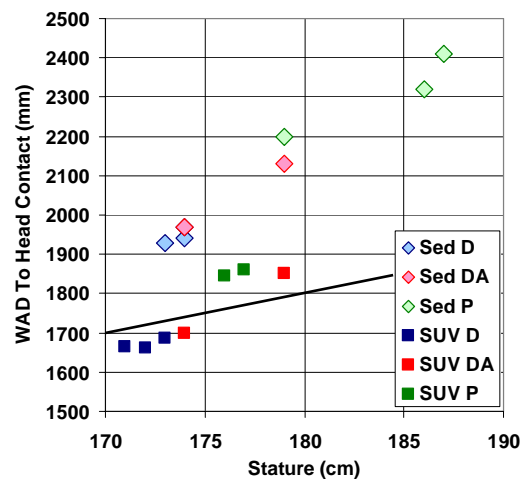


Figure 6. WAD to Head Contact vs. stature for all tests. The black line indicates a WAD equal to stature.

In the case of the sedan, all WAD measurements were greater than stature (Figure 6), which suggests that subjects slide up the vehicle prior to head contact, with the amount of sliding also positively correlated with stature. The repeated dummy tests and the first adjusted dummy test (DA1) on the SUV resulted in WAD measurements slightly less than the stature, which means that not only does the dummy not exhibit sliding (like in the sedan tests), but that the dummy did not evenly wrap around the vehicle in the SUV cases. (Figure 5).

High speed video images (1 kHz) from each test were analyzed to determine the time of head-to-vehicle contact. Because of the temporal resolution (1 ms) of the video images, the exact time of head contact to the vehicle could not be determined. However, the last imager frame prior to head contact (HC1) and the first imager frame after contact (HC2) initiated were determined, and since the change in the resultant head linear velocity relative to the vehicle velocity (Appendix Figure A1) over this short (1 ms) time interval was relatively high, head impact velocities are reported as the average (“Impact Velocity” in Table 2) and as the average and range over the time interval (Figure 7). Head impact velocities exceeded the vehicle velocity between 6% (P3) and 43% (DA1) in the sedan cases. In the SUV cases, the head impact velocities were less than the vehicle velocity in the repeated dummy tests (6%-16%) and in one PMHS test (4%), but higher than the vehicle velocity in the adjusted dummy tests (3%-8%) and in the other PMHS test (9%).

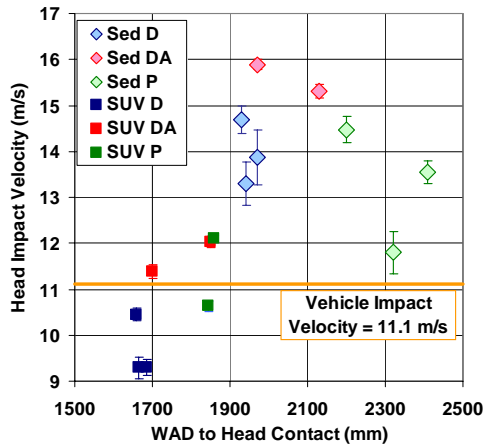


Figure 7. Impact velocity vs. WAD to head contact for all tests.

With regard to the risk of injury resulting from linear acceleration, the 15 ms Head Injury Criteria (HIC15) (Table 2)—calculated from the head CG resultant linear acceleration (Appendix Figure A1)—was compared to

the impact velocity (Figure 8) and the WAD to head contact (Figure 9). In general, HIC15 values increased with head impact velocity for each vehicle with some exceptions.

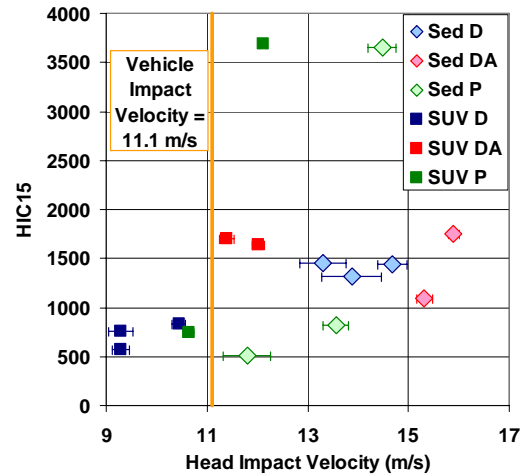


Figure 8. HIC15 vs. head impact velocity for all tests.

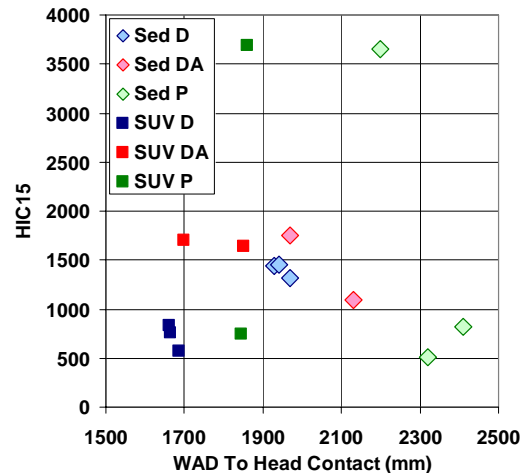


Figure 9. HIC15 vs. WAD to head contact for all tests.

The first adjusted dummy test (DA1) on the sedan resulted in the highest impact velocity (15.89 m/s), which was only slightly higher than that in the repeated dummy tests (13.3-14.7 m/s). This resulted in DA1 having only a slightly higher HIC than the repeated tests (1749 vs. 1321-1447) since head contact was in a similar location in each case (WAD 1930-1970 mm). In DA2, the dummy sustained a substantially lower HIC15 (1091) by impacting the windshield farther up (near the center) at a slightly lower impact velocity (15.9 vs. 15.3 m/s) than DA1. The second PMHS endured head impact at location similar to in DA2 and a lower velocity (14.48 vs. 15.89 m/s), yet it sustained a much higher HIC15 (3647 vs. 1091) than DA2. While the other two

PMHS, which had head impacts to the top third of the windshield (12 and 21 cm higher up than P2), sustained head impacts at lower velocities (11.8 and 13.6 m/s) and recorded drastically lower HIC15 values (824 and 511).

The lowest impact velocities of all of the cases in this study were sustained by the dummy in the repeated SUV tests. Although the dummy sustained HIC values that were only among the lowest recorded in the study. In SUV DA1 the dummy sustained a higher HIC15 than in the repeated dummy tests (1704 vs. 577-826) despite impacting the vehicle at a similar location and only a slightly higher impact velocity (11.4 vs. 9.3-10.5 m/s). Raising the dummy up by 7 cm between DA1 and DA2 resulted in a 15 cm increase in WAD to head impact, and a slightly higher impact velocity (11.4 vs. 12.0 m/s) yet a slightly lower HIC15 (1642 vs. 1704). Looking at the PMHS SUV tests, there is a large discrepancy in HIC values between the two tests (3694 and 745) despite having similar impact locations (rear 10% of the hood) and a small difference in impact velocity (12.11 m/s vs. 10.64 m/s). Furthermore, DA2 and P1 have similar impact locations and similar velocities, but DA2 has a substantially lower HIC15 (1642).

By examining the vehicle hood and underhood components in the area of the impacts, it became clear that both the SUV PMHS (and SUV DA2) endured head impacts at a location on the vehicle hood just above the passenger compartment-engine compartment firewall. It is hypothesized that this structure is very stiff, and thus has substantial influence on HIC15 values. Further analysis of the video images showed that the chin of P2 contacted the right arm/shoulder 4-5 ms prior to contacting the hood. It is hypothesized that the head/arm impact resulted in the substantially reduced HIC15 value, and that if the head/arm impact had not occurred, the HIC15 value recorded by SUV P2 would be similar to that recorded by P1.

Linear Kinetics

Dummy neck forces (Appendix Figure A2) at head impact (HC1) were dominated by z-direction forces, which exceeded 2300 N in every test in this study, 2500 N in all but two tests, and 3000 N in four tests (Figure 10). Neck forces are presented as forces applied to the head, so the positive z-forces at impact indicate significant neck tension. X and y-forces were all below 400 N at impact, and on average, x and y-forces were only 4% and 10% of the of the tensile (z) forces, respectively. The repeated dummy tests resulted in the highest tensile forces at impact, followed by the adjusted SUV tests, and lastly by both

the adjusted sedan tests and the repeated SUV tests, which sustained similar tensile forces at impact. Overall however, the average tensile force at impact was 2902 N with only a 15% coefficient of variation across all tests despite differences in vehicle geometry. Similar coefficients of variation in tensile force, 17% and 10% for the sedan and SUV tests respectively, were seen when considering impacts only with the same vehicle.

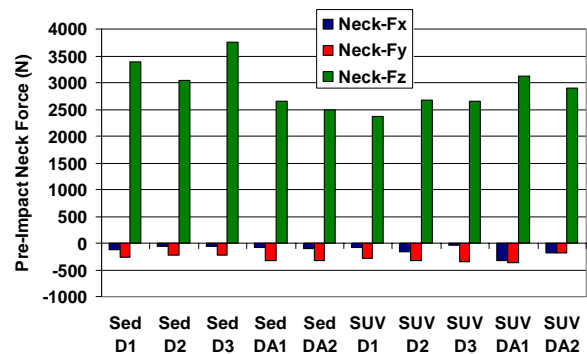


Figure 10. Dummy neck forces at the time of head contact (HC1).

Tensile forces similarly dominate neck forces throughout the interaction between the head and the vehicle. It is difficult to discern a robust kinematic marker for the end of the interaction time, so to examine the effect over the period of head-vehicle interaction, neck forces were averaged over the times used to calculate HIC15 (Figure 11). While z-direction forces still dominate neck forces throughout impact (1600-2500 N), x and y-forces were higher on average at 6% and 25% of the tensile force, respectively. The difference in tensile impact forces by test type is less clear than in the pre-impact forces. Overall, the average tension in the neck during the impact interaction was 2155 N with only 14% coefficient of variation across all tests. Similarly also, averaged tensile forces had only 16% and 12% coefficients of variation when considering sedan and SUV cases separately.

In contrast to neck forces, impact forces (Appendix Figure A2) are dominated by y-direction forces resulting from the vehicle impacting the right lateral side of the head. When impact forces are averaged over the times used to calculate HIC15 (Figure 12), the data show that in the SUV cases (except DA2) x-direction forces are commensurate with y-forces, but that y-forces are much larger than x-forces in the sedan cases. In the sedan cases, averaged y-impact forces were only slightly higher, on average, than z-neck forces (2590 vs. 2112 N). However, in the case of the SUV, averaged neck tensile forces were substantially

larger, on average, than y-impact forces (2199 N vs. 1381 N). This difference is still apparent, yet to a lesser degree, when comparing y and z-neck forces with x and y-impact forces in the SUV cases.

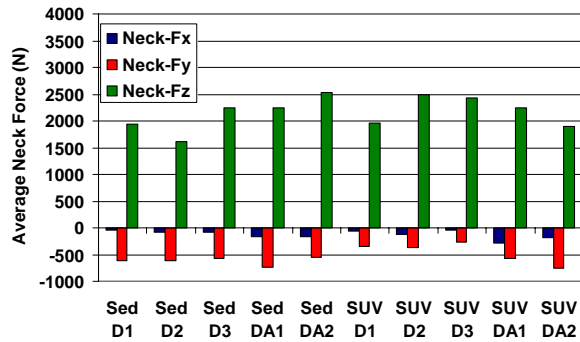


Figure 11. Dummy neck forces averaged over the times used to calculate HIC15.

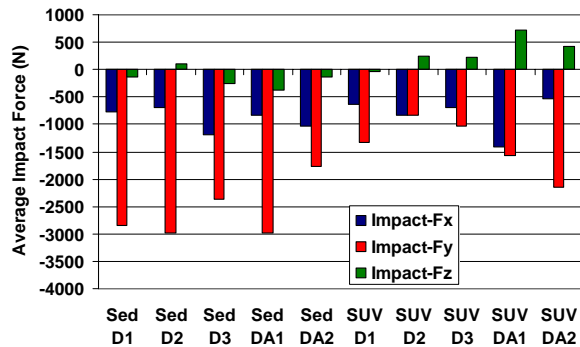


Figure 12. Dummy head impact forces averaged over the times used to calculate HIC15.

While there was no way to determine the neck or impact forces applied to the head during impact, Equation 1 and Equation 2 suggest that comparing local-frame accelerations between the dummy and PMHS tests, can shed light on the forces in the PMHS tests (Figure 13). In both Sed DA1 and SUV DA2, for example, the dummy shows that there are high z-accelerations at the time of impact (71 and 73 g, respectively), with virtually no x or y-direction accelerations (between 2 and 16 g). Similarly, there are high z-direction neck forces at the time of impact in both cases, but there was virtually no x and y-direction forces. Similarly in the PMHS, examining Sed P1 and SUV P1 for example, z-direction accelerations are relatively high at impact (54 and 80 g, respectively), and x and y-direction accelerations are lower (30 and 12 g in Sed 1, and 21 and 6 g in SUV 1, respectively), but slightly higher than in the dummy tests.

During the head-vehicle impact interaction, the dummy data shows that the z-direction acceleration and neck force reduces to zero by t_2 with the z-direction impact forces remaining small. Despite the smaller magnitude, the z-direction impact force in Sed DA1 opposes the z-direction neck force. However, in the case of the SUV, the opposite occurs and the z-neck force points in the same direction as the z-impact force. In contrast to the dummy tests, the z-direction PMHS accelerations remain relatively high throughout the interaction.

During the interaction, y-direction accelerations and impact forces in the dummy grow and remain relatively high, with smaller, yet still not negligible, y-direction neck forces, which point in the same direction as the impact force in both cases. The same is true for the x-direction accelerations and impact forces, but their magnitude is lower than those measured in the y-direction. Similarly in the PMHS tests, y-direction and x-direction accelerations grow and remain high throughout the interaction, with the y-accelerations being higher than the x-accelerations.

Overall, the averaged (between t_1 and t_2) resultant neck forces in the dummy were 61%-115% and 95%-190% of resultant impact forces in the sedan and SUV cases, respectively. On average, resultant neck forces were 79% and 128% of resultant impact forces in the sedan and SUV cases.

ANGULAR KINEMATICS

Resultant angular velocity and angular acceleration time histories (Appendix Figure A2) show that angular velocities are relatively high at the time of impact, and angular accelerations reach high values as a result of impact. Angular velocities at the time of impact are close to, or equal to, peak angular velocities measured in all tests. In general, the subjects reached peak angular accelerations during head-vehicle impact that spanned a large range between 4522 rad/s^2 (Sed P3) and 39126 rad/s^2 (SUV DA2). Averaging over the times used to calculate HIC15 (t_1 - t_2), the dummy predicted higher angular accelerations in the sedan tests than in the SUV tests, despite having similar peak angular velocities in some cases (Figure 14). In the PMHS cases on the other hand, averaged angular accelerations were similar with one high case for each vehicle ($\sim 15600 \text{ rad/s}^2$) and the other cases lower (2300 - 4300 rad/s^2). Interestingly though, the peak angular velocities measured in the sedan PMHS tests were less than those measured in the SUV PMHS tests.

Furthermore, it is interesting to note that, other than in the adjusted dummy tests on the SUV, all of the tests showed that HIC15 and averaged angular acceleration

were well correlated (Figure 15). Additionally sedan test P2 and SUV test P1 resulted in very similar and quite high HIC15 and peak angular acceleration values,

whereas the other PMHS tests predicted lower levels of injury risk.

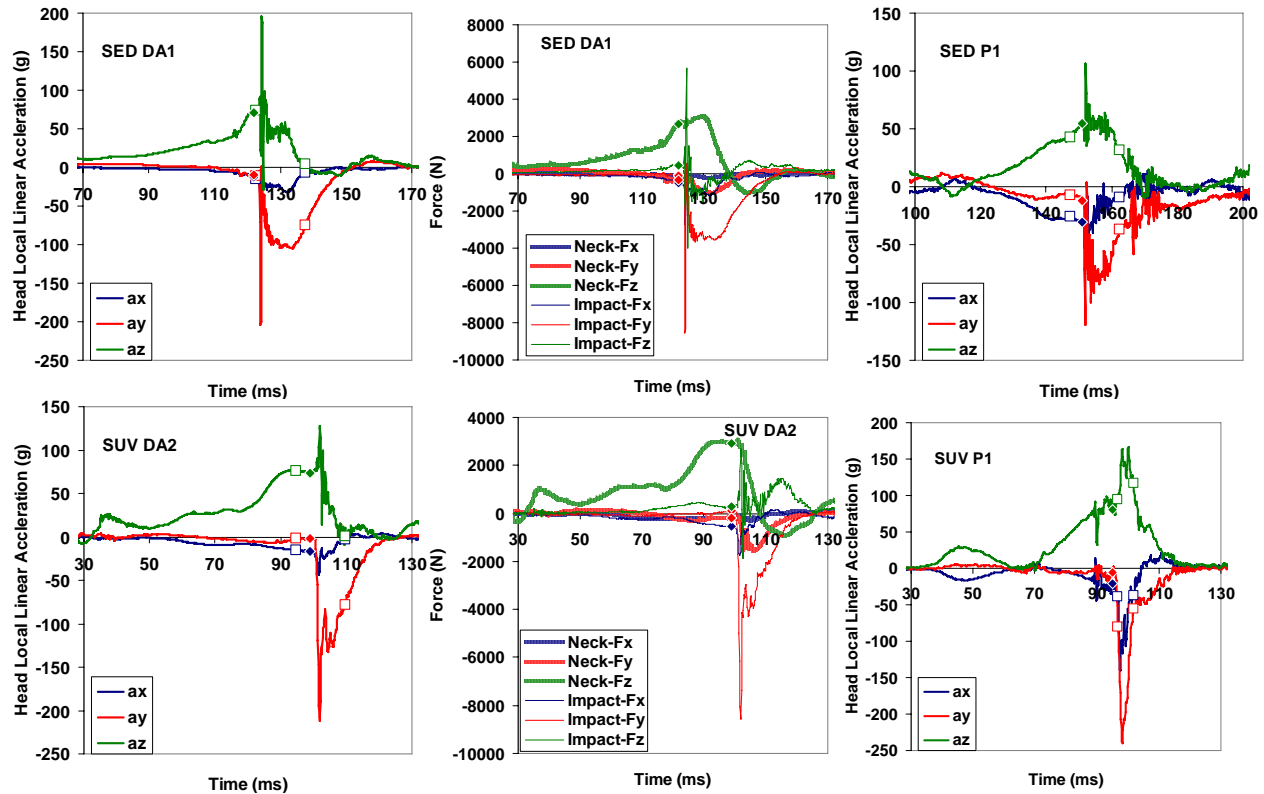


Figure 13. Head local accelerations from a sedan (top) and an SUV (bottom) dummy test (left), with neck and head impact forces (center), compared to head local accelerations from two PMHS tests (right). Times used to calculate HIC values are shown in each plot with squares, and the head impact time (HC1) is shown with a diamond.

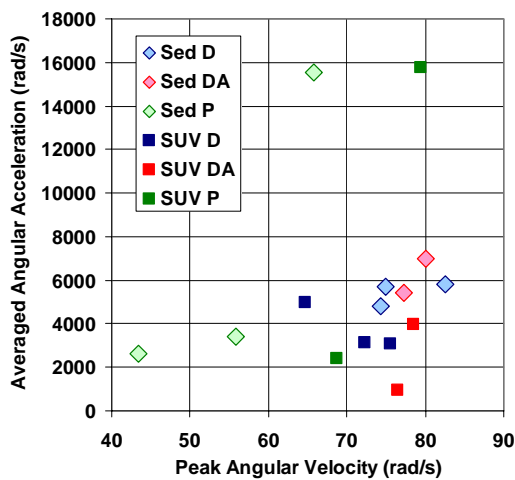


Figure 14. Resultant angular acceleration averaged over t_1-t_2 vs. peak angular velocity for all tests.

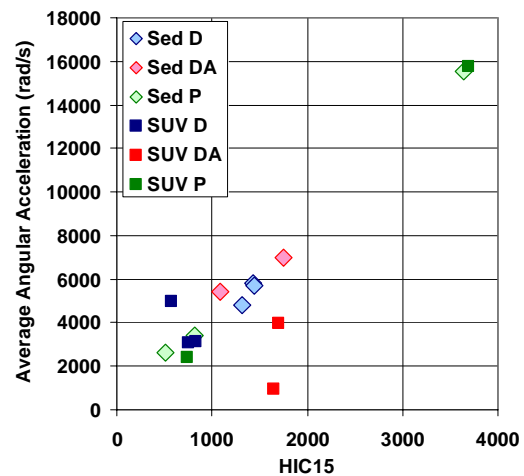


Figure 15. Resultant angular acceleration averaged over t_1-t_2 vs. HIC15 for all tests.

DISCUSSION

If head injury risk is measured in vehicle/pedestrian collisions using the linear acceleration (which determines HIC15) during interaction with the vehicle, solving Equation 2 for the head acceleration vector

$$\mathbf{a} = \frac{\mathbf{F}_I}{m_{head}} + \frac{\mathbf{F}_N}{m_{head}} \quad (3)$$

shows that head injury risk is equally affected by the forces applied to the head through the neck, and by the forces applied to the head by the vehicle. Neck forces were shown to be dominated by z-direction (tensile) forces that increase to high levels well prior to head impact, and remain at relatively high levels throughout the impact interaction. High tensile neck forces prior to impact are easily explained by the overall kinematics of the subjects (Kerrigan et al. 2005a and Kerrigan et al. 2005b). The subjects' upper bodies undergo rotations about the x (anterior-posterior) axis with center of rotation near the pelvis. This results in the head, which is farthest from the pelvis, having the highest linear velocity, and its inertia causing high tensile forces in the neck. Okamoto and Kikuchi (2006) showed similarly high tensile forces in the dummy neck prior to and at the time of head impact (~1500 N and ~4000 N in SUV and sedan impacts, respectively).

Since the distribution of neck forces at impact (high z-force and low x and y-forces) does not change dramatically during interaction with the vehicle, it can be concluded that head impact with the vehicle does not dramatically affect the force transmission from the neck to the head. Impact forces, on the other hand, are dominated by y-direction (lateral) forces, with somewhat high forces also in the x-direction, and virtually no forces measured in the z-direction. Since these forces are caused by vehicle impact, it makes sense that they are directed in the right-to-left lateral direction and in the anterior-to-posterior direction because head impacts occur to the right-anterior side of the head (Figure 5).

Equation 3 also shows that when impact forces and neck forces point in the same direction, the effect on the acceleration is additive. Another way of saying this is that when the neck force points in the same direction as the impact force, the neck force results in increased head acceleration, and when the forces have opposite polarities, neck forces decrease head accelerations. Data from this study shows that the neck force has an additive effect on the acceleration magnitude, on average, in the x, and y directions in all of the tests and in the z-direction in the SUV tests. In

the sedan tests, on average, the z-impact force opposes the neck force, but is only 8% of the neck force (162 N vs. 2112 N) the mitigating effect on the z-acceleration is low.

In this study, all of the force applied to the head through the neck is assumed to be measured by the dummy's upper neck load cell, when the structure of the dummy (Figure 16) as well as the presence of impact forces prior to head contact (Appendix Figure A2) suggests that this is not true. Firstly, the dummy has anterior and posterior cables designed for the THOR dummy to increase the flexion-extension stiffness of the neck, that provide for a load path between the head and the neck that is parallel to that which passes through the neck load cell. While the THOR dummy contains load cells to measure the tension in the cables, the Polar-II dummy did not. Since the cables can only support loads in tension, data from this study show that neck tensile loads are underestimated. The time histories of z-direction impact forces (Appendix Figure A2) show that a tensile "impact" force (between 67 and 420 N) was measured prior to impact in all of the tests.

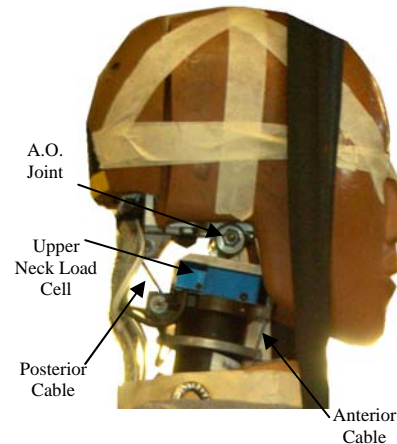


Figure 16. Photo depicting Polar-II head/neck connection and instrumentation.

Additionally, the dummy neck has a pin joint between the dummy neck and the head (A.O. joint), which permits the head's coordinate system to be rotated about the y-axis between -8 degrees (extension) and 25 degrees (flexion). Thus the orientation of the head's acceleration coordinate system was not necessarily aligned with the neck's coordinate system. This difference explains why there are impact forces measured in the x-direction prior to impact (between 80 and 560 N). Negative x-direction forces applied through the neck that result in these pre-contact "impact" forces, suggest that prior to impact the A.O. joint is in extension, and if the neck forces could be

corrected for A.O. joint angle (which is measured by a potentiometer in THOR) these x-direction impact forces would actually be recorded as increased tensile forces.

While it is not possible to measure neck forces in the PMHS directly, it is hypothesized that force transmission from the neck to the head is different in PMHS than in the dummy. A primary justification of this hypothesis can be explained by the lack of active musculature. Since the PMHS lacks active musculature, and the dummy's neck was designed to have the stiffness of a living human with active musculature (Akiyama et al. 2001) there are some differences in the head trajectory (Kerrigan et al. 2005a and Kerrigan et al. 2005b) and head linear and angular velocity (Appendix Figure A1) between the dummy and the PMHS. The linear velocity time histories show that PMHS reach lower peak head velocities than the dummy, and the angular velocity time histories show an early peak not seen in the dummy tests, which results from the motion of the thorax being out of phase with the motion of the head. In other words, as the thorax of the dummy rotates down toward the car, the relatively stiff neck of the dummy keeps the head in line with the thorax (see Kerrigan et al. 2005a and Kerrigan et al. 2005b for more high speed imagery from the tests). But in the PMHS tests, as the thorax rotates, the inertia of the head and relatively low stiffness of the neck caused a delayed reaction of the PMHS head.

Further evidence of the difference in force transmission between the head and neck of the PMHS and dummy can be seen in the differences in head impact dynamics between the DA2 dummy tests and PMHS tests Sed D2 and SUV D1. Despite sustaining similar head impact velocities at similar (or the same) impact location, DA2 in the sedan and SUV resulted in much lower HIC15 values than in the Sed P2 and SUV P1. Since impact accelerations are determined by neck and impact forces (Equation 3), the sum of the neck and impact forces must have remained much higher during the impact in Sed P2 and SUV P1 than in the DA2 tests. While it is not possible to know whether it was the neck force or the impact force (or both) that was higher in the PMHS tests, comparing accelerations and impact forces in two dummy tests (Figure 13) showed that z-direction accelerations correlated with z-direction neck forces before and during head impact, and that x and y-direction accelerations correlated with impact forces during the head impact. In comparing SUV P1 with SUV DA2, while y-direction accelerations appear to remain at similar levels through out the impact, x and z-direction accelerations in the PMHS remain higher than those in the dummy

tests, which suggests that both neck forces and impact forces were higher in the PMHS. Ideally though, to provide a more accurate estimate of this difference, a universal (not representing any particular vehicle) with instrumented impact surfaces should be used to measure impact forces directly.

It is hypothesized that SUV P2 would have resulted in similar impact dynamics as those seen in SUV P1, had it not endured a head/arm impact prior to (and during) the head/hood impact. Not only did the arm impact reduce the linear acceleration and HIC15 value, but it reduced the peak and averaged angular acceleration values.

In comparing head impacts to the sedan and to the SUV, the difference in impact velocity between the two vehicles, on average, showed that the dummy impacted the sedan at a 39% higher velocity in the sedan tests than in the SUV tests (14.6 vs. 10.5 m/s). Looking at the forces, on average, averaged resultant neck forces were similar between the two vehicles, but impact forces were 57% higher in the sedan tests than in the SUV tests (2930 vs. 1862 N). The higher impact velocities resulted in higher impact forces causing the dummy to predict higher HIC15 values and higher angular accelerations in windshield impacts in the sedan tests than in hood impacts in the SUV tests. This result is further supported by epidemiology data showing that the windscreen causes greater Harm to pedestrians than any other vehicle structure (Fildes et al. 2004) and almost half of all AIS 2-6 head injuries are caused by the windscreen (Mizuno 2003).

CONCLUSIONS

In the current study, head impact dynamics experienced by pedestrians struck by a small sedan and a large SUV were examined using data from impacts with both a pedestrian dummy and PMHS. Despite analyzing only lateral impacts with two vehicle geometries at 40 km/h, the results and analyses presented in this study provide insights into pedestrian head impact dynamics that can be used to improve passive and active pedestrian injury countermeasures.

In general, the results of the dummy tests showed that the Polar-II dummy is repeatable but that differences in the pre-test position, support and clothing of the dummy can dramatically affect head impact dynamics, with a greater effect seen in the SUV tests compared to the sedan tests. Additionally, the dummy shows good biofidelity in comparing it to the PMHS tests, however, differences in stature and neck stiffness between the PMHS and dummy affect head dynamics before and during head impacts

The data also showed that, for both vehicles, dummy neck forces contribute a substantial and additive effect to head impact accelerations because the component-wise neck forces point have the same polarity as the component-wise impact forces, and because the neck forces are of comparable magnitude to the impact forces: neck forces were, on average, 79% and 128% of resultant impact forces in the sedan and SUV cases, respectively. In the case of the SUV, averaged resultant neck forces exceeded averaged impact forces, suggesting that neck forces affect head accelerations more than impact forces in the SUV.

While inclusion of the PMHS data complicates the relationship, the dummy predicted higher HIC15 values and higher angular accelerations in windshield impacts in the sedan tests than in hood impacts in the SUV tests. This difference is due to the higher impact velocities in the sedan tests compared to the SUV tests (14.6 m/s vs. 10.5 m/s), which result in higher impact forces transmitted to the head by the vehicle.

REFERENCES

- Akiyama A, Okamoto M, Rangarajan N. (2001) Development and application of the new pedestrian dummy. Paper 463, 17th Conference on the Enhanced Safety of Vehicles, Amsterdam, The Netherlands.
- Fildes B, Gabler HC, Otte D, Linder A, Sparke L. (2004) Pedestrian impact priorities using real-world crash data and harm. 2004 International Conference on the Biomechanics of Impacts (IRCOBI), Graz, Austria.
- Kam C, Kerrigan J, Meissner M, Drinkwater C, Murphy D, Bolton J, Arregui C, Kendall R, Ivarsson J, Crandall J, Deng B, Wang JT, Kerkeling C, Hahn W. (2005) Design of a full-scale impact system for analysis of vehicle pedestrian collisions. Paper 2005-01-1875, Society of Automotive Engineers, Warrendale, PA.
- Kerrigan J, Crandall J, Deng B. (2007) Pedestrian kinematic response to mid-sized vehicle impact. *International Journal of Vehicle Safety*. 2007; 2(3): 221–240.
- Kerrigan, J, Crandall, J, Deng, B. (2008a) A Comparative Analysis of the Pedestrian Injury Risk Predicted by Mechanical Impactors and Post Mortem Human Surrogates. *Stapp Car Crash Journal*, 52, pp. 527-567.
- Kerrigan J, Kam C, Drinkwater C, Murphy D, Bose D, Ivarsson J, Crandall J. (2005a) Kinematic Comparison of the Polar-II and PMHS in Pedestrian Impact Tests with a Sport-Utility Vehicle. 2005 International Conference on the Biomechanics of Impacts (IRCOBI), Prague, Czech Republic.
- Kerrigan J, Murphy D, Drinkwater D, Kam C, Bose D, Crandall J. (2005b) Kinematic corridors for PMHS tested in full-scale pedestrian impact tests. NHTSA, Paper 05-0394, Proc. 19th Conference on the Enhanced Safety of Vehicles (ESV), Washington DC, United States.
- Kerrigan J, Rudd R, Subit D, Untaroiu C, Crandall J. (2008b) Pedestrian lower extremity response and injury: a small sedan vs. a large sport utility vehicle. Paper Number 2008-01-1245, Society of Automotive Engineers, Warrendale, PA.
- Mizuno Y. (2003). Summary of IHRA pedestrian safety WG activities (2003)-proposed test methods to evaluate pedestrian protection afforded by passenger cars. NHTSA Paper 580, Proc. 18th Conference on the Enhanced Safety of Vehicles (ESV), Nagoya, Japan.
- Neal-Sturgess CE, Carter E, Hardy R, Cuerden R, Guerra L, Yang J. (2007) APROSYS European In-Depth Pedestrian Database. Proc. 20th Conference on the Enhanced Safety of Vehicles (ESV), Lyon, France.
- Okamoto Y, Kikuchi Y. (2006) A study of pedestrian head injury evaluation method. Proc. 2006 International IRCOBI Conference on the Biomechanics of Impact, pp. 265-276.
- Padgaonkar AJ, Krieger KW, King AI. (1975) Measurement of angular acceleration of a rigid body using linear accelerometers, *J. Appl. Mechanics*, 42, 552–556.
- Robbins, D.H. (1983) Anthropometric Specifications for Mid-Sized Male Dummy, Volume 2. Report number UMTRI-83-53-2, University of Michigan Transportation Research Institute, Ann Arbor, MI.
- Society of Automotive Engineers, Inc., “Instrumentation for Impact Tests,” SAE J211/1 MAR95, March 1995, 10 p.

APPENDIX

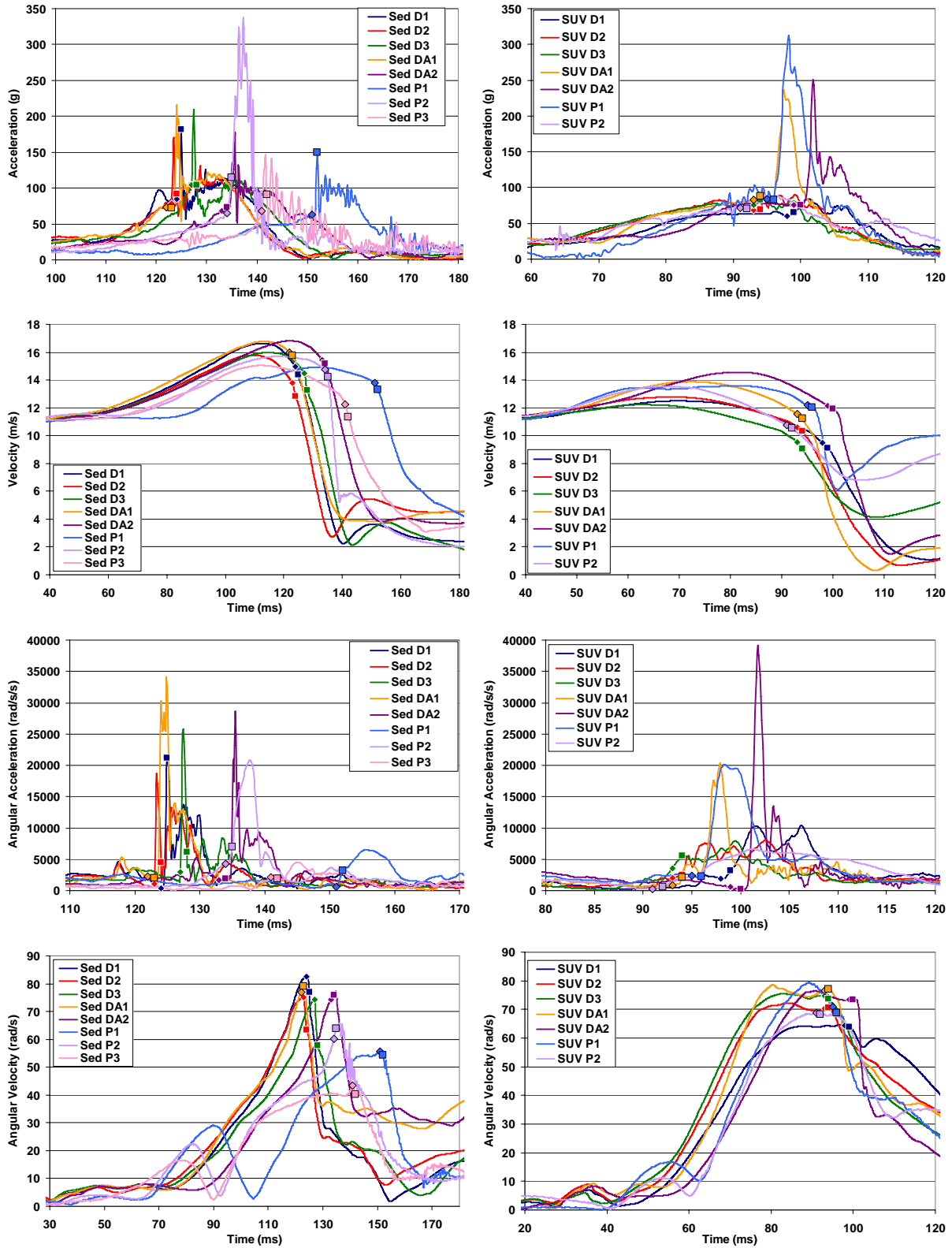


Figure A1. Head resultant linear acceleration and velocity, and angular acceleration and velocity time histories from the sedan (left) and SUV (right) tests. The diamond indicates HC1 and the square indicates HC2.

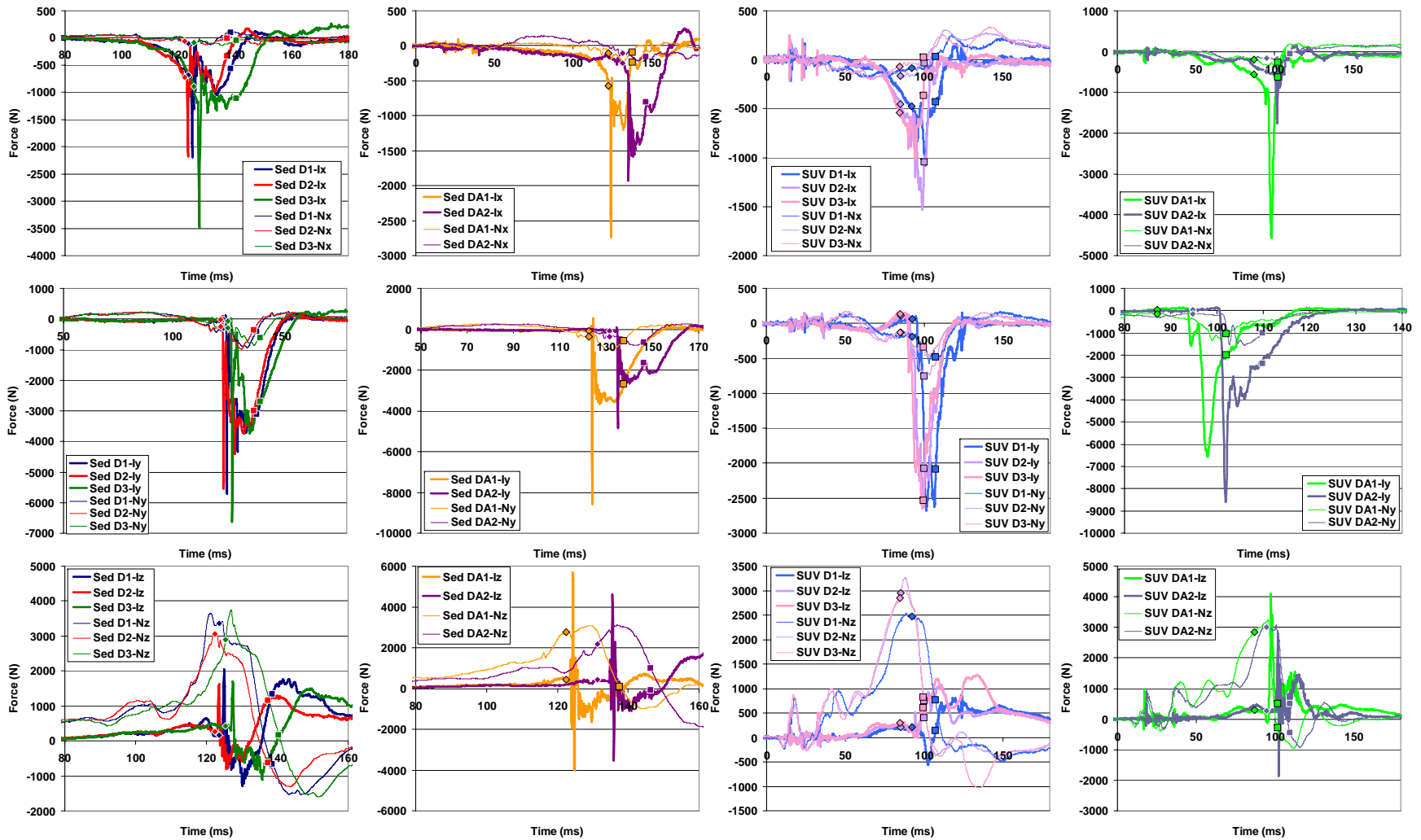


Figure A2. Impact forces (“Ix”, “Iy”, and “Iz”) and neck forces (“Nx”, “Ny”, and “Nz”) applied to the head. Forces are in the head’s local coordinate system as defined by SAE J211 (Figure 4). The diamond and square indicate HIC calculation times t_1 and t_2 , respectively. Note that time and force scales vary.

DEVELOPMENT OF AN HYBRID HOOD TO IMPROVE PEDESTRIAN SAFETY IN CASE OF VEHICLE IMPACT

Giovanni Belingardi

Alessandro Scattina

Politecnico di Torino

Enrico Gobetto

Fiat Group Automobiles S.p.A.

Italy

Paper number 09-0026

ABSTRACT

In recent years car manufacturers when developing new car designs have paid great attention to two main aspects. On one hand there are the pollutant emissions and in particular the carbon dioxide emissions which are directly connected to the fuel consumption of cars, on the other hand there is the always increasing safety level required for the cars, with a particular attention to the safety of pedestrian and other vulnerable road users (VRU).

The present paper reports some results of a recent research activity developed in this perspective and specifically devoted to the design of a bonnet for a middle/low segment car. A global overview on the different solutions which can be used to obtain a lightweight and pedestrian safe bonnet will be illustrated.

The main part of the work deals with the design of a hybrid metal/plastic bonnet. All the aspects examined during the design of a new bonnet will be taken into consideration, starting from the technical performance and going through the manufacturing and economical aspects.

Then some considerations on a bonnet with a peripheral frame solution will be presented. At the end, the study on a further concept of hybrid bonnet characterized by a particular wire design of the inner structure will be addressed.

INTRODUCTION

In the recent years substantially two main objectives are put in evidence as the main targets in the automotive design. On one hand cars are one of the most important sources of pollution. There are different reasons to explain why vehicles are a source of pollution [1-4], first of all there are the products of engine combustion, the primary ones, the carbon dioxide (CO₂) and the secondary ones,

such as carbon monoxide (CO), oxides of nitrogen (NO_x) and unburned hydrocarbons (HC). Then the cars are also an important source of noise pollution [5], and at last but not least, the vehicles have to be considered as a solid pollution at the end of their life. Among these types of pollution, in the recent years the pollution due to the emission of carbon dioxide is certainly considered the most important one, because it is a green house gas and is considered responsible for the planet climatic changes. In particular, as it is possible to see in Figure 1, if in the last years the emissions of carbon dioxide from different sectors have decreased, the contribution from the transport sectors has continuously grown [1].

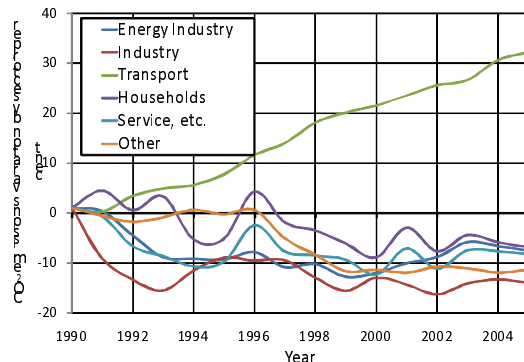


Figure 1. Variation of the global CO₂ emissions by sectors as a function of the years.

In this field, from many years a series of regulations have been proposed and emitted by different source such as the national Governments but also by association of car manufacturers, with the scope of a relevant reduction of the production and the emission of carbon dioxide. In order to face this more and more strict limits, the car manufacturers are currently engaged to improve the global efficiency of the vehicles, working on different aspects: engine, transmission and aerodynamics efficiency. However, in order to

meet the targets, one of the most important aspects is the lightweight, in fact the production of carbon dioxide is directly related to the fuel consumption and therefore to the weight of cars.

The other main subject in the automotive design is the safety. In recent years many improvements have been achieved in the field of safety for the occupants of the vehicles, by working both on active and passive safety. Nowadays the attention of the public opinion and of the car manufactures is focused on the safety of the vulnerable road users (pedestrians and cyclists), in fact the number of dead and injuries due to road accidents that involve these categories is very important [3,9,11]. Also in this field more and more strict regulations have been proposed, not only by the national Governments but also by rating institutes such as the Euro NCAP [12]. A series of impact tests have been introduced which replicate possible accident involving a pedestrian, and a series of target have been established which have to be reached to get the approval for the vehicle [10, 16, 17]. Since 2009 the total score obtained in the rating tests includes the score referred to pedestrian protection; it is unnecessary to remind here how Euro NCAP score is considered now a marketing key for the car manufacturers.

In this perspective it is possible to collocate the present research work, made in collaboration between Fiat Research Centre and Politecnico di Torino, aimed to the development of a hybrid metal/plastic bonnet for a car of medium/low segment. The progressive development of the bonnet design, starting from a reference solution, will be illustrated. The main targets of the work have been a weight reduction of about 30% in comparison with the reference bonnet, together with a reduction of the injuries to the pedestrian head in case of impact. Further the final solution should have competitive total industrial cost when compared to a full aluminium solution, and to ensure the same quality and functionality of the reference solution. The development has started from a predefined hybrid concepts, but different solutions in terms of shapes and materials have been considered. During the development the main stream has been focused on the technical performance, but also manufacturing considerations such as the compatibility with the current assembly line and some economical aspects have been taken into account. All the development phase has been done by means of virtual

simulations, in particular using the finite element model technique.

At the end also some considerations on alternative solutions made by a peripheral reinforcement as bonnet frame will be illustrated together with a further hybrid bonnet concept with a particular wire design for the inner structure.

The reference bonnet is shown in an exploded view in Figure 2, it is completely made by stamped steel sheet parts and it is composed by an outside panel, which will be considered constrained by the aesthetic style of the car (for this reason its shape cannot be changed but it is only possible to modify the sheet thickness and the material), by an inner structure aimed to structural functions, and by a series of reinforcements applied near the hinges and above the locking mechanism.

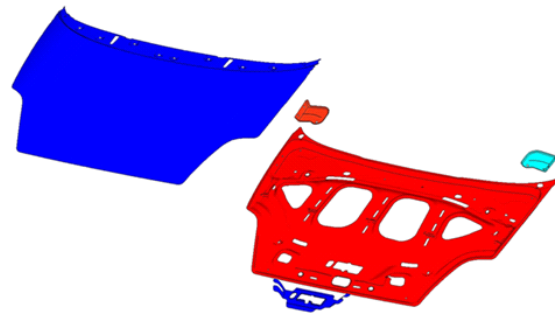


Figure 2. An exploded view of the reference bonnet.

HYBRID BONNET

The main hybrid concept has been defined starting from the experiences made in other similar activities [6-8], in particular focused on a tailgate. This concept is characterized by a thermoplastic inner structure, in order to exploit the potentials of this material in terms of freedom in shape and thickness distribution, and by an outside metal panel in order to meet the quality requirements. Starting from these concepts, and on the basis of information obtained in a preliminary benchmarking activity, where the geometries and the materials used for a series of bonnets currently in production have been investigated, some initial ideas for the hybrid bonnet have been proposed. In particular the design of the inner thermoplastic structure has been considered. The first solution consists of a simple perimeter structure, the other ones are characterized by a perimeter structure with a series of longitudinal and crossed ribs. These initial concepts are shown in Figure 3.

As the main targets of this work is lightweight together with reduction of injury risks for the impacted pedestrian head, the different proposed solutions have been evaluated first under the pedestrian safety point of view, then the most promising ones have been evaluated also versus other structural performance: stiffness and indenting resistance

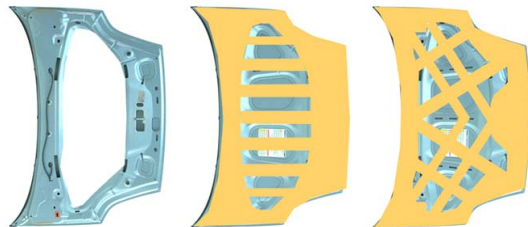


Figure 3. Three main preliminary concepts for the inner structure of hybrid bonnet.

For what concerns the pedestrian head impact tests, simulations have been performed according the ACEA phase II regulations. The test parameters have been an impact speed of 40 km/h with an impact angle of 50°.

Before to examine the first proposed solutions, the quality of the prepared FEM model has been assessed by comparing the numerical results of some pedestrian head impact tests with the available experimental values. In particular three different impact points, namely C2C, C3D and C4C, (their positions on the bonnet surface are shown in Figure 4) have been examined for the reference bonnet solution. For this work the well known software LS-Dyna®, that is based on a step by step explicit integration scheme, has been used. The results have been examined in terms of HIC_{15} and acceleration curves recorded during the test execution in the head form centre of gravity. The diagrams shown from Figure 5 to Figure 7 establish a systematic comparison between the experimental and numerical acceleration curves, while and the HIC_{15} values are reported and compared in Table 1. The results of this quality assessment are very good, not only because the numerical values of HIC_{15} are very close to the experimental one but also because all the acceleration curves have remarkable accordance both in values and in trend with the experimental ones. It has been possible to conclude that this model can be used for the following development of the hybrid hood because it has simulated very well the real behaviour.

Table 1. Comparison between the numerical and experimental HIC_{15} results for the reference solution

Points	HIC_{15}	
	Experimental	Numerical
C2C	1852	1912
C3D	1181	1381
C4C	943	945

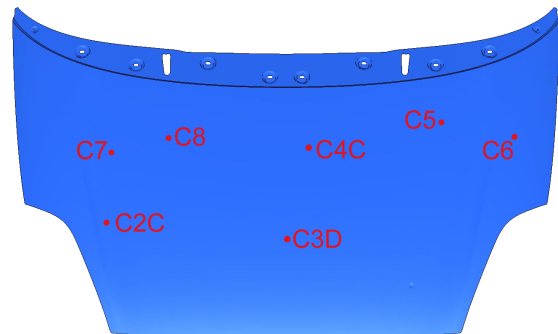


Figure 4. Position of the impact points on the bonnet surface.

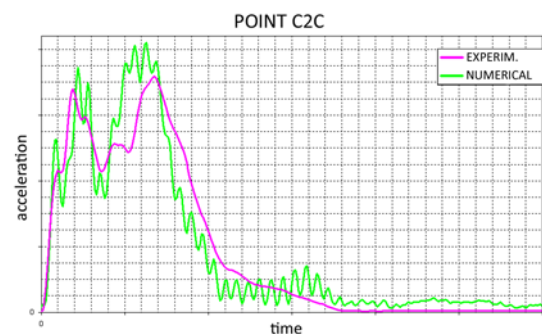


Figure 5. Comparison between the experimental and numerical acceleration curves for the point C2C.

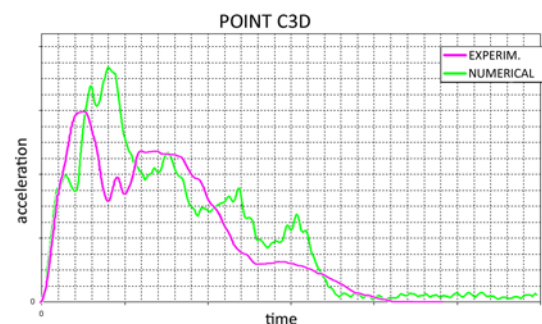


Figure 6. Comparison between the experimental and numerical acceleration curves for the point C3D.

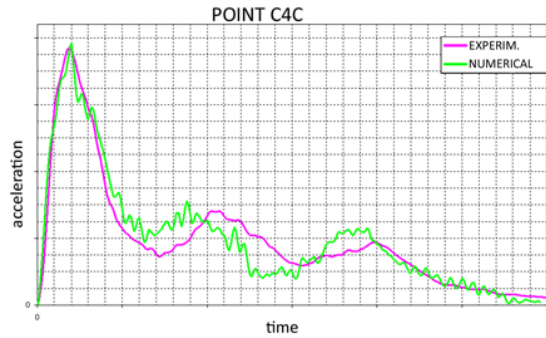


Figure 7. Comparison between the experimental and numerical acceleration curves for the point C4C.



Figure 8. Two different designs for the inner structure, G1 on the left, G2 on the right.

At this stage the design of the hybrid bonnet has begun and some solutions for the thermoplastic inner structure have been drawn, according to the information obtained in the first preliminary benchmarking phase. In particular, as shown in Figure 8, two different solutions have been proposed, namely the G1 and the G2.

The G1 solution is characterized by a series of longitudinal ribs, while the G2 solution has a series of cross ribs. For what concerns the material to be adopted for this part, the thermosetting materials have been discarded, because they cannot be recycled in an easy way. An interesting solution for the material, both from lightweight and cost point of view, could be the polypropylene, which is one of the most used thermoplastic material for automotive applications, but this material can have problems with the temperature due to the proximity of the engine. For this reason it is necessary to consider a material with better thermal and mechanical properties, and in this case a polyamide reinforced by glass fibres has been chosen. In particular, in a first development, a long glass fibre reinforcement with a weight fraction of 40% has been selected. The main mechanical properties of this material are: tensile modulus of 9300 MP and tensile strength of 146 MPa. For what concerns the thickness of the inner structure, initially two

different values have been considered, in particular 2.5 and 1.2 mm but the second one has been immediately discarded because, from the manufacturing point of view, is not feasible. The plastic material has been modelled using the card *MAT_PIECEWISE_LINEAR_PLASTICITY. The stress-strain curve of the material has been supplied at room temperature. The design of the hybrid bonnet has been completed by the same parts of the reference solution: an outside steel skin and a series of steel reinforcements. The join between the different parts has been made by structural adhesive bonding.

The pedestrian safety performance of this first hybrid bonnet has been evaluated in the same impact points considered up to now. The obtained results are shown in Table 2 in term of HIC₁₅.

Table 2
HIC₁₅ results for the first hybrid bonnets

HIC ₁₅	Impact point		
Solution	C2C	C3D	C4C
Reference	1912	1385	941
G1 Th. 2.5	2429	2222	2112
G1 Th. 1.2	2027	1507	1016
G2 Th. 2.5	2515	-	-
G2 Th. 1.2	1966	-	-

The obtained value are generally too high, and by examining also the acceleration curves which have led to these results, it has been possible to conclude that these first solutions for the hybrid bonnet have resulted too stiff for this type of performance. For this reason a series of corrective modifications have been introduced.

First of all a third design for the thermoplastic inner structure, as shown in Figure 9 and called G3, has been proposed. This solution is made once again by longitudinal ribs but in a lower number and with a lower height in order to reduce bending stiffness. Then, on the three considered inner structures, a series of cuts have been applied in order to reduce further both the weight and the bending stiffness. The new obtained solutions, identified by the extension .1 are shown again in Figure 9. For what concerns the materials, for the inner structure, it has been decided to reduce the mechanical properties of the fibre reinforced polyamide by using a short glass fibre reinforcements, with the same weight fraction, while for the outside panel it has been decided to evaluate the behaviour of different types

of aluminium alloys, series 6xxx, varying at the same time, the panel thickness.

The behaviour of these modifications has been evaluated initially only for the pedestrian safety performance with a complete test plan on the impact point C4C. Results allow to compare all the possible solutions. A summary the results are shown in Table 3. Substantially, the solutions which have a thermoplastic inner structure reinforced with long glass fibre, have to be discarded because are too stiff, even if the external panel has been made in aluminium. A similar thing can be said also for the solutions characterized by a steel outside panel.

For what concerns the inner structure, the best results have been obtained with the G3 design, but also the results obtained with the design G1.1 and G2 are quite interesting, finally, as it has already seen before, the design G1 appears too stiff.

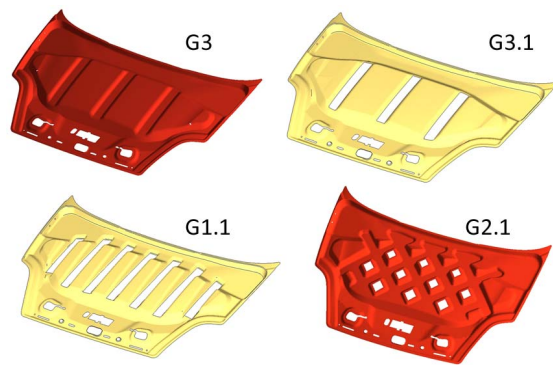


Figure 9. Different considered designs for the thermoplastic inner structure.

**Table 3
Comparison of the HIC₁₅ results obtained for the different examined solutions.**

HIC ₁₅	Impact Point C4C						
	Solution	Ref.	G1	G2	G3	G1.1	G3.1
Inner Structure: PA long fibre Skin: aluminium	941	1904	1263	1104	1277	902	
Inner Structure: PA short fibre Skin: aluminium	941	1540	1097	937	1074	812	

On the most promising solutions a further simulation loop has been done, aimed to evaluate the effect of some different types of aluminium alloys and to define the best material and thickness.

At this point of the development it has been necessary to take into consideration a second important performance for the bonnet, the torsional stiffness. This value is obtained with an experimental test after having positioned horizontally the bonnet and by applying a vertical load at one of the two rubber pads, where usually the bonnet is leaned. The vertical displacement of the load application point is measured and then, through a geometric procedure, the applied torque and the related deformation angle are calculated. The ratio between these two values allows to evaluate the torsional stiffness.

Starting from the previous results on pedestrian safety, the bonnet typologies taken into consideration for the torsional stiffness analysis have been designed by an external aluminium skin and an inner structure made by short glass fibre reinforced polyamide. In particular the behaviour of the different design for the inner structure has been investigated. Once again they have been evaluated by means of the results obtained with of finite element simulations. At this stage the scope of these numerical analysis has been to understand the global trend of the different solution taken into consideration. By examining the results collected in Table 4, it is possible to note a deep decrease from the value of reference solution, but it is also necessary to say that this value is much higher than the target. These results have put in evidence as the design G2 is the best solution from the torsional stiffness point of view. The loss in stiffness is also rather low for the cut solution G2.1. The other two solutions G1 and G3 can be considered in target also if the decrease of the stiffness is quite high. Finally the use of cuts in these latter design has been quite relevant because they have caused a dramatic loss in stiffness for the solution G1.1 and G3.1.

Then two different types of lateral stiffness, which are two other important missions usually taken into consideration during the design of a bonnet, have been calculated. In this case the bonnet has been opened at two different angle and a lateral load (in the Y direction) has been applied on the stricker of the lock and then on the mobile hinge. Also in this case the displacement of the load application points has been measured and then the related stiffness has been calculated. The results of these virtual tests have substantially confirmed those obtained for torsional stiffness, for this reason it is possible to make the same considerations mentioned before.

Table 4
Torsional stiffness results for the different design of the inner structure

Torsional stiffness test	
Solution	Δ stiffness vs reference (%)
G1	-53.1
G2	-21.4
G3	-55.3
G1.1	-82.9
G2.1	-22.7
G3.1	-65.1

At this point of the development, by integration of the results obtained during the pedestrian head impact test and the stiffness results, it has been possible to define the most promising solution to be investigated in more details. This solution is characterized by an external skin of series 6xxx aluminium, with a defined thickness, and an inner structure, with the G3 design, made with short glass fibre reinforced polyamide, with a thickness of 2.5 mm. By comparison of the weight of this solution with that of the reference one, it is put in evidence a very interesting weight reduction of about 30%. Further this last solution has been examined in more details and, in order to get more information, has been compared with another reference solution made by aluminium. Substantially this second reference bonnet has been obtained simply by substituting the steel with aluminium (series 6xxx for the reinforcements and for the skin, series 5xxx for the inner panel) and appropriately increasing the thickness of the metal sheets. The weight reduction obtained with this aluminium solution has been about 45% once again in comparison with the reference steel bonnet. First of all a complete analysis has been performed for the pedestrian impact test by simulating the head impact in the first three impact points considered up to now, in the above described impact conditions. The results of these simulations, in terms of HIC₁₅, are shown in Table 5.

Table 5
HIC₁₅ results for the most promising hybrid solution compared to the reference ones

HIC ₁₅	Impact point		
	C2C	C3D	C4C
Solution			
Reference	1912	1382	946
Aluminium	1876	1723	837
Hybrid	2048	1739	852

Examining the results it is possible to note that the HIC₁₅ values at point C2C are generally not satisfying. This can be explained considering that this point is quite near the perimeter of the bonnet, and in particular near the lamp groups, and for this reason the impact performance are heavily influenced by that near structure. The HIC₁₅ values for the lightweight solutions on point C3D are very close, this is due to the low local stiffness of these solutions, as a consequence during the impact the bonnet has reached and hit the lower crossbeam. Point C4C is the more significant for this performance because its behaviour is influenced only by the structure of the bonnet. In this point with the hybrid solutions there is an important reduction of the HIC₁₅ value. At this stage of the design development, the three different types of stiffness have been studied for these three solutions. The non linear FE software Abaqus ® has been used. The results for this second type of performance substantially has not evidenced particular problems, the decrease of the stiffness is lower than that assessed during the first analysis, but all the values for the hybrid solution bonnet are completely in target.

The functionality of the bonnet has been further evaluated in term of denting resistance. In this test an increasing load is applied on determined points of the bonnet (usually on the front central part, above the lock zone), and the displacements of the load application points are measured. The maximum and residual displacements have to be lower than target values. Substantially with this test the formation of a visible impression on the bonnet surface has to be investigated. The points of application of load are defined with a geometric procedure. Also this analysis has been performed using the Abaqus software. Once again this test has not shown particular problems because all the displacements are well below than the limit target values.

At this point, in order to get a deep exam of the pedestrian safety performance, the three bonnets under evaluation, the new hybrid one and the two reference ones, have been tested on four additional impact points. These points have been chosen choosing the potential most critical points examining the structure of the bonnets and the engine compartment. A complete picture of the results of this last simulation loop, once again in terms of HIC₁₅, is shown in Table 6.

Table 6
HIC₁₅ results for the additional impact points

HIC ₁₅	Impact Point			
Solution	C5	C6	C7	C8
Reference	995	1061	1124	1050
Aluminium	865	1059	979	815
Hybrid	948	1308	1182	792

The results obtained at these additional impact points, substantially have confirmed the trend obtained at the first three considered points. It is possible to conclude that the best solution is the aluminium one because the decrease on the HIC₁₅ values is the highest, once again there is a confirmation that the use of aluminium is the best choice for the bonnet design considering the technical performance. However also the proposed hybrid solution is very interesting, the results obtained for the pedestrian impact test are interesting and also considering the other performance the hybrid bonnet can be considered in target.

Before to conclude the development of the hybrid solution, also some economical considerations has been done. In particular, in this economical analysis the total, the industrial and the variable costs have been calculated. This evaluation has been done by means of cost models developed by Fiat Research Centre. The main results of this activity has put in evidence as the hybrid solution has a cost nearly comparable with the aluminium reference solution, it is also important to say that the analysis has been heavily influenced by the cost of raw materials.

It has been also interesting to examine the trend of these costs as a function of the annual production, but also in this perspective the curves of the hybrid solution and the aluminium one have substantially the same trend although there are some steps due to the substitution of the mould. For this reason for very low production volumes, the hybrid solution results to be cheaper, the opposite effects it has been obtained for very high production volumes.

PERIPHERICAL FRAME BONNET

Before to start with the design of the hybrid solution, some considerations on a peripheral frame bonnet solution has been done, in fact, as it has been put in evidence in the preliminary benchmarking activity, this type of solution can be

considered a state of art. For this reason a simple modification has been made on the FEM model of the reference bonnet by erasing the central part of the inner structure, without changes in material and thickness. This type of bonnet has been tested for the pedestrian head impact, at the three initial considered impact points (C2C, C3D, C4C). This solution has shown excellent results in fact, there is an important reduction of the HIC₁₅ values. Due to the obtained interesting results in the first mentioned analysis, it was decided to examine in more details only the pedestrian safety performance of this bonnet, in particular all the impact points used up to now for the hybrid bonnet have been considered. The design used in this phase has been the same used for the preliminary analysis, it is shown in Figure 10.

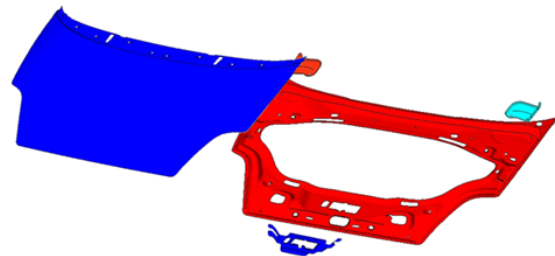


Figure 10. The examined perimeter bonnet.

On this geometry two different bonnets have been prepared, the first one has been made by the same material used for the reference solution, the second one has been an aluminium version, in particular, once again, for the external skin and the reinforcements a 6xxx series alloys has been used, instead for the perimeter inner structure a 5xxx series has been adopted. This choice of materials has been done starting from the information obtained in the preliminary benchmarking activity. When compared to the reference solution made by steel, the weight reduction reached by the perimeter bonnet made by steel has been of about 14%, instead for the perimeter bonnet made in aluminium the weight reduction has been of 46%. A global overview on the obtained results is shown in Table 7.

These results are quite interesting, first of all there has been a global reduction of the HIC values, but it is interesting to note as the use of aluminium, that is very important to obtain the weight reduction, has not led to significant improvements for the pedestrian safety, in fact at some impact points the best performance have been obtained with the steel version. This is substantially due to the higher

deformations obtained with the aluminium bonnet. There is a further confirmation that, in order to obtain the best pedestrian safety performance, it is necessary to start the design with a global approach considering all the design aspects and case by case, because also the near body structure is very important for the global behaviour. It is not possible to define at the beginning an optimum solution.

Table 7
HIC₁₅ results for the perimeter bonnet compared to the previous solutions

HIC ₁₅	Solution				
	Ref.	Al.	Hyb.	<i>Perimeter bonnet in steel</i>	<i>Perimeter bonnet in aluminium</i>
C2C	1912	1876	2048	1637	1429
C3D	1382	1723	1739	918	833
C4C	941	837	852	380	526
C5	995	865	948	575	667
C6	1061	1059	1308	936	1100
C7	1124	979	1182	669	662
C8	1050	815	792	448	475

WIRE CONCEPT BONNET

From the results illustrated up to now, two fundamental aspects can be put in evidence. First of all it is clear that the multi material approach represents one of the best way to obtain excellent results in terms of lightweight and pedestrian safety without loss in others performance. A second important subject is that, to improve the pedestrian safety performance, a inner structure made with a distribute or perimeter design have to be preferred because they absorb better the crash impact energy against the pedestrian head. Starting from these considerations, a further concept of hybrid bonnet has been developed. The main idea for this further hybrid bonnet has been a thermoplastic inner structure made with a perimeter design and with a wire net central part. To better understand this solution it is possible to see Figure 11.

In particular, as it has already been done with the other previous solutions, it was decided to use an external metal panel, to reach the quality requirements, besides the inner structure has been thought in thermoplastic to lightweight the structure. Once again, the material used for the external skin has been the series 6xxx aluminium

and for the inner structure the same polyamide used in the previous part of the wok has been chosen. A first model has been designed. For what concerns the innovative inner structure, the perimeter has been taken by the reference structure, so it has the same shape and geometry, instead for the central wire part, the width of the sticks has been chosen 25 mm and the step between the stick about 100 mm. The thickness of the inner structure has been again 2.5 mm. The hybrid bonnet has been completed with the same reinforcements used in the reference subframe. The joint between the different parts has been thought by structural adhesive bonding. The weight reduction obtained with this first solution has been about 47% which is an excellent value if compared with those obtained in the previous part of this work. This first solution has been submitted to pedestrian impact tests on the same impact points used in the previous part of the work.



Figure 11. The wire hybrid concept bonnet.

The obtained results (summarised in Table 8) have been excellent because there has been an important reduction in the HIC₁₅ value. At this point also the torsional stiffness has been considered, in order to evaluate if the bonnet can be suitable also from the point of view of the static performance. The results for this performance have not been very good in fact the obtained values are too low and very far from the minimum target. At this point a series of modifications have been thought to improve the stiffness of this solution. In particular the influences of the elastic modulus of the adopted plastic material and the thickness of the inner structure have been taken into consideration. However, both these types of modification have not lead to a sufficient increase of the stiffness value, for this reason, the inner structure has been

partially redesigned defining a larger perimeter crown. Once again, the torsional stiffness results obtained after a simulation loop have been too low. To reach the stiffness target, at this point a further modification in the philosophy of the solution has been done. In particular it was decided to make the perimeter crown in aluminium always with a central wire part in thermoplastic. This last change has not influenced the weight reduction that remains about 44%. With these last modifications, the stiffness results obtained from the simulations result to be in target and even better than with the hybrid solution developed in the previous part of the activity. At this point a further simulation loop concerning the pedestrian head impact has been done, in order to evaluate if these last modifications have influenced also this performance. A summary of the obtained results are proposed on Table 8.

Table 8
HIC₁₅ results for the wire bonnet compared to the previous solutions

HIC ₁₅ Impact Point	Solution				
	Reference	Wire first version	Wire	Aluminium	Hybrid
C2C	1912	1722	1766	1876	2048
C3D	1382	884	960	1723	1739
C4C	941	506	565	837	852
C5	995	781	656	865	948

Before to conclude the development of this hybrid solution, also some considerations on the manufacturing technology have been done. In particular the aluminium parts of this last proposed solution, can be made by common stamping technology instead the wire thermoplastic part can be made by different technologies such as injection or compression moulding but also some other possibilities can be taken into consideration. For what concerns the connection between the wire central part and the aluminium crown, some different joining technologies can be used, such as the riveting or the adhesive bonding. The development of this second solution has been stopped at this point, without any economical consideration, in fact the main target of this second part of the work was to investigate the behaviour of this wire concept bonnet. Obtained results have confirmed the first idea. This solution has improved the performance in particular for the pedestrian safety because the central wire part distributes

better the energy of an head impact and can avoid the contact between the deformed inner part of the bonnet and stiff part inside the engine compartment.

CONCLUSIONS

This work has illustrated a global overview on the different solutions which can be adopted for the bonnet of medium/low segment car, in order to reach lightweight and pedestrian safety targets. First of all the development of an hybrid bonnet has been presented. Starting from a benchmarking activity an hybrid concept composed by a thermoplastic inner structure and an outside metal skin has been proposed. During the activity different types of materials for the different parts and some geometries for the inner structure have been evaluated. The final solution has been characterized by an aluminium skin and a short fibre reinforced polyamide inner structure with a specific design. This solution allows a weight reduction of about 30% compared to the reference solution with a further important reduction of the pedestrian head impact evaluated in terms of HIC₁₅. Also the manufacturing and the economical aspects have been taken into consideration during the development.

After that some considerations on the perimeter bonnet solutions have been done, they can be considered an excellent solution for the bonnet to reach the targets of lightweight and reduction of the risks of pedestrian and VRU head injuries. At the end the study on a concept hybrid solution, characterized by an inner structure with a wire design has been illustrated. This last solution can ensure a better distribution of the impact energy between the bonnet and the pedestrian head, with a consequent reduction of the injury risks.

REFERENCES

- [1] U.S. Environmental protection agency office of transportation and air quality. 2005. "Average carbon dioxide emissions resulting from gasoline and diesel fuel." Washington.
- [2] U.S. Environmental protection agency office of transportation and air quality. 2006. "Greenhouse gas emissions from the U.S. transportation sector, 1990 – 2003." Washington.

- [3] Office for official publications of the European Communities. 2008. "EU energy and transport in figures – Statistical pocketbook 2007/2008." Luxembourg.
- [4] Jos Dings. 2008. "Reducing CO₂ emissions from new cars: a study of major car manufacturers, progress in 2007. Brussels." European federation for transport and environment AiSBL.
- [5] L.C. den Boer, A. Schroten. 2007. "Traffic noise reduction in Europe." CE Delft.
- [6] G. Belingardi, M. Avalle. 2004. "Advanced materials for automotive applications." *Mobility and Vehicle Mechanics*, 30 (2), 51-65.
- [7] G. Belingardi, E. Gobetto, A. Scattina. 2007. "Development of a lightweight solution for a front subframe." Proc. of 11th EAEC conf., Budapest.
- [8] F.I.M. Geoff Davies. 2003. "Materials for Automobile Bodies." Elsevier, Oxford.
- [9] Viano D., Von Holst H., Gordon E. 1997 "Serious brain injury from traffic-related causes: priorities for primary prevention", *Accident analysis and prevention*, Vol. 29, pp. 811-816.
- [10] Mizuno Y. 2003 – "Summary of IHRA pedestrian safety WG activities – Proposed test methods to evaluate pedestrian protection afforded by passenger cars", *Proceedings 18th International Technical Conference on the Enhanced Safety of Vehicles*, paper n. 580.
- [11] Yang J. 2005 – "Review of injury biomechanics in car-pedestrian collisions", *Int. Journal of Vehicle Safety*, Vol. 1, No. 1-2-3, pp. 100-117.
- [12] Nishimoto T. 2003 – "Introduction of the regulation of pedestrian head protection in Japan", *Proceedings 18th International Technical Conference on the Enhanced Safety of Vehicles*, paper n. 503.
- [13] Kerkeleing C., Schäfer J., Thompson G.M. 2005 – "Structural hood and hinge concepts for pedestrian protection", *Proceedings 19th International Technical Conference on the Enhanced Safety of Vehicles*, paper n. 05-0304.
- [14] Kwak D.Y., Jeong J.H., Cheon J.S., Im I.T. 1997 – "Optimal design of composite hood with reinforcing ribs through stiffness analysis", *Composites structures*, Vol. 38, No. 1-4, pp. 351-359.
- [15] Fredriksson R., Håland Y. 2001 – "Evaluation of a new pedestrian head injury protection system with a sensor in the bumper and lifting of the hood's rear part", *Proceedings 17th International Technical Conference on the Enhanced Safety of Vehicles*, paper n. 131.
- [16] Stammen J.A., Saul R.A., Ko B. 2001 – "Pedestrian head impact testing and PCDS reconstructions", *Proceedings 17th International Technical Conference on the Enhanced Safety of Vehicles*, paper n. 326.
- [17] Yang J. 2003 – "Pedestrian head protection from car impacts", *Int. J. Vehicle Design*, Vol. 32, No. 1-2, pp. 16-27.

DEVELOPMENT OF THE POP-UP ENGINE HOOD FOR PEDESTRIAN HEAD PROTECTION

Yusuke Inomata
Nobuhiro Iwai
Yoshinori Maeda
Seiichi Kobayashi
Hiroyuki Okuyama
Nobuhiko Takahashi

NISSAN MOTOR CO., LTD.,
Japan
Paper Number 09-0067

ABSTRACT

The “Pop-up Engine Hood” helps makes it possible for automobile designers to help reduce head injury during pedestrian impact while maintaining streamlined hood design.

Some countries have adopted pedestrian protection regulation and there is an on-going discussion in the United Nations WP29 about Global Technical Regulations (gtr) and there is a possibility such regulations may be enhanced in the future.

Many car manufacturers have been planning to improve pedestrian safety by various technical applications. In general, pedestrian head protection is achieved by creating space between the hood (which is deformable) and the engine component (which is not). However, this concept is difficult to apply to some vehicles, especially low engine hood vehicles, such as coupes and sport cars.

The “Pop-up Engine Hood System” which has recently been used in mass production vehicles in Japan may help with this issue.

This paper will describe the system outline and key technologies incorporated in the system e.g.:

- Effectiveness of injury reduction mechanism (evaluated using CAE analysis and tests) when a pedestrian contacts directly above or near the actuator, which lifts up the hood.
- Technique to help reduce the dispersion of head injury due to hood vibration during the hood raising process.
- Human kinematics during system operation evaluated by using Polar-II dummy (currently available as a pedestrian full scale dummy), and human body FE model.

INTRODUCTION

There were 6,639 traffic accident fatalities in Japan in 2007.^[1] The number of fatalities has been on a downward trend for many years, but pedestrian

fatalities now account for more than 30% of the total and are almost equal to vehicle occupant fatalities (Fig. 1). At the result of governmental efforts concerning pedestrian protection, the regulation (e.g. EEC 2003/102) has been adopted in Europe and Japan beginning 2005. The United Nations is also proceeding with the work of developing Global Technical Regulations (gtr). Other countries around the world are also examining the introduction of pedestrian protection regulations.

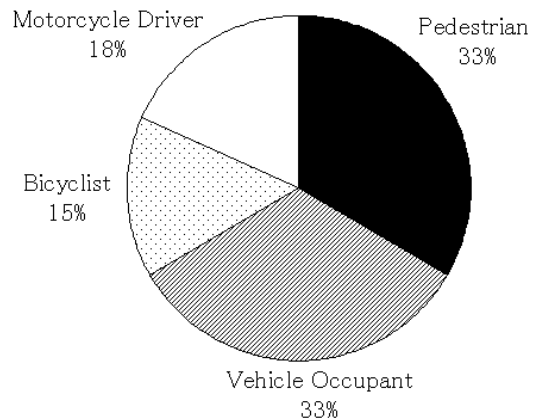


Figure 1. Ratio of traffic accident fatalities in Japan in 2007.

Head injuries are the main cause of pedestrian fatalities.^[2] One factor is the presence of high-stiffness parts such as the engine and battery in the engine compartment. After a pedestrian's head strikes the engine hood in the primary impact, the risk of head injury increases due to a secondary impact with such high-stiffness parts. One general design measure adopted in recent years is to raise the height of the hood so as to secure more buffer space above high-stiffness parts after the primary impact. This measure reduces the risk of head injury because it can help prevent a secondary impact by using the extra space to absorb the kinetic energy of a pedestrian's

head.

However, it is difficult to apply to some vehicles, especially low engine hood vehicles, such as coupes and sport cars. The pop-up engine hood presented here has been developed to help resolve this issue by immediately raising the rear of the hood approximately 100 mm upon detection of a collision with a pedestrian. This pop-up engine hood has recently been installed on a production vehicle having limited space under the hood.

This paper explain the system configuration and the newly developed techniques.^[3] It especially describes the energy absorbing mechanism of the actuators, the method used to reduce the dispersion of head injury due to hood vibration, and the results of tests conducted with a pedestrian dummy and using human body FE model to verify the operation of the system.

Pop-up Engine Hood System

This section describes the basic structure and mechanisms of the pop-up engine hood system. As illustrated in Fig. 2, the system consists of the following three basic components.

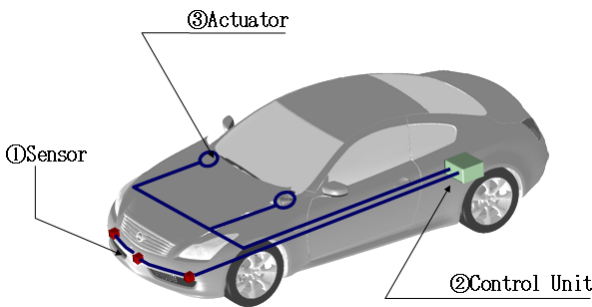


Figure 2. System overview.

- (1) Sensors : Detect a collision between the vehicle and a pedestrian.
 - (2) Control unit : Judge the necessity of raising the hood.
 - (3) Actuators : Raise the rear of the hood.
- The function of each component is explained in detail below.

Sensors - Three sensors for detecting a collision with a pedestrian are installed behind the front bumper fascia as shown in Fig. 3. This structure was adopted because the front bumper is usually the first part to come in contact with a pedestrian's body in a collision with a vehicle.^[4] The sensors are positioned on the right and left sides and in the center. The sensors function to detect a change in acceleration and have experience of use as the airbag sensors. These devices detect the movement of the bumper fascia caused by contact with a pedestrian's legs.

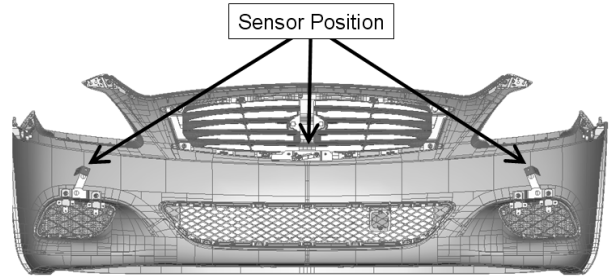


Figure 3. Sensor for pedestrian detection.

Control Unit - The flowchart in Fig. 4 shows the sequence of events involved in the judgment made by the control unit. The control unit judges the necessity of raising the hood based on the detection signals from the three sensors and also the vehicle velocity at the time of a collision. The use of this judgment logic achieves reliable system deployment in the vehicle velocity range where it is necessary to raise the hood.

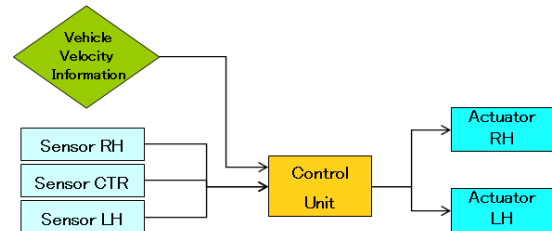


Figure 4. Flow chart of sensor.

Actuators - The actuators that provide the driving force for raising the rear of the hood are constructed with an extendable cylinder operated by pyrotechnics. As shown in Fig. 5, the length of the three-stage cylinder before operation is less than one-half of its extended size.

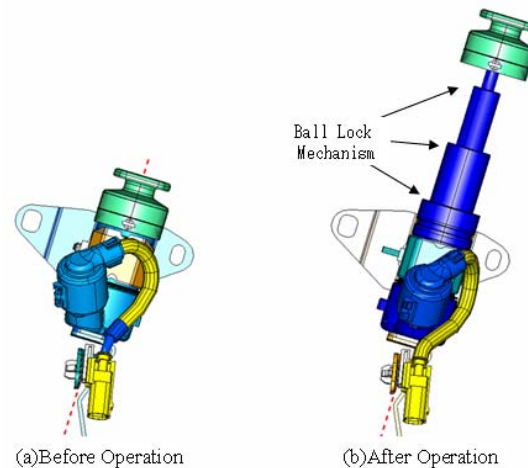


Figure 5. Actuator.

Figure 6 shows the relationship between the operation of the actuators and the hood hinges for opening/closing the hood. Normally, the hood opens or closes by rotating upward or downward centered on the hood hinges (Fig. 6 (a) and (b)). In contrast, when the pop-up system is deployed, the rear of the hood is raised centered on the hood lock at the front of the vehicle (Fig. 6 (c)).

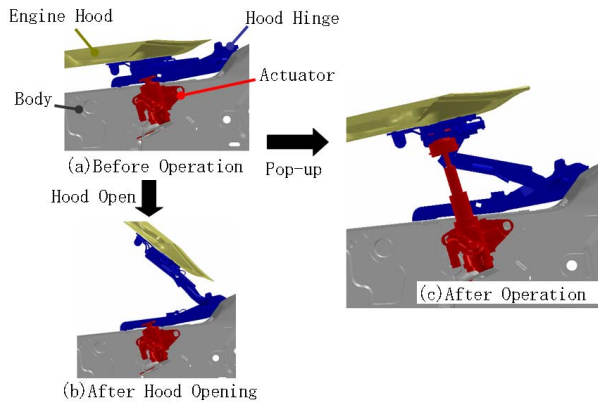


Figure 6. Operation of hinge and actuator.

A detailed diagram of the hood hinge mechanism is shown in Fig. 7. During normal opening or closing of the hood, the lock lever fixes link (a) and link (b), allowing only link (a) to rotate. When the pop-up hood system is deployed, the actuator head presses on the lock lever, allowing link (b) to rotate. The actuator cylinder extends to raise the rear of the hood, with the hood lock serving as the fulcrum of the hood's upward rotation. As a result of these operations, the rear of the hood is raised by approximately 100 mm to secure buffer space between the hood and the high-stiffness parts beneath it.

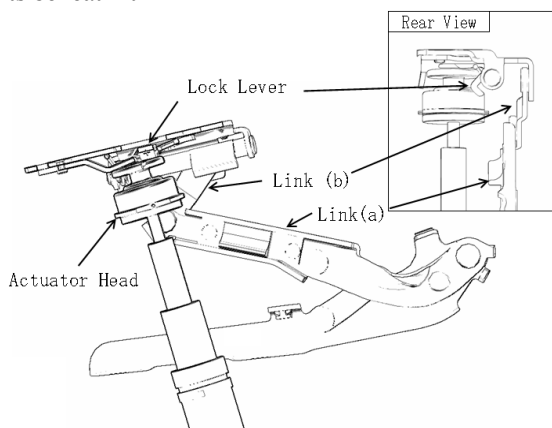


Figure 7. Pop-up mechanism of hood hinge.

Following the extension of the actuators, the rear of the hood is supported on each side by a ball lock mechanism built into the cylinders to prevent them from returning to their original state (Fig. 5). In the

event of a collision with a pedestrian, primarily this mechanism enables the actuator cylinders to support the rear of the hood. The system is constructed such that in certain impacts the pedestrian's kinetic energy is absorbed by the primary impact and a secondary impact with the engine compartment components is avoided. Secondly the ball lock mechanism also has a collapsible structure that allows the cylinders to retract again if force above a certain threshold is applied. This helps to reduce the risk of injury in the event a pedestrian collides with the hood directly above or near the actuators.

Collapsible Mechanism of Actuators - This section presents an example of numerical simulations^{[5], [6]} that were conducted to validate the effectiveness of the collapsible mechanism of the actuators. These simulations were performed with the PAM-CRASH software using a headform impactor.

Figure 8 shows acceleration histories of the headform impactor when it struck the hood surface near one of the actuators. The impactor acceleration is indicated along the vertical axis in relation to its displacement along the horizontal axis. The solid line is for a pop-up hood system with collapsible actuators and the dashed line is for a system with rigid actuators. The waveform for the system without the collapsible mechanism indicates that, following the initial peak for the primary impact with the hood surface, the secondary impact with the actuator produced a relatively large acceleration peak. In contrast, the waveform for the system with the collapsible mechanism indicates that the actuators initially supported the rear of the hood until the preset load was reached, after which the collapsible mechanism worked to avoid another increase in impactor acceleration. As a result, the system with the collapsible mechanism kept the subsequent impactor acceleration below that of the level of the primary impact with the hood, thereby verifying the effectiveness of this mechanism.

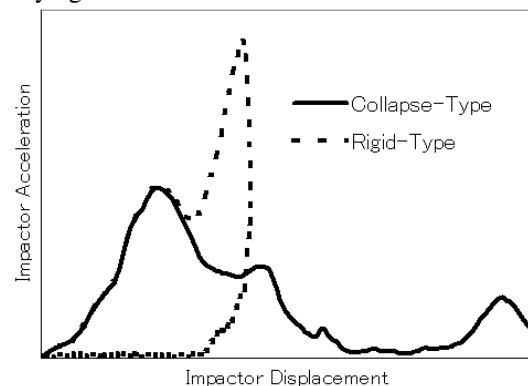


Figure 8. Example of acceleration history of headform impactor.

System Deployment

Targeted System Deployment Time - On a time line of a vehicle-to-pedestrian collision, the earliest event is when the bumper strikes the pedestrian's legs and the final event is when the head strikes the hood. This time interval from bumper contact with the legs to the head's striking the hood is called the head impact time (HIT). The deployment criteria is to have complete deployment of the pop-up hood system sufficiently earlier than HIT.

In developing this system, HIT was calculated by conducting simulations using a pedestrian model, an approach shown to be suitable on the basis of the research done by Ishikawa, H., et al.^[7] HIT is mainly influenced by the front-end geometry of a vehicle and a pedestrian's physique. Accordingly, simulations were conducted using pedestrian models with different physiques to calculate HIT values for vehicle front-end geometry considered (Fig. 9).

A specific example is presented here to explain the procedure for calculating the targeted time for completion of pop-up hood deployment. For the vehicle front-end geometry considered here, HIT of a 50th percentile adult male is assumed to be 1.0. Accordingly, HIT of the 5th percentile adult female is 0.67 and that of the 6 years old child is 0.38. This smallest HIT value for the 6 years old child was adopted as the targeted completion time for system deployment.

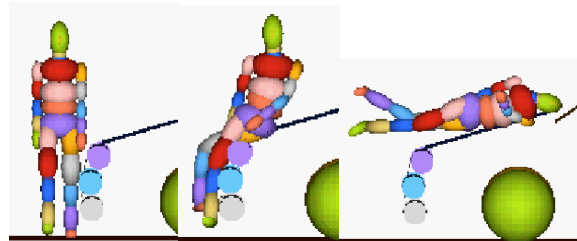


Figure 9. Example of car to pedestrian dummy collision simulation.

Validation of System Deployment Completion

Time - In order to validate that the pop-up engine hood system could be deployed before the targeted system deployment completion time explained in the preceding section, tests were conducted with impactors that simulated the mass of pedestrians. Figure 10 shows an example of the displacement history of the pop-up hood, where the amount of hood displacement near the actuators is shown along the vertical axis in relation to elapsed time along the horizontal axis. The results indicate that the hood was raised the specified amount with sufficient time to spare in relation to the targeted deployment time from the moment of the impactor contact with the front bumper.

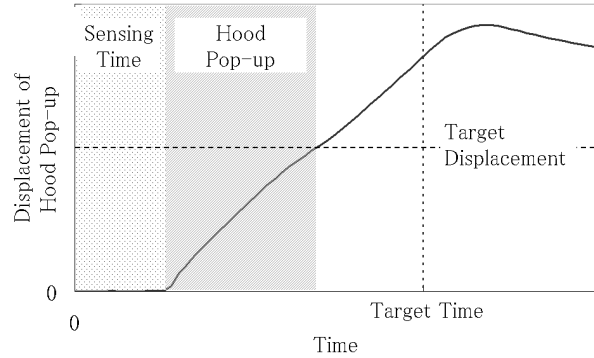


Figure 10. Example of displacement history of pop-up.

Dynamic Hood Behavior and Its Stabilization

Numerical simulations^{[5], [6]} were conducted with a headform impact to analyze the dynamic behavior of the hood in this system. The analysis results revealed that the dispersion of head injury values was due to vibration at the center of the hood. This section presents an example of a mechanism that was developed to reduce this dispersion.

Method of Evaluating Head Protection Performance

- The headform impactor was projected against the hood and other areas of the vehicle front-end to investigate head protection performance, which was evaluated using the head injury criterion (HIC) as defined in Eq. (1) below.

$$HIC = \left((t_2 - t_1) \left[\frac{\int_{t_1}^{t_2} A dt}{t_2 - t_1} \right]^{2.5} \right)_{MAX} \quad (1).$$

where $t_2 - t_1 \leq 15\text{msec}$

Where A is the acceleration of the headform impactor and t_1 and t_2 are the initial and final times. In order to reduce the HIC, the mean acceleration should be low and there should not be any pronounced acceleration peak.

Effect of Raising the Hood on Reducing HIC

- Figure 11 shows an example of the effect of the pop-up hood on improving the acceleration history of the headform impactor when the system was installed on a vehicle with little available space underneath the hood. The vertical axis shows the impactor acceleration and the horizontal axis indicates the impactor displacement in terms of the amount of indentation made in the hood. The dashed line is for an ordinary hood without the pop-up system. The first peak was produced by the reaction force from the hood due to the primary impact. The large peak observed after that is attributed to the secondary impact of the hood with a high-stiffness component in the engine compartment. In contrast, the solid line for the pop-up hood system

indicates that a secondary impact was avoided or reduced by raising the rear of the hood to secure sufficient space for absorbing the primary impact energy. As a result, the HIC calculated with Eq. (1) is reduced.

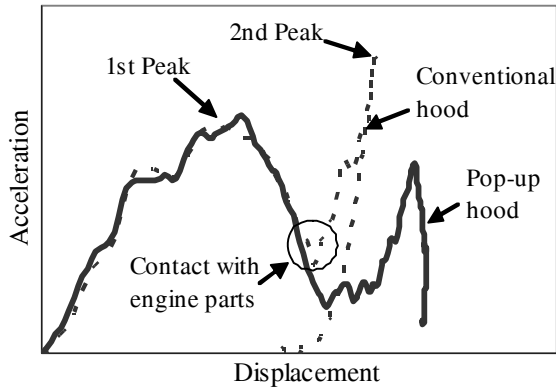


Figure 11. Example of acceleration history of headform impactor.

The Dispersion of HIC Value due to Dynamic Hood Behavior - The boldface solid line in Fig. 12 is for the dynamic behavior of the hood when it was raised. The vertical axis indicates the displacement of the hood outer panel at a representative point in the center of the hood in relation to time along the horizontal axis. As indicated in the rectangular area enclosed in the dashed line, the hood vibrated after initially reaching its maximum displacement and its behavior was not stable. This vibration was presumably induced by the force applied to the hood when the actuator cylinders were extended.

The dashed line in Fig. 12 shows a displacement history when the headform impactor struck the hood at time (a) of the hood displacement. The thin line and the solid line show displacement histories for impacts at time (b) and time (c) of the hood displacement, respectively. The impact at time (a) occurred after the hood began its downward vibration, so the displacement following the impact was greater and would require larger space for absorbing the impact energy. The impact at time (b) occurred at approximately the moment the downward vibration was completed, so the displacement was smaller. The impact at time (c) occurred during the upward vibration of the hood, so the displacement was even smaller.

Because the relative velocity between the headform impactor and the hood at the time of impact became larger in the order of (a) < (b) < (c), the reaction force toward the impactor also became larger in the same order. As a result, the HIC ratio of (a), (b) and (c) was 0.83:1.11:1.34 (i.e., the ratio nondimensionalized by the HIC value in a static hood state), which indicated HIC variation due to the time of impact. Therefore, the

method explained in the following section was developed to resolve this variation.

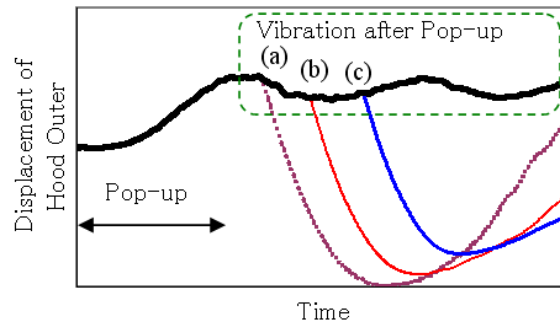


Figure 12. Time history of displacement of impact point of hood (initial design).

Outline of Structure for Reducing HIC Variation - Assuming that the above-mentioned HIC variation was ascribable to the time of impact, the principal reason for that variation was thought to be the fluctuation of the relative velocity of the impactor and the hood due to hood vibration. Accordingly, it was reasoned that the HIC variation could be reduced by mitigating the hood vibration. Therefore, this question was simplified by assuming that the vibration induced by raising the hood could be represented as a sine wave as indicated by the dashed line in Fig. 13. Then, by inducing a vibration (thin solid line) having the opposite phase at the time of phase 2π , it would produce a superimposed wave (boldface solid line) for canceling the initial vibration.

Figure 14 shows an example of a specific structure for inducing the opposite phase vibration. If the rate of actuator extension is known, the relationship between time and the amount of actuator extension can be uniquely determined. Accordingly, the amount of hood hinge opening corresponding to the time (one cycle) when the vibration induced by popping up the hood becomes 2π can also be uniquely determined. A stopper is provided at that position, as shown in the figure. The deceleration produced by the action of the stopper generates a force input in the opposite direction of the input induced by the operation of the actuators. The application of that force to the hood at the time of phase 2π cancels out the vibration excited by raising the hood.

The effect of this structure is shown in Fig. 15. Compared with the results in Fig. 12, the boldface solid line shows stable dynamic behavior at the time the hood is raised. The dashed line, thin line and solid line in Fig. 15 show the displacement history when the headform impactor struck the hood at impact times of (a), (b) and (c), respectively. The results indicate that the difference in displacement histories due to the

method explained in the following section was developed to resolve this variation.

impact time has been reduced. That resulted in a HIC ratio in this example of 1.05:0.97:1.01, indicating that the variation in head injury values was also reduced. The proposed structure is effective if the onset of deceleration occurs near the vibration phase 2π . The time when the vibration phase is 2π is determined almost entirely by the natural vibration frequency of the hood. Therefore, this structure can stably reduce hood vibration under various real-world conditions.

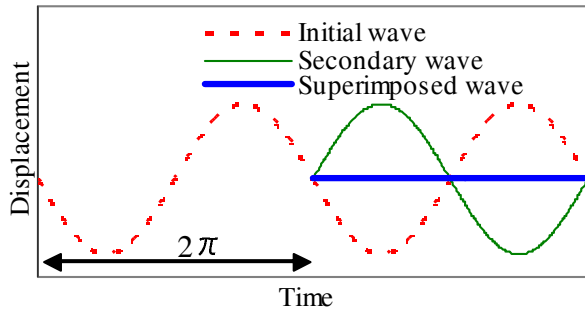


Figure 13. Cancellation of vibration by superposition.

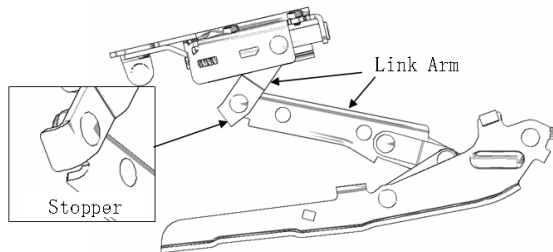


Figure 14. Example of hood hinge structure.

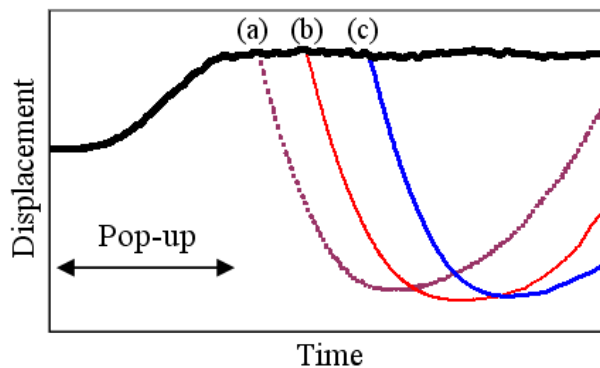


Figure 15. Time history of displacement of impact point of hood (robust design).

System Validation Using a Pedestrian Dummy

This section describes an example of the validation of the operation of the pop-up engine hood system using a Polar-II pedestrian dummy.^{[8],[9]}

Test Conditions - The validation example described here is for a vehicle impact speed of 35 km/h. As shown in Fig. 16, the dummy was set in a walking pedestrian stance (WP2) as defined in IHRA/PS 215. The dummy was positioned such that the center of its head was at the centerline of the vehicle laterally.



Figure 16. Dummy setting.

Validation of System Operation - Figure 17 shows the dummy's behavior at the time deployment of the actuators was completed. The dummy's upper body has not moved clearly from its initial condition. It is clear that the deployment of the pop-up hood was completed sufficiently in advance of the subsequent impact of the dummy's head against the hood.

The dummy's behavior at the moment of shoulder contact with the hood is shown in Fig. 18. At this time, the extended actuators were holding the hood at a higher position above the engine compartment components. It is clear that the system secured the necessary buffer space for absorbing the head's impact energy.

This test verified that the series of operations explained in the previous section were completed according to the intention of the system design, even under these conditions of an actual car-to-pedestrian accident.



Figure 17. Dummy behavior after actuator operation.



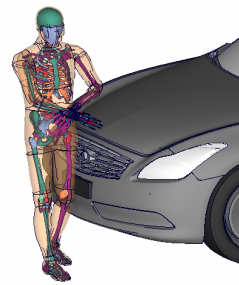
Figure 18. Dummy behavior before head contact.

Validation of System Deployment by Using Human Body FE Model

This section describes an example of validation of the system operation and confirmation of the effect on potential injury by using human body FE model. This human body FE model⁽¹⁰⁾ is based on the model that is developed by Japan Automobile Manufacturers Association (JAMA). Joint development by Japanese car manufacturers recently started because the human body FE model can be used by all car manufacturers. In Japan, JAMA coordinates Japan Automobile Research Institute (JARI) and domestic car manufacturers will work jointly to develop the future human body FE model.

The application the human body FE model to evaluate the pop-up engine hood system that is mounted on the coupe style vehicle is presented here. The numerical simulation introduced here is for the final validation of the system operation in more practical condition.

Fig. 19 shows an outline of the simulation. The representative parameter is “with” or “without” pop-up engine hood system in this simulation.



Vehicle Model	
Impact V	40 km/h
Human Body Model	
Height ⁺	172 cm
Weight	71.9 kg
# of Nodes	66,249
# of Elems.	95,304
⁺ in a walking posture	

Figure 19. Simulation model setup of pedestrian collision with vehicle with Pop-up engine hood.

As a representative simulation example in more practical condition, the vehicle speed is set to 40km/h. The relation between pedestrian behavior and hood pop-up is validated. Fig. 20 shows behavior of human body FE model. This example shows that it is clear that the deployment of the pop-up engine hood was completed sufficiently in advance of the subsequent impact of the head against the hood.

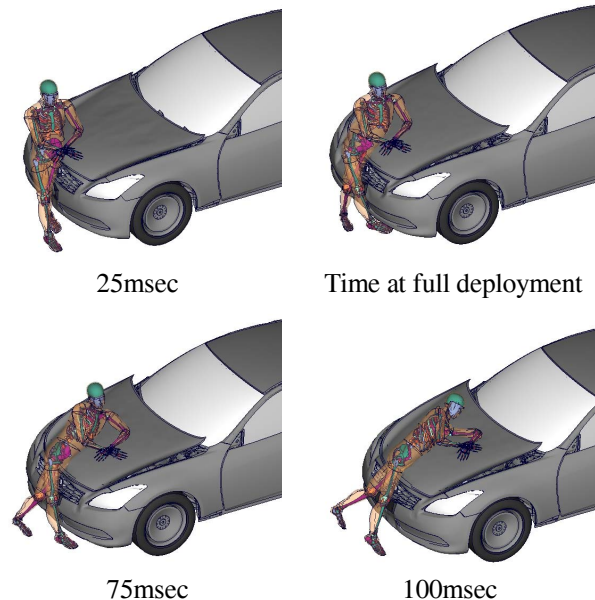


Figure 20. A simulation (FEM) result of pedestrian collision with Pop-up engine hood.

Fig. 21 shows the head contact behavior after the full deployment. At this time, the extended actuators were holding the hood at a higher position above the engine compartment components. It is clear that the system secured the necessary buffer space for absorbing the head's impact energy.

The simulation result of the pedestrian behavior by using human body FE model is described under the condition showing in Fig. 19. Additionally, this

simulation result shows that the pop-up engine hood system did not cause the specific concentration of stress on human body. The result presented here by using human body FE model is validated under limited conditions.

So, additional improvement is needed to allow more predictive injury analysis. It is necessary to note that it is not presented that the head injury of the pedestrian can be completely predicted.

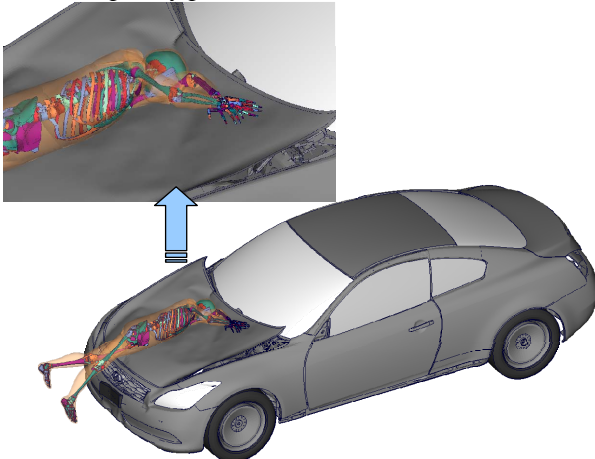


Figure 21. Close-up of pedestrian collision with Pop-up engine hood in FEM.

CONCLUSIONS

This paper has described a pop-up engine hood system that has been developed and applied to a production vehicle to improve pedestrian head protection performance while maintaining a sporty, streamlined styling. An outline of the system was presented along with an explanation of its functionality, focusing in particular on the following points.

- The results of numerical simulations conducted with a headform impactor were presented to show the effect of the collapsible actuator structure on mitigating the secondary impact of a pedestrian's head.

- Raising the rear of the hood initially caused it to vibrate at its center, resulting in dispersion of HIC values. A method was developing for reducing that dispersion, and its effectiveness was verified by the results of numerical simulations.

- Human kinematics during the system operation in the pedestrian accident by using Polar-II dummy which is currently available as pedestrian full scale dummy, and human body FE model. The results verified that the pop-up engine hood system operated as it was designed to.

REFERENCES

- [1] National Police Agency, "Traffic Accident Fatalities within 30 Days of the Accident in Fiscal 2007," <http://www.npa.go.jp/toukei/#koutsuu>, 2008 (in Japanese).
- [2] Institute for Traffic Accident Research and Data Analysis, *2000 Annual Report on Traffic Accident Statistics* (in Japanese).
- [3] Inomata, Y., et al., "Development of the Pop-up Engine Hood for Pedestrian Protection," *Nissan Technical Review*, No. 63, 2008 (in Japanese).
- [4] Ishikawa, H., "Pedestrian Behavior and Protection in Collisions with Vehicles," *Journal of the Society of Biomechanisms Japan*, Vol. 27, 128-133, 2003 (in Japanese).
- [5] Iwai, N.: "Computational Simulation for Head Impact on Vehicle Hoods Using the Precise Finite Element Model", 18th ESV Conference, 2003.
- [6] Iwai, N., "Numerical Simulation of Vehicle Body Structures for Pedestrian Head Protection, *Lecture Series Abstracts of The Japan Society for Computational Engineering and Science*, Vol. 8, No. 1, 187-190, 2003 (in Japanese).
- [7] Ishikawa, H., et al. : "Computer Simulation of impact Response of the Human Body in Car Pedestrian Accidents." SAE Paper No. 933129, 1993
- [8] Akiyama, A., et al. : "Development and Application of the New Pedestrian Dummy." 17th ESV Conference, 2001
- [9] Jason, R. Kerrigan, et al. : "Kinematic Corridors for PMHS tested in Full-Scale Pedestrian Impact Tests." 19th ESV Conference, 2005
- [10] Sugimoto, T., et al.; "First Results from the JAMA Human Body Model Project", 19th International Technical Conference on the Enhanced Safety of Vehicles, Paper Number 05-0291, (2005-6).

EFFECT OF MUSCLE CONTRACTION IN LOW SPEED CAR-PEDESTRIAN IMPACT – SIMULATIONS FOR WALKING POSTURE

Anurag Soni

Anoop Chawla

Sudipto Mukherjee

Department of Mechanical Engineering
Indian Institute of Technology Delhi, India

Rajesh Malhotra

Department of Orthopaedics,
All India Institute of Medical Sciences, Delhi, 110016 India
Paper Number 09-0366

ABSTRACT

This paper investigates the effect of muscle contraction on lower extremity injuries in low-speed car-pedestrian lateral impacts for a walking pedestrian. The full body model, PMALE, which was configured in symmetric standing posture, has been repositioned in the walking posture. FE simulations have then been performed for its impact with the front structures of a car. Two impact configurations, i.e. impact on the right and on the left leg have been simulated. Two pre-impact conditions, that of a symmetrically standing pedestrian, representing a cadaver and an unaware pedestrian have been simulated for both the impact configurations. Stretch based reflex action was modeled for the unaware pedestrian. It is concluded that (1) with muscle contraction, risk of ligament failure decreases whereas risk of bone fracture increases (2) in lateral impacts, MCL could be considered as the most vulnerable and LCL as the safest ligament and (3) for a walking pedestrian, PCL would be at a higher risk in case of impact on rear leg whereas, in case of impact on front leg, ACL would fail.

Keywords: PMALE, Lower extremity model, Finite element model, Dynamic simulation, Muscle

contraction, Standing posture, Walking posture, Car-pedestrian impact, Knee injury

INTRODUCTION

Pedestrians constitute 65% of the 1.17 million people killed annually in road traffic accidents worldwide (World Bank 2001). Epidemiological studies on pedestrian victims have indicated that after the head, the lower extremities are the most frequently injured body region (Chidester et al. 2001; Mizuno 2003). Pedestrian Crash Data Study (PCDS) (Chidester et al. 2001) reports that passenger cars have the biggest share in vehicle-pedestrian accidents. Further, the front bumper was the major source of injury to the lower extremity when injuries were caused by a vehicle structure (Mizuno 2003). This has posed a challenge for vehicle designers to design pedestrian friendly car front structures. To devise effective pedestrian protection systems, it is essential to understand the injury mechanism.

So far, lower limb injury mechanism in car-pedestrian crashes have been studied through tests on human cadaver specimens (Kajzer et al. 1990, 1993, 1997, 1999; Bhalla et al. 2005) and simulations using validated passive FE models (Schuster et al. 2000; Maeno et al. 2001; Takahashi et al. 2001; Nagasaka et al. 2003; Chawla et al.

2004; Soni et al. 2007). However, the major shortcoming in these experimental and computational studies was that they did not account for reflex muscle action. Therefore, effects of pre-crash muscle contraction on the response of lower limbs in car-pedestrian crashes remained unclear.

Of late, Soni et al. (2007) have investigated the probable outcome of muscle contraction using a lower limb (single leg) FE model with active muscles (A-LEMS). More recently, Soni et al. (2008) have extended the single leg model A-LEMS to a full body Pedestrian Model with Active Lower Extremities (PMALE) and studied the effects of muscle contraction on the response of lower extremity for a symmetrically standing pedestrian (with legs in side by side stance) in full scale car-pedestrian impact. They concluded that with muscle contraction the risk of knee ligament failure is likely to be lower than that predicted through the cadaver tests or simulations with the passive FE models. However, Pedestrian Crash Data Study (PCDS) (Chidester et al. 2001) reported that prior to the crash, only 4% pedestrians were found standing stationary whereas, a majority, i.e. 55%, was walking.

The present study extends our earlier studies to investigate the effect of muscle contraction on the response of lower limb for the walking pedestrian in low speed car-pedestrian lateral impact using FE simulations. The PMALE, which was configured in standing posture, has been repositioned in walking posture in the current study. The real world car-pedestrian lateral impact has been simulated using the PMALE configured in the walking posture and front structures of a validated car FE model. Two impact configurations, i.e. impact on right and on left leg have been simulated. This is to account for the equal chances of impact on either leg of a walking pedestrian in real world crashes. Two sets of simulations, i.e. with deactivated muscles

(cadaveric) and with activated muscles (including reflex action), mimicking an unaware walking pedestrian have been performed for both the impact configurations. Strains in knee ligaments and VonMises stresses in bones for two levels of muscle activation have been compared to assess the effect of muscle contraction.

METHODS

PMALE in Walking Posture

In the present study, PMALE (Soni et al. 2008), which was configured in symmetrically standing posture of a pedestrian with legs in side by side stance, has been adopted as the base model. Body segments of the PMALE configured in the standing posture have then been repositioned in the walking posture in the current study. Relative angles between the body segments required to define the alignment of the walking posture (Table 1) are taken from Mizuno et al. (2003).

Table 1 Definition angles for pedestrian walking posture (Mizuno et al. (2003))

	Definition Angle	
	Left Leg	Right Leg
BA (deg)	+5	
SA (deg)	-15	+15
EA (deg)	0	+27
HA (deg)	+29	-12
KA (deg)	-14	-10
FA (deg)	0	+22

A series of FE simulations have then been performed with the PMALE in standing posture to reposition its body segments in the walking posture. Figure 1 shows the PMALE in walking posture (referred as PMALE-WP) obtained after the repositioning process. In PMALE-WP, right leg (positioned in rear) corresponds to the terminal stance phase of the human gait cycle whereas; left leg (positioned in front) corresponds to heel strike

phase. Upper body is leaned forward by 5 degrees with the vertical axis.

Simulation Setup

Figure 2 shows the simulation setup used in the present study. Here, the real world car-pedestrian impact has been reproduced using the PMALE-WP and front structures of a validated car FE model. PMALE-WP represents a pedestrian walking on rigid ground in gravity field. The coefficient of friction between shoe and ground is set to 1.0 as suggested for grooved rubber on road (Li K.W. et al. 2006). Car model with a total mass of 1158 kg (mass of the front structures is 355 kg and 803 kg is

modeled as added mass to account for the remaining car structures) is propelled with a speed of 25 kmph towards the PMALE-WP. Since in real world car-pedestrian crashes, a car may hit any one of the two legs of a pedestrian; therefore, to account this variability, two impact configurations, i.e. impacting the right leg (Figure 1 (a)) and the left leg (Figure 1 (b)) on the lateral side, have been simulated. In both the impact configurations, the PMALE-WP is placed in front of the car model such that it interacts with mid portion of the bumper whereas; the car model is positioned at a height above the ground such that it corresponds to the car rolling on its tyres.

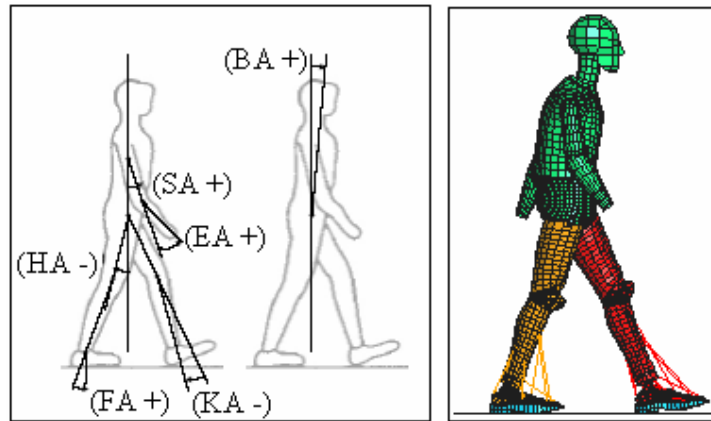


Figure 1 (a) Definition angles with sign conventions for pedestrian walking posture (Mizuno et al. 2003) and (b) PMALE in walking posture (i.e. PMALE-WP)

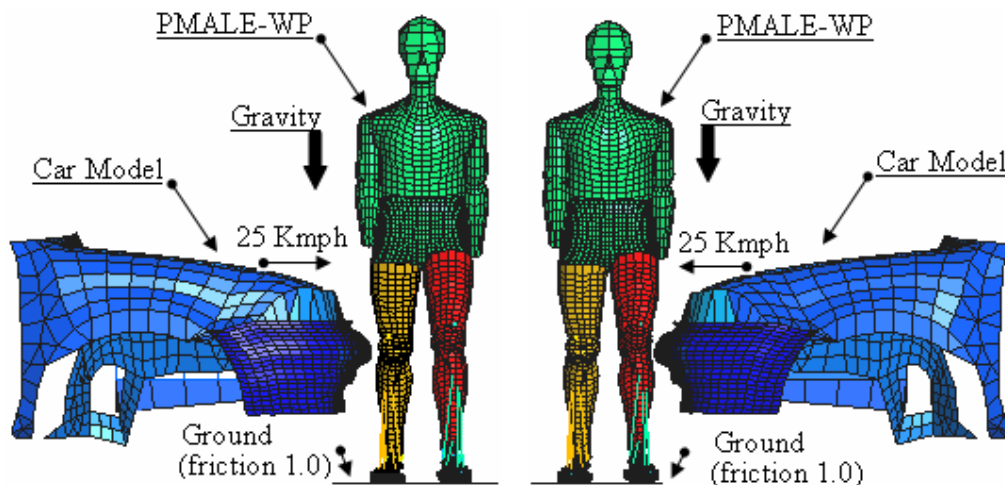


Figure 2 Simulation set up used in the present study for (a) impact on right leg and (b) impact on left leg

Pedestrian Pre-Impact Conditions

Two pre-impact pedestrian conditions, i.e., one with deactivated muscles (cadaveric) and the other with activated muscles (including reflex action) for an unaware pedestrian have been simulated for both the impact configurations in the present study. We call these conditions cadaveric and reflex conditions respectively. These conditions differ in terms of initial activation levels in muscles and whether the reflex action is enabled. By enabling the reflex action for a muscle, the activation level in that muscle rises with time during the simulation; thereby increasing the force produced by that muscle.

Cadaveric Condition - In this condition, a cadaver aligned in walking posture has been simulated. To model a cadaver in FE simulation, all the muscles in PMALE-WP have been assigned the minimum value of 0.005 as the initial activation level. The reflex action is disabled. As a result, in this condition, activation levels in each muscle remain at the minimum value (i.e. 0.005) for the entire duration of the simulation. Therefore, all the muscles function at their minimum capacity.

Reflex Condition - In this condition, a pedestrian who is walking on road and is unaware of an impending crash has been simulated. Here, we have considered that prior to the impact, pedestrian's right leg (in rear) is in terminal stance phase (i.e. right heel is about to leave the ground) of the human gait cycle and left leg (in front) is in heel strike phase (i.e. left heel is just landed on the ground). To model an unaware pedestrian in such walking posture, right leg muscles have been assigned the activation levels corresponding to the terminal stance i.e. 60% gait whereas, muscles in the left leg have been assigned the activation levels corresponding to heel strike i.e. 0% gait. Values of these muscle activation levels (Table A1 in

Appendix A) have been taken from the electromyography (EMG) levels recorded in human subjects during the gait cycle by Winter (1987).

A stretch based involuntary reflex action has also been enabled in this condition. For enabling the reflex, a threshold value of elongation is to be defined in Hill material card of a muscle. When the elongation in muscle crosses the threshold value, stretch reflex in a muscle gets activated. However, the increase in muscle force starts only after a certain time known as reflex time. This delay between the activation of stretch reflex and the onset of increase in muscle force represents the time taken by the signal to travel through the central nervous system (CNS) circuitry (muscle-spinal cord-muscle). A delay of 20 ms has been assigned to all the muscles in PMALE-WP (Ackerman 2002). This mimics the ability of live muscle to respond to a small stretch produced by an outside agency. In medical terms, this kind of reflex action is known as "stretch reflex" (Vander et al. 1981).

Data Analysis

Element elimination approach has been enabled to simulate the failure in the ligaments and the bones. Strain time history of each knee ligament and VonMises stress contours in bones of the impacted leg of the PMALE-WP have been recorded from the simulations. Response in cadaveric and reflex conditions has then been compared to determine the role of muscle contraction.

RESULTS AND DISCUSSION

In all, four simulations, each of 100 ms duration, have been performed in the present study. For the first 50 ms (stabilization duration), PMALE-WP has been stabilized under gravity load in each simulation. At the end of first 50 ms, car front impacts the right leg or the left leg of the stabilized PMALE-WP. Ligament strains and VonMises

stresses in bones have been recorded from the simulations to assess the effect of muscle contraction. Results presented here are for the impact duration and the initial time (i.e. 0 ms) corresponds to the time of contact.

Impact on Right Leg

In this section we present the results obtained from the simulations of impact on right leg in both cadaveric and reflex conditions.

Strain in Knee Ligaments - Figure 3 illustrates the calculated strain time history in knee ligaments of the right leg of PMALE-WP for both cadaveric and reflex conditions. It is apparent that strains in knee ligaments have reduced significantly in the reflex conditions as compared to the cadaveric condition.

ACL: Figure 3 (a) compares the strain time history in ACL for both the conditions. It is

observed that upto 30 ms, ACL remained nearly unstrained in both the conditions. At about 30 ms, strain in ACL has kicked-in and then increased for the remaining portion of the simulations in both the conditions. However, active muscle forces in the reflex condition (peak strain 2.96%) have significantly reduced the strain in ACL as compared to the cadaveric condition (peak strain 4.37%).

PCL: Strain time history in PCL is compared for both the conditions in Figure 3 (b). It is observed that upto 28 ms, PCL is strained equally (approx. 3.5%) in both the conditions. However, after 30 ms, strain in PCL has suddenly increased in the cadaveric condition and reached to the peak value of 13.1% at around 45 ms. Whereas, in the reflex condition, active muscle forces have shared the load and hence reduced the strain in PCL (peak strain reached only up to 8% at 50 ms).

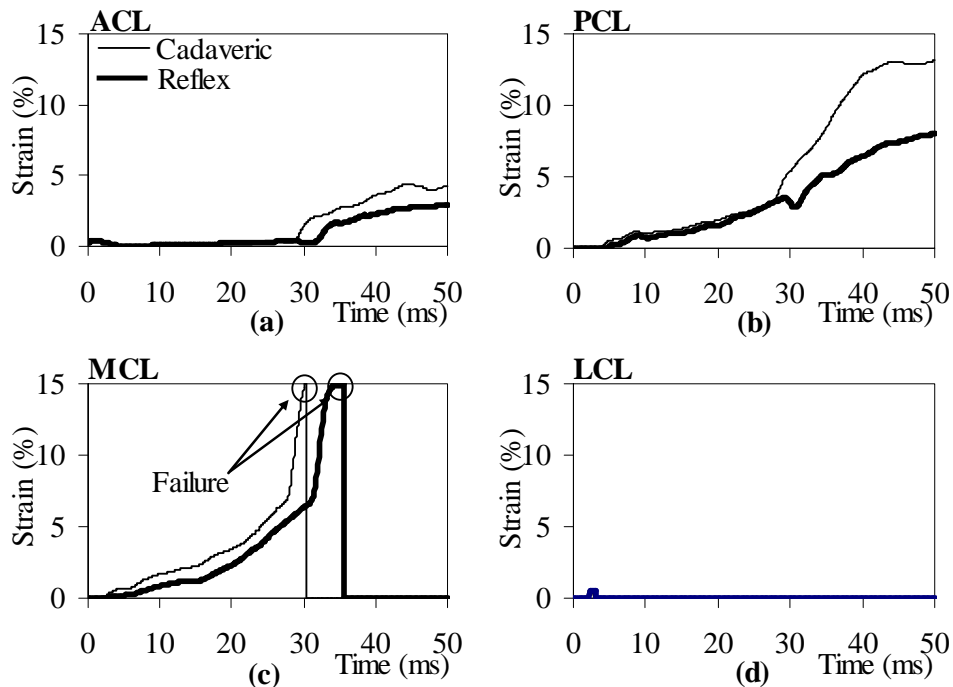


Figure 3 Comparison of strain time history in knee ligaments (a) ACL (b) PCL (c) MCL and (d) LCL of the right leg

MCL: MCL strain for both the conditions is shown in Figure 3 (c). It is observed that peak MCL strain

has reached the ligament failure limit of 15% in both the conditions. However, in comparison to the

cadaveric condition (30 ms), failure is delayed by 5 ms in the reflex condition (35 ms). Effect of rupture of MCL is reflected as a sudden increase in strain in ACL (Figure 3(a)) and PCL (Figure 3(b)) around 30 ms in both cadaveric and the reflex conditions.

LCL: It is observed that LCL (Figure 3 (d)) has remained unstrained in both the conditions. This can be ascribed to the lateral impact which forces tibia to bend medially and consequently keeps the LCL slackened.

VonMises Stresses in Bones - Figure 4 compares the VonMises stress distribution in the bones (i.e. femur, tibia and fibula) of the right leg at 34 ms in both cadaveric and reflex condition. It is apparent that stresses in bones have increased significantly in the reflex condition as compared to the cadaveric condition.

It is observed that in the reflex condition, stresses in the bones have reached up to 124 MPa at the lateral femoral condylar region and 118 MPa at the medial side of mid tibia whereas; it has reached only up to 104 MPa in the cadaveric condition.

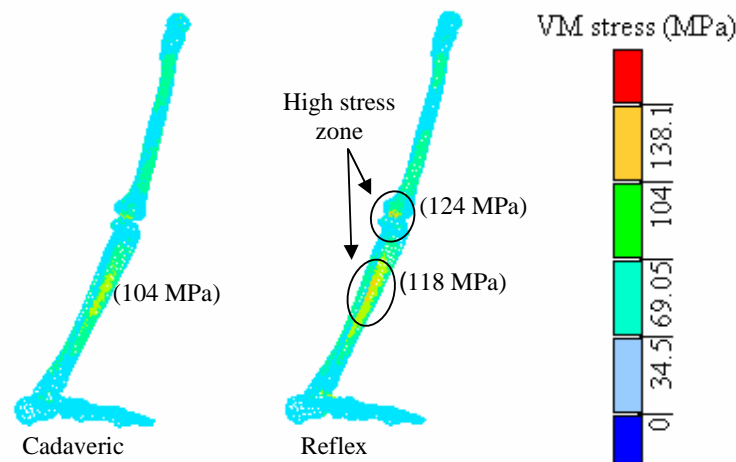


Figure 4 Comparison of VonMises stress distribution in bones (peak stress values are also given) of the right leg in both cadaveric and reflex conditions at 34 ms state

This can be attributed to the higher compressive forces caused by the muscle pull in the reflex condition.

Impact on Left Leg

Now, we present the results obtained from the simulations of impact on left leg in both cadaveric and reflex conditions.

Strain in Knee Ligaments - Figure 5 illustrates the calculated strain time history in knee ligaments of the left leg of PMALE-WP for both cadaveric and reflex conditions. It is evident that strains in knee ligaments have reduced significantly in the reflex conditions as compared to the cadaveric condition.

ACL: Figure 5 (a) compares the strain time history in ACL for both the conditions. It is observed that peak ACL strain has reached the ligament failure limit of 15% in both the conditions. However, active muscle forces in the reflex condition (47 ms) have delayed the failure by 7 ms as compared to the cadaveric condition (40 ms).

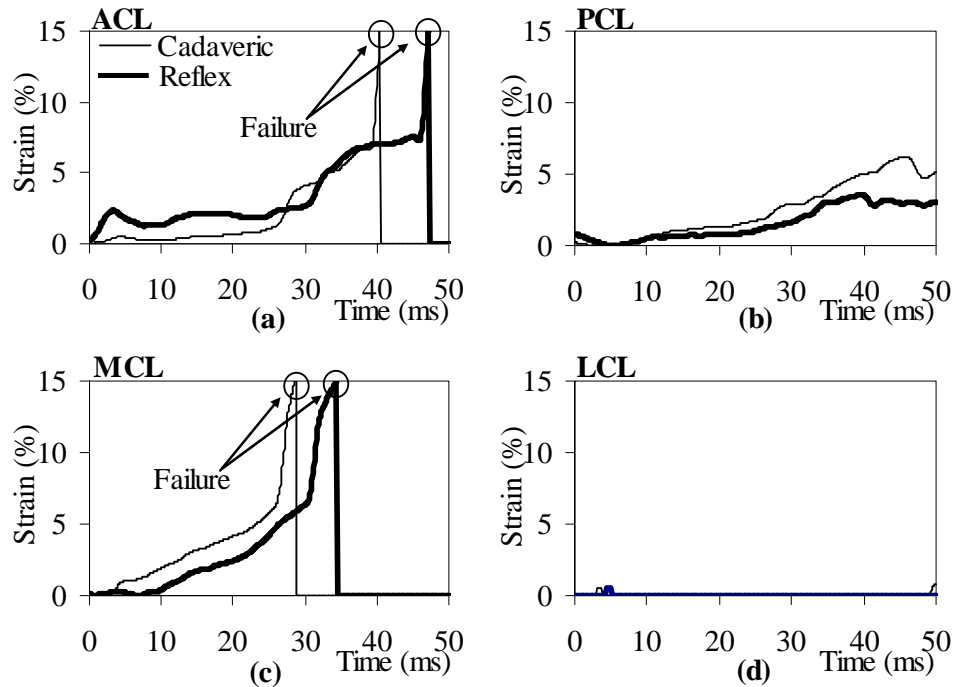


Figure 5 Comparison of strain time history in knee ligaments (a) ACL (b) PCL (c) MCL and (d) LCL of the left leg

PCL: Strain time history in PCL is compared for both the conditions in Figure 5 (b). It is observed that, in the reflex condition, strain in PCL has remained lower than the cadaveric condition for the entire duration of the simulation. It is found that peak strain in PCL has dropped by a factor of 1.78 in the reflex condition (3.5%) as compared to the cadaveric condition (6.2%).

MCL: MCL strain for both the conditions is shown in Figure 5 (c). It is observed that peak MCL strain has reached the ligament failure limit of 15% in both the conditions. However, in comparison to the cadaveric condition (29 ms), failure is delayed by 6 ms in the reflex condition (35 ms). Effect of rupture of MCL in both the conditions is reflected as a sudden increase in strain in ACL (Figure 5 (a)) between 29-32 ms in both the conditions.

LCL: It is observed that LCL (Figure 5 (d)) has remained unstrained in both the conditions. This can be ascribed to the lateral impact which forces tibia to bend medially and consequently keeps the LCL slackened.

VonMises Stresses in Bones - Figure 6 compares the VonMises stress distribution on the bones (i.e. femur, tibia and fibula) of the left leg at 36 ms in both cadaveric and reflex condition.

It is apparent that stresses in bones have increased significantly in the reflex condition as compared to the cadaveric condition.

It is observed that in the reflex condition, stresses in the bones have reached up to 120 MPa at medial side of mid tibia; whereas, it has reached only up to 98 MPa in the cadaveric condition. This can be attributed to the higher compressive forces caused by the muscle pull in the reflex condition.

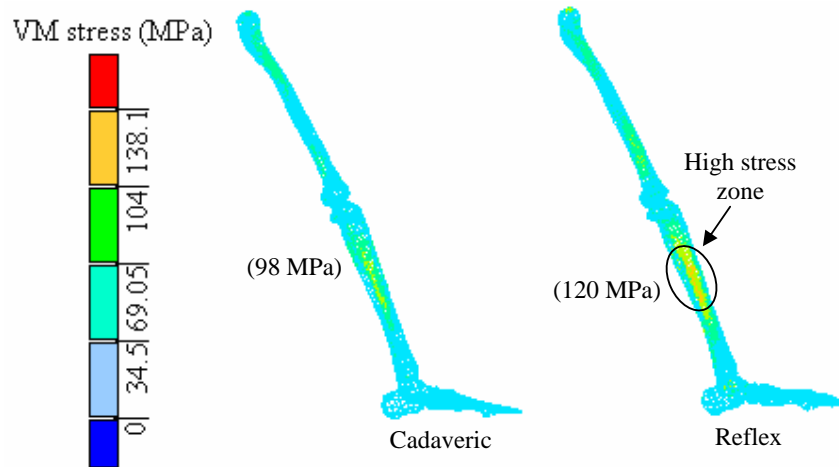


Figure 6 Comparison of VonMises stress distribution in bones (peak stress values are also given) of the left leg in both cadaveric and reflex conditions at 36 ms state

CONCLUSIONS

In the present study, effect of muscle contraction on the response of lower limb in low speed lateral impact has been studied for the pedestrian walking posture. The full body model with active lower extremities i.e. PMALE, which was configured in standing posture, has been repositioned in the walking posture. The real world car-pedestrian lateral impact has been simulated using the PMALE-WP and front structures of a validated car FE model. Two impact configurations, i.e. impact on the right leg and on the left leg have been simulated. For each impact configuration, two sets of simulations, i.e. one with deactivated muscles (cadaveric condition) and the other with activated muscles (including reflex action) mimicking an unaware walking pedestrian have been performed. Differences in responses of a cadaver and an unaware pedestrian have been then studied. To assess the effect of muscle activation, strains in knee ligaments and VonMises stresses in bones have been compared. It has been concluded that:

1. For both impact configurations, peak strains in knee ligaments were lower in the reflex condition (with active muscles) as compared to the cadaveric condition. This supports our previous

findings that the risk of ligament failure in real life crashes is likely to be lower than that predicted through cadaver tests or simulations.

2. For both impact configurations, VonMises stresses in the bones were significantly higher in the reflex condition as compared to the cadaveric condition. This leads to the conclusion that chances of bone fracture increase with muscle contraction.

3. In all the four simulations, MCL has failed, whereas, LCL remained nearly unstrained. This implies that in lateral impacts, MCL could be considered as the most vulnerable and LCL as the safest ligament.

4. In the right leg impact configuration, strain in PCL is found to be significantly higher than that in ACL. This suggests that in case of impact on rear leg of a walking pedestrian, PCL would be at a higher risk than ACL.

5. In the left leg impact configuration, ACL has failed in both the conditions. This indicates that in case of impact on front leg of a walking pedestrian, ACL would be at a higher risk.

ACKNOWLEDGEMENT

The authors would like to acknowledge the support from the Transportation Research and Injury Prevention Program (TRIPP) at Indian Institute of

Technology Delhi and the Volvo Research Education Foundation.

REFERENCES

1. Bhalla, K., Takahashi, Y., Shin, J., Kam, C., Murphy, D., Drinkwater, C., and Crandall, J., Experimental investigation of the response of the human lower limb to the pedestrian impact loading environment, In Proceedings of the Society of Automotive Engineer World Congress 2005, SAE Paper 2005-01-1877.
2. Chawla, A., Mukherjee, S., Mohan, D., and Parihar, A., Validation of lower extremity model in THUMS, In Proceedings of the IRCOBI 2004, pp. 155-166.
3. Chawla, A., Mukherjee, S., Soni, A., and Malhotra, R., Effect of active muscle forces on knee injury risks for pedestrian standing posture at low speed impacts, In Proceedings of the IRCOBI conference, pp. 95-112, 2007.
4. Chidester, A. B., and Isenberg, R. A., Final report - the pedestrian crash data study, In Proceedings of the 17th ESV conference 2001.
5. Kajzer, J., Cavallero, S., Ghanouchi, S., and Bonnoit, J., Response of the knee joint in lateral impact: Effect of Shearing Loads, In Proceedings of the IRCOBI 1990, pp. 293-304.
6. Kajzer, J., Cavallero, S., Bonnoit, J., Morjane, A., and Ghanouchi, S., Response of the knee joint in lateral impact: Effect of Bending Moment, In Proceedings of the IRCOBI 1993.
7. Kajzer, J., Schroeder, G., Ishikawa, H., Matsui, Y., and Bosch, U., Shearing and bending effects at the knee joint at high speed lateral loading, In Proceedings of the Society of Automotive Engineers 1997, SAE Paper 973326.
8. Kajzer, J., Ishikawa H., Matsui Y., and Schroeder G., Shearing and bending effects at the knee joint at low speed lateral loading, In Proceedings of the Society of Automotive Engineers 1999, SAE Paper 1999-01-0712.
9. Kerrigan, J., Bhalla, K., Madeley, N., Funk, J., Bose, D., Crandall, J., Experiments for establishing pedestrian impact lower injury criteria, In Proceedings of the Society of Automotive Engineers 2003, SAE Paper 2003-01-0895.
10. K. W. Lia, H. H. Wub and Y. C. Linb, The effect of shoe sole tread groove depth on the friction coefficient with different tread groove widths, floors and contaminants, Applied Ergonomics 37 (2006), pp. 743-748.
11. Maeno, T., and Hasegawa, J., Development of a finite element model of the total human model for safety (THUMS) and application to car-pedestrian impacts, In Proceedings of the 17th ESV conference 2001, Paper No. 494.
12. Mizuno, Y., Summary of IHRA Pedestrian safety WG activities (2003) – proposed test methods to evaluate pedestrian protection afforded by passenger cars, In Proceedings of the 18th ESV conference 2003.
13. Nagasaka, K., Mizuno, K., Tanaka, E., Yamamoto, S., Iwamoto, M., Miki, K., and Kajzer J., Finite element analysis of knee injury in car-to-pedestrian impacts, Traffic Injury Prevention 2003, Vol. 4, pp. 345-354.
14. Schuster, J. P., Chou, C. C., Prasad, P., and Jayaraman, G., Development and validation of a pedestrian lower limb non-linear 3-D finite element model, Stapp Car Crash Journal 2000, Paper No. 2000-01-SC21.
15. Soni, A., Chawla, A., and Mukherjee, S., Effect of muscle contraction on knee loading for a standing pedestrian in lateral impacts, In proceedings of the 20th ESV conference 2007, Paper No. 467.
16. Soni, A., Chawla, A., Mukherjee, S. and Malhotra R., Response of lower extremity in car-pedestrian impact - influence of muscle contraction, In Proceedings of the IRCOBI conference, 2008, pp. 469-472.

17. Takahashi, Y., and Kikuchi, Y., Biofidelity of test devices and validity of injury criteria for evaluating knee injuries to pedestrians, In Proceedings of the 17th ESV conference 2001.

18. Winter, D. A. (1987). 'Biomechanics & Motor Control of Human Gait', University Waterloo Press.

APPENDIX-A

Values of activation levels used in the present study to model the 42 active muscles in each leg are listed in the Table A.1. These values are taken from Winter (1987). Here, right leg muscles are modeled for 60 % gait (i.e. terminal stance) and left leg muscles are modeled for 0 % gait (i.e. heel strike).

Table A-1 Activation levels in muscles of left and right leg (Note: Activation levels labeled with (*) are taken from Winter (1987))

Lower extremity muscles	Activation levels	
	Left	Right
Vastus Lateralis	0.5*	0.1*
Vastus Intermedius	0.005	0.005
Vastus Medialis	0.005	0.005
Rectus Femoris	0.5*	0.1*
Soleus	0.2*	0.35*
Gastrocnemius Medialis	0.2*	0.2*
Gastrocnemius Lateralis	0.2*	0.3*
Flexor Hallucis Longus	0.005	0.005
Flexor Digitorum Longus	0.005	0.005
Tibialis Posterior	0.005	0.005
Tibialis Anterior	0.4*	0.1*
Extensor Digitorum	0.4*	0.1*
Extensor Hallucis Longus	0.005	0.005
Peroneus Brevis	0.005	0.005
Peroneus Longus	0.4*	0.2*
Peroneus Tertius	0.005	0.005
Biceps Femoris (LH)	0.4*	0.1*
Biceps Femoris (SH)	0.4*	0.1*
Semimembranosus	0.4*	0.1*
Semitendinosus	0.4*	0.1*
Piriformis	0.005	0.005
Pectineus	0.005	0.005

Obturator Internus	0.005	0.005
Obturator Externus	0.005	0.005
Gracilis	0.005	0.005
Adductor Brevis 1	0.005	0.005
Adductor Brevis 2	0.005	0.005
Adductor Longus	0.5*	0.5*
Adductor Magnus 1	0.25*	0.1*
Adductor Magnus 2	0.25*	0.1*
Adductor Magnus 3	0.25*	0.1*
Gluteus Maximus 1	0.5*	0.15*
Gluteus Maximus 2	0.5*	0.15*
Gluteus Maximus 3	0.5*	0.15*
Gluteus Medius 1	0.5*	0.05*
Gluteus Medius 2	0.5*	0.05*
Gluteus Medius 3	0.5*	0.05*
Gluteus Minimus 1	0.005	0.005
Gluteus Minimus 2	0.005	0.005
Gluteus Minimus 3	0.005	0.005
Sartorius	0.4*	0.25*
Tensor Fascia Lata	0.005	0.005

SAFETY REQUIREMENTS FOR CYCLISTS DURING CAR IMPACTS TO THE LEGS

R.N. Hardy

J.W. Watson

Cranfield Impact Centre

K. Kayvantash

Cranfield University

United Kingdom

Paper Number 09 –0462

ABSTRACT

The term vulnerable road user (VRU) is most commonly associated with pedestrians and in particular children and the elderly. In many European countries cyclists make up a significant number of VRU casualties – typically around one-third. In the context of the European 6th Framework Integrated Project APROSYS (Advance PROtection SYStems), a study was conducted to examine the safety requirements for cyclists and whether these were addressed by current pedestrian safety assessments of cars.

An examination of accident statistics was first conducted to determine the principal accident scenarios for cyclists. Since insufficient cyclist cases were recorded in a detail database of VRU accidents compiled during APROSYS, a programme of virtual testing was then conducted. The objective was to identify the most significant parameters during cyclist impacts with a range of cars sizes and the likely injury consequences. The primary region of investigation was impacts to the legs and knees – the points of first contact.

The study indicated that cyclists interacted differently with cars than pedestrians, resulting from the geometric configuration of their legs, the presence of the bicycle and their elevated riding position. The potential for injury was different and the current sub-system impactor tests used by Euro NCAP and for vehicle certification purposes did not address all these differences. It was determined that the relevance of the current pedestrian impact safety assessments of cars for cyclists could be improved by minor changes to the test parameters. However, the study also identified new injury mechanisms that may require further biomechanical investigations.

Although this study has considered a wide range of cyclist impact configurations it should not be considered as definitive. Further work including

physical testing is needed in order to take forward improved safety test procedures.

INTRODUCTION

Cycling is a popular mode of transport associated with commuting, sport and leisure activities. The bicycle has been in existence for over 100 years, but has had to share the roads with other forms of transport. Cyclists, along with pedestrians are known as vulnerable road users as they do not have the protection of a structure around them and do not have passive safety features associated with their bicycles, such as airbags and seatbelts, to improve their chances of surviving an accident. Of the 37,000 people killed on European roads every year, 2000 of them are cyclists and 7000 are pedestrians, while several hundred thousands are injured (European Commission, Directorate-General for Energy and Transport, 2008).

Few researchers have considered in detail the differences between cyclists and pedestrian accidents. One of the first attempts to reconstruct bicycle accidents using a mathematical technique was performed by Huijbers and Janssen (1988). One of their principle conclusions was that vehicle shape had a considerable influence on the relative head impact velocity of the cyclist. Other papers by Maki et al. (2003) and Verschueren et al. (2007) have investigated cyclist accidents by using modelling techniques, but only Maki reviewed accident statistics for both road user types, although no modelling was performed for pedestrians.

There are fundamental differences between the two user groups in terms of their kinematics and injuries sustained, Carter et al. (2005); Janssen and Wismans (1985) and Otte (2004). Cyclists strike the vehicle in a different orientation and contact different parts of the vehicle, which have different levels of stiffness.

Similarities do exist between the two road users, such as the exposure of limbs to direct contact with

the vehicle and the impact speeds. However, cyclists have a higher centre of gravity compared to pedestrians due to their positioning on the bicycle and their feet not being in contact with the ground on impact. In the majority of cases, a cyclist will also be travelling at a greater speed compared to a pedestrian. This has consequences for their impact conditions with the vehicle.

Nevertheless, current European legislation (European Parliament and Council 2003) that has been targeted at protecting pedestrians, assumed that the introduction of pedestrian legislation would also contribute to protecting cyclists, as they generally come into contact with the front of the vehicle.

This paper examines and contrasts the differences between cyclists and pedestrians from the first point of contact with a vehicle, that is impacts to the legs.

BASIS OF MODELLING

Preliminary cyclist related activities in APROSYS (Hardy et al, 2007, Bovenkerk et al, 2008) have reported that the Detailed Accident Database from Work Package (WP) 3.1 did not contain sufficient bicyclist cases to examine the type, range of injuries or the severity of the injuries sustained by bicyclists. Therefore, a programme of parametric studies using mathematical models was conducted to examine vehicle to bicyclist impacts during loadings to the legs, to ascertain the likelihood and extent of injuries. In order to draw comparisons with pedestrians, since the current legal and consumer sub-system lower leg impactor tests are designed for pedestrians, vehicle to pedestrian impacts were also included in the parametric study.

Bicycle, cyclist and pedestrian models

Physical dimensions were measured from an adult aluminium bicycle frame and an FE model was developed in LS-DYNA. The main tubing was represented by shells and joined together by using localised rigid bodies at the frame joints. It was assumed that the joints do not fail, but the region immediately surrounding the joints had the capability to deform. This was to allow for the collapse mechanism observed in a series of dynamic tests that were conducted.



Figure 1. Finite element model of adult bicycle.

The bicycle model, see Figure 1, was constructed with aluminium properties for the main tubes, with the seat and handlebars constructed of a rigid material. The wheels were modelled by representing the spokes as beams and the tyres as an elastic material.

A human model, as developed by Cranfield Impact Centre from a previous project (Howard et al 2000), was used to model the cyclist and the pedestrian and by virtue of the properties and dimensions represented an average 50th percentile human of 16 to 35 years of age. The bicycle and human model combination is shown in Figure 2.



Figure 2. Human and bicycle model combined.

The bicycle model was developed to include pedals and cranks to accommodate the human model's feet and create a more realistic starting position for the simulation. The cranks had the ability to turn through 360 degrees by the use of a cylindrical joint positioned at the bottom bracket. The steering column and front forks of the bicycle were further advanced to represent the movement of the handlebars if they were struck by a vehicle.

Details of the pedals and crank with the feet positioning is shown in Figure 3.



Figure 3. Details off pedals and crank.

A contact characteristic was defined for the feet to pedal and crank contact. However, for the hand to

handlebar connection an altogether different arrangement was required. As the geometry of the hands, including the fingers and compression of the soft tissue were not modelled in detail, a spring was used to represent the hand to handlebar connection. At a designated force and displacement level the spring extended to simulate the releasing of the hand from the handlebars. The springs for each hand were programmed to work independently. Based on a literature search, the displacement release level was set at 10 mm with an 860N force level (Incel et al 2002).

Four different sizes of vehicle were considered in the parametric study:

- Supermini
- Large Family Car (LFC)
- Multi-purpose vehicle (MPV)
- Sports utility vehicle (SUV)

The geometric shapes and stiffness characteristics of each vehicle model were based on the results from APROSYS WP 3.1, Carter (2006) and Martinez et al (2006), respectively.

INITIAL GEOMETRIC CONSIDERATIONS

A number of factors need to be considered in examining the suitability of the pedestrian lower leg impactor for use to assess the safety of cyclists during impacts with passenger vehicles. The first concerns the relative positioning of a cyclist's lower limbs, as compared to a pedestrian's, with respect to the front geometry of these vehicles. Two difference 'stances' were considered for the cyclist, struck leg up (SLU) and struck leg down (SLD), and two difference 'stances' were considered for the pedestrian, struck leg forward (SLF) and struck leg back (SLB). This is illustrated for the four different vehicle sizes in Figure 4 to Figure 7.

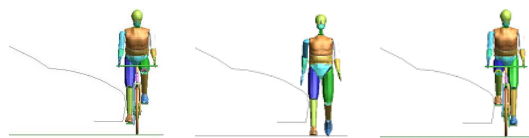


Figure 4. Cyclist and pedestrian leg positioning with respect to Supermini front.

In the case of impacts with the Supermini model, the knee region of the pedestrian's struck leg (middle picture of Figure 4) is just below the bonnet leading edge with subsequent bumper impacts lower down the lower leg. The knee region of the pedestrian's non-struck leg is similarly positioned. Conversely, for the cyclist in the struck leg down configuration (left most picture of Figure 4), the knee is just above the bonnet leading edge.

In addition, although the height of the cyclist's head is almost the same distance from the ground plane, the pelvis is significantly higher up. The cyclist's non-struck leg is positioned with the knee well above the bonnet leading edge and only the foot overlapping the bonnet leading edge. In the case of the cyclist in the struck leg up configuration, (right most picture of Figure 4), the locations are effectively reversed from the previous cyclist case. Therefore, already the likelihood of different levels for the leg injury indices from the simulations for pedestrians and cyclists seems clear.

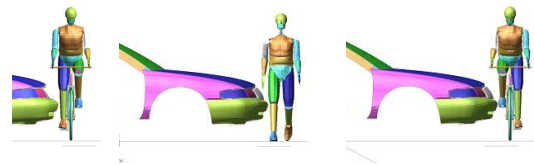


Figure 5. Cyclist and pedestrian leg positioning with respect to Large Family Car front.

In the case of impacts with the Large Family Car model, the knee regions of the pedestrian's struck leg (middle picture of Figure 5) and the non-struck leg are close to the top of the bumper. Conversely, for the cyclist in the struck leg down configuration (left most picture of Figure 5), the knee is above the top of the bumper but below the bonnet leading edge and the non-struck leg is positioned with the knee well above the bonnet leading edge and only the foot overlapping the bumper. In the case of the cyclist in the struck leg up configuration, (right most picture of Figure 5), the locations are effectively reversed from the previous cyclist case. Again, the likelihood of different levels for the leg injury indices from the simulations for pedestrians and cyclists seems clear.

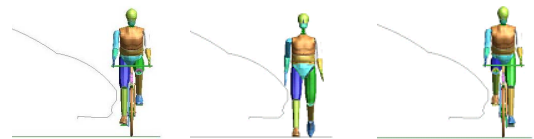


Figure 6. Cyclist and pedestrian leg positioning with respect to MPV front.

In the case of impacts with the MPV, the knee regions of the pedestrian's struck leg and the non-struck leg are below the bonnet leading edge (middle picture of Figure 6). Conversely, for the cyclist in the struck leg down configuration (left most picture of Figure 6), the knee is just above the bonnet leading edge and the non-struck leg is positioned with the knee well above the bonnet leading edge but the foot below the bonnet leading edge. In the case of the cyclist in the struck leg up configuration, (right most picture of Figure 6), the

locations are effectively reversed from the previous cyclist case. Again, the likelihood of different levels for the leg injury indices from the simulations for pedestrians and cyclists seems clear.

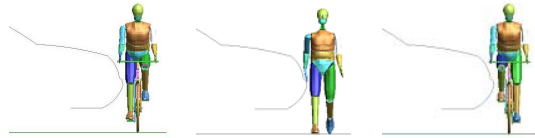


Figure 7. Cyclist and pedestrian leg positioning with respect to SUV front.

In the case of impacts with the SUV model, the whole of the pedestrian's lower body is below the bonnet leading edge (middle picture of Figure 7). Similarly, for both cyclist configurations the legs and a significant proportion of the pelvis are below the leading edge of the bonnet. For the SUV, the likelihood is that similar levels for the leg injury indices from the simulations for pedestrians and cyclists may occur.

SIMULATION PARAMETERS

Simulations were conducted at vehicle impact speeds of 5, 10 and 15 m/s with the cyclist or pedestrian aligned with the centre-line of the vehicle and stationary. The two different cyclist 'stances', struck leg up (SLU) and struck leg down (SLD), and the two different pedestrian 'stances', struck leg forward (SLF) and struck leg back (SLB), were used for human model.

The following parameters were monitored on the struck leg and non-struck leg of the pedestrian or cyclist model: accelerations at the tibia (accelerometer location in the same relative vertically position compared to the knee joint as in the sub-system leg impactor), bending moments at the knee and shear forces at the knee.

In the cases of the leg bending moments and shear forces, a sign convention was used to identify in which directions the knee was bending and shearing, since it changes according to the vehicle geometry, between cyclists and pedestrians and between initial leg orientations. In the simulations the car moved from left to right, according to the view point shown by the geometric vehicle and cyclist/pedestrian configurations in the Figures 4 to 7 above. The sign convention is defined in Figure 8.

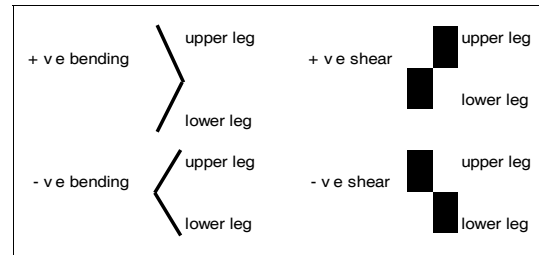


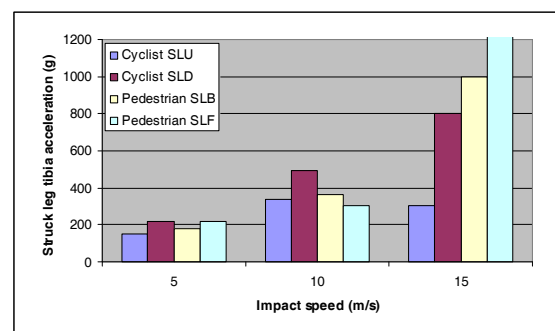
Figure 8. Sign convention for knee bending and shear.

Therefore, by reference to the pedestrian configuration given by the middle picture in Figure 4, the pedestrian's struck leg will initially experience positive bending, due to movement of the knee in the direction of car movement and relative to the hip and ankle regions of the struck leg. Shear force were similarly defined so that positive shear represented movement of the upper leg to the right relative to the lower leg (or the movement of the lower leg to the left relative to the upper leg). The inverse was the case for negative shear.

RESULTS

Impact forces – Supermini

The maximum tibia accelerations for the struck leg, Figure 9, were all above the 150g level set for the EEVC WG17 lower leg impactor test – although it is important to point out that 150g may not be a sufficiently robust or bio-mechanically correct criteria for a human leg. The levels increased with increasing vehicle speed and until at the highest speed the cyclist and pedestrian values were generally similar. For the non-struck (or second struck) leg the tibia acceleration levels were generally lower than for the struck leg and generally similar at each car impact speed.



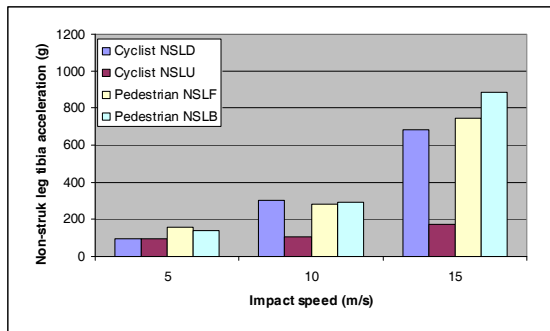


Figure 9. Tibia accelerations for the struck and non-struck legs.

The maximum bending moments for the struck leg, Figure 10, were reversed for cyclists compared to pedestrians although the numerical values were generally lower for cyclists. The positive bending moments for pedestrians were in-line with the injury mechanism assessed by the lower leg sub-system impactor. Therefore, these results suggested the possibility of an alternate injury mechanism for cyclists. The knee ligaments were then loaded in the reverse direction and specifically the lateral collateral ligaments on the outside of the knee were subjected to tensile loadings.

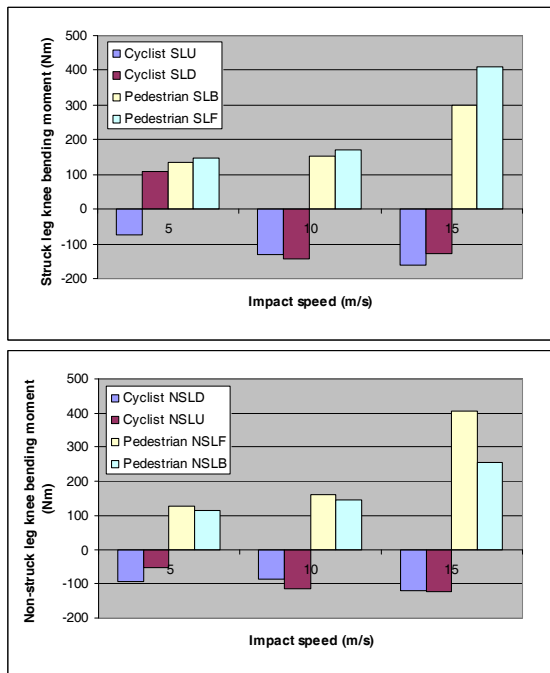


Figure 10. Knee bending moments for the struck and non-struck legs.

The maximum bending moments for the non-struck leg also showed an asymmetry between the cyclist and pedestrian cases but again the numerical values were generally lower for cyclists. However, now, the negative bending moments for cyclists reflected a direction of bending compatible with the injury mechanism assessed by the lower leg sub-system impactor (medial collateral ligaments, on the inside

of the knee, in tension). In contrast, these results now suggested an alternate injury mechanism for the non-struck or second struck leg of pedestrians. This situation has real world implication for pedestrians.

In these simulations, at a car impact speed of 10 m/s, the results for the non-struck leg of the pedestrian were probably on the borderline of injury/no injury.

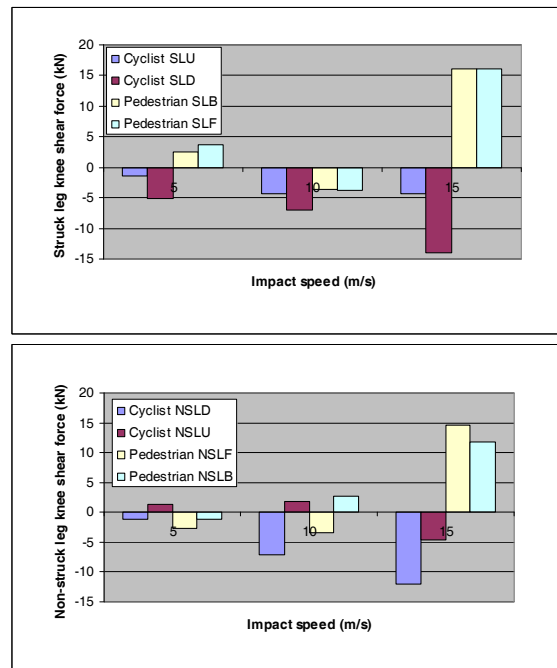


Figure 11. Knee shear forces for the struck and non-struck legs.

The maximum shear forces for the struck and non-struck legs, Figure 11, showed a mixed trend for cyclists and pedestrians. In general, the numerical values of the cyclist and pedestrian results were similar at each impact speed for the struck leg cases and mostly similar at each impact speed for the non-struck leg cases. The values at each speed were lower for all the non-struck leg cases.

Impact forces – Large Family Car

The maximum bending moments for the struck leg, Figure 12, were reversed for the cyclist cases with the struck leg up compared to the cyclist case with the struck leg down and all pedestrian cases. The trend was the same for the non-struck leg results, except at an impact speed of 5 m/s. In almost all scenarios the numerical values were lower for cyclists than pedestrians and lower for the non-struck leg than the struck leg.

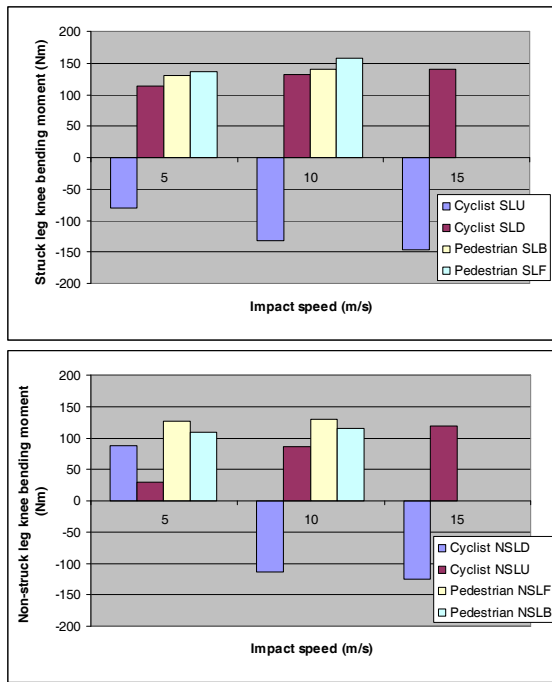


Figure 12. Knee bending moments for the struck and non-struck legs.

The negative values for the cyclist struck leg up scenarios again highlighted the possibility of an alternate injury mechanism, where the knee ligaments were loaded in the reverse direction from the injury mechanism assessed by the lower leg sub-system impactor. For the non-struck leg cases the positive values again highlighted the possibility of an alternate injury mechanism, in this case for all pedestrian scenarios and many of the cyclist scenarios. As in the case of the Supermini, this situation has real world implication for pedestrians and some cyclists.

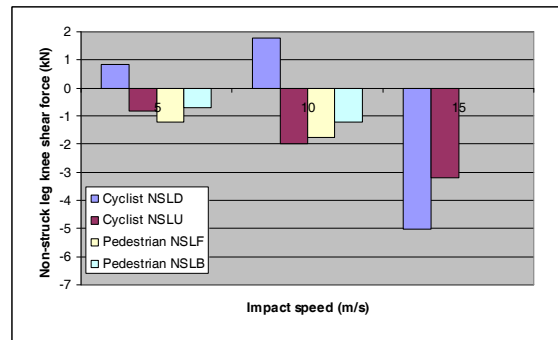
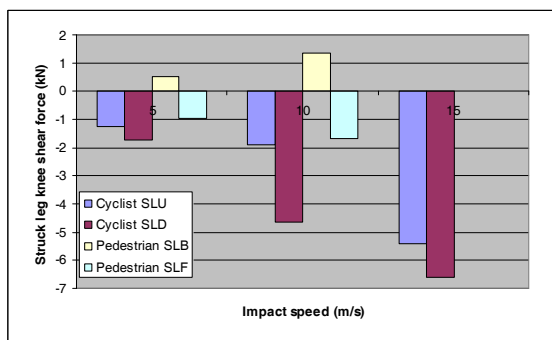
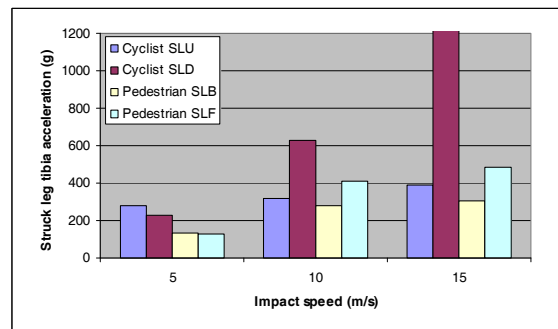


Figure 13. Knee shear forces for the struck and non-struck legs.

The maximum shear forces for the struck and non-struck legs, Figure 13, showed a mixed trend for cyclists and pedestrians. In general, the numerical values of the cyclist results were higher than the values from the pedestrian results at each impact speed for the struck and non-struck leg cases. The numerical values at each speed were generally lower for all the non-struck leg cases.

Impact forces – MPV

The maximum tibia accelerations for the struck leg, Figure 14, were nearly all above the 150g level set for the EEVC WG17 lower leg impactor test – although as mentioned earlier, it is important to point out that 150g may not be a sufficiently robust or bio-mechanically correct criteria for a human leg. The levels increased with increasing vehicle speed and the cyclist values were generally higher than the pedestrian values at each impact speed. For the non-struck (or second struck) leg cases, the tibia acceleration levels were generally lower than for the struck leg cases and the cyclist results were generally lower than the pedestrian values at each speed.



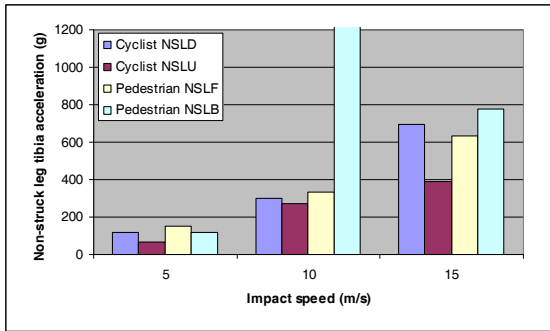


Figure 14: Tibia accelerations for the struck and non-struck legs

As in the case of the large family car impacts, the maximum bending moments for the struck leg, Figure 15, were reversed for the cyclist cases with the struck leg up compared to the cyclist cases with the struck leg down and all the pedestrian cases.

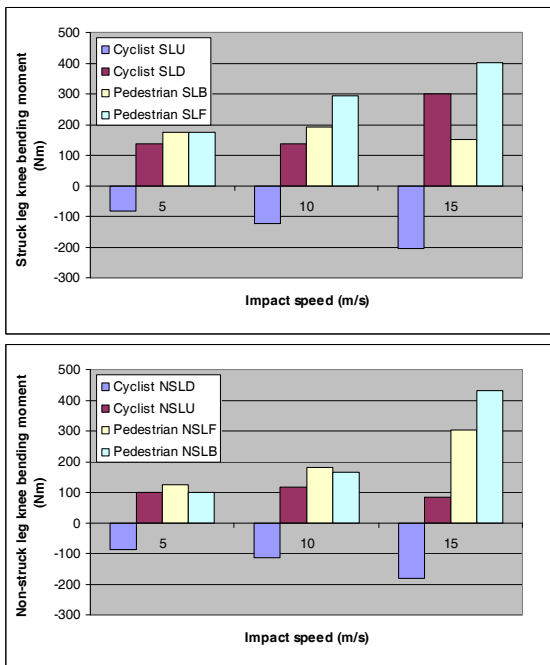


Figure 15. Knee bending moments for the struck and non-struck legs.

The trend was the same for the non-struck leg results. In all scenarios the numerical values were lower for cyclists than pedestrians and lower for the non-struck leg than the struck leg.

The same possibility of an alternate injury mechanism for cyclist struck leg up cases (negative values) again existed - as it does also for cyclists in the non-struck leg up cases and for all the pedestrian non-struck leg cases.

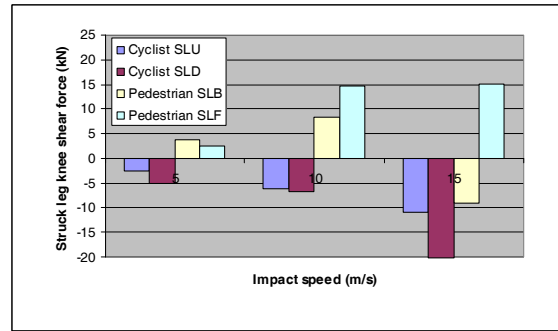


Figure 16. Knee shear forces for the struck and non-struck legs.

The maximum shear forces for the struck and non-struck legs, Figure 16, showed a clearer trend than for the previous vehicles with most results from the cyclists cases the reverse sign of those from the pedestrian cases. The numerical values were generally lower for the cyclist cases compared to the pedestrian cases at each impact speed and the numerical values at each speed were generally lower for the non-struck leg cases – with the exception of the pedestrian cases at an impact speed of 15 m/s.

Impact forces – SUV

The maximum tibia accelerations for the struck leg, Figure 17, were generally below the 150g level set for the EEC WG17 lower leg impactor test for impacts at 5 m/s but at higher speeds the values were all above this limit – although as mentioned earlier, it is important to point out that 150g may not be a sufficiently robust or bio-mechanically correct criteria for a human leg. The levels increased with increasing vehicle speed and the cyclist values were generally lower than the pedestrian values – except at an impact speed of 5 m/s. For the non-struck (or second struck) leg cases, the tibia acceleration levels were generally lower than for the equivalent struck leg cases - except at an impact speed of 15 m/s - and the cyclist results were generally lower than the pedestrian values – except at an impact speed of 5 m/s.

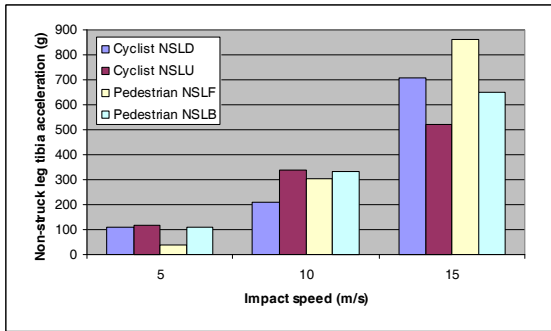
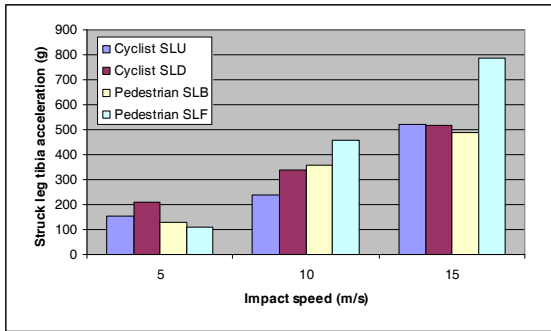


Figure 17: Tibia accelerations for the struck and non-struck legs.

As in the cases of the large family car and MPV impacts, the maximum bending moments for the struck leg, Figure 18, were reversed for the cyclist cases with the struck leg up compared to the cyclist cases with the struck leg down and all the pedestrian cases – again highlighted the possibility of an alternate injury mechanism from that tested for by the lower leg sub-system impactor. However, the trend was different for the non-struck leg results where all the values were the same (positive) sign – a direction of bending in the reverse direction from the injury mechanism assessed by the lower leg sub-system impactor. This situation has real world implication for pedestrians and cyclists.

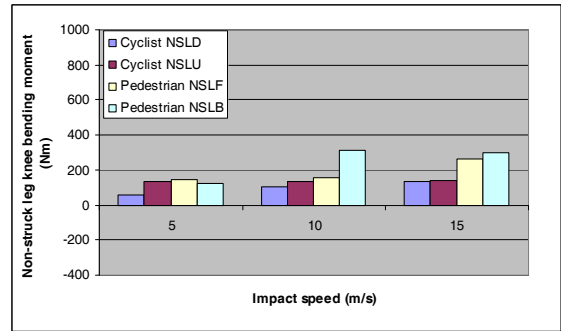
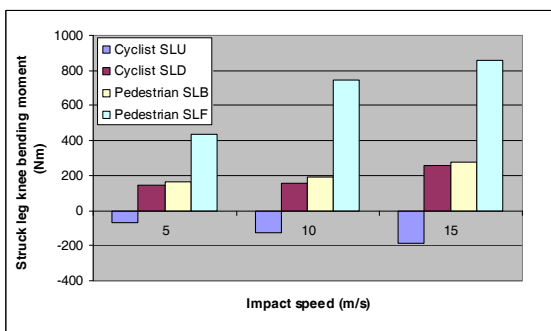


Figure 18: Knee bending moments for the struck and non-struck legs.

In all scenarios the numerical values were lower for cyclists than pedestrians (marginally in some cases) and lower for the non-struck leg than the struck leg.

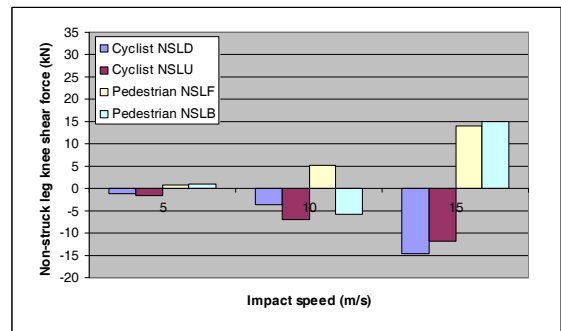
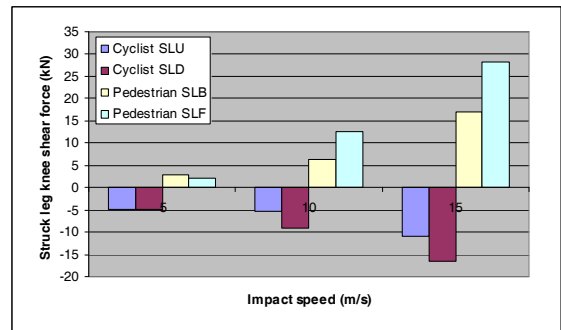


Figure 19. Knee shear forces for the struck and non-struck legs.

The maximum shear forces for the struck and non-struck legs, Figure 19, showed a clearer trend than for the Supermini and Large Family Car, with most results from the cyclist cases the reverse sign of those from the pedestrian cases. In the struck leg cases, the numerical values were generally lower for the cyclist cases compared to the pedestrian cases – except at an impact speed of 5 m/s. In the non-struck leg cases, the numerical values were generally similar for the cyclist and pedestrian cases at each impact speed. The numerical values at each speed were generally lower for the non-struck leg cases.

DISCUSSION

In this parametric study of the differences and similarities between comparable cyclist and pedestrian impact scenarios, the numerical values of the leg injury indices were lower for cyclists in nearly two-thirds of the scenarios. In just over one-fifth of the scenarios the values were similar and in just over one-eighth of the scenarios the cyclist values are higher.

With only one exception (tibia accelerations during impacts with the SUV at 15 m/s) the leg injury indices were lower for the non-struck (or second struck) leg than for the struck (or first struck) leg. But this did not mean that the non-struck leg would register injury indices that were below the threshold values.

Over the range of impact speeds, the cyclist tibia accelerations were slightly lower than those for pedestrians. In general, the SUV was the vehicle model that produced the lowest range of tibia accelerations values across the cyclist and pedestrian impact scenarios and impact speeds. The geometric shape and, in particular, the height of the bumper may have been contributory factors in this situation.

Over the range of impact speeds, the cyclist knee bending moments (numerical values) were lower than those for pedestrians. In general, the Supermini and Large Family Car were the vehicle models that produced the lowest ranges of knee bending moment values across the cyclist and pedestrian impact scenarios and impact speeds.

Over the range of impact speeds, the cyclist knee shear forces (numerical values) were either lower than or similar to those for pedestrians, except for one vehicle model, the Large Family Car, where the values were higher than those for pedestrians. Nevertheless, the Large Family Car was the vehicle model that produced the lowest range of knee shear force values across the cyclist and pedestrian impact scenarios and impact speeds.

The simulation results have confirmed the initial geometric considerations, that differences in cyclist and pedestrian injury risks were likely. In fact, the simulations have demonstrated that this was not solely attributable to the numerical value of the injury indices but also the sign of the values, indicating the mode of deformation under the action of the applied loads.

Therefore, the physical positioning of a cyclist, particularly height from the ground, in front of a

vehicle is an important consideration for meaningfully evaluating the injury risk potential of an impact. The orientation of the cyclists' limbs is also an important consideration in assessing cyclist safety. The current testing regimes assume that a vulnerable road user presents themselves for impact with a vehicle in a straight legged 'gait'. This is not wholly accurate for a pedestrian but for a cyclist it is even more unrealistic, given the range of leg orientations during the rotation of the crank. Recognition of the important physical orientation differences between cyclists and pedestrians immediately prior to an accident is fundamental to providing the same levels of protection for both.

Another aspect of the differences between cyclists and pedestrians is the presence of the bicycle itself. In addition to the physical positioning differences that arise, as discussed above, the inertia of the bicycle can have an important role in the kinematics of the cyclist. The struck leg may be pinned between the front of the vehicle and the bicycle, inducing differences in the loads applied to the legs and the duration of these loadings. To represent this situation it may be necessary to represent an element of the bicycle mass in a testing regime to enhance cyclist safety. Further analytical work will be necessary to determine if this is necessary or not and if so, the magnitude of this mass, its position and its attachment to a sub-system leg impactor.

In the parametric study the struck leg knee bending moments for the cyclist struck leg-up scenarios were consistently the opposite sign of those for all the pedestrian scenarios, as they were also for the entire Supermini to cyclist impact scenarios, except at a vehicle speed of 5 m/s. This implied a 'reverse' bending situation compared to conventional thinking for pedestrian impacts and raises the question as to whether the current knee bending criteria for pedestrians are relevant for cyclists in these scenarios. Similarly, while the non-struck leg bending moments in all the pedestrian impact scenarios had a positive value, this now indicated a 'reverse' bending phenomenon and raises the issue of whether the current testing regimes adequately protect pedestrians. There were also some cyclist impact scenarios where the non-struck leg bending moments also indicated this same 'reverse' bending phenomenon.

The current legform criteria are based on the assumption that, using the sign convention defined in this report (see Figure 8), the lateral knee bending is positive during loading of the leg by the car - that is, the knee is forced forwards in the

direction of car motion whilst the ankle and hip joints lag behind. One of the consequences of this motion is that the medial ligaments in a pedestrian's leg experience tensile forces and if these are too high they may cause ligament damage – work defining the characteristics of this mode of knee bending have been reported by a number of researchers including Levine et al (1984) and Kajzer et al (1993). Damage to other knee ligaments may also occur. If the loading is reversed, negative using the sign convention above, with the knee lagging behind the hip and ankle joints, the lateral collateral ligaments on the opposite (outer) side of the knee experience tensile forces. The injury criterion used for knee bending in the current sub-system impactor leg does not represent the capabilities of the knee in this opposite (or reverse) model of bending.

Therefore, where this type of bending occurs in the real world or in realistic computer simulations of the real world, then no biomechanical criterion exists that can be applied to assess the potential for injury risk. To address the safety requirements of cyclists (and the non-struck leg of pedestrians) where this reverse mode of bending occurs, research to identify the capabilities of the lateral collateral ligaments of the knee will be needed and implementation of these characteristics in a test impactor. In addition, the procedure of conducting a test for this reverse bending scenario will need to be addressed.

The lateral knee shear forces from the simulations also had values for cyclists that in many cases were the opposite sign to those for pedestrians. Further investigations to understand the exact mode that is addressed by the current testing regimes is needed and then further research may be required to determine if the human knee behaves in a symmetric manner under the application of lateral shearing loads.

In general, the numerical values for the lower leg injury indices from these simulations suggested that the current pedestrian consumer and legislative test criteria are likely to be appropriate to provide adequate levels of safety for cyclists. Nevertheless, improvements in the testing procedures to enhance the levels of safety for cyclists are feasible. In summary, among the factors that should be considered are:

- The appropriate height above the ground for the positioning of a lower leg sub-system impactor;
- Representation of the knee region in other than a 'straight' orientation;

- The possible need to represent an element of bicycle mass;
- The appropriate criteria to assess injury risk in lateral modes of knee bending;
- Review, and if necessary, determine the appropriate criteria to assess injury risk in lateral modes of knee shearing.

CONCLUSIONS

1. The impact forces that the legs of a cyclist are exposed to during a collision with a car can be subtly different than those experienced by a pedestrian.
2. The greater pelvis height of the cyclist generally causes the impact points to be lower down on the cyclist's legs.
3. Depending on vehicle shape, generally for vehicles having a low bumper or low bonnet leading edge height, the struck leg knee bending moments and shear forces can be in the opposite direction to those experienced by a pedestrian when struck by the same vehicle.
4. New injury criteria and adjusted impact test procedures are needed to address the differing needs of cyclists in providing a safety environment equivalent to that for pedestrians.
5. Use of any new criteria and use of the existing pedestrian criteria for cyclist impact tests should be reviewed taking into account leg and knee heights, use of an impactor with a bent knee and the influence of the bicycle mass (or an element of it).

ACKNOWLEDEMENT

This research was funded by the 6th Framework project APROSYS (Advanced PROtective SYStems) with support from the European Commission, under the title of Sub-Project 3 Pedestrian and Pedal Cyclist Safety.

REFERENCES

- Bovenkerk, J., Hardy, R.N., Neal-Sturgess, C.E., Hardy, B. J., van Schijndel - de Nooij, M., Willinger, R. and Guerra, L. J. (2008), "Biomechanics of real world injuries and their associated injury criteria", APROSYS EC Project Report Deliverable D3.3.1, AP-SP33-001.
- Carter, E., Ebdon, S. and Neal-Sturgess, C. (2005), "Optimization of passenger car design for the mitigation of pedestrian head injury using a genetic algorithm", Proceedings of Genetic and Evolutionary Computation Conference, pp. 2113, June 2005, Washington DC, USA.

Carter, E. (2006), "The generalised geometry corridors, generic shapes and sizes of the vehicle fleet covering cars, MPVs and SUVs", APROSYS document AP-SP31-007R, Deliverable D3.1.2A.

European Commission, Directorate-General for Energy and Transport (ed.) (2008), EU Energy and Transport in Figures, European Communities, Belgium.

European Parliament and Council, (2003), Directive 2003/102/EC of the European Parliament and of the Council of 17th November 2003 relating to the protection of pedestrians and other vulnerable road users before and in the event of a collision with a motor vehicle and amending Council Directive 70/156/EEC, Directive ed., EU, Brussels, Belgium.

Hardy, R.N., Watson, J. W., Carter, E., Neal-Sturgess, C.E, Joonekindt, S., Yang, J., Hermann, K., Baumgartner, D., Guerra, L.J., Martinez, L. (2007), "Impact conditions for pedestrians and cyclists", APROSYS document AP-SP32-009R, Deliverable D3.2.3.

Howard, M., Thomas, A., Koch, W., Watson, J. and Hardy, R.N. (2000), "Validation and Application of a Finite Element Pedestrian Humanoid Model for use in Pedestrian accident simulations", Proc. of the Int. IRCOBI Conference on the Biomechanics of Impacts, Montpellier (France).

Huijbers, J. J. W. and Janssen, E. G. (1988), "Experimental and Mathematical Car-Bicycle Collision Simulations", Proceedings of 32nd Stapp Car Crash Conference, October 1988, P215, paper SAE 881726, SAE, Atlanta, Georgia, USA.

Incel, N.A., Ceceli, E., Durukan, P.B., Erdem, H.R., Yorgancioglu, Z.R. (2002), "Grip Strength: Effect of Hand Dominance", Singapore Med J 2002 Vol 43(5), pp 234-237.

Janssen, E. G. and Wismans, J. S. H. M. (1985), "Experimental and Mathematical Simulation of Pedestrian-Vehicle and Cyclist-Vehicle Accidents", Proceedings of 10th International Technical Conference on Experimental Safety Vehicles, pp.977-988, July 1985, Oxford, England.

Kajzer, J., Cavallero, C., Bonnoit, J., Morjane, A., Ghanouchi, S. (1993), "Response of the Knee Joint in Lateral Impact: Effect of Bending Moment", International IRCOBI Conference on The Biomechanics of Impacts, September 8-9-10th 1993 Eindhoven (The Netherlands), pp 105-116.

Levine, R. S., Begeman, P. C., King A. I. (1984), "An Analysis of the Protection of Lateral Knee Bracing in Full Extension using a Cadaver Simulation of Lateral Knee Impact", American Academy of Orthopedica Surgical, 17th August, 1984.

Maki, T., Kajzer, J., Mizuno, K. and Sekine, Y. (2003), "Comparative analysis of vehicle-bicyclist and vehicle-pedestrian accidents in Japan", Accident Analysis and Prevention, vol. 35, no. 6, pp. 927-940.

Martinez, L., Guerra, L.J., Ferichola, G., García, A., Yang, J., Yao, J. (2006), "Stiffness corridors for the European flee", APROSYS document AP-SP31-009R, Deliverable D3.1.2B.

Otte, D. (2004), "Use of Throw Distances of Pedestrians and Bicyclists as Part of a Scientific Accident Reconstruction Method", in SAE (ed.), 2004 SAE World Congress, Vol. Accident Reconstruction 2004, paper 2004 -1-1216, 8th-11th March 2004, Detroit, Michigan, USA, SAE International, USA.

Verschueren, P., Delye, H., Depreitere, B., Van Lierde, C., Haex, B., Berckmans, D., Verpoest, I. Goffin, J., Vander Sloten, J. and Van der Perre, G. (2007), "A new test set-up for skull fracture characterisation", J. Biomechanics, vol. 40, no. 15, pp. 3389-3396.

DEVELOPMENT AND VALIDATION OF PEDESTRIAN SEDAN BUCKS USING FINITE ELEMENT SIMULATIONS; APPLICATION IN STUDY THE INFLUENCE OF VEHICLE AUTOMATIC BRAKING ON THE KINEMATICS OF THE PEDESTRIAN INVOLVED IN VEHICLE COLLISIONS

Costin Untaroiu

Jaeho Shin

Jeff Crandall

Center of Applied Biomechanics, University of Virginia
United States

Rikard Fredriksson

Ola Bostrom

Autoliv Research
Sweden

Yukou Takahashi

Akihiko Akiyama

Masayoshi Okamoto

Yuji Kikuchi

Honda R&D Co., Ltd.

Japan

Paper Number 09-0485

ABSTRACT

Previous vehicle-to-pedestrian simulations and experiments using pedestrian dummies and cadavers have shown that factors such as vehicle shape, pedestrian anthropometry and pre-impact conditions influence pedestrian kinematics and injury mechanisms. Generic pedestrian bucks, that approximate the geometrical and stiffness properties of current vehicles, would be useful in studying the influence of vehicle front end structures on pedestrian kinematics and loading. This study explores the design of pedestrian bucks, intended to represent the basic vehicle front-end structures, consisting of five components: lower stiffener, bumper, hood leading edge and grille, hood and windshield. The deformable parts of the bucks were designed using types of currently manufactured materials, which allow manufacturing the bucks in the future. The geometry of pedestrian bucks was approximated based on the contour cross-sections of two sedan vehicles used in previous pedestrian dummy and cadaver tests. Other cross-sectional dimensions and the stiffness of the buck components were determined by parameter identification using FE simulations of each sedan vehicle. In the absence of a validated FE model of human, the FE model of the POLAR II pedestrian dummy was used to validate a mid-size sedan (MS) pedestrian buck. A good correlation of the pedestrian dummy kinematics and contact forces obtained in dummy - MS pedestrian buck with the corresponding data from dummy - MS vehicle

simulation was achieved. A parametric study using the POLAR II FE model and different buck models: a MS buck and a large-size sedan (LS) buck were run to study the influence of an automatic braking system for reducing the pedestrian injuries. The vehicle braking conditions showed reductions in the relative velocity of the head to the vehicle and increases in the time of head impact and in the wrap-around-distances (WAD) to primary head contact. The head impact velocity showed greater sensitivity to the different buck shapes (e.g., LS buck vs. MS buck) than to the braking deceleration. The buck FE models developed in this study are expected to be used in sensitivity and optimization studies for development of new pedestrian protection systems.

INTRODUCTION

Pedestrian fatalities comprise a considerable percentage of total traffic fatalities in industrialized nations: from 11 % in USA (NHTSA 2009) to nearly 50 % - South Korea (Youn et al. 2005). Additionally, the probability for a pedestrian to be injured or killed during a traffic accident is much higher than that for a vehicle occupant. In 2007, 6.7 % of vehicle-pedestrian impacts in the US were fatal, whereas the corresponding fatality rate for occupants in crashes was only 1.3 % (NHTSA, 2009). Protection of pedestrians in vehicle-to-pedestrian collisions (VPC) has recently generated increased attention with regulations implemented or proposed

in Europe (EU 2003, EU 2009), Korea (Youn et al. 2005), and Japan (Mizuno 2008). While subsystem experiments are currently being used as the basis of evaluations for these regulations, car-to-pedestrian dummy impact tests (Fredriksson et al. 2001, Crandall et al. 2005) or car-to-human/dummy impact simulations (Untaroiu et al. 2008) provide complementary data that can better characterize whole body response of vehicle-pedestrian interactions.

An advanced pedestrian dummy, called the POLAR II, has been developed and continuously improved by Honda R&D, GESAC, and the Japan Automobile Research Institute (JARI) (Akiyama et al. 1999, 2001; Okamoto et al. 2001, Takahashi et al., 2005, Crandall et al., 2005). The primary purpose of the POLAR II dummy has been to reproduce pedestrian kinematics in a collision with a vehicle. Kerrigan et al. (2005) performed vehicle impact tests on the POLAR II and post mortem human surrogates (PMHS) in identical conditions and showed that the POLAR II dummy generally replicates the complex kinematics of the PMHS.

A FE model of the POLAR II dummy has been developed, validated in component tests (Shin et al. 2006), and verified at the full scale level against kinematic data (Shin et al. 2006, 2007) recorded during the vehicle-dummy impact experiments performed by Kerrigan et al. (2005). The POLAR II FE model was developed using Hypermesh (Altair Engineering) and Generis (ESI) as pre-processors and PAM-CRASH/PAM-SAFE FE solver (version 2001, ESI) was used for impact simulations. The model contains 27,880 elements that represent the head, neck, thorax, abdomen, pelvis, upper arms, forearms, hands, thighs, knees, legs, and feet and has a total mass and height close to that of the 50th percentile male. Recently, injury thresholds for the POLAR II dummy FE model are being established based on FE simulations with a human model (Takahashi et al. 2008) that may extend the applicability of the dummy model to injury prevention applications. While vehicle-to-PMHS tests or simulations may provide a better understanding of new protection devices, the high cost of tests and the lack of a fully validated human models have turned attention of many researchers toward simple tests or models. Vehicle sled bucks were used in pedestrian PMHS tests by Snedeker et al. 2005 to assess the pelvis and upper leg injury risk. While these simplified bucks approximated reasonable the geometric characteristics of current vehicle front-ends, no information about a correlation with the vehicle stiffness was provided. To study the influence of the pre-impact position of pedestrian arms on pedestrian head injury, Ogo et al. (2009) developed a scaled

human model and vehicle buck. The values of head injury criteria (HIC) recorded in the vehicle buck-to-dummy tests showed a significant variation with respect to the arm pre-impact position. Neal et al. (2008) developed a simplified buck FE model (rigid surfaces connected by nonlinear springs) to predict the performance of different vehicle front-end designs in pedestrian leg impact tests.

The objective of the current study was to design two FE models of simplified vehicle bucks with geometrical and stiffness characteristics similar to those of a mid-size sedan (MS) and a large sedan (LS). To show a possible application of the buck FE models in the development of new measures for pedestrian protection, a numerical study related to influence of braking on the pedestrian kinematics was performed.

METHODOLOGY

The pedestrian kinematics during impact with a vehicle are generated by the vehicle-dummy contact forces. These loads highly depend on the geometry and stiffness properties of the front-end structures of the vehicle involved in the crash. Since a pre-impact position of the dummy along the vehicle centerline has been used in previous vehicle-to-pedestrian dummy/PMHS tests (Kerrigan et al. 2005, Kerrigan et al. 2007), the vehicle geometry and stiffness properties along the centerline were used in current study for the development of MS and LS bucks. It was hypothesized that five vehicle components (lower stiffener, bumper, hood leading edge and grille, hood and windshield) can reasonably approximate the front-end of the vehicle during a pedestrian impact. Each component was designed as a combination of deformable parts connected to a rigid part. Since a physical implementation of the pedestrian buck is ultimately planned, material selection for the deformable components of the buck was based on readily available materials: steel, Expanded Polypropylene Particle (EPP) foam (JSP Japan), and polypropylene fascia (Boedeker Plastics, TX, US). The shape and locations of buck components were defined based on the exterior geometry of the MS and LS vehicles used in previous testing (Kerrigan et al. 2005, Kerrigan et al. 2007). The material used for each deformable component of the buck was chosen based on the stiffness characteristics of corresponding sedan component determined by FE simulations. Then, FE simulations in similar conditions were run to calibrate the thickness of deformable parts of the bucks. Detailed information about the development of each vehicle component is provided in the following sections.

Development of a mid-size sedan (MS) pedestrian buck

A pedestrian simulation was performed using the POLAR II FE model (Shin et al. 2006 and 2007) and the FE model of a MS vehicle in order to determine the maximum level of dummy-vehicle forces during a 40 km/h impact. In addition to the upper body kinematics of pedestrian recorded at specified locations (head center of gravity (CG), T1, T8, pelvis – Untaroiu et al. 2008), the time histories of resultant force were calculated at the contact points of the dummy with four components (lower stiffener, bumper, leading edge and grille, hood – Figure 1).

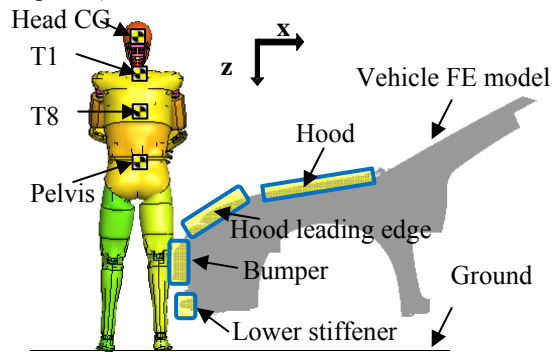


Figure 1. Pedestrian - mid-size (MS) sedan vehicle FE simulation setup

To determine the stiffness characteristics of the lower stiffener and bumper, a cylindrical rigid impactor (220 mm length, 120 mm diameter, and 10 kg mass) was launched freely with a 40 km/h initial velocity toward the vehicle at the middle sections of the lower stiffener (Figure 2), and then at the corresponding section of the bumper (Figure 3). The time histories of the resultant force in the impactor were calculated during the simulations, and then were normalized with the sum of the highest forces calculated in these components in the POLAR II – vehicle simulation.

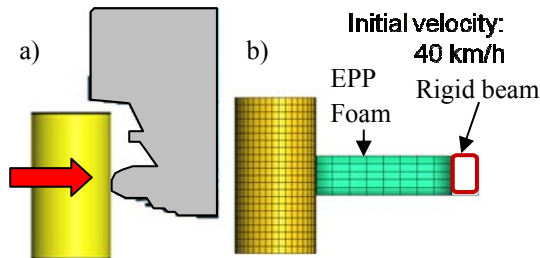


Figure 2. Impactor – vehicle/buck FE simulations at lower stiffener location a) MS vehicle and b) MS buck

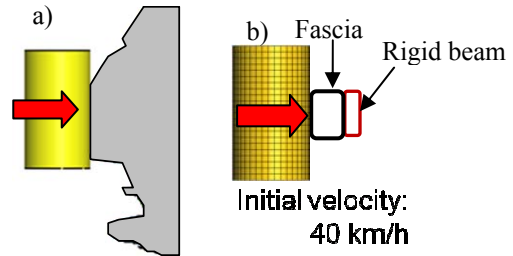


Figure 3. Impactor – vehicle/buck FE simulations at bumper location a) MS vehicle and b) MS buck

It was observed that the EEP foam and the fascia could approximate the stiffness characteristics of the lower stiffener, and the bumper respectively. While the vertical lengths of the chosen deformable components were approximated from the vehicle cross-section (Kerrigan et al. 2007), the other dimensions were adjusted to match the stiffness curves of vehicle components.

A cylindrical rigid impactor (350 mm length, 150 mm diameter, and 10 kg mass) was also used to determine the stiffness of the hood leading edge-grille region of the vehicle. The impactor was launched freely at 40 km/h with an angle of 40 degrees towards the hood vehicle leading edge (Figure 4). The time histories of the resultant forces in the impactor were calculated during the simulations, and then were normalized with the sum of the highest forces calculated in the hood leading edge and grille components in the POLAR II – vehicle simulation. After evaluating several different potential solutions, it was determined that two EFF foam parts (20g/l density) covered with a steel sheet could reasonably represent the leading edge and the grille stiffness.

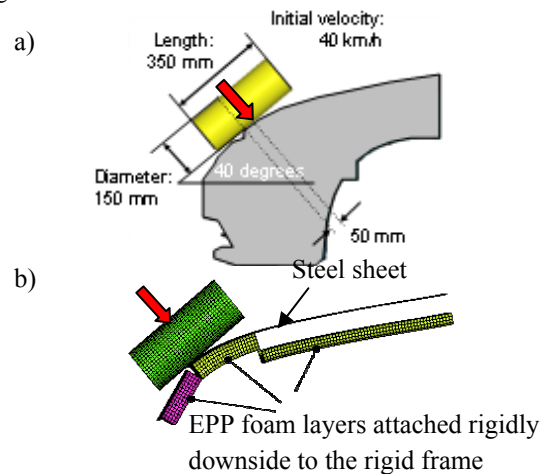


Figure 4. Impactor – hood leading edge FE simulations a) MS vehicle and b) MS buck

Since the stiffness of the hood varies from the leading edge to the cowl, two locations were chosen to

determine the hood stiffness, and then were used in the buck calibration: 1) the middle region at a wrap-around distance (WAD) = 1200 mm – the location frequently struck by the dummy upper extremities and 2) the cowl region at WAD = 1500 mm – the location often struck by the dummy shoulder or head. A head impactor FE model developed by Untaroiu et al. (2007) and validated against static and dynamic tests reported by Matsui and Tanahashi (2004) was used in the hood impact simulations (Figure 5). The head impactor was launched freely at an impact angle of 65° in agreement with the requirements of the International Organization for Standardization (ISO) and the European Enhanced Vehicle Safety Committee (EEVC) protocols for a sedan type vehicle (Untaroiu et al. 2007). The time histories of the resultant forces in the impactor were calculated during the simulations, and then were normalized with the maximum force calculated in the hood in the POLAR II – vehicle simulation.

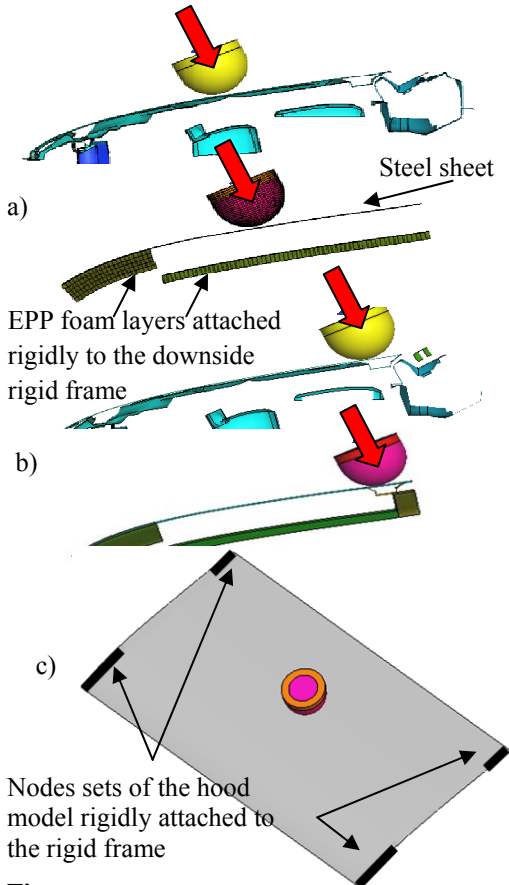


Figure 5. Head adult impactor – hood FE simulations a) at WAD = 1200 mm, b) at WAD = 1500 mm, and c) The attachment of hood to the rigid buck frame

A glass windshield similar to that of the MS vehicle was used in the MS buck. All deformable parts were

rigidly connected to the buck frame, with the total mass adjusted to that of the actual MS vehicle.

To verify the MS buck model, an impact simulation was performed with the POLAR II FE dummy with a configuration matched to those used in the POLAR II - MS vehicle simulation (Figure 1). The kinematics of the POLAR II and the reaction forces with the buck were calculated and then compared with the corresponding data from the POLAR II - MS vehicle simulation.

Development of a large-size sedan (LS) pedestrian buck

A similar design approach to that used for the MS pedestrian buck was utilized in the development of the LS pedestrian buck. The geometry of the LS buck was approximated based on the exterior contour of the LS vehicle (Kerrigan et al. 2007). Following Kerrigan et al. (2008), the rigid impactors were constrained to move in the impact direction with a prescribed velocity of 40 km/h. The stiffness curves obtained by FE simulations of that vehicle (Kerrigan et al. 2008) were used to calibrate the lower stiffener, the bumper, and the hood leading edge-grille components of the LS pedestrian buck. In the lower stiffener impact test, a cylindrical impactor (220 mm length, 120 mm diameter) was used. While a similar design to the MS buck was able to reasonably approximate the stiffness characteristics in the lower stiffener component of the LS buck (Figure 6 a), a different design approach was required for the LS bumper component. As in Kerrigan et al. 2008, an impact simulation with a rigid cylindrical impactor (800 mm length, 120 mm diameter) striking the MS buck complex of lower stiffener and bumper at 40 km/h was performed (Figure 6 b). The structure consisted of two EPP foam layers that were shown to provide the best approximation of the LS vehicle bumper in terms of the stiffness characteristics during the impact simulation.

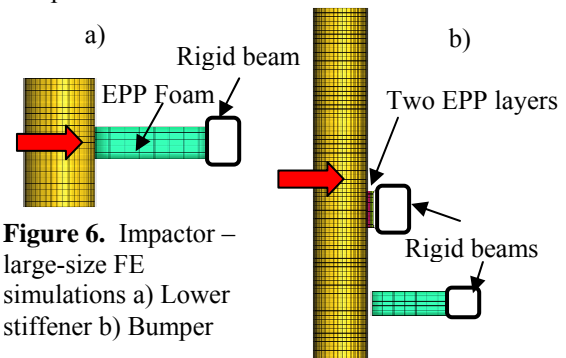


Figure 6. Impactor – large-size FE simulations a) Lower stiffener b) Bumper

A similar structure consisting of one EPP foam layer covered by a steel sheet was used for the hood leading edge-grille LS buck model. A impact simulation with a cylindrical impactor (300 mm

length, 200 mm diameter) at a 40 degree angle from the vertical was performed as in Kerrigan et al. (2008) (Figure 7). The thickness of the foam layer and the steel sheet was adjusted to approximate the stiffness characteristics of the leading edge structure of the LS vehicle. Since stiffness of the hood structure in the LS vehicle model was not directly available, the hood design determined for the MS buck was also applied to the LS buck.

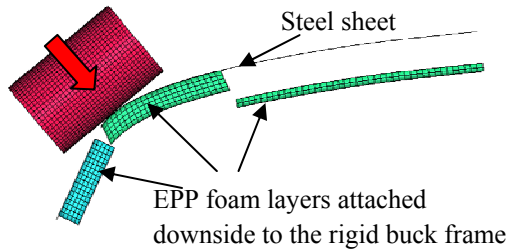


Figure 7. Impactor-to-hood leading edge – grille FE simulation (LS sedan)

Application: Study the influence of pre-braking and vehicle shape on the pedestrian kinematics

A study of the influence of braking and vehicle shape on the pedestrian kinematics was performed. A constant deceleration (1.0 g) and a forward pitching rotation (1 deg) were applied to the vehicle bucks based on the test data recorded in a large sedan during an in-house braking test (Autoliv). Two FE simulations with braking and non-braking conditions were run using MS and LS bucks, and POLAR II dummy in the same initial posture (Figures 1 and 8). The pedestrian dummy kinematics and the contact forces with the buck were calculated and compared among the cases.

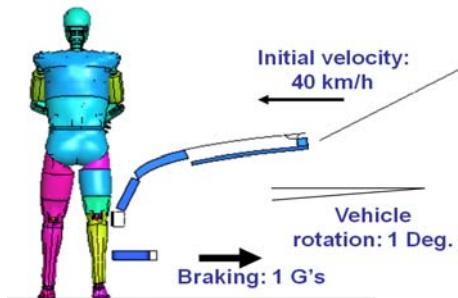


Figure 8. Pre-Impact Configuration of POLAR II – MS Buck impact FE simulation with braking condition

RESULTS

Development of a mid-size sedan (MS) pedestrian buck

A nonlinear trend was observed in the force time history in the lower stiffener impact simulation of the MS vehicle (Figure 9a). A rectangular

prismatic part (200 x 55) made of EPP foam (20 g/l) and connected rigidly to the frame (Figure 10) provided an almost linear force time history which was considered to reasonably approximate the corresponding curve of the lower stiffener in MS vehicle. For the force time history of the bumper, a slightly increasing force was obtained until about 3 ms, followed by a high spikes in force at later times (Figure 9b). A fascia sheet with a 1.7 mm thickness (Figure 10) and a rectangular shape (34 mm x 67 mm) was used to model the bumper and exhibited a trend similar to the MS vehicle.

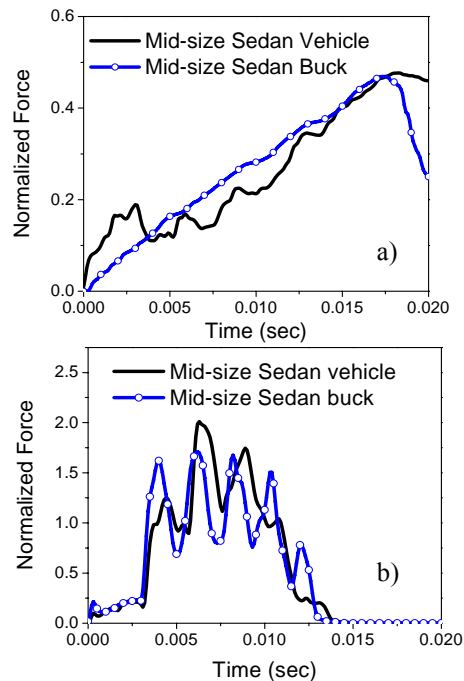


Figure 9. Time histories of the normalized contact force in FE simulations at a) lower stiffener and b) bumper locations

The force time history obtained in the impact with the MS vehicle at the hood leading edge location showed an almost linear increasing force (above the maximum force recorded in the pedestrian impact) that was followed by a plateau region at later times (Figure 11). Several designs of the buck hood leading edge which matched well the linear part of this curve in the component test were proposed. However, these designs recorded in the POLAR II – buck simulation much higher force levels at the hood leading edge location than the levels recorded in the POLAR II – vehicle simulation. The impact force obtained using a hood leading edge design of two rectangular prismatic layers of EPP foam 20 g/l (the final design) also showed a linearly increasing force trend, but with a lower slope than that of MS vehicle (Figure 11).

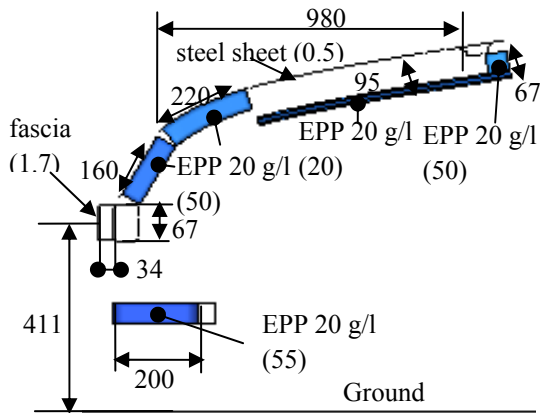


Figure 10. Schematic drawing of the MS pedestrian buck. All dimensions are in mm (thickness in parenthesis)

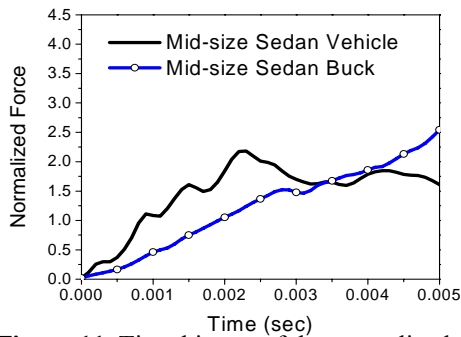


Figure 11. Time history of the normalized force in impactor-hood leading edge FE simulations

The time history of force at the interface between the head impactor and the hood showed a peak at about 4 ms followed a second slightly higher peak. The impactor simulation using a MS hood design, which consists of a steel sheet (0.5 mm thickness) connected at its corners (Figure 10), showed a very good match in the first part of the impact force time history. An EPP foam layer (20 g/l) was added under the hood in order to reduce the second peak of impact force (Figure 12). Several peaks were observed in the time history of impact force at the headform-cowl region impact (Figure 13). In the ME buck design, the force levels of the first and the last peaks were adjusted by changing the gap under the steel sheet and the thickness of EPP foam, respectively (Figure 10).

Validation of a mid-size sedan (MS) pedestrian buck in vehicle-to-pedestrian impact

The time histories of the impact forces calculated in the lower stiffener during POLAR II - MS buck simulation showed similar overall trend to the corresponding data calculated from the POLAR II - MS vehicle simulation (Figure 12). However, the force time history of the buck lower stiffener showed

a slightly higher load peak, corresponding to the impact with the right leg (about 10 ms), and less fluctuation at the later times than the corresponding data from the vehicle simulation (Figure 14 a). A pattern of bi-modal peak forces, corresponding to the impacts with the right knee and then the left knee regions, were observed in both simulations (Figure 14 b). While the first peak had similar values to those in the MS vehicle simulations, the second peak in the MS buck simulation was about 40% higher.

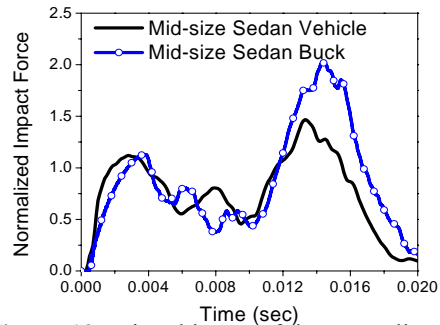


Figure 12. Time history of the normalized force in impactor-hood simulations at WAD = 1200 mm impact locations

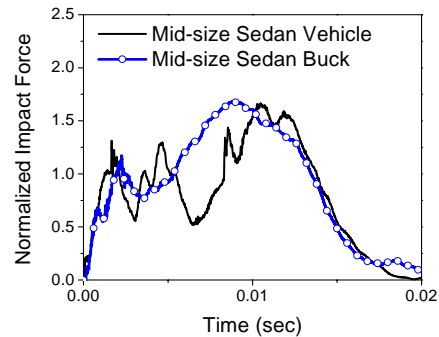


Figure 13. Time history of the normalized force in impactor - hood simulations at WAD = 1500 mm impact locations

The time histories of the forces at the hood leading edge and grille location showed a similar trend in the vehicle and buck simulations with a uniformly increasing force response during pelvis loading, and a decreasing force during the rebound of the pelvis (after 30 - 50 ms). However, the peak forces in the hood leading edge and the grille were higher in the MS buck simulation than in the MS vehicle simulation (Figure 14 c). The contact between the upper extremities and the hood occurred at the last part of the dummy- MS vehicle (buck). The time histories of the hood contact showed a similar trend in the vehicle and buck simulations, with slightly lower values in the buck simulation (Figure 14 d).

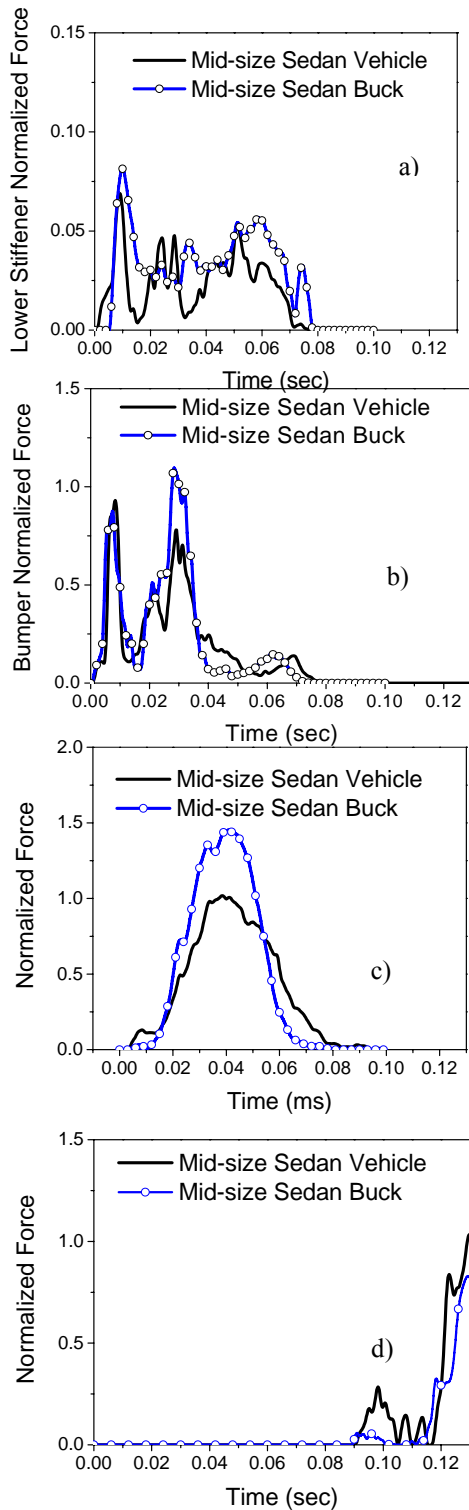


Figure 14. Time history of the normalized forces in POLAR II - vehicle/buck simulations a) lower stiffener contact b) bumper contact c) hood leading edge + grille contact, and d) hood contact

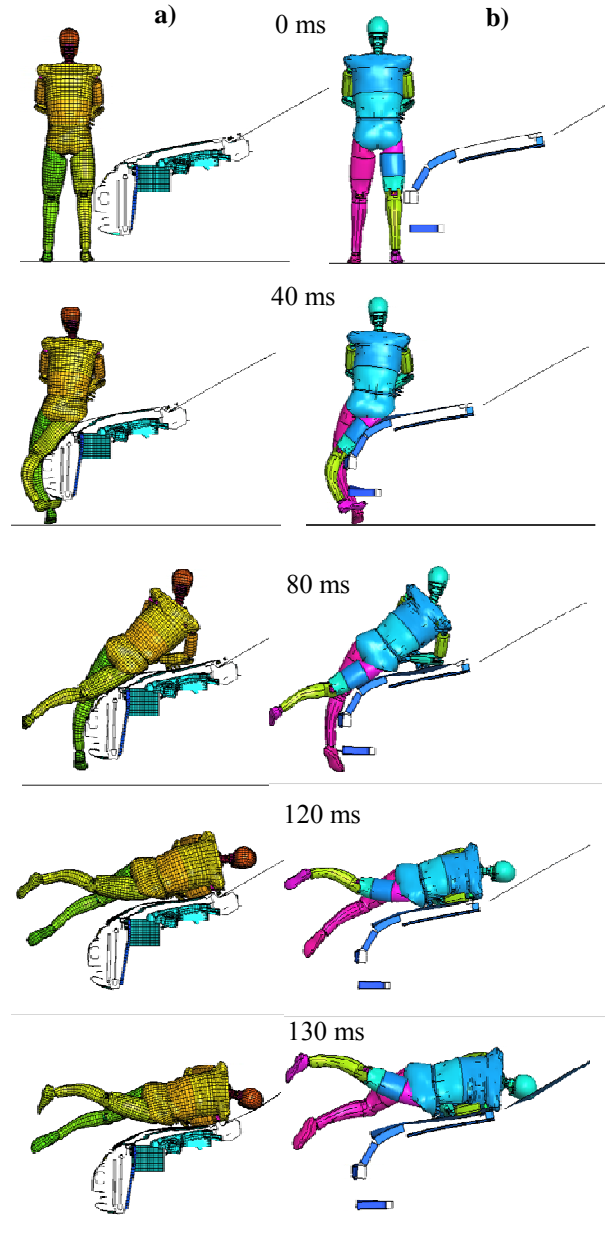


Figure 15. POLAR II dummy kinematics during the impact with a) mid-size sedan FE model and b) mid-size sedan buck FE model

The overall kinematics of the dummy during the impact with the MS buck model showed good visual correlation with the corresponding data from the MS vehicle impact simulation. However, at 120 ms and 130 ms it was observed that the right leg and the pelvis exhibited higher vertical displacements in the MS buck simulation than in the MS vehicle simulation.

The design of the MS lower stiffener was also used in the LS buck design (Figure 16). Although the time histories curves of the LS vehicle LS buck (Figure 17

a) have different trends (linear in LS buck, and nonlinear in LS vehicle), relatively small differences were observed up to about 1.5 kN. Similar trends and relatively small differences were observed in the stiffness curves of the LS vehicle and buck calculated during impact simulations at bumper plus lower stiffener (Figure 17 b) and hood leading edge plus grille (Figure 17 c) locations.

Good correlation can be observed between the trajectories of the upper body trajectories of the POLAR II dummy in the MS buck and vehicle simulations. The T1 and T8 trajectories for the MS vehicle and buck simulations are similar. However, the higher rotation of the POLAR II in the sagittal plane for the MS buck simulation compared to the MS vehicle simulation (Figure 15) generated a slightly lower and higher trajectory of the head location (Figure 18 a) and the pelvis location (Figure 18 d), respectively.

Significant differences are observed between the POLAR II upper body kinematics obtained in the LS and MS buck simulations. While the location of head-vehicle impact was at almost the same vertical level (about 1.1 m) in the LS and MS simulations, the horizontal level in the LS simulation was approximately 100 mm lower than in MS simulations. In addition, the dummy head contact for the MS vehicle occurred in the windshield region (Figure 19 a), while the dummy head - LS vehicle was observed in the cowl region (Figure 19 c). While the trajectories of T1 and T8 calculated in the impacts with MS and LS vehicles were almost identical, the horizontal level at head impact was shorter in the LS simulation than in MS simulation. A higher trajectory of the pelvis marker impact was observed after pelvis-buck interaction in the simulation with LS buck than with MS buck (Figure 18 d).

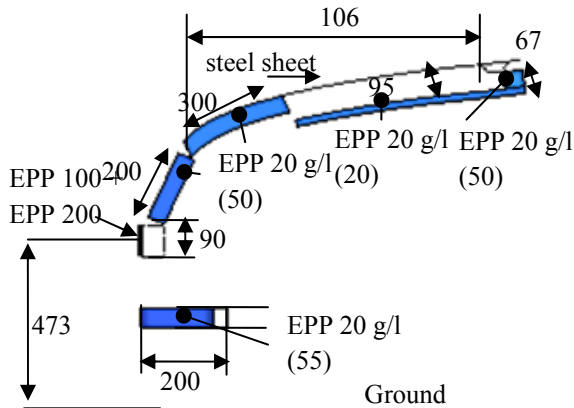


Figure 16. Schematic drawing of LS pedestrian buck. All dimensions are in mm (thickness in parenthesis)

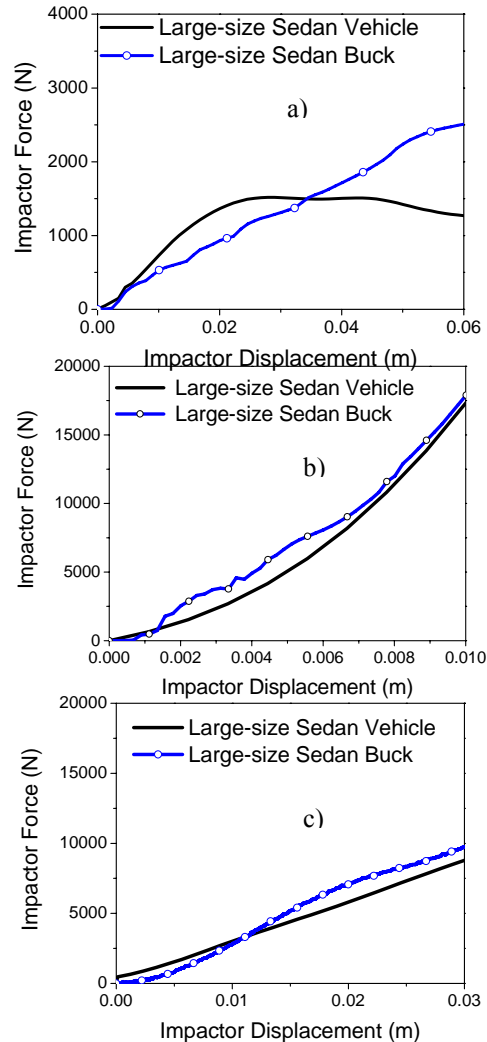


Figure 17. Force-displacement curves in impactor simulations a) lower stiffener b) bumper, and c) hood leading-edge

Application: Study of pre-braking and vehicle shape on the pedestrian kinematics

A comparison between the dummy configurations at the times of head-to-vehicle impacts showed that vehicle (buck) shapes and braking conditions have a significant influence on the head-to-vehicle contact locations (Figure 19) and to the velocity of dummy head relative to the vehicle (buck) (Figure 20). The contact points on the buck for the head-to vehicle impacts were located in the MS windshield regions (Figure 19 a-b) and the LS cowl regions (Figure 19 c-d) for both the braking and no-braking conditions. However, the braking conditions introduced a delay in the head contact time, and generated an increase in the WADs. In addition, both

vehicle/buck shape and the braking conditions influenced the head velocities relative to the vehicle/buck (Figure 20). The velocity of the head relative to the vehicle was lower in the LS simulations than in the MS simulations and in the braking conditions relative to the no-braking conditions (Figure 20).

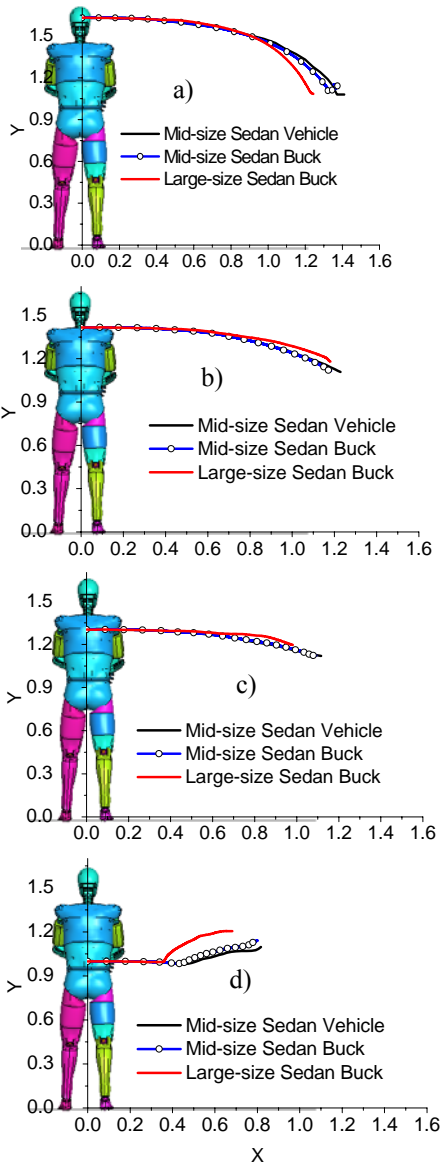


Figure 18. Comparisons of POLAR II upper body trajectories during the impacts with mid-size sedan vehicle, mid-size sedan buck, and large-size sedan buck. a) head, b) T1, c) T8, and d) pelvis

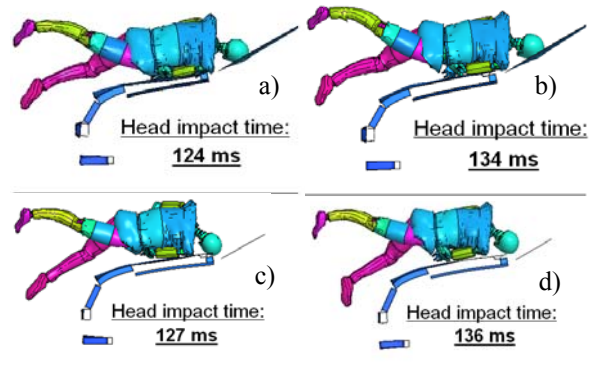


Figure 19. POLAR II - pedestrian buck configurations at the times of head-vehicle impacts a) mid-size buck b) mid-size buck with braking c) large-size buck and d) large-size buck with braking

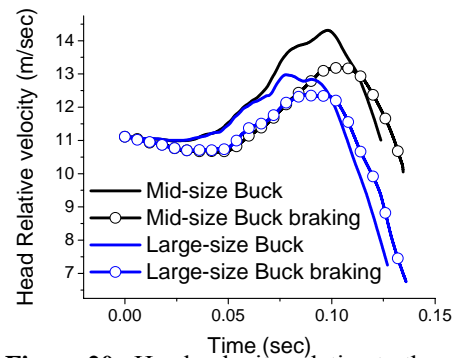


Figure 20. Head velocity relative to the mid/large-size sedan buck in braking/non-braking conditions

DISCUSSION

In addition to the pedestrian impactor tests used currently in regulations and consumer tests, the pedestrian dummy-to-vehicle impact test is a complementary way of investigating pedestrian protection. Given the high cost of experimentally testing a large number of vehicle front-end concepts, an alternative solution could be replacing the vehicle front end with a pedestrian buck that allows simple design changes in terms of vehicle shape and component stiffness parameters.

The design of a generic pedestrian buck (MS and LS configurations), which may reasonably replicate the behavior of sedan front ends in a pedestrian impact, was investigated in the current study. The deformable parts of the bucks were designed using three types of currently manufactured materials: steel, EPP (Expanded PolyProylene) foam (JSP Japan), and plastic fascia used in vehicle bumpers, which allow manufacturing the bucks in the future. While the contour cross-sections of the bucks were approximated based on the corresponding data of

vehicles (Kerrigan et al. 2006, 2007), other cross-sectional dimensions were determined using FE simulations to approximate the stiffness characteristics of front end structures. Impactor-to-vehicle simulations were used to determine the dynamic stiffness of main components of vehicle front ends, such as: lower stiffener, bumper, grille, hood leading edge and hood.

The lower stiffener is located below the bumper system, and prevents the pedestrian's leg from moving underneath the vehicle. Its main role for pedestrian interactions is to reduce the risk of severe knee joint injuries such as ligament ruptures by limiting the knee bend angle (Schuster 2006). A buck component with a prismatic shape (55mm x 200 mm in cross-section) and made of EPP foam (20 g/l) was chosen in the buck design. The force time histories and stiffness curves of the vehicle lower stiffeners showed a nonlinear increasing trend in impactor tests, in contrast to linear trend observed in the lower stiffener of the buck. However, the time history of lower stiffener force in dummy - MS buck simulation had similar trend like the corresponding data from MS vehicle impact, but slightly higher peaks values. Although the lower stiffener component have a low influence on the pedestrian kinematics (especially on upper body) by low load applied during the impact, future studies should try to improve the current design, especially if the buck will be used in prevention studies of lower extremities injuries.

The bumper is the first vehicle component to contact the pedestrian and the level of impact force is high. The bumper system in sedan vehicles usually consists of an energy absorber component (bumper cover, deformable foam etc.) in front of a semi-rigid beam. A fascia sheet (1.7mm thickness) connected to a rigid beam approximated the MS bumper up to the maximum force observed in the dummy-MS simulation. In addition, the time histories of the bumper force in the dummy-MS buck simulation showed similar trends and values as the MS vehicle simulation. The higher peak values predicted at 30 ms may be caused by the higher stiffness of buck bumper at larger deformations. The stiffness of the LS bumper showed an increasing trend, which was well matched using a two-layer bumper design (EPP foams with densities of 100 g/l and 200 g/l, respectively). Although current designs of buck bumpers showed to approximate well the stiffness properties of vehicle bumpers, better designs can be obtained using optimization techniques (Untaroiu et al. 2007).

The leading edge of the hood is the vehicle component that usually contacts the pelvis of adult pedestrian during the impact. Depending on its

position relative to the hip joint, the pelvis can slide along the hood or can be pinned at the contact point (Kerrigan et al. 2007, Untaroiu et al. 2007). Since the pelvis-to-vehicle contact is complex, the design of this region was the most challenging task of the pedestrian buck design. After trying several design concepts, it was decided that a design consisting of two low densities EPP (20 g/l) blocks, which approximate the shape of the hood leading edge and the grille, reasonably replicate this vehicle component response in the buck design. The time history of MS buck force shows a linear trend with values relatively close to the curve obtained from the MS vehicle impact which has an initial slope followed by a plateau region. However, the results of the dummy-MS vehicle simulation showed a higher stiffness for the MS buck in the contact with the dummy pelvis, especially in the grille region. While the MS buck was softer than the vehicle in the impactor test, this finding suggests that the leading edge impactor test may poorly approximate the conditions of a dummy pedestrian impact. Therefore, a new impactor test or even the whole dummy-vehicle simulation should be used for a better stiffness calibration of this region in a future design. The stiffness curve, obtained from the impact between the constrained impactor with a constant impact velocity (40 km/h) and the hood leading edge - grille component of the buck, showed a closed trend to the stiffness curve reported by Kerrigan et al. (2008).

A steel sheet rigidly connected at its corners, with one EPP foam layer showed to approximate well the hood behavior during simulations with adult headform impactor at both middle and cowl impact locations. Although the hood contact force in MS vehicle and MS buck showed good correlation with the corresponding data from the POLAR II - MS vehicle simulation, the level of force between shoulder and hood was low because the head impacted the windshield. Therefore, future studies of MS vehicle impacts with a dummy having a different anthropometry (e.g., the 5th female used in Untaroiu et al. 2008) may be used to verify the hood design of buck in a dummy-vehicle simulation.

Since previous pedestrian studies have investigated the pedestrian kinematics until the head-to-vehicle contact (Kerrigan et al. 2005, 2007), the windshield was included as a buck component but stiffness studies of this component were not performed in the current study. FE models of the buck may be improved in future studies by using recently developed material model of laminated glass (Timmel et al. 2007) when dynamic test data of the sedan windshields will be available.

A parametric study using the same dummy FE model, but different buck shapes (MS and LS) showed a possible application of buck models in the study of an automatic braking system for reducing pedestrian injuries. While the pre-braking condition showed reductions in the relative velocity of head with the vehicle at the head-vehicle impact and increase the pedestrian WAD, the vehicle shape showed a significant influence on the velocity speed and the vehicle component impacted by the pedestrian head. More parametric studies may be run in the future, with different braking parameters, and dummy anthropometries. The simplified FE models of vehicle can be easily used in different optimization studies of vehicle shape and stiffness and restraint systems for pedestrian protection. In addition, a physical buck developed based on the design concepts of this study may be manufactured and used to validate the new pedestrian protection design in dummy-pedestrian buck crashes.

CONCLUSIONS

This numerical study showed that a simplified pedestrian buck consisting of five components: lower stiffener, bumper, hood leading edge-grille, hood and windshield; can reasonably approximate the vehicle front structures during the lateral impact of a POLAR II dummy. The geometry of the buck FE models was developed based on the contour-cross-sections corresponding to a mid-size and a large-size sedan vehicle used in previous vehicle-to-dummy and cadaver tests. The material properties of current polymeric products were used for the FE models of the buck components in order to allow manufacturing a physical implementation of the generic pedestrian buck in the future. Simulations of interactions between impactors and vehicle component were used to correlate the dynamic stiffness of buck components with the corresponding data of vehicle models. The hood lower edge-grille component designed based on impactor simulations showed poor correlation during the dummy –vehicle impact simulations. This poor correlation may be caused by the complex contact between the pelvis and vehicle which is poorly reproduced in the component test. In a parametric study using FE impact simulations of POLAR II dummy and pedestrian buck models, it was shown that the vehicle braking conditions reduce the relative velocity of the head to the vehicle and increase the time of head impact and wrap-around-distances (WAD) to primary head contact. In addition, different buck shapes (e.g. MS buck and a large-size sedan - LS buck) showed a higher sensitivity to pedestrian kinematics (e.g. relative head impact velocity) than to the braking conditions over the

range of conditions examined in this study. The pedestrian buck models developed in the current study may be used for future optimization studies of pedestrian protection systems (e.g. airbags, automatic braking etc) and in manufacturing a physical pedestrian buck, which could, in turn, be used to validate pedestrian protection systems.

REFERENCES

- [1]. Akiyama A., Yoshida S., Matsushashi T., Moss S., Salloum M., Ishikawa H., Konosu A. (1999) Development of Human-like Pedestrian Dummy, Paper 9934546, Japanese Society of Automotive Engineers, Chiyoda-Ku, Tokyo, Japan.
- [2]. Akiyama A., Okamoto M., N. Rangarajan (2001) Development and Application of the New Pedestrian Dummy, Paper 463, Proceedings of the 17th International Technical Conference on the Enhanced Safety of Vehicles (ESV), Amsterdam, The Netherlands.
- [3]. Crandall J., Wiley K., Longhitano D., Akiyama A. (2005). Development of Performance Specifications for a Pedestrian Research Dummy, Paper 389, Proceedings of the 19th International Technical Conference on the Enhanced Safety of Vehicles (ESV), Washington, USA.
- [4]. EU (2003). Directive 2003/102/EC of the European Parliament and of the Council of 17 November 2003 relating to the protection of pedestrians and other vulnerable road users before and in the event of a collision with a motor vehicle and amending Council Directive 70/156/EEC. Brussels, Official Journal of the European Union.
- [5]. EU (2009). Regulation (EC) No 78/2009 of the European Parliament and of the Council of 14 January 2009 on the type-approval of motor vehicles with regard to the protection of pedestrians and other vulnerable road users, amending Directive 2007/46/EC and repealing Directives 2003/102/EC and 2005/66/EC. Strasbourg, Official Journal of the European Union.
- [6]. Expanded Polypropylene (EPP) ARPRO®, http://www.jsp.com/en/home/products/arpro/arpro_ch.php
- [7]. Fredriksson, R., Y. Håland, et al. (2001). Evaluation of a New Pedestrian Head Injury Protection System with a Sensor in the Bumper and Lifting of the Bonnet's Rear Part. 17th ESV Conference, Amsterdam, Netherlands.

- [8]. Kerrigan J., Kam C., Drinkwater C., Murphy D., Bose D., Ivarsson J., Crandall J. (2005) Kinematic Comparison of the POLAR II and PMHS in Pedestrian Impact Tests with a Sport-Utility Vehicle, Proceedings of the 2005 International Research Council on the Biomechanics of Impact (IRCOBI), Prague, Czech Republic.
- [9]. Kerrigan R., Crandall J., Deng B. (2007) Pedestrian kinematic response to mid-sized vehicle impact. *Int. J. Vehicle Safety*, 2(3) pp.221-240
- [10]. Matsui Y and Tanahashi M. (2004) "Development of JAMA-JARI pedestrian headform impactor in compliance with ISO and IHRA standards", *Int J Crashworthiness*, 2004 9(2) 129–139.
- [11]. Mizuno Y. (2008) "Development and Process of the Pedestrian Safety Global Technical Regulation" *Review of Automotive Eng. (JSAE)* 29(1), pp. 43-48
- [12]. Neal M.O. Tu J., Jones D. (2008) A response Surface Based Tool for evaluating vehicle performance in the pedestrian leg impact test, *SAE Congress 2008*, 2008-01-1244.
- [13]. National Highway Traffic Safety Administration (NHTSA), (2009) *Traffic Safety Facts 2007*. DOT HS 811 017.
- [14]. Okamoto Y., Akiyama A., Okamoto M., Kikuchi Y. (2001) A Study of the Upper Leg Component Tests Compared with Pedestrian Dummy Tests, Paper 380, Proceedings of the 17th International Technical Conference on the Enhanced Safety of Vehicles (ESV), Amsterdam, The Netherlands.
- [15]. Ogo Y., Sakai H., Maki T. (2009) Influence of the arms on pedestrian head injury at the time of vehicle collision, *JSAE Review of Automotive Engineering*, 30 (1), pp. 85-90.
- [16]. Pam System International, (2004) *PAM-CRASH / PAM-SAFE REFERENCE MANUAL*, Version 2004.
- [17]. Polypropylene –fascia (Boedeker Plastics, TX, US)
- [18]. Shin J., Untaroiu C., Kerrigan J., Crandall J., Subit D., Takahashi Y., Akiyama A., Kikuchi Y., Longitano D. (2007) Investigating Pedestrian Kinematics with the POLAR II Finite Element Model, Paper 2007-01-0756 Society of Automotive Engineers.
- [19]. Shin J., Lee S., Kerrigan J., Darvish K., Crandall J., Akiyama A., Takahashi Y., Okamoto M., Kikuchi Y. (2006) Development and Validation of a Finite Element Model for the POLAR II Upper Body, Paper 2006-01-0684, Society of Automotive Engineers
- [20]. Schuster P (2006) "Current trends in bumper design for pedestrian impact." Proceedings, 2006 SAE World Congress, April 2006.
- [21]. Snedeker, J.G., Walz, F.H., Muser, M.H., Lanz, C., and Schroeder, G. (2005) Assessing femur and pelvis injury risk in car-pedestrian collisions: comparison of full body PMTO impacts, and a human body finite element model Paper05-0130, Proc. 19th Conference on the Enhanced Safety of Vehicles (ESV), Washington DC, United States
- [22]. Takahashi Y., Kikuchi Y., Okamoto M., Akiyama A., Ivarsson J., Bose D., Subit D., Shin J., Crandall J. (2005) Biofidelity Evaluation for the Knee and Leg of the Polar Pedestrian Dummy, Paper 05-0280, Proceedings of the 19th International Technical Conference on the Enhanced Safety of Vehicles (ESV), Washington DC, United States.
- [23]. Takahashi Y., Okamoto M., Kikuchi Y., Akiyam A. (2008) Injury threshold and a measurement technique for thigh and leg of a pedestrian dummy, *IRCOBI Conf.*
- [24]. Timmel M, Kolling S, Osterrieder P, Du Bois PA (2007) A finite element model for impact simulation with laminated glass, *International Journal of Impact Engineering*, 34(8):1465-1478
- [25]. Untaroiu C., Shin J. and Crandall J. (2007). "A Design Optimization Approach of Vehicle Hood for Pedestrian Protection". *International Journal of Crashworthiness*, 12(6):581-589.
- [26]. Untaroiu C., Kerrigan J., Kam C., Crandall J., Yamazaki K., Fukuyama K., Kamiji K., Yasuki T., Funk, J. (2007). "Correlation of Strain and Loads Measured in the Long Bones with Observed Kinematics of the Lower Limb during Vehicle-Pedestrian Impacts". *Stapp Car Crash Journal*, 51:433-466
- [27]. Untaroiu C., Shin J., Ivarsson J. Crandall, Subit D., Takahashi Y., Akiyama A., Kikuchi, Y. (2008). "A Study of the Pedestrian Impact Kinematics using Finite Element Dummy Models: the Corridors and Dimensional Analysis Scaling of Upper-Body Trajectories" *International Journal of Crashworthiness*, 13(5):469-478.

- [28]. Untaroiu C., Meissner M., Crandall J., Takahashi Y., Okamoto M., Ito O. (2009). "Crash Reconstruction of Pedestrian Accidents using Optimization Techniques". *International Journal of Impact Engineering*, 36(2):210-219
- [29]. Youn Y., Kim S., Oh C., Shin M., Lee C. (2005) Research and Rule-Making Activities on Pedestrian Protection in Korea, Paper 05-0117, Proceedings of the 19th International Technical Conference on the Enhanced Safety of Vehicles (ESV), Washington DC, United States.